An investigation into the molecular mechanisms underlying retinitis pigmentosa 17 with the view to developing novel gene-based therapies

By

Aisha Pandor

Thesis presented for the Degree of Doctor of Philosophy in Human Genetics in the Department of Clinical and Laboratory Sciences, Faculty of Health Sciences, University of Cape Town

February 2012

DECLARATION

I, Aisha Pandor, hereby declare that the work on which this thesis is based is my original work (except where acknowledgements indicate otherwise) and that neither the whole work nor any part of it has been, is being, or is to be submitted for another degree in this or any other University. I empower the University to reproduce for the purpose of research either the whole or any portion of the contents in any manner whatsoever.

The Human Genetics journal referencing convention has been used.

……

February 2012

Acknowledgements

I wish to thank the following wonderful individuals:

My parents for unconditional love, support and encouragement through the years. They have sacrificed so much for us. I thank my amazing siblings Faz, Suraya and Haroon for being there for me and lifting me up at the end of a long day. Ajla couldn't ask for a more awesome aunt and uncles.

Thanks to my girlfriends Sampa, Kath, Justine, Liz, Kia, Cali, Michaela and Tracey for never giving up on my social life, even when I did.

To Sharon and Raj, thank you for being role models, mentors, and friends. In addition to the scientific skills that I have learnt from you both, you have taught me to strive for excellence, to be ethical in my work, and to have passion for what I do. I will take these lessons with me wherever I go.

To my grandparents, Joe and Fikile Matthews, I wish you were here to share my successes with me, I know you would both have been so proud.

To the Human Genetics and T-Box laboratories, thank you for being a shoulder to cry on when experiments failed, and a cheering party when they did not. Your support, friendship, and enormous assistance made every day at the lab a great one.

I am greatly indebted to:
Drs Deeya Ballim and Wendy Kroger, Sabina Wansleben, and Lisa Roberts, for the enormous amount of time spent in their critical reading of this thesis.

Dr Putuma Gqamana and The Professor Jonathan Blackburn Lab, University of Cape Town Health Sciences Faculty, for assistance with proteomics work. Thanks too to Dr

Salome Smit at the University of Stellenbosch Proteomics Laboratory for facilitating the mass spectrometry work.

The David and Elaine Potter Fellowship Society for the immense financial support and invitation to be part of a great network. Their work encourages me to “be the change I want to see in the world”.

I am thankful too, to the South African Medical Research Council for financial support during this degree.

Last but not least, I am so grateful to Alen for supporting me through the hardest times, and standing by me through decisions that were difficult. You are my rock. I cannot describe how thankful I am every day that you are in my life.

This thesis is dedicated to Ajla Ribic, the light of our lives.

Table of contents

Materials and Methods

Results

Genetics of RP17

List of Figures and Tables

Table **Page**

ABSTRACT

Retinitis pigmentosa (RP) is a highly heterogeneous form of inherited blindness that affects more than 1.3 million individuals worldwide. The RP17 form of the disease is caused by an arginine to tryptophan (R14W) mutation in the signal sequence of carbonic anhydrase IV (CAIV). In an effort to elucidate the molecular mechanisms underlying RP17, three cell types were transfected with the wild type (WT) and the R14W mutant form of the protein. We show using immunocytochemistry that unlike transfected WT CAIV which is transported to the plasma membrane of transfected COS-7 and HT-1080 cells, R14W mutant CAIV is retained in the endoplasmic reticulum when transfected into the same cell type. Further analyses of these cells by western blotting reveal that whereas the WT CAIV is processed to its mature form in both these cell lines, significant levels of the R14W mutant protein remain in its immature form. Importantly, flow cytometry experiments demonstrate that compared to WT CAIV protein, expression of specifically the R14W CAIV results in an S and G2/M cell cycle block, followed by apoptosis. Interestingly, when the above experiments were repeated in the human embryonic kidney cell line, HEK-293, strikingly different results were obtained. These cells were unaffected by the expression of the R14W mutant CAIV and were able to process the mutant and WT protein equally effectively. These findings regarding cell type specificity were used as a basis to explore methods of therapy for RP17. In particular, allele-specific small hairpin RNA was used to silence expression of R14W mutant CAIV, and to rescue cells from undergoing cell cycle arrest and apoptosis. A study of specific chaperones involved in protein folding, as well as gene and protein expression studies (microarray and mass spectrometry analysis), were also carried out to determine which proteins that were expressed in HEK-293 cells play a part in the ability to fold, process and transport R14W mutant CAIV. The results of this study have important implications for our understanding of the RP17 phenotype, and in investigating gene and protein therapy for the prevention and treatment of RP17.

Introduction

1.1. Retinitis Pigmentosa

Retinitis pigmentosa (RP) is a leading cause of blindness, occurring at an incidence of approximately 1 in 3500 people, and affecting a total of 2 million individuals worldwide (Dejneka et al. 2001; Phelan and Bok, 2000). This debilitating disease can cause loss of vision from as early as birth in some individuals, with the majority of affected individuals being declared legally blind by the age of 60 years (Berson, 1996). Night blindness is the earliest symptom of RP, but as the disorder progresses, all aspects of day vision may also be affected. In RP, peripheral vision is affected to varying degrees, and the result is a narrowing visual field, or "tunnel vision", which often progresses to functional blindness (Kalloniatis et al. 2004). The identification of numerous genes involved in RP in the last 20 years has highlighted the high degree of heterogeneity of the disease, and its widespread nature (it is not limited to a particular age, ethnicity, or regional group) has triggered much interest in studying the various classes of the disease.

Most recently, gaining an understanding of the molecular mechanisms underlying different types of RP has allowed researchers to investigate possible modes of therapy for the disease. In previous studies, gene therapy (both silencing and replacement) (Cideciyan, 2010; Millington-Ward et al. 2011; Tam et al. 2008), stem cell therapy (Enzmann et al. 2009; Jin et al. 2009), the application of molecular chaperones and other small molecules (Kosmaoglou et al. 2008; Mendes and Cheetham, 2008; Noorwez et al. 2003; Noorwez et al. 2008), vitamin supplementation (Berson et al. 1993a; Berson et al. 1993b; Berson et al. 2004) and protein inhibitors (Clemson et al. 2011) have all been attempted, with varying degrees of success. Currently, none of these methods have provided a "silver bullet" solution to treating the large burden of RP (Jacobson et al. 2010), and the prognosis for the majority of RP sufferers is still poor.

1.1.1. Categorisation and classification

RP was first described in 1857 by the German physician Franciscus Donders, who discovered night blindness in his patients, which he later termed "retinitis pigmentosa". Upon funduscopic examination he found these patients to have "bone spicule pigmentation" in the retina. Although the name RP was a misnomer (the implied "inflammation" is not a primary defect in RP), it is still used today, and describes a highly heterogeneous group of inherited ocular diseases that are characterized by progressive degeneration of the retina (Dryja and Li, 1995; Phelan and Bok, 2000). RP comprises a highly complex group of diseases, which may be associated with an exclusively ocular phenotype, or may occur as part of a syndrome (Shintani et al. 2009). More than a century and a half since Donders' discovery, new forms of RP and their causal genes are still being discovered.

In RP, retinal pigment epithelium (RPE) cells in the eye degenerate and consequently release their pigment into the surrounding tissue. The result is a cluster of dark spots (bone-spicule formations) in the retina, which are used as a definitive clinical characteristic in the diagnosis of the disease. Other features of RP may include constriction of retinal arterioles, a waxy pallor of the optic disk, cataracts, astigmatism, myopia, and a reduced electroretinogram (ERG) response (Hims et al. 2003; Wang et al. 2001). Interestingly, half of the reported cases of RP appear to be sporadic or isolated, with no apparent family history of disease and the other half are apparently familial, and exhibit different modes of inheritance. It is estimated that autosomal dominant (adRP) inheritance accounts for 16% of RP cases, autosomal recessive (arRP) inheritance for 31%, and X-linked inheritance for 6% (Kalloniatis et al. 2004). In a minority of cases, RP may also be inherited mitochondrially. It is speculated that the "sporadic" cases may in fact be due to X-linked or recessive inheritance, or to gene mutations that have as yet not been identified (Shintani et al. 2009).

Although there is a broad spectrum of phenotypes relating to disease severity and the rate of disease progression in RP, age of onset can generally be correlated with the mode of

inheritance. X-linked RP generally has the earliest age of onset; followed by arRP, while adRP generally shows a relatively later age of onset of disease (Phelan and Bok, 2000).

The heterogeneity of this disease is underscored by reports that more than 58 loci involving 47 genes are implicated in non-syndromic RP, with numerous more mutations identified in the various syndromic forms (Hims et al. 2003; http://www.retina-international.org/sci-news/disloci.htm). It is now possible to group causative genes and proteins mutated in RP according to their function. For example, some of the most common mutations linked to RP occur in genes that are expressed in the photoreceptor cells of the retina, or whose products are associated with the phototransduction cascade or visual cycle. These mutations usually cause arRP. Mutations in genes encoding structural proteins, transcription factors, splicing factors, intracellular transport and signalling proteins, and cell-cell adhesion proteins, generally cause adRP (Hims et al. 2003). In a more rare and less well-defined group of RP, mutations occur in miscellaneous genes, making it harder to correlate the phenotype with the molecular pathology underlying the disease. This may occur when non-syndromic RP occurs as a result of a mutation in a gene not exclusively expressed in the retina. These mutations may indirectly cause retinal cell death through the death of supporting cells that are directly affected by the mutations.

An example of non-photoreceptor-expressed genes being involved in photoreceptor degeneration is in retinitis pigmentosa 17 (RP17). Mutations in the carbonic anhydrase 4 gene (*CA4* describes the gene, CAIV the protein), which is not expressed in photoreceptor cells, cause a dominant form of the disease. The disease is believed to result from misfolding of mutant CAIV protein, there has however, been controversy over the exact cause (this will be discussed in detail in section 1.2). In order to better understand the pathology of RP17, it may help to begin by exploring P23H RP, which is another, more common form of the disease. P23H RP is an archetypal form of "misfolding RP", which is believed to share with RP17, at least some of the molecular mechanisms that eventually lead to disease.

1.1.2. Protein misfolding retinitis pigmentosa

P23H RP

In many cases of RP, the mutation resulting in disease is in the gene encoding rhodopsin (RHO), the visual pigment responsible for mediating rod cell based vision (Sung et al. 1991). *RHO* was the first gene in which mutations linked to RP were identified, and to date, over 200 mutations have been identified in this gene, the most frequent of which is P23H (which causes a proline to histidine substitution at amino acid 23). This mutation accounts for about 10% of all cases of RP (Chadderton et al. 2009; Noorwez et al. 2003; Noorwez et al. 2004), and is the "single most common RHO mutation among patients with adRP", accounting for over 50% of RHO RP (Noorwez et al. 2003). The P23H mutation results in misfolding of RHO and its subsequent aggregation in the endoplasmic reticulum (ER), and Golgi body of the cell. Furthermore, in P23H RP, small amounts of the mutant opsin may escape the quality control mechanisms of the ER and enter the cytosol, forming aggregates with itself and other proteins (Mendes et al. 2005). The aggregated RHO protein that is trapped in the ER cannot translocate to the plasma membrane, and is therefore unable to reconstitute with 11-cis retinal as part of the phototransduction process that mediates vision.

Phototransduction occurs in the retinal cells during normal vision. During this process, light signals, in the form of photons, are converted into electrical signals that relay the visual stimulus to the brain. The process is mediated by opsins (like RHO), which are G-protein coupled receptors (GPCRs) that contain the chromophore 11-cis retinal. When opsins are stimulated by light, 11-cis retinal undergoes photoisomerisation to form all-trans retinal. The conformational change of the opsin leads to a signal transduction cascade that causes the closure of cyclic nucleotide guanosine monophosphate-gated channels and hyperpolarisation of photoreceptor cells. This hyperpolarisation activates neighbouring cells, and eventually sends an excitatory signal to the optic nerve and down the neural pathway (Moiseyev et al. 2005; Yau, 1994).

In P23H RP, the mutant opsin is targeted for degradation by the ubiquitin proteasome system (Illing et al. 2002), but when the load of unfolded protein is too high, this causes ER stress, leading to the instigation of the unfolded protein response (UPR) (Saliba et al. 2002).

In transfected cells, P23H mutant RHO protein that accumulates in the ER and Golgi is found in a complex with the molecular chaperones BiP and Grp94, supporting the notion that it is misfolded (Chapple et al. 2001; Mendes et al. 2005; Saliba et al. 2002). This form of RP is therefore thought to be caused by photoreceptor cell death by apoptosis, in response to the burden of misfolded proteins on the ER (Kalloniatis et al. 2004, Mendes et al. 2005).

In vivo experiments have revealed that heterozygous *RHO* knockout mice display little photoreceptor cell death, again suggesting that it is not failure of RHO to translocate to the outer segment which causes RP, but rather the toxic "gain of function" effect of the misfolded protein (Chapple et al. 2001). Indeed, the Drosophila transgenic model for the P23H form of RP has shown that most of the mutant RHO is trapped in the ER, while some of it is partially active and interferes with the phototransduction pathway (Galy et al. 2005). The observed mechanism of disease of P23H RP provides a valuable case on which to build our understanding of another form of retinitis pigmentosa, RP17.

1.2. Retinitis Pigmentosa 17

Retinitis pigmentosa 17 (RP17) is an autosomal dominant form of RP caused by an arginine to tryptophan missense mutation at residue 14 (R14W) of the CAIV protein (Rebello et al. 2004). Like the P23H RHO mutation, the R14W CAIV mutation is thought to lead to incorrect protein folding in cells where it is expressed. The CAIV protein is a glycosylphosphatidylinositol membrane-anchored zinc metalloenzyme that is localised on the luminal surface of microcapillaries and is highly expressed in the choriocapillaris of the human eye (Bonapace et al. 2004). CAIV belongs to the carbonic anhydrase family of enzymes, and plays a role in pH buffering in cells in which it is

expressed, due to its role in the hydration of carbon dioxide (CO_2) to form bicarbonate (HCO_3^-) and acids. This family of RP is particularly interesting to some researchers not only because of the protein misfolding aspect of the disease, but also because CAIV is not expressed in the retina. RP17 therefore belongs to the less-defined group of RP cases where mutations occur in miscellaneous non-photoreceptor-specific proteins. As a result, the exact molecular pathogenesis leading to disease may be more difficult to elucidate.

The RP17 locus was mapped in 1995 by our research group at the Division of Human Genetics at the University of Cape Town. The disorder was initially identified in a South African family of German descent, and then later in other South African families that all shared common haplotypes associated with the disease phenotype (Bardien et al. 1999; Bardien-Kruger et al. 1997). Detailed phenotypic analysis of RP17 patients has revealed a distinctive chorioretinal atrophy aspect of the disease (Ramesar et al. unpublished), which deteriorates with age. This is in keeping with a choroidal origin of the disease, as first suggested by Hageman et al. (1991).

In 2004, Rebello et al. showed that a C>T substitution in the *CA4* gene was causative of RP17. The change occurs at base 40 of the cDNA sequence, leading to the R14W mutation in the signal sequence of the protein. The mutation occurs at position -5 relative to the signal sequence cleavage site, and is therefore thought to result in incorrect signal peptide cleavage of CAIV after transfer of the nascent polypeptide to the ER lumen. As a result of incorrect cleavage of the signal sequence, the mutant CAIV protein is thought to be retained in the ER, leading to its misfolding, and consequently, to ER stress and apoptosis of cells in which it is expressed. This hypothesis was supported by experiments in COS-7 cells transfected with either wild type (WT) or R14W mutant CAIV constructs. Results from these experiments showed that expression of the mutant protein: (i) reduced steady-state levels of CAIV activity by 28%; (ii) led to up-regulation of BiP, PERK, and CHOP, the markers of the UPR and endoplasmic reticulum stress in eukaryotic cells; and (iii) induced apoptosis, as revealed by Annexin V binding and terminal deoxynucleotidyltransferase-mediated dUTP nick-end label staining in most cells

expressing the mutant (but not the WT) form of the protein (Rebello et al. 2004). Based on these results, our research group hypothesised that the high levels of expression of the mutant protein in choriocapillaris cells leads to apoptosis. This hypothesis and experimental results were also confirmed by various other groups in subsequent studies (Bonapace et al. 2004; Datta et al. 2009; Datta et al. 2010).

The choriocapillaris has a crucial role in removing waste from, and supplying oxygen to the adjoining RPE of the eye, which in turn supplies nutrients to the retina (Jeppesen et al. 2007). Apoptosis of the cells of the choriocapillaris could therefore lead to ischemia in the overlying RPE and the consequential lack of nutrient supply to the retina (and no efficient removal of waste). This possibility is supported by experiments in the pig eye that have shown that mechanical closure of the choriocapillaris fenestrae leads to severe RPE and retinal degeneration, which in turn causes more intensified closure and increased deterioration of the choriocapillaris as part of a type of "feedback loop" effect (Kiilgaard et al. 2007). As demonstrated by this study, the death of choriocapillaris cells is ultimately extremely detrimental to retinal cells, and will eventually lead to the RP phenotype and loss of vision.

Early in 2005, concurrent with the Rebello et al. (2004) work, Yang et al. (2005) performed separate studies that led them to suggest an alternate mechanism of retinal cell death in RP17. During these studies, Yang et al. (2005) co-transfected HEK-293 cells with sodium bicarbonate co-transporter 1 (NBC1) protein and either WT- or R14W mutant-CAIV constructs and measured intracellular pH and bicarbonate flux. Using fluorescence microscopy, the group showed that the R14W mutant CAIV did not bind effectively to transfected NBC1 protein. Since an earlier study had shown in *in vitro* experiments that ectopically-expressed CAIV and NBC1 form a transporter system complex on the plasma membrane of HEK-293 cells (Alvarez et al. 2003), Yang et al. (2005) proposed that the R14W mutation compromises this system in these cells. The latter study speculated that the mutation in the CAIV protein leads to imbalances in pH homeostasis within choriocapillaris cells and surrounding tissue, due to the disrupted

transporter system. Based on their results, the Yang group (2005) concluded that high levels of WT CAIV protein are vital, and that haploinsufficiency of functional CAIV protein contributes to disease pathogenesis and the RP17 phenotype. Interestingly, in the previous work by Alvarez et al. (2003), a mutation in the CAIV-binding site of NBC1 disrupted the binding of the two proteins, but did not decrease the functional activity of the NBC1 protein.

Included in the same study by Yang et al. (2005) was the identification of two new RP17 CAIV mutations, one in exon 7 (R219S), and the other in the 3'- UTR, which segregated with the disease phenotype in Caucasian families. In a separate but similar study, Alvarez et al. (2007) identified a novel CAIV mutation in a cohort of Chinese individuals. A simplex or sporadic R69H mutation was identified in an 11-year-old boy who presented with night blindness and poor vision at the age of 3 years. Based on experiments analogous to those of Yang et al. (2005), the concept of a "bicarbonate metabolon" was again put forward, with the proposal that CAIV in the choriocapillaris associates with NBC1 in a transporter system metabolon. As with the Yang et al. study, the mechanism of disease in the cases of the CAIV mutations was suggested to be a pH imbalance caused by a build-up of acid within these CAIV-expressing cells.

While the studies carried out by Yang et al. (2005) and Alvarez et al. (2007) were performed by transfecting WT- and mutant CAIV expression constructs into HEK-293 cells, subsequent studies have also looked at CAIV expression *in vitro*. Sun et al. (2008) used cultured bovine epithelium to examine the activity and localisation of CAIV protein with the view to investigating the role of the protein in pH recovery and bicarbonate flux. Firstly, using immunofluorescence assays with CAIV-specific antibodies, they show that the protein is localised to the apical membrane of endothelial cells. They then measured flux and transport of CO_2 and HCO_3^- in the cultured cells by perfusing cells with CO_2 and HCO_3^--rich and CO_2 and HCO_3^--free Ringer solution. Using cell-permeable and impermeable carbonic anhydrase inhibitors as well as knockdown of endogenous (WT) CAIV protein using an siRNA approach, Sun et al. (2008) demonstrated that CAIV

facilitates apical CO_2 flux and the conversion of CO_2 to HCO_3^- at the apical membrane, but does not facilitate apical HCO_3^- flux, or determine cell membrane permeability to HCO_3^-. Results from these experiments also indicated that CAIV does not have a role in net CO_2 flux, and instead suggested a role of CAIV in buffering capacity at the apical surface only, suggesting a more minor role in pH buffering than that proposed by Yang et al. (2005).

Results from their studies in bovine corneal epithelial cultures also led Sun et al. (2008) to challenge the theory of a bicarbonate transport metabolon, based on the incapability of siRNA or benzolamide (an impermeable carbonic anhydrase inhibitor) to reduce HCO_3^- permeability or flux. However, more than one study has provided evidence to suggest that CAIV interacts with an anion transporter on the plasma membrane of cells in various tissues (Boron et al. 2010; Dinour et al. 2004; Sterling et al. 2002). The contrasting results of the Sun et al. (2008), and Yang et al. (2005) and Alvarez et al. (2003; 2007) studies may, therefore, be explained by (i) the substitution of CAIV with another analogous and functional carbonic anhydrase as suggested by Ogilvie et al. (2007) and Shahidullah et al. (2009), (ii) the substitution of CAIV with another type of protein, (iii) the ability of other membrane metabolons to perform the same function, or (iv) an ability of these anion transporters to successfully perform HCO_3^--coupled transport even without an interaction with CAIV, albeit at a decreased rate.

Adding further to the complexity surrounding RP17 is the high level of CAIV protein expression in the renal proximal tubules (Brown et al. 1990; Carter et al. 1990) in addition to the choriocapillaris. However, while mutations in CAIV result in loss of vision, RP17 patients do not show evidence of a kidney phenotype (Rebello et al. 2004). Rather, mutations in NBC1 protein (suggested to be the functional partner of CAIV in the bicarbonate transporter system) cause proximal renal tubular acidosis of the kidney (Dinour et al. 2004) and a different ocular phenotype to RP (cataract, glaucoma and band keratopathy) (Dermici et al. 2006). This suggests that NBC1, as opposed to CAIV, is the most important component of the transporter metabolon in terms of pH buffering.

Nevertheless, the results of all of these studies suggest that tissue-specific differences exist to determine whether cells can fold and process mutant CAIV, and whether cells expressing the mutant CAIV protein undergo apoptosis.

In the studies of RP in general, there appears to be no clarity on the exact mechanisms of cell death, and in cases where apoptosis is suggested, the molecular causes are not always clear (Shintani et al. 2009). This, together with the conflicting studies by Rebello et al. (2004), Sun et al. (2008), Yang et al. (2005) and Alvarez et al. (2007) regarding the importance of levels of WT CAIV protein as well as the reported lack of kidney phenotype in RP17 affected individuals, emphasises the need to re-examine CAIV mutation pathogenesis. In order to provide sufficient background information, the next section will describe the structure of the eye in more detail, and in particular, the choriocapillaris where CAIV is highly expressed.

1.3. The choriocapillaris

The choriocapillaris is a continuous network of vascular channels, which spans the entire outer retina surface. Choriocapillaries are fenestrated, containing 60-70 nm pores which are involved in the bidirectional exchange of molecules between blood and tissue (Cavallotti et al. 2005; Strauss, 2005). The choriocapillaris provides vital oxygen and nutrients, as well as a means of waste disposal, to the highly metabolic tissue it encases, and it is these fenestrae, which facilitate the rapid choroid-RPE exchange (Flower, 1993). Figure 1.1 shows the position of the choriocapillaris in relation to other layers in the retina. It is important to note the close proximity of the choriocapillaris layer to the rod and cone cells of the retina, which underlines its importance in maintaining these structures. In fact, it is separated only by the single layer retinal pigment epithelium and the Bruch's membrane. This membrane separates the pigmented layer of the retina from the choroid, and consists of five layers:

1. The basement membrane of the retinal pigment epithelium (RPE)
2. The inner collagenous zone

3. A central band of elastic fibres
4. The outer collagenous zone, and
5. The basement membrane layer of choriocapillaris

The retinal pigment epithelium transports metabolic waste from the photoreceptors on its basal membrane, across Bruch's membrane to the choroid, which then conducts the circulation of this waste material from, as well as nutrient-containing fluids towards, the retina (Browning et al. 2005).

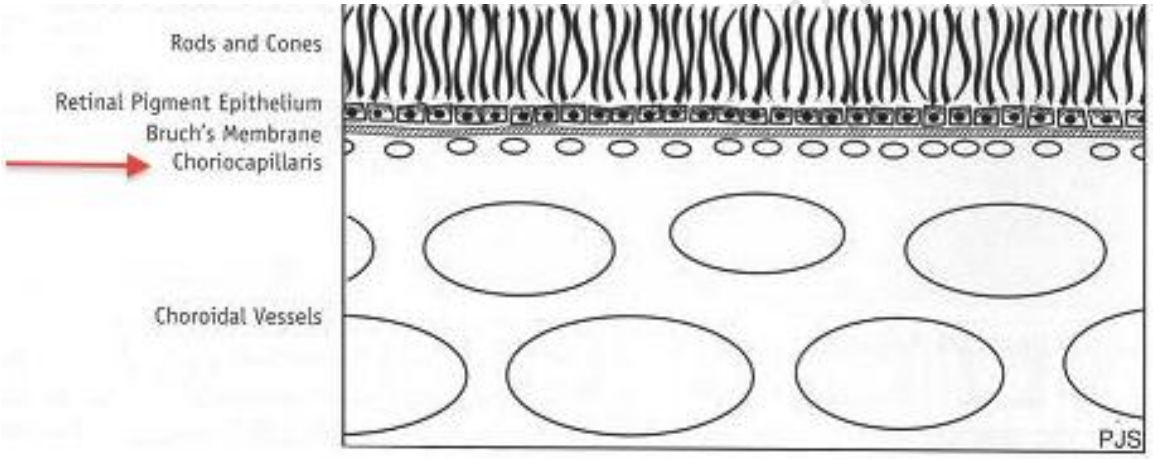

Figure 1.1. Cross-section showing the position of the choriocapillaris in the choroid. The choriocapillaris (indicated by an arrow) is immediately adjacent to the Bruch's membrane and choroidal vessels, and in very close proximity to the rod and cone cells of the retina. (Adapted from PJ Saine and ME Tyler. Ophthalmic photography. Boston: Butterworth-Heinemann, 1997;46)

The small depiction of the choriocapillaris in Figure 1.1 should not undermine the worth of this extremely valuable layer. A feature of the choriocapillaries is that they are much larger than standard capillaries (being between 18-50 microns in diameter) as part of their specific adaptation to service the metabolically overactive photoreceptor layers. The choriocapillaris provides as much as 80% of the blood supply to the eye in mammals (Denton, 1999), and due to the extremely high metabolic load of the RPE and retina, the

choriocapillaris needs to be extremely efficient in supporting these tissues. This vascular layer performs its functions with a tightly regulated system of protein expression. This includes the expression of growth factors that play a key role in maintaining choriocapillaris structure such as vascular endothelial growth factor (VEGF) (Blaauwgeers et al. 1999; Marneros et al. 2005, Ohno-Matsui et al. 2003), and proteins like CAIV, which aid in maintaining choriocapillaris function. The importance of CAIV in the choriocapillaris is underscored by its high expression in this tissue from as early as 7 weeks into gestation (Baba et al. 2009).

1.4. Carbonic anhydrase IV

The *CA4* gene that encodes the CAIV protein is localised on chromosome 17q22 (Bardien et al. 1997). CAIV mRNA consists of 1104 base pairs (www.ncbi.nlm.nih.gov/entrez), and the 312 amino acids of the protein have a combined weight of 35kD (www.ncbi.nlm.nih.gov/entrez). As shown in a schematic diagram of the protein in Figure 1.2, the precursor protein has at its N-terminus a 19 amino acid signal sequence, which is responsible for directing CAIV to the plasma membrane. This is followed by the functional protein sequence, which is then succeeded by a 28 amino acid C-terminus GPI (glycosylphosphatidylinositol) sequence, which physically attaches the protein to the plasma membrane. The 19 amino acid signal sequence is cleaved off from the protein as CAIV is folded in the ER, and does not form part of the mature protein. Under normal circumstances, as this signal sequence is cleaved off, a signal recognition particle is simultaneously bound to the folding CAIV protein, directing it to the cell surface.

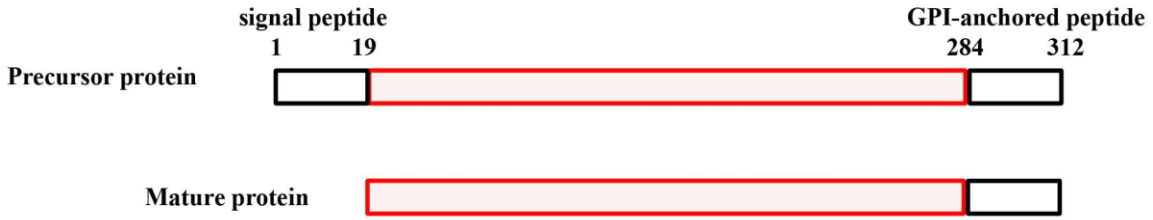

Figure 1.2. Schematic diagram of CAIV. The precursor protein has a 19 amino acid signal sequence at its N-terminus, which is cleaved off from the mature protein. A GPI-anchored peptide is found at the C-terminus of the protein, and is responsible for attaching the protein to the plasma membrane.

CAIV belongs to the carbonic anhydrase family of enzymes, which comprises of 16 isoforms of carbonic anhydrase (CA), each one characterized by tissue-specific expression and differing subcellular localizations. The family of CAs describes a group of zinc-containing enzymes that catalyse the reversible hydration of carbon dioxide to form bicarbonate ($H_2O + CO_2 \leftrightarrow HCO_3^- + H^+$). In addition to catalysing the hydration of carbon dioxide, carbonic anhydrases also regulate acid-base balance in the various organs in which they are found (Carter, 1972, in Alvarez et al. 2001). Some CAs are cytosolic (CAI, CAII, CAIII, CAVII, CAXIII), others are membrane-bound (CAIV, CAIX, CAXII, CAXIV, CAXV), two are mitochondrial (CAVA, CAVB), and one (CAVI) is secreted in milk and saliva. Among the 16 isoforms three are acatalytic CA-related proteins (CARP), CARPVIII, CARPX and CARPXI (Ogilvie et al. 2007; Suparan and Scozzafava, 2007). Figure 1.3 shows the anchoring of four of the five membrane-bound CAs on the plasma membrane, while Figure 1.4 provides a picture of the crystal structure of CAIV to show this binding in greater detail.

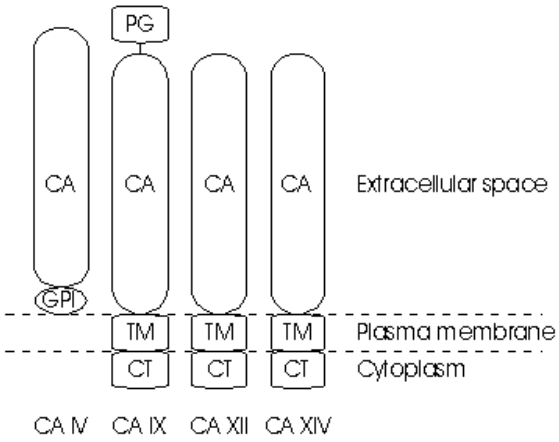

Figure 1.3. Anchoring of CAIV, CAIX, CAXII and CAXIV on the plasma membrane. Note that CAIV is the only carbonic anhydrase attached to the membrane by a glycosylphosphatidylinositol (GPI) link. (Figure from Antti Kivelä, 2003).

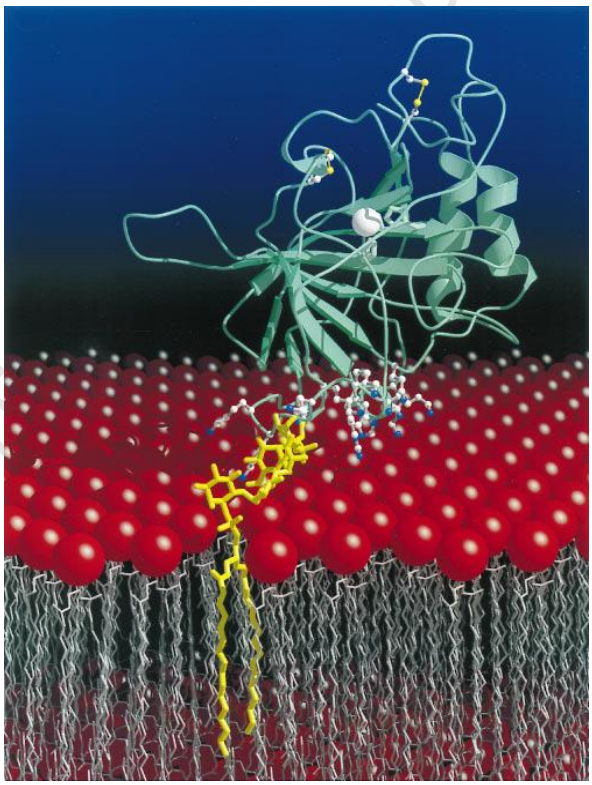

Figure 1.4. Chrystal structure of CAIV. CAIV is anchored to the membrane by a GPI link provided by the GPI-tail at its C-terminus (yellow). The active-site zinc ion appears as a white sphere, and the two disulphide linkages are indicated by bonded yellow spheres. (Figure from Stams et al. 1996).

The carbonic anhydrase enzymes have crucial roles in the eye, particularly those associated with enhancing the CO_2/HCO_3^- buffering capacity of the membrane. Studies performed to assess endothelial fluid transport in the absence of HCO_3^- and presence of carbonic anhydrase inhibitors also suggest that endothelial fluid transport is governed by carbonic anhydrase-facilitated HCO_3^- transport (Sun et al. 2007; Svitchar et al. 2009). There are five membrane-associated carbonic anhydrase isoforms, of which three are associated with corneal endothelium.

CAII is a well-characterized isoform (Alvarez et al. 2001), and the first of the membrane-associated carbonic anhydrases to be identified in the retina more than two decades ago (Wistrand et al. 1986). It is expressed in the ciliary body of the eyes where it regulates intraocular pressure, and is most abundant in the cytosol of Müller glial cells (Ogilvie et al. 2007). CAXIV has been identified as another membrane-bound member of the CA family that is expressed in the eye. This form of CA is an integral membrane protein that has its catalytic domain on the extracellular surface of the eye. Like CAII, it is highly expressed in Müller glial cells, but is also localised on the retinal pigment epithelium (Ogilvie et al. 2007).

CAIV is highly expressed in the choriocapillaris cells adjacent to Bruch's membrane in the eye (Fig. 1.1) (Ogilvie et al. 2007). The protein is also found at high levels in segments of the proximal renal tubular epithelium (Purkerson et al. 2007), the pulmonary endothelial cells and pancreatic duct cells (Fanjul et al. 2002), and to a lesser degree, in various other microcapillary beds in the body (Carter et al. 1990; Fleming et al. 1993; Fleming et al. 1995; Parkkila et al. 1994; Zhu et al. 1990). Although the choriocapillaris supplies nutrients and removes waste from the retina, CAIV has not been shown to be expressed in the photoreceptors. Despite this finding, CAIV has generated much interest related to retinal function, due to the identification of the arginine to tryptophan (R14W) signal sequence mutation in the CAIV protein, which is associated with RP17 (section 1.2). As mentioned previously, in order to understand the molecular pathology of RP17 and how the R14W mutation eventually leads to apoptosis, it is imperative to understand

the nature of normal folding within the cell, and in particular, within the endoplasmic reticulum. This will allow an appreciation of the interactions of CAIV with other molecules, and the effects on the cell of disruptions in these interactions.

1.5. CAIV membrane complexes

Membrane-bound carbonic anhydrases like CAIV catalyse a reversible reaction that converts CO_2 to HCO_3^-. In some cases, these CAs are bound by bicarbonate transporters in order to maximise the coupled catalytic/transport flux. In such cases, the CA and coupled transporter, form a transport metabolon (Alvarez et al. 2005). Examples of such a metabolon are of that formed between CAII and SLC26A6 (solute-carrier family 26 member 6), a plasma membrane Cl^-/HCO_3^- exchanger with a role in pancreatic HCO_3^- secretion (Alvarez et al. 2005). CAII has also been shown to bind to the Cl^-/HCO_3^- exchangers AE1 (anion exchanger 1) and NBC1 (sodium bicarbonate transporter 1) (Pushkin et al. 2004; Reithmeier, 2001; Vince and Reithmeier, 2000) as well as NHE1 (Na^+/H^+ exchanger 1) (Li et al. 2006). In studies on the interactions of CAIV, this protein has also been shown to form transport metabolons with AE1, NBC1 (Alvarez et al. 2003; Sterling et al. 2002) and cystic fibrosis transmembrane (CFTR) protein (Fanjul et al. 2002). An example of a CAIV/CAII/AE1 metabolon is depicted in Figure 1.5.

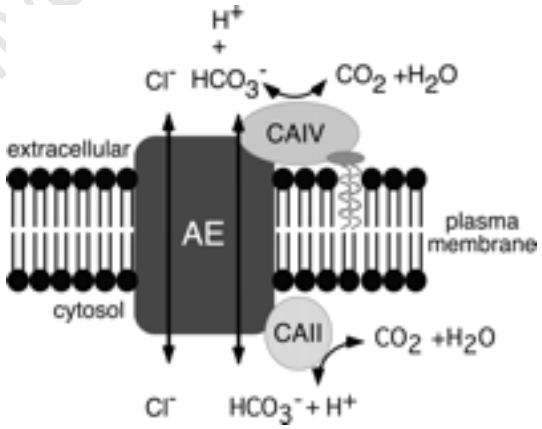

Figure 1.5. CAIV metabolon. A schematic diagram shows a metabolon between CAIV, CAII, and anion exchanger AE1. This metabolon is found in kidney cells in which these carbonic anhydrases are expressed (Figure from Sterling et al. 2002).

The interaction between CAs and bicarbonate transporters in the process of vision has been studied by Alvarez et al. (2007), who found that AE3/Slc4a3 null mice had inner retinal defects. These mice displayed late-onset blindness, and had elevated levels of CAII, CAXIV and NBC1 in their retinas (suggesting compensation for the defunct AE3). While this study identified the lack of AE3 as a cause of blindness in mice, it must be noted that CAIV is not expressed in the mouse retina, and these results therefore cannot be directly applied to humans.

The functional effect of the disruption of the interaction of CAIV with two ion exchangers has been studied in an attempt to determine the importance of the CAIV metabolons in cells in which they are formed.

1.5.1. CAIV and NBC1

A direct interaction between CAIV and NBC1 was first described by Alvarez et al. (2003) following their experiments in HEK-293 cells transfected with both CAIV- and NBC1 expression constructs. They used immunodetection and gel overlay assays to observe the interactions between the proteins (as well as between NBC1 and CAII), and used a mutated NBC1 to show that when the CAIV-binding loop of the protein is affected, the interaction between the two is abolished. Interestingly, this study showed the interaction of CAIV and NBC1 to occur on the extracellular surface of the membrane, while the interaction between CAII and NBC1 occurs on the intracellular surface. This finding emphasises the unique nature of the CAII and CAIV interactions, and implies that caution must be used when attempting to suggest that CAII and CAIV have overlapping or redundant roles.

As reviewed in section 1.2, disruptions in the CAIV-NBC1 metabolon, as a result of the R14W mutant CAIV, were suggested by Yang et al. (2005) to be behind the RP17 phenotype.

1.5.2. CAIV and CFTR

A 2002 report published by Fanjul et al. studied the relationship between the Cystic Fibrosis Transmembrane conductance Regulator (CFTR) protein and CAIV in a human pancreatic duct cell line. Their aim was to examine a possible interaction between CFTR, a Cl^-/HCO_3^- transporter, and CAIV on the plasma membrane of epithelial tissues in the lung and pancreas. This study investigated the targeting of CAIV to the plasma membrane in CFPAC-1 pancreatic duct cells expressing ΔF508 CFTR protein. The ΔF508 mutation which causes the deletion of a phenylalanine residue in the protein, is the most common found in cystic fibrosis patients and has been identified in over 70% of those with symptoms of the disease (Kerem et al. 1989). The Fanjul et al. study found that while CAIV was localised to the plasma membrane of WT human pancreatic duct cells, it was not targeted to the plasma membrane in CFPAC-1 cells. This suggested an interaction between CFTR and CAIV, which was abolished in the presence of the ΔF508 mutation. The authors concluded that the elimination of the interaction might contribute to a disruption in HCO3- secretion in cystic fibrosis epithelia, and could account for at least some of the cystic fibrosis phenotype.

The studies above highlight the importance of interactions between CAIV and the relevant bicarbonate transporter in a number of tissues. They show that a mutation in either one of the two proteins results in a disruption of the metabolon. The phenotypic effect of this disruption, however, is not immediately clear. Furthermore, in addition to the kidney, lung, and pancreas, CAIV is also expressed in the heart, gall bladder, distal small intestine and colon (Purkerson and Schwartz, 2005). It is likely that on examining the interactions of CAIV with anion and cation transporters in these tissues, many more functional complexes or metabolons, will be discovered.

1.6. Protein folding

In order to become fully functional, proteins have to acquire a unique tertiary structure. This occurs via a complex folding pathway that involves a variety of factors with very specific roles (Chaudhauri et al. 2006; Outeiro et al. 2007). The progression of folding,

and the ultimate 3D conformation of the protein, depends primarily on the order of the amino acids in the primary sequence of the protein (Anfinsen, 1973). A number of possible conformations exist for each amino acid sequence, and a string of amino acids will progressively fold along a pathway of several conformations, with preference for the structure that has the lowest free energy. In most cases, this conformation will be identical to the native state of the protein.

During the correct folding of a protein, a string of amino acids will interact with itself in order to assemble into a stable and low-energy three-dimensional structure (Miller, 2004) which is able to operate within the cell, or be exported for extracellular function. Much of the protein folding and maturation occurs in the ER, and is a rapid process, which should result in a conformation that is stable, and with specific biological function.

Correct folding not only provides structural conformity, but also prevents inappropriate interactions between proteins (Hammarström, 2009). The folding of a protein is initiated by a hydrophobic collapse, during which hydrophobic side chains of the protein shield each other from water in the surrounding environment. This collapse also serves to bury electrostatic interactions such as salt bridges and hydrogen bonds, eliminating the possibility of the time-consuming formation of high free-energy structures. Individual structures like α-helices and β-turns can fold within 0.1-1 μs, while small proteins can assemble in less than 50 μs (Schröder and Kaufman, 2005).

In order for secondary and tertiary (3-dimensional) structural elements such as β-sheets and disulphide bonds to form, the participating residues must be held in a "folding-competent" state until the specific interacting partners and folding-facilitative enzymes such as the heat shock proteins (HSPs) are allowed access to the polypeptide chain (Schröder and Kaufman, 2005). This situation is exacerbated by the high protein concentration in the ER, which can reach from 100 mg/mL (≈ 2mM) to over 400 mg/mL (Outeiro and Tetzlaff, 2007). Thus, it is necessary to shield folding proteins from collisions that may result in interaction with other mature and maturing proteins.

Ultimately, the three-dimensional folding of proteins will also serve to hide these volatile stretches of the amino acid sequence that, if exposed, would react non-specifically with other proteins (Miller, 2004).

Once proteins are correctly folded into their native state, a process termed quality control occurs (Ellgaard and Helenius, 2003), during which folded proteins are exported to the Golgi complex for direction to their final destination through a "packaging and labelling" route. Incorrectly folded proteins, on the other hand, are retained by proteins involved in the folding process for the completion of folding, or to be targeted for degradation (Schröder and Kaufman, 2005).

1.6.1. Endoplasmic reticulum protein folding

The endoplasmic reticulum (ER) is the membrane-surrounded organelle in which transmembrane, secretory, and ER-resident proteins are processed. The ER is a crucial protein-processing compartment in the eukaryotic cell, with its protein load being second only to that of the cytosol (Schröder and Kaufman, 2005). Proteins are directed to the ER through a hydrophobic signal sequence, and have to traverse the ER membrane, either co- or post-translationally. Once proteins are within the ER lumen, the signal sequence peptide is cleaved from the polypeptide being processed, and protein folding continues (Fig. 1.6).

The presence and timing of signal sequence cleavage and folding of a polypeptide, bear great effect on the protein-folding pathway. As part of folding and processing, proteins may also undergo a multitude of post-translational modifications such as asparagine-linked glycosylation, and the formation of inter- or intra-molecular disulphide bonds (Schröder and Kaufman, 2005). Once proteins are correctly folded in the ER, they are packaged into transport vesicles that correspond to the "destination" specified in the signal sequence. These vesicles transport the proteins to the Golgi body for further processing, after which they are packaged into secretory vesicles and sent to their final destination (Fig. 1.7).

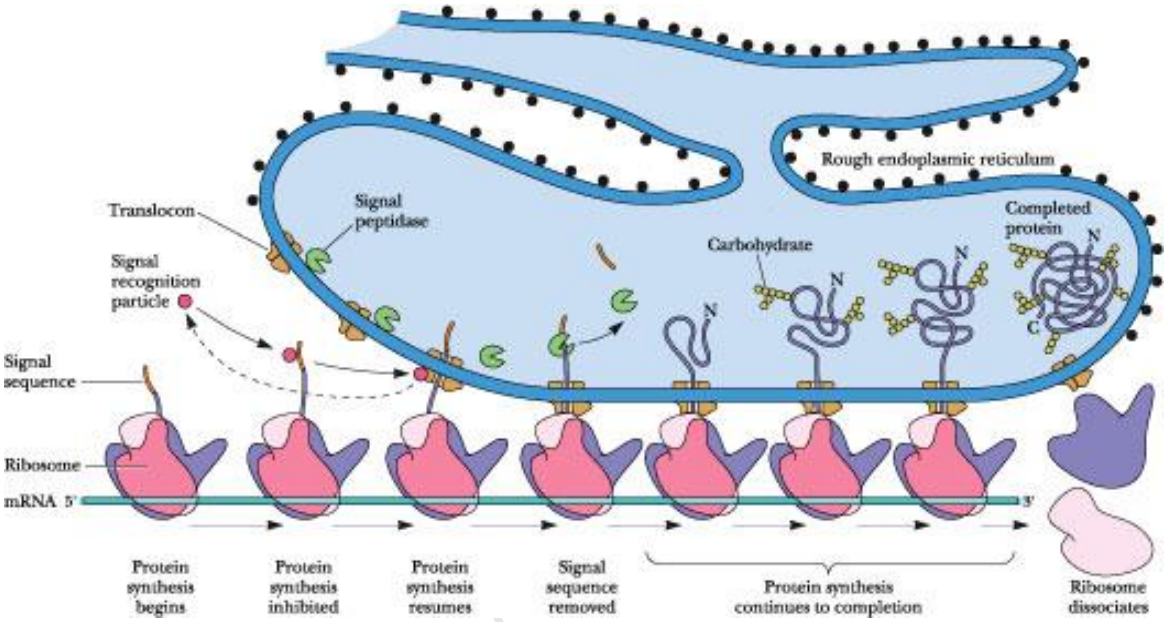

Figure 1.6. Processing of proteins in the ER. Proteins are translated from ribosomes and simultaneously pulled through pores into the ER lumen. Once in the ER, the signal sequence is cleaved from the nascent protein, and it is folded and modified. The completed protein is then ready to be packaged into transport vesicles to begin its journey to the Golgi body.

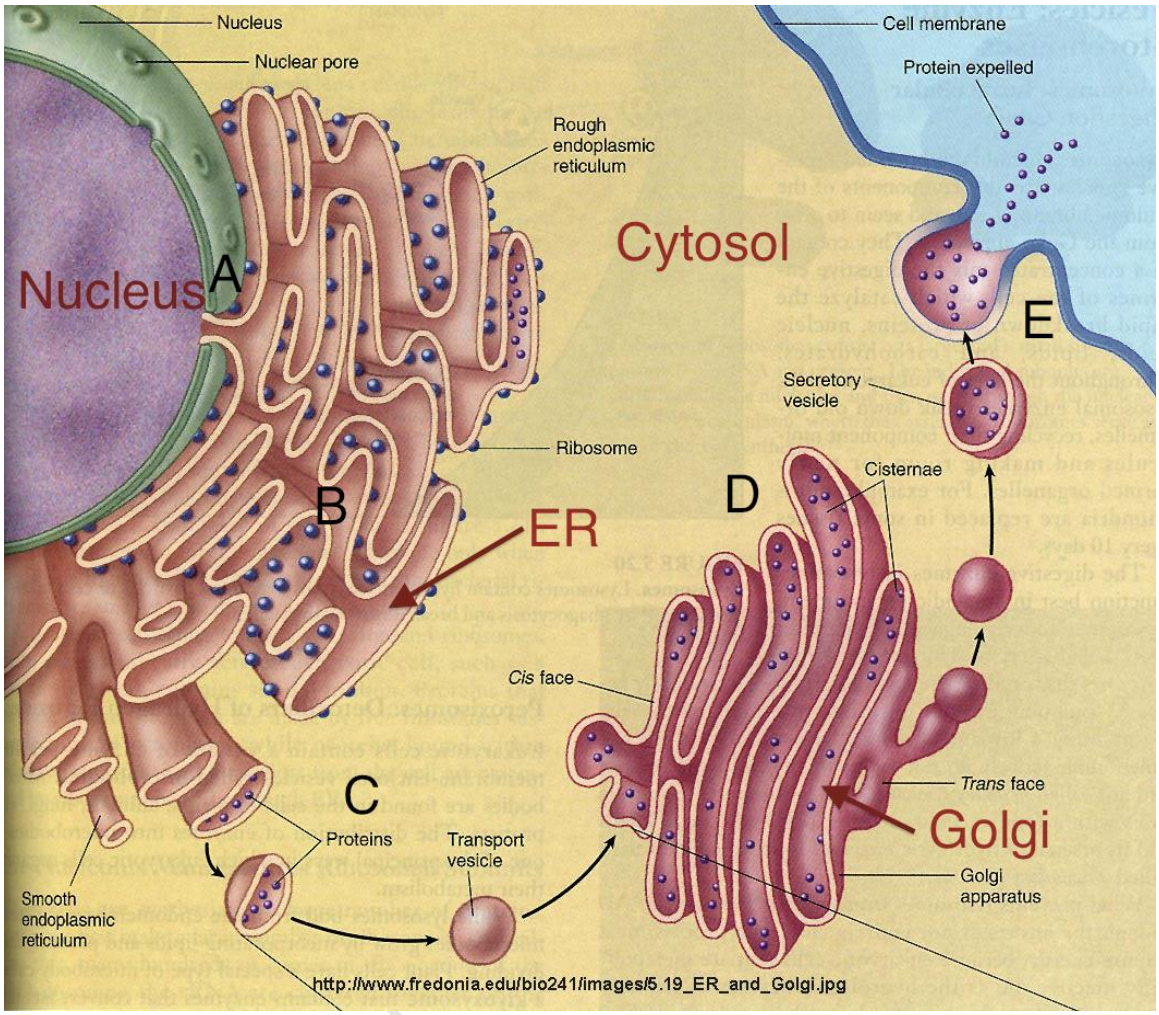

Figure 1.7. ER processing pathway of a newly translated protein. (A) The protein is translated from ribosomes and pulled into the ER lumen for folding (B). Once protein folding is complete, proteins are packaged into transport vesicles (C) and sent to the Golgi body for further processing (D). The completely folded and processed protein is then packaged into secretory vesicles, and (E) transported to the cytosol, the plasma membrane or the extracellular environment, where it can perform its function.

Folding in the ER differs from that which occurs in the cytosol in a number of respects, including the topology of the ER, its chemical composition (including the high concentration of Ca^{2+}, which may alter hydrophobic interactions in proteins by participating in electrostatic interactions), and the ability of the ER-resident proteins to perform a multitude of post-translational modifications. These modifications may include

N-linked glycosylation, disulphide bond formation, lipidation, hydroxylation, and oligomerisation (Hartl et al. 2002; Schröder and Kaufman, 2005; Shen et al. 2004).

N-linked glycosylation is a process that is common to many membrane and secretory proteins. It involves the transfer of a 14-oligosaccharide core (N-acetylglucosamine$_2$-mannose$_9$-glucose$_3$, or Glc-NAc$_2$-Man$_9$-Glc$_3$) from a membrane-bound phosphate anchor to a consensus Asn-X-Ser/Thr residue in the polypeptide chain (Malhotra and Kaufman, 2007; Nakatsukasa and Brodsky, 2008). This process increases the solubility of the protein so that it can traverse the cytoplasm. The large oligosaccharide volume also protects the peptide from surrounding proteins, and acts to stabilise the protein conformation (Shröder and Kaufman, 2005).

During the folding process, lectins "report" on the folding status of the protein by monitoring the sequential trimming of sugar residues from the 14-oligosaccharide chain. This monitoring is carried out chiefly by calnexin and calreticulin (Shen et al. 2004). During this trimming process, three terminal glucose residues of the oligosaccharide are cleaved sequentially by glucosidases I and II, and the result is a Glc-NAc$_2$-Man$_9$ structure. When polypeptides are not folded properly, a UDP-glucose:glycoprotein glucosyltransferase (UGGT) recognises the unfolded nature of the protein, and reglucosylates the core oligosaccharide. The restoration of this glycosidic linkage re-institutes bonds with calnexin and calreticulin, and the bound protein is unable to exit the ER.

This process is an important step in the quality control process that occurs in the ER to assess protein-folding progress, and determines whether peptides may be exported to the Golgi for further modification, or are targeted for ER-associated degradation (Shen et al. 2004; Shröder and Kaufman, 2005). Peptides re-bound to these lectins may also be cleaved of their mannose residues and transferred to ER Degradation Enhancing α-Mannosidase-like protein (EDEM), a molecular chaperone that facilitates degradation of unfolded proteins (Anelli and Sitia, 2008; Nakatsukasa and Brodsky, 2008).

In addition to the three lectins mentioned above (calnexin, calreticulin and EDEM), the ER also has in its arsenal of protein folding machinery two further classes of enzymes: foldases and molecular chaperones. Foldases catalyse the steps in protein folding in order to increase the rate of folding, while molecular chaperones facilitate correct folding of proteins by shielding unfolded regions of a maturing protein from surrounding proteins. It is important to note that they do not directly increase the rate of folding of proteins (Shen et al. 2004; Shröder and Kaufman, 2005). Molecular chaperones work on substrates through successive cycles of binding and release, and are aided by various cochaperones and powered by adenosine triphosphatase activity (Outeiro and Tetzlaff, 2007).

Chaperones can be classified into several broad groups, which include class HSP70 chaperones (including BiP and GRP170, which also participate in the transfer of nascent polypeptide chains into the ER), class HSP90 chaperones, which, in coordination with other chaperones, recognise particular protein substrates, and PDI (protein disulphide isomerase), which has disulphide-dependent and independent chaperone activity (Barral et al. 2004; Höhfeld et al. 2001). Due to their importance in the process of ER-associated folding, the function and activities of three of these chaperone proteins will be described briefly.

Binding Protein

Binding Protein (BiP) is an ER-specific chaperone protein and a member of the HSP70 family (Hampton, 2000). It binds exposed hydrophobic patches on the surface of unfolded proteins and releases these protein substrates upon ATP binding (Kaufman, 2002). Studies with BiP have shown this protein to play a key role in protein folding in both the normal and stressed ER (Beckmann et al. 1990). During normal folding, BiP binds co-translationally to polypeptide chains and inserts them into Sec61p, a co-chaperone complex that forms channels in the ER membrane (Goder et al. 2003). Once BiP has pulled the polypeptide chain through the Sec61p complex and into the ER lumen, it holds them in a conformation that facilitates their folding into secondary and tertiary structures (Fig. 1.8) (Dudek et al. 2006; Fink, 1999; Gething, 1999).

BiP is dependent on ATP in order to perform its functions, and has an N-terminal ATPase domain and a C-terminal substrate-binding domain that has an affinity for hydrophobic patches, and thus binds unfolded proteins. Affinity for these substrates depends on ATP binding at the N-terminal domain, and hydrolysis of ATP to ADP results in an N-terminal conformational change, and the release of the substrate (Anelli and Sitia, 2008; Malhotra, 2007). In cells not burdened by misfolded proteins, BiP also binds the luminal domains of three stress sensor membrane proteins: inositol-requiring enzyme 1 (IRE1), pancreatic ER kinase-like kinase (PERK), and activating transcription factor 6 (ATF6). Binding to BiP maintains these proteins in an inactive state (Malhotra, 2007), and when these proteins are released, they transmit messages of ER-stress to the rest of the cell. Once released, IRE1, PERK, and ATF6 form bonds via their luminal domains which are stronger than that formed with BiP, preventing the possibility of further inhibition of these proteins by BiP binding (Shen, 2004). The activity of BiP in cells undergoing ER stress, is discussed further in section 1.6.1 (Fig. 1.8).

Glucose-Regulated stress Protein 170

Glucose-Regulated stress Protein 170 (GRP170) is another member of the HSP70 family, and has roles in the ER that are closely tied to that of BiP. While the activity of this chaperone has not been studied in as much detail as that of BiP (Dudek et al. 2006), recent research has shown GRP170 to have a role as a nucleotide exchange factor. Due to its close relationship with the BiP protein, it is assumed that GRP170 is directly involved in the exchange of nucleoside diphosphates and nucleoside triphosphates between ATP and BiP (Andréasson et al. 2010; Dudek et al. 2006). Like BiP, GRP170 is involved in normal folding, with its expression also being up-regulated as part of the unfolded protein response (UPR).

Protein disulphide isomerase

The chaperone cofactor protein disulphide isomerase (PDI) is concerned with the formation of disulphide bonds in proteins that are being folded in the ER. PDI plays a

critical role in the ER as many secreted proteins have multiple disulphide bonds, which have to be paired correctly during folding (Fig. 1.8). The cofactor carries out this function by catalysis of oxidative folding, and its levels in the ER can reach millimolar concentrations (Fink, 1999). PDI binds hydrophobic polypeptide residues as well as unfolded and folding proteins, and has been shown to have a chaperone activity that is distinct from its disulphide bond interactions (Cai et al. 1994).

These three chaperones play key roles in the endoplasmic reticulum, however, cells may simultaneously express multiple versions of a member of a particular chaperone class, as well as members of different classes, leading to a complex and adaptable chaperone response. The interaction of unfolded proteins with these molecular chaperones is an integral component of the quality control process in the ER (Outeiro and Tetzlaff, 2007).

The entry of an amino acid sequence into the folding pathway, its folding into the correct native state, any modification which must occur, and its appropriate exit from the ER to the Golgi body, are all vital factors in the tightly controlled and intricate process of correct protein folding (Outeiro and Tetzlaff, 2007; Szegezdi et al. 2006). Disruption of this pathway at any of these points can lead to the accumulation of unfolded proteins, and in response to this stress, activation of the UPR.

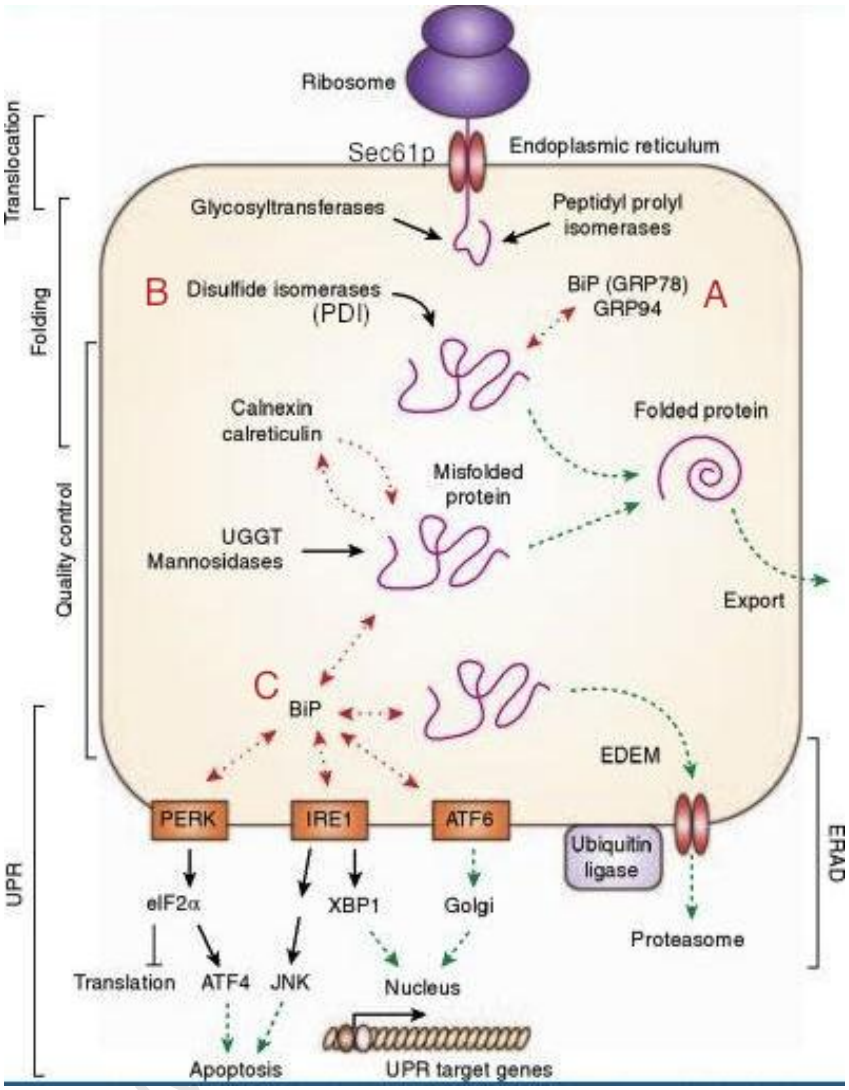

Figure 1.8. The roles of BiP and PDI during ER-associated protein folding. BiP is responsible for pulling nascent polypeptides through the Sec61p complex and into the ER lumen, and then holding these proteins in a conformation that is compatible with folding. Its activity is partly facilitated by co-chaperones like GRP-170 (A). PDI catalyses the formation of disulphide bonds in folding proteins (B), which are then processed further. In its secondary role, BiP is also associated with signalling pathways that are initiated when proteins are misfolded (C). (Figure adapted from Cybulsky, 2010; Kidney International)

1.7. Protein misfolding

1.7.1. Endoplasmic reticulum stress and the UPR

When there is a mutation in the gene coding for a protein, or in one of the stages of protein assembly, a number of responses are initiated in order to effectively manage the misfolding of the protein and to respond with mechanisms that will allow for minimal cell damage. These are carried out as part of the UPR (Schröder and Kaufman, 2005).

During the UPR, intracellular signals transmit information about the protein folding status in the ER lumen to the cytoplasm and nucleus. This process serves to balance the folding capacity of the ER with its unfolded protein burden, and in doing so, return the ER to its normal physiological state. The UPR includes two simple adaptive mechanisms: (1) transcriptional induction of UPR genes (including BiP, PERK, and CCAAT/enhancer-binding protein homologous-protein (CHOP), and other ER-resident chaperones and foldases), in order to increase the folding capacity of the ER. This is accompanied by an increase in the size of the ER; and (2) transcriptional and translational attenuation of protein synthesis, in order to decrease the biosynthetic load of the ER (Schröder and Kaufman, 2005). This is coupled by an increase in the clearance of unfolded proteins from the ER as part of ERAD, or ER-associated degradation (Liu and Kaufman, 2003). These procedures provide adaptive responses for survival. However, if the protein folding defect is not adequately corrected, cells undergo apoptosis.

Unfolded proteins are recognised thermodynamically as being in a state with a higher free energy than the native state. The hydrophobic regions exposed on the surface of a non-native conformation will contact surrounding water, raising the free surface energy. In an *in vitro* setting, where such a definition may be difficult to test experimentally, an unfolded protein is defined as one that interacts with molecular chaperones. Of course, different chaperones will react with different proteins, and chaperone specificity may limit interaction to just one, or a few, proteins. Protein folding status thus depends on the particular protein and chaperone under investigation.

Perhaps the simplest method of combating protein misfolding is the molecular chaperone-mediated sequestering of protein intermediates and misfolded proteins. These chaperones deliver protein substrates to other quality control complexes in the cell, which then escort them from the ER to the proteasome (Anelli and Sitia, 2008; Nakatsukasa and Brodsky, 2008). This action serves to attenuate the continuation of attempts to refold aberrant proteins, prevents misfolded proteins from interacting with other proteins in the ER, and allows degradation of misfolded peptides (Malhotra, 2007). BiP plays a key role in the sequestering of aberrant proteins and when these proteins are persistently not able to fold correctly, a set of reactions is initiated which leads to the release of a number of proteins that play vital roles in the UPR. Under normal conditions, BiP binds the transmembrane proteins IRE1, PERK, and ATF6 at their luminal ends. When there is a high load of unfolded proteins within the ER, BiP releases these three proteins (Kaufman, 2002).

IRE1, PERK, and ATF6 are transmembrane proteins that regulate the production and quality of transcription factors for a number of UPR-expressed genes. One of the first mechanisms employed by the cell to combat protein misfolding is the transcriptional induction of this set of genes whose products increase the folding capacity and volume of the ER. Thus, the task of these proteins is to act as proximal sensors, setting off the complex network of physiological responses that occur in conditions of ER stress (Kaufman, 2002). Each of the three proteins has distinct and important roles in the up-regulation of ER stress proteins.

IRE1 is a glycoprotein that contains kinase and RNase activities. ER stress causes IRE1 to autophosphorylate, which in turn activates its RNase activity. Splicing of the mRNA target of IRE1 leads to its binding of the ER stress element (ERSE) which is present in the promoter of many UPR genes. ATF6 responds to ER stress in a similar way, moving first into the Golgi, and then the nucleus, where its altered form binds ERSEs (Liu and Kaufman, 2003). Binding to the ERSE leads, in particular, to up-regulation of molecular chaperones and catalysts of protein misfolding and increases the folding capacity of the

ER, providing a protective effect for cell survival (Lin et al. 2007; Lin et al. 2008; Liu and Kaufman, 2003).

PERK is a kinase that phosphorylates a translation initiation factor in response to ER stress. This phosphorylation reduces the formation of translation initiation complexes, reducing the recognition of AUG codons and therefore attenuating translation in general to reduce the number of unfolded proteins in the ER and counteracting ER overload (Lin et al. 2007; Lin et al. 2008; Liu and Kaufman, 2003).

Together, these three sensors serve to lighten the burden of ER stress imposed on the cell in response to misfolding. However, when the UPR response is not enough to alleviate ER stress, and misfolded proteins accumulate, these same stress sensors initiate pathways which lead to activation of pro-apoptotic transcription factors such as CHOP (Nishitoh, 2011; Shore et al. 2011; Szegezdi et al. 2006), and the cell undergoes apoptosis.

The combined effect of these factors is to generate diversity in the responses of different subsets of UPR-responsive genes, endowing the cell with a highly adaptive mechanism of dealing with ER stress (Hetz, 2012). It must be noted that UPR activity can also be observed in cells that are not undergoing "stress", suggesting that all or most cells undergo a minimal basal stress level. This suggestion is supported by the observation that yeast cells which are defective in the UPR and ERAD are synthetic lethal (Hampton, 2000; Schröder and Kaufman, 2005). This basal UPR activity is thought to occur as part of nutrient sensing and the control of cellular responses to fluctuations in nutrient levels, and these minor changes in the protein load may well serve as an indicator of the cell's overall metabolic state.

1.8. Protein misfolding diseases

Protein misfolding and aggregation are the cause of a number of inherited human diseases known collectively as Protein Conformational Disorders. In this group of diseases, mutations which alter the folding pathway or final conformation of a protein

result in the disruption of the process of folding in the ER, and may lead to activation of the UPR. Proteins are the main effectors in the cell and they play crucial roles in all biological processes. Therefore, as the number of new proteins being identified rises and their functions become clear, researchers are also being made aware of a host of new and interesting protein conformational disorders. According to prion researcher Susan Lindquist, "protein misfolding could be involved in up to half of all human diseases" (Bradbury, 2003).

In many cases, severely misfolded proteins may be recognised as undesirable by the HSPs and will thus be directed to the protein degradation (ERAD) machinery in the cell. Disease in these cases will be caused by lack of this particular protein due to its degradation (Chaudhauri and Paul, 2006; Guerriero and Brodsky, 2012; Miller, 2004; Wang et al. 2011) and include α-1 antitrypsin deficiency, Marfan syndrome, Gaucher's disease, and retinitis pigmentosa 3. In addition, some cancers are thought to be associated with the misfolding and consequent degradation of tumour-suppressor genes such as p53 (Chaudhauri and Paul, 2006). Treatment for these diseases might include expression of WT protein, manipulation of ER quality control machinery, or the development of chemical chaperones specifically tailored to aid in correctly folding the mutant protein (Schröder and Kaufman, 2005).

In cases where mutations are minor and result in proteins with partially functional activity, disease occurs as these proteins may not pass quality control criteria, and are therefore retained in the ER and cannot perform their function. A prominent example is cystic fibrosis, ~90% of which is caused by a F508 deletion in the cystic fibrosis transmembrane conductance regulator (CFTR) protein (Amaral, 2006; Ellgaard and Helenius, 2003). The presence of partial activity in the mutant form of this protein suggests that allowing affected cells to bypass the stringent quality control process may be key to treating the disease.

Other protein misfolding diseases (e.g. Alzheimer's disease, Type III diabetes, and Parkinson's disease) are characterised by the deposition of insoluble protein aggregates within the cell, rather than their disappearance. Disease symptoms arise because of a "gain of toxic function" (Outeiro and Tetzlaff, 2007), which occurs as a result of the aggregation process or of a combination of both the toxic function and loss of normal functioning protein. This class of misfolding diseases is characterised by an unusually high propensity of the protein to aggregate under physiological conditions (Anelli and Sitia, 2008). Biophysical studies on the aggregation behaviour of a wide array of proteins has revealed that even small perturbations in the sequence, stability, or environment of predisposed proteins will affect their propensity to aggregate (Luheshi et al. 2008).

In yet another group of diseases, the loss of function of the protein in its cellular or extra-cellular location is obscured by aggregation of misfolded protein in the ER. The consequences of this class of disease are activation of ER stress and the UPR, and in over-stressed cells, the result is apoptosis. Diseases of this kind are usually dominant and associated with increased ER-chaperone levels (Schröder and Kaufman, 2005). RP17 is thought to be included in this class (Rebello et al. 2004) along with P23H RHO RP (Illing et al. 2002; Medes and Cheetham, 2008), β-amyloid toxicity disease, type 1 diabetes in the Akita mouse (Schröder and Kaufman, 2005), and some autoimmune diseases (Kim et al. 2008).

Distinguishing between these classes of disease is imperative as it bears great effect on the type of gene therapy that should be used to effectively treat the disorder. For example, while loss-of function mutations may be treated by insertion of a WT copy of the mutant gene into organ tissue, gain-of-function misfolding mutations will be much less amenable to such therapy, which may in fact exacerbate disease conditions (Kaufman, 2002).

1.9. RP Therapy

The heterogeneity of RP has been underlined by the numerous genes and varying genetic mutations involved with the disease. The identification of scores of these mutations over

the past two decades has allowed for greater understanding of the underlying molecular defects and pathophysiology of many forms of RP. This in turn has lead to the investigation of various modes of therapy for the disease. Among these are vitamin therapy (Berson et al. 1993), cell transplantation including stem cell therapy (Buchholz et al. 2009), the application of small molecules to affected cells, chaperone therapy (Noorwez et al. 2003), and gene therapy (Acland et al. 2001; Cideciyan, 2010; Shintani et al. 2009). For the purposes of this study, only chaperone therapy and gene therapy will be discussed.

1.9.1. Chaperones

As explained in section 1.5, chaperone proteins aid in the folding of nascent polypeptides both in the ER lumen, and in the cytosol. The importance of these enzymes and co-factors has been demonstrated in studies that show the lethality of insufficiency of some of the key chaperones mentioned earlier (Mori, 2009; Nagai et al. 2000; Wang et al. 2009). Chaperones have hydrophobic surfaces, which initiate contact with the exposed hydrophobic regions of unfolded proteins, and in doing so, protect them from inappropriate interactions with other proteins within the cell (Outeiro and Tetzlaff, 2007).

The ability of chaperones to bind folding and unfolded proteins, and the identification of protein misfolding as the cause of cell death in some forms of RP, has led researchers to investigate the application of this family of protein folding facilitators to cells expressing misfolded proteins, as a mode of therapy (Kosmaoglou et al. 2008).

Chaperone-mediated folding has been shown to rescue photoreceptor cells using in vitro models of the P23H RHO form of RP associated with protein misfolding (Phelan and Bok, 2000). In P23H RP, disease occurs as the result of a mutation in RHO, the photoreceptor molecule from retinal rod cells (Phelan and Bok, 2000). In vitro studies with the P23H RHO have shown that this mutant protein is misfolded and retained within the ER, leading to apoptosis of cells expressing it (Noorwez et al. 2003). The retaining of RHO in the ER and its resultant inability to be translocated to the outer segments appear

not to be the cause of the RP phenotype. Humphries et al. (1997), using heterozygous *RHO* knockout mice, showed that very little photoreceptor cell death occurs from having only one correct copy of the *RHO* gene. Instead, it seemed that the misfolded RHO acquired a toxic "gain of function" that lead to cell death.

Following these observations, a study by Noorwez et al. (2003) demonstrated that the P23H opsin could be induced to fold correctly by introducing a ring variant of 11-cis retinal into cell cultures during opsin biosynthesis. This variant acted as a pharmacological chaperone and was able to preferentially bind to the mutant protein, stabilising it to promote correct folding and trafficking (Noorwez et al. 2003; Noorwez et al. 2004). In studies with the same mutation, Gorbatyuk et al. (2010) showed that delivery of BiP into P23H RHO transgenic rats by adeno-associated viral vector did not increase transport of the mutant protein to the plasma membrane of rod cells, but reduced mutant RHO aggregates, the UPR, and levels of apoptosis, and was thus able to restore vision. This affinity and selectivity of the introduced chaperones for the mutant opsin suggests that a pharmacological intervention could be found for this misfolding disease.

Following the early success of *in vitro* experiments involving the use of chaperones in cell culture models of some diseases including P23H RP (Noorwez et al. 2004), a group of researchers including scientists from the University of Cape Town, investigated the ability of chaperone-like agents, in the form of small molecules, to rescue photoreceptor cells in cultures which represented R14W mutant CAIV protein misfolding in RP17.

In their earlier studies, Rebello et al. (2004) noted that a portion of R14W mutant CAIV precursor in transfected cells was more slowly converted to mature enzyme, and more rapidly degraded, than the WT protein. Following this, Bonapace et al. (2004) used the highly specific carbonic anhydrase inhibitor acetazolamide as a chemical chaperone, in order to slow down degradation. They were also able to achieve the same results using sodium 4-phenylbutyrate (4-PBA), which acts as a non-specific chemical inhibitor. In addition to decreasing the degradation of R14W CAIV, treatment of cells with PBA

caused increased conversion of the unfolded mutant and WT CAIV to be processed (which includes the formation of disulphide bonds) to the mature form. When tested on their ability to "rescue" cells from the effects of the mutant enzyme, both types of chemical chaperones reduced the markers of ER stress and the UPR, as well as those indicating apoptosis of cells.

Studies which followed on from the initial research on the effects of "chaperones" on the folding of mutant CAIV used dorzolamide, another carbonic anhydrase inhibitor, to successfully rescue COS-7 and HEK-293 cells expressing two different CAIV mutations (R69S and R219S), from undergoing apoptosis (Datta et al. 2008). While this study showed the effectiveness of carbonic anhydrase inhibitors in protecting cells from the harmful effects of the mutant CAIV, the importance of other carbonic anhydrases both in the eye and in other tissues, highlights the very real threat of inhibitors affecting the expression of other vital proteins. Furthermore, a study by Sauvé et al. (2006) showed that treatment with carbonic anhydrase inhibitors depressed electroretinogram responses in mice, and suggested that this form of therapy would likely have a long-term adverse effect on vision.

In an alternative approach to CA inhibitors, Datta et al. (2010) investigated the effect of the R219S and R14W CAIV mutations in transgenic mice (which express a renal as opposed to an ocular phenotype), and found that an aggravated phenotype was observed in mice that were also deficient for the ER specific co-chaperone $p58^{IPK}$ (Datta et al. 2010). This co-chaperone plays a role in renal-specific protein processing, and these studies again highlighted the importance of chaperones and co-chaperones in correct protein folding. This group used $p58^{IPK}$ because of the accessibility of the heterozygous mouse line that could be used as a background on which to cross the CAIV mutations. It however becomes obvious the benefit that would be derived from performing similar studies in models of RP17 in which chaperones like BiP are either knocked out in order to assess whether their absence causes exacerbation of the molecular pathology, or added to cells in an attempt to develop therapy.

1.9.2. RNA interference

In the late 1980s, researchers discovered an auto-regulated method of genetic "co-suppression" in the petunia plant (Napoli et al. 1990; van der Krol et al. 1990). They observed that transgenes coding for purple pigment yielded reduced as opposed to increased levels of the pigment. This unexpected finding was reiterated by the similar effect of expression of the alcohol dehydrogenase (Adh) gene in *Drosophila melanogaster* (Pal-Bhadra et al. 1997). Subsequent studies identified RNA as the common target of these silencing transgenes, and showed that expressing high levels of antisense RNA led to suppression of endogenous genes (Fire et al. 1991; Ratcliff et al. 1997).

Preliminary work on RNA silencing was followed by a major breakthrough after 1995, when Guo and Kemphues (1995) showed that extremely low levels of sense RNA could be used to silence endogenous gene expression. These studies were put to the test in *in vivo* models when a study by Fire et al. (1998) showed that long double-stranded RNA (dsRNA) could produce gene-specific knockdown in an animal model (*C. elegans*). In contrast to the knockdown observed in previous studies, Andrew Fire and Craig Mello were able to achieve sustained and specific knockdown with the presence of only a few copies of dsRNA (Fire et al. 1998). This knockdown was passed on through a generation of progeny, and won these co-workers a Nobel Prize in 2006. The success of the gene knockdown led this group to postulate that there existed an endogenous biological method of gene silencing, and what is now known as micro RNA (miRNA), was thus discovered.

This discovery of gene knockdown was halted somewhat by the realisation that these long dsRNA strands triggered an antiviral immune response in mammals, resulting in non-specific mRNA destruction and an inhibition of protein synthesis (Clemens et al. 1996). As an alternative, short dsRNA fragments were therefore used to imitate the effects of the longer dsRNA, and eventually chemically synthesized short dsRNA (RNAi) became widely used as a tool for the specific knockdown of gene expression.

Processing in RNAi

During the processing of endogenous miRNA, transcript expression is driven mainly by RNA Polymerase II promoters. miRNA transcripts then standardly fold into a secondary hairpin structure, which is bound by the Drosha-DGCR-8 (DiGeorge critical region-8) complex for processing. While the transcript is bound by DGCR-8, it is cleaved by Drosha, and the resulting precursor miRNA (pre-miRNA) is transported across the nuclear membrane by exportin-5 (Han et al. 2006). Once outside of the nucleus, the hairpin loop is cleaved by Dicer (a ribonuclease III enzyme), which leaves a small RNA duplex with 3'overhangs (Bernstein et al. 2001). The RISC complex then binds this duplex, retaining the guide (sense) strand, and releasing the anti-guide (passenger) strand.

The single stranded miRNA, bound to RISC, is then directed to a complimentary mRNA transcript, to which it binds, leading to cleavage of the now double-stranded target mRNA, and as a result, inhibition of translation (Martinez et al. 2002). While miRNA is reported to cause a powerful and sustained knockdown, endogenous small interfering RNA (siRNA), in which mismatches to the target exist, is though to result in transient knockdown by binding to the target mRNA to inhibit translation, without actually facilitating cleavage (Valencia-Sanchez et al. 2006) (Fig. 1.9).

In attempting to harness RNAi, researchers have designed hairpin RNA structures with a stem of 19-21 bases, separated by a loop sequence, which is expressed off a strong Pol III promoter (Brummelkamp et al. 2002; Elbashir et al. 2001). These short hairpin RNAs (shRNAs) mimic pre-miRNA, and are incorporated into the endogenous miRNA-processing pathway and are also able to evade the immune response elicited by long dsRNAs. These modified hairpin structures have been shown to be 12 times more effective (Silva et al. 2005) than traditional siRNAs, providing an obvious benefit in terms of translational silencing for the purposes of gene therapy.

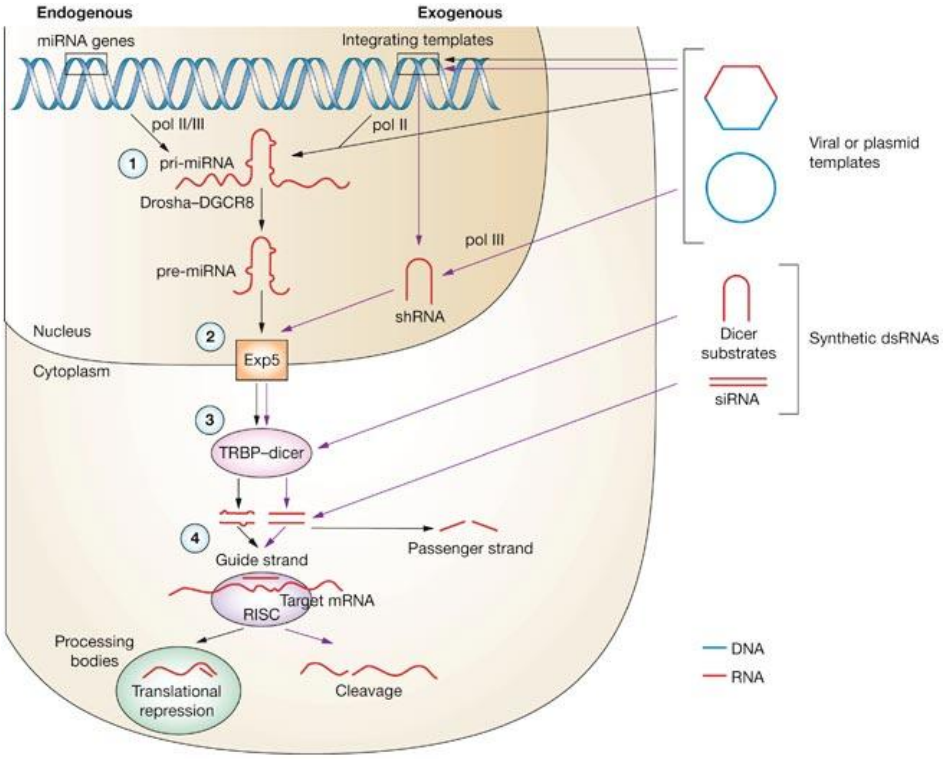

Figure 1.9. Entry points of manipulation of RNAi in mammalian cells. The diagram shows how to manipulate the RNAi pathway in order to achieve knock down. (1) Viral or DNA plasmid vectors can be introduced into the cell nucleus to result in stable expression of hairpin structures. These can be designed to mimic pri-miRNA based hairpins which are processed by the Drosha-DGCR8 complex into pre-miRNA based hairpins expressed off Pol II promoter. Alternatively, shRNAs can be designed to resemble the pre-miRNA structure and are usually expressed off Pol III promoters. (2) Processed structures are exported into the cytoplasm and (3) processed by TRBP-dicer to yield siRNAs, which can alternatively be directly introduced into the cell. (4) The guide strand is incorporated by RISC and leads to translational repression or target mRNA cleavage. (Adapted from Gonzalez-Allegre and Paulson, 2007).

When using an shRNA approach for silencing of genes, both sequence specificity and the accessibility of the target site (secondary structure of mRNA) have been reported to play an important role on the extent of knockdown (Ameres et al. 2007). In a 2003 study, Miller et al. investigated the possibility of discriminating between two alleles of the atxn3 gene in vitro. This group used siRNA complimentary to a mutant atxn3 transcript and, varying the position of the mismatch to the WT transcript, achieved selective knockdown of the mutant protein. Their results showed that the addition of another mismatch in

addition to the one complimentary to the mutant protein, decreased silencing of the WT ataxin-3 protein. Furthermore, by expressing siRNA off a U6 promoter in an adenovirus backbone, they were able to show sustained knockdown in their systems.

Following the research of Miller et al. (2003), Scholefield et al. (2009) also used RNAi to silence expression of a mutant protein (ataxin-7). In these studies however, they found that applying an additional mismatch did not increase specificity to the mutant allele. Interestingly, their knockdown of mutant ataxin-7 in mammalian cell models also led to restoration of normal expression of the WT protein in heterozygous cells.

The use of RNAi in cell models of dominant protein misfolding disease, brings forward the prospect of using RNA to silence the mutant form of CAIV in RP17. When considering RP17, it must be noted that it was demonstrated by Shah et al. (2005) that heterozygous CAIV knockout mice had no phenotypes, although homozygous knockout mice showed low female pup survival rates. This finding portends potential success in the use of mutant CAIV-targeted RNAi as a means of therapy, as it appears that cells can survive with one functional copy of the protein. Studies performed to assess the effect of CAIV absence in systems where functional copies of either CA II or CA XIV are expressed, suggest a complimentary effect of the isozymes on one another (Ogilvie et al. 2007; Shah et al. 2005; Sun et al. 2008). Gene therapy for RP has been considered in the past, and apart from the very successful use of newly introduced transcripts to replace mutant RPE65 in Leber's congenital amaurosis (Cideciyan et al. 2009), silencing RNA has been suggested for various forms of the dominant disease (Cashman et al. 2005; Gaur, 2006; Shinohara et al. 2008; Tam et al. 2008).

The studies mentioned in section 1.9 have thus shown that siRNA, CA inhibitors, and non-specific chaperones can be effective tools for the prevention of R14W mutant CAIV-mediated apoptosis *in vitro*. Furthermore, the work that has been done so far has shown proof of concept mechanisms of how a number of methods can be used to attempt therapy for RP and other diseases. Building on these admirable attempts for gene therapy

could reveal promising results, and could also possibly herald a new approach to delaying the onset of, or even preventing, a wide range of diseases caused by protein misfolding.

1.10. General and specific aims of the study

The R14W mutation in CAIV has been linked to RP17 in a number of studies. However, characterisation of the RP17 phenotype has not been carried out to date and the exact cause of the phenotype at the molecular level is not clear. Work performed by our group (Rebello et al. 2004) showed the cause of cell death in RP17 to be accumulation of mutant CAIV protein, while another group (Yang et al. 2005) contend that RP17 is caused by the absence of functioning CAIV protein. These conflicting studies necessitated an investigation into the molecular mechanisms of disease in RP17. The aim of this study was therefore to describe the RP17 phenotype and determine how the R14W mutation in CAIV leads to RP17, and to use the results to explore methods of therapy for the disease.

The specific aims of the study were therefore to:

(i) Describe and characterise the UCT RP17 cohort and disease phenotype.

(ii) Express the WT- and R14W mutant-CAIV in three different cell lines and to examine protein processing and localisation of R14W mutant protein, as well as its effect on cell cycle progression and apoptosis.

(iii) Design shRNA to R14W mutant CAIV in an effort to specifically knock down and consequently inhibit the effects of the mutant protein.

(iv) Use microarray analysis and mass spectrometry to identify genes and proteins respectively that could account for the RP17 phenotype and consequently be exploited in the development of treatment for this disease.

Materials and Methods

Prior to commencement of the study, the research proposal was approved by the University of Cape Town Human Research Ethics Committee (HREC/REF 243/2009). In accordance with the Declaration of Helsinki, October 2000, the recruitment of patients and relatives involved obtaining informed consent from each individual from whom blood was drawn.

2. Genetics of RP17

2.1. Characterisation of RP17 cohort

Since the initiation of the Retinal Degenerative Disease (RDD) project in 1990, the Division of Human Genetics at the University of Cape Town (UCT) has collected and archived samples from over 1284 South African RDD families. To date, biological material from 3043 individuals in these families, with a clinical history of various forms of retinal disease, has been archived at the Division.

The RP17 cohort consists of 64 individuals with the R14W CAIV mutation. For the purpose of this study, this cohort was characterised in terms of ages of onset and RP symptoms, in order to better define the cohort, perform a broad genotype-phenotype analysis, and identify typical trends in terms of symptoms for RP17.

2.2. Screening of *CA4* gene in the UCT 'dominant RP' cohort

Subsequent to the identification of the R14W CAIV mutation by Rebello et al. (2004), three more *CA4* mutations were identified in RP17 patients. Therefore, in order to update the RP17 cohort to include patients with the more recently identified CAIV mutations (R69H, R219S, G>A +59UTR), samples from all individuals classified as having adRP, but in whom no mutation had as yet been identified, were screened for *any* mutations in the *CA4* gene.

2.2.1. Patient recruitment and cohort selection

For the mutation screen of the *CA4* gene, 56 individuals with RP showing autosomal dominant inheritance (adRP) due to an as yet unidentified mutation were chosen.

2.2.2. DNA isolation and cataloguing

Following collection, blood samples were stored at 4°C. Blood was catalogued according to the standard sample coding procedure of the UCT Division of Human Genetics. Biological material for each disorder and subject has a unique identifier. For example, the fictional code RPD 157.19NAG identifies a sample as being from a family affected with autosomal dominant RP (RPD). The family identifier, 157, denotes this sample as being from the 157th family from which samples have been taken under this particular category (RPD), while 19 refers to the 19th member of this family to have been recruited. The three letter "confirmatory code" (NAG) usually indicates the first three letters of the individual's first name.

The DNA used for this study was isolated using the PureGene^{TM} DNA Isolation kit (Biozym, The Netherlands) as per the manufacturer's protocol. In order to assess DNA quality, samples were loaded onto 2% agarose gels containing 0.6 µg/ml ethidium bromide (EtBr). Electrophoresis was carried out at 100 V for 30 min. Samples in which DNA was found to be markedly degraded were not included in the mutation detection study.

2.2.3. Gene annotation and primer design

The annotation of the *CA4* gene was based on the genomic sequence downloaded from the National Centre for Biotechnology Information (NCBI) website (www.ncbi.nih.gov). The annotations were based on the version of the genome available as of November 2005. The sequence file was converted into the annotated form using a perl script designed by Dr George Rebello (personal communication), which included a genomic sequence approximately 2 kb upstream and downstream of the gene. The final form of this annotation is shown in the Appendix (section 14.1).

All of the primers used for mutation screening of the *CA4* gene had been designed prior to the start of this project by other researchers. In order to verify the suitability of the primers for use in the present study, several *in silico* analyses were performed. Primers were aligned onto the *CA4* genomic sequence to confirm their location, and to ensure that the amplicon generated by extension of these primers included the intron-exon boundary. The melting temperature and GC content of the designed primers was calculated using the Primer3 website-based program (http://frodo.wi.mit.edu/).

To ensure primers would bind to only the appropriate regions of *CA4*, sequence specificity was analysed using the standard nucleotide BLAST (Basic Local Alignment Search Tool) program (Altschul et al. 1990), which is accessible via the NCBI website (www.ncbi.nih.gov/BLAST). In order to analyse the potential of primers to form hairpin loops and/or primer-primer dimers, the web-based OligoAnalyzer program (http://www.idtdna.com/analyzer/ Applications/OligoAnalyzer) was used.

Exon 1, spanning over 500 bp, was divided into two separate amplicons - exon 1a and exon 1b. Exon 1a was further divided into exon 1a3-1 and exon 1a3-2. This was done in order to separate the exon into smaller sizes that could accurately be analysed by Denaturing High Performance Liquid Chromatography or by direct sequencing. Small exons, with short intervening sequences, were combined into single amplicons by the positioning of primer pairs that flank more than one exon. This was the case for exons 3, 4, 5 and 6, which were amplified as amplicons "3 and 4" (3/4), and "5 and 6" (5/6).

For mutation detection of the *CA4* gene, a total of seven primer pairs spanning the seven *CA4* amplicons (1a3-1, 1a3-2, 1b, 2, 3/4, 5/6 and 7) were verified. Primer size (in bp), sequences, and melting temperatures are listed in the Appendix (section 14.2) along with the positions of these primers on the annotated gene sequence (Appendix 14.1).

2.2.4. Mutation detection

2.2.4.1. Polymerase chain reaction

The polymerase chain reaction (PCR) for the seven amplicons of CAIV was prepared using the standard reaction mixture (Appendix 14.3). Reactions included 0.4 μM of both forward and reverse primer, 0.2 μM dNTPs (deoxyribonucleotide triphosphates) (Bioline, USA), and 1 X GoTaq® PCR buffer (Promega, USA) (containing 20 mM TRIS-HCl (pH 8.4) and 50 mM KCl). GoTaq® (Promega, USA) was used as a DNA polymerase, with 0.5 U added to reactions. SABAX sterile distilled water was added to make a final reaction volume of 25 μl. DNA samples at a concentration of 200 ng/μl were added as a template at a volume of 1 μl into the final volume of 25 μl. Annealing temperatures used for PCR amplification of *CA4* amplicons were selected based on the primer melting temperature predicted from *in silico* analyses

Figure 2.1 is an agarose gel image of the results of a PCR on amplicon 3/4 showing how PCR amplification resulted in a single, specific product. In the PCR, water blanks (instead of DNA) were used as negative controls.

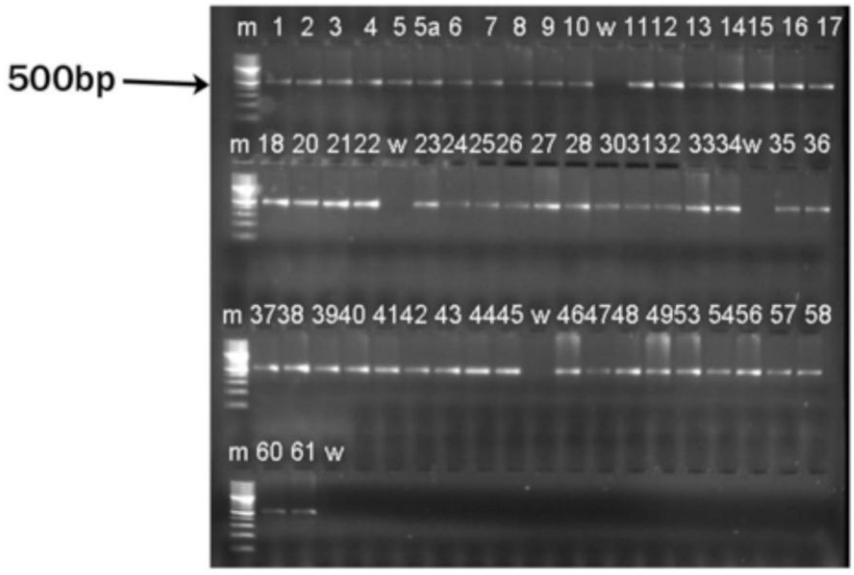

Figure 2.1. PCR on amplicon 3/4 of *CA4* in the adRP cohort results in a product of 513 bp. Lane m: 100 bp molecular weight size standard, w: water blank.

The PCR amplification protocol consisted of an initial denaturing step of one cycle at 95°C for 5 min. Thirty cycles were repeated, in which each cycle consisted of a second denaturing step at 95°C for 30 s, followed by an annealing step at a specific temperature for each primer pair (Table 2.1). An elongation step (72°C for 40 s) followed the annealing step. After the thirty cycles were completed, a final elongation step at 72°C for 7 min was carried out for one cycle.

Table 2.1. Melting temperatures selected for the 7 amplicons of *CA4*, as determined by temperature gradient PCR.

	Exons						
	1a3-1	**1a3-2**	**1b**	**2**	**3&4**	**5&6**	**7**
Tm (°C)	*55*	*60*	*60.5*	*59.5*	*61.9*	*59.2*	*63.4*

Where PCR failed to amplify a product, a magnesium titration ($MgCl_2$) was carried out with the aim of increasing the efficiency of the Taq enzyme. $MgCl_2$ was added to the PCR reaction mixture at final concentrations of 1.5 to 5 mM, and the concentration of $MgCl_2$ that resulted in the highest yield of (specific) PCR product was selected for use. A $MgCl_2$ titration increased the PCR amplification of exon 7. As a result of the titration, PCR on this exon was carried out with $MgCl_2$ added to the reaction at a final concentration of 4 mM (Fig. 2.2).

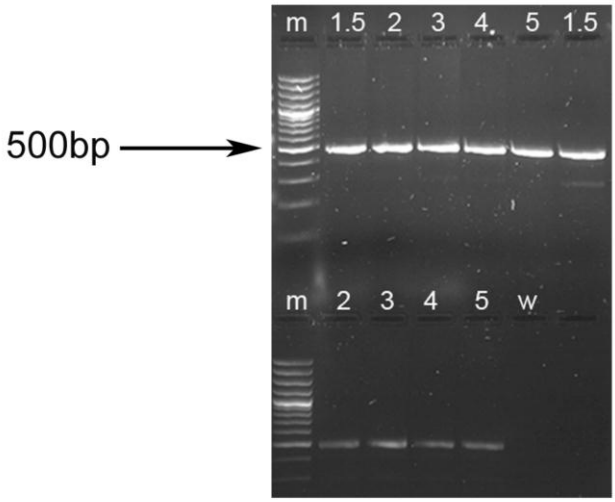

Figure 2.2. $MgCl_2$ titration carried out during PCR of exon 7 of *CA4*. $MgCl_2$ was added to samples at final concentrations of 1.5, 2, 3, 4, and 5 mM. Lane m: 100 bp molecular weight size standard, w: water blank.

PCR reactions were performed on the PCR Thermal Cycler apparatus GeneAmp® 9700 PCR System (Applied Biosystems, USA), the Px2 Thermal Cycler (Thermo Electron Corporation, USA) or the Techne Touchgene Gradient Thermocycler (Adcock Ingram, RSA).

2.2.4.2. Agarose gel electrophoresis

The products of PCR were resolved by electrophoresis on agarose gels prepared as described in section 2.2.2. Electrophoresis was carried out at 160 V for 30 min. The Generuler™ 100 bp DNA Ladder Plus (Fermentas Inc., Canada) (Appendix 14.4) was used as a DNA size standard.

2.2.4.3. Heteroduplex analysis

Denaturing High Performance Liquid Chromatography (dHPLC), or WAVE analysis, is a sensitive and high throughput system for mutation detection. PCR-amplified DNA was screened for mutations using the Transgenomic® WAVE System Model 4500 (Transgenomic Inc. USA).

Using the Transgenomic® WAVE System, duplex DNA is fixed to a Triethylammonium Acetate (TEAA) buffered column. TEAA buffer is an ion-pairing reagent that binds to the negatively charged phosphate group of the DNA backbone with its positively charged ammonium groups. The hydrophobic groups of the TEAA interact with the hydrophobic C-18 chains on the column, allowing TEAA to form a bridge between the DNA and the cartridge matrix of the Transgenomic® WAVE System. A 0.1 M solution of TEAA mixed with 25% acetonitrile is used as the elution buffer. As increasing concentrations of acetonitrile flow across the cartridge matrix, the hydrophobic interaction between the column and the DNA/TEAA is broken, and the DNA will elute. Heteroduplex strands, which are less hydrophobic, elute first as the unstable mismatched region begins to melt. The more hydrophobic homoduplexes elute at a later stage.

DNA was denatured at 95°C for 5 min using the PCR Thermal Cycler apparatus (Hybaid, USA). After heat denaturing, samples were steadily cooled down to room temperature (±25°C) over a period of at least 45 min, allowing re-annealing of DNA strands. The re-annealing period allows for the formation of homoduplexes, where wild type control samples anneal to identical wild type cohort samples. In cases where variations exist in cohort DNA, even if at a single nucleotide, heteroduplexes form between these and the wild type control samples. The heteroduplexes have different elution profiles on the Transgenomic® WAVE System to homoduplexes.

Mutation detection was performed by partial denaturing of the duplex DNA at oven temperatures that were selected based on the melting profiles of each amplicon. These melting profiles showed the predicted melting behaviour of the amplicon as determined by its sequence. Melting profiles were calculated in silico for each amplicon using the Mutation Detection application of the WAVEMAKER® software, version 4.1 (Transgenomic Inc., USA). Different sections of an amplicon have different melting temperatures, which are dependent on stretches of DNA sequence. As such, several melting temperatures may be required to partially denature a particular DNA fragment,

section by section. Two methods (i.e. Two different melting temperatures for one fragment) were used for each amplicon in this study in order to ensure partial denaturing that would result in the entire fragment being analysed. In cases where four or more WAVE methods were required in order to melt a fragment (amplicon 1a3-1), or where fragments were extremely GC-rich and thus not amenable to melting analysis (amplicon 1b), sequencing analysis was used for mutation detection. In total, 5 amplicons were screened by dHPLC.

WAVE Low-range™ and High-Range Mutation Control Standards ™ (Transgenomic Inc. USA) were included at the beginning and end of every dHPLC run in order to calibrate the oven temperature. Wild type samples were analysed prior to mutation detection screening of the cohort, in order to optimise WAVE methods for the selected melting temperatures, and to ensure that wild type samples did not contain any variants in each amplicon, which would be seen as distortions in the melting profile.

Optimisation of WAVE methods

When the amplicons of some wild type samples were analysed by dHPLC in order to test optimisation of WAVE methods, the melting profile was such that fragments would elute outside of the predicted separation times. Broad peaks were also observed in some cases, resulting in difficulty in the analysis of the elution profile. In such cases, timeshifts were introduced to shift elution times to occur over longer or shorter periods. Figure 2.3 shows an example of how a short elution time (Fig. 2.3a) can mask some aspects of an elution profile. When a timeshift is added (Fig. 2.3b), the peaks of the elution profile can be resolved, and mutation detection analysis can be carried out. A timeshift was added to the dHPLC methods of amplicon 2 in order to carry out mutation detection for this amplicon.

(a)

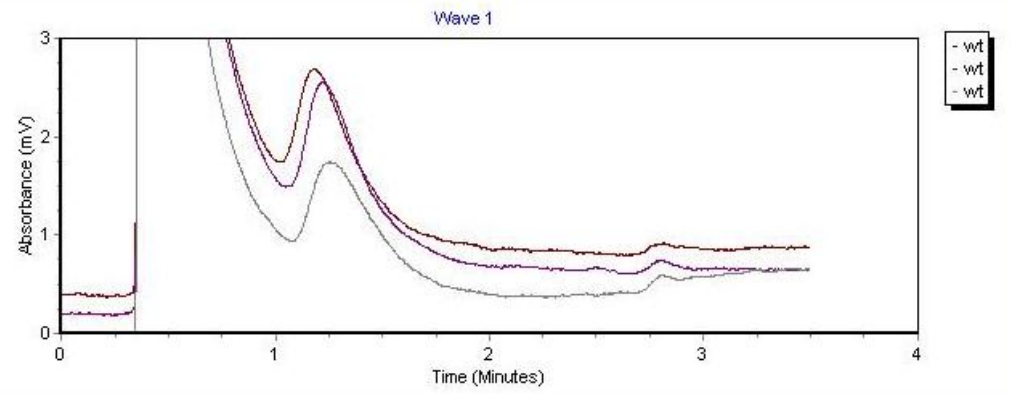

Figure 2.3a. A dHPLC chromatogram showing the elution profile of a wild type fragment of an exon at 63.7 ºC (top), 62.7ºC, and 61ºC (bottom). A time shift was added to the WAVE method (b) in order to extend and resolve the elution profile.

(b)

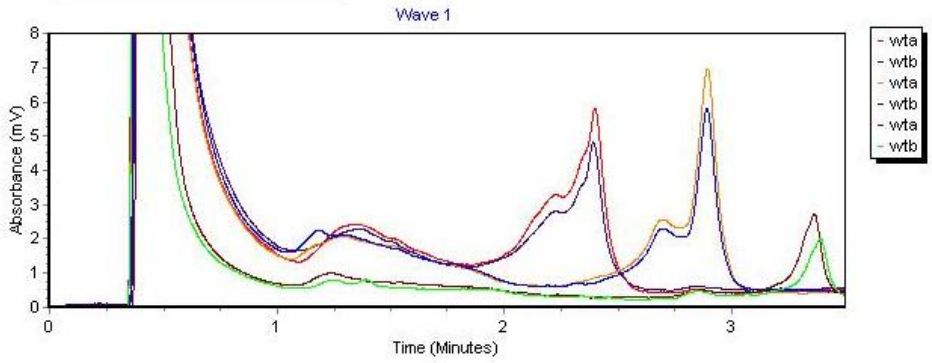

Figure 2.3b. A dHPLC chromatogram showing the elution profile of the same exon as in 2.3a, at 63.7 ºC (top), 62.7ºC, and 61ºC (bottom) in two wild type samples. Addition of a time shift resolved the peaks of the elution profile.

For the majority of amplicons, the "Rapid DNA Mutation Detection" function was used to analyse DNA samples. Using this function, fragments elute after 1.1 to 2.5 minutes. This fast elution time is due to a higher concentration of acetonitrile in the eluent than under the slower standard conditions. When the rapid method was not sufficient for effective analysis of DNA samples, as shown in Figure 2.4, a "Slow DNA Mutation Detection" method, with lower acetonitrile concentrations, was also used in order to

resolve the elution profile of the samples. In addition to a timeshift, the "Slow DNA Mutation Detection" method was also used for mutation detection on amplicon 2.

(a)

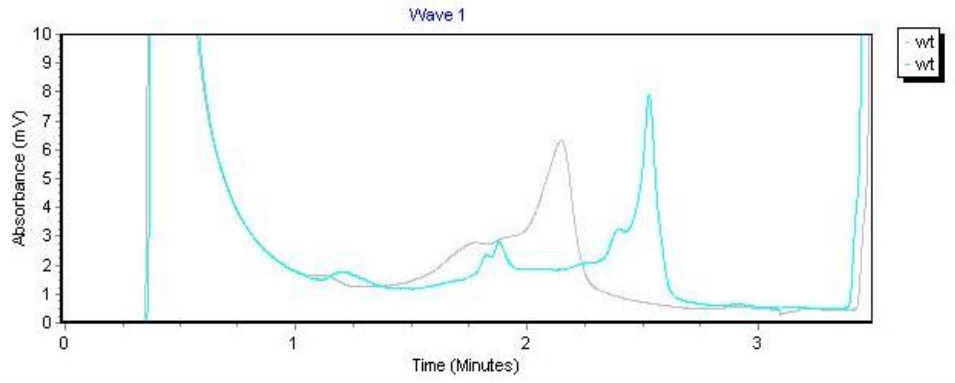

Figure 2.4a. A dHPLC chromatogram showing the "rapid" method elution profile of a wild type sample of an exon at 62.5ºC (top, in grey) and 61.3ºC (bottom peak). A slow method (b) was used in order to resolve the profile better at 62.5ºC.

(b)

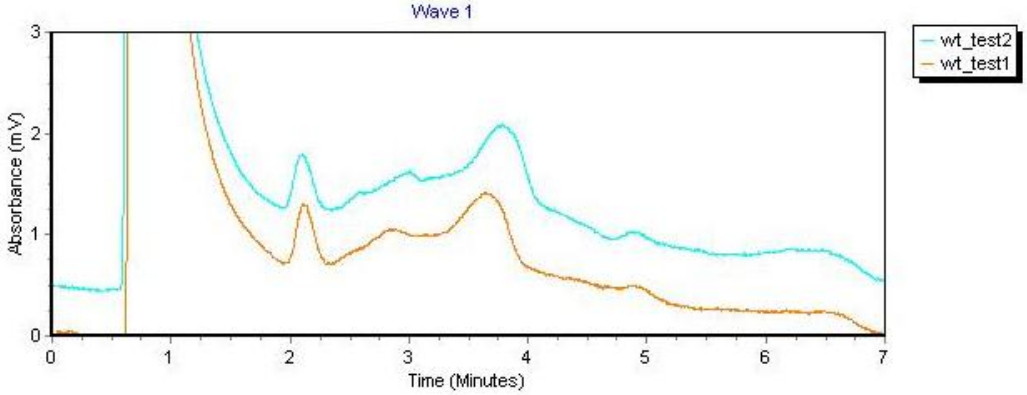

Figure 2.4b. A dHPLC chromatogram showing the "slow" method elution profile of the same exon as in 2.4a for two wild type samples at 62.5ºC. The use of the slow elution method enabled better analysis of the elution profile compared to the rapid method (a).

Once WAVE methods were optimised for a particular amplicon, the DNA obtained from PCR on that amplicon (for each individual in the cohort) was run on the Transgenomic® WAVE System. Results were analysed using the WAVEMAKER® Software, version 4.1 (Transgenomic Inc. USA).

Elution profiles that differed significantly to those of the wild type control were subjected to sequencing analysis in order to investigate the suspected variant.

2.2.4.4. DNA sequencing analysis

Direct sequencing

For sequencing, DNA samples from PCR were electrophoresed through 2% agarose gels under conditions described in section 2.2.2. In this case, the entire volume of 25 µl of PCR product was loaded onto the agarose gel. The PCR products were viewed under UV trans-illumination and excised using a scalpel. PCR products were purified from agarose gels using the QIAquick Gel Extraction Kit (Qiagen, Southern Cross Biotechnology, SA) protocol as per the manufacturer's instructions.

Cycle sequencing of DNA samples was carried out using the ABI PRISM® BigDye™ Terminator v3.1 Cycle Sequencing Kit (Applied Biosystems, USA). The reaction mixtures used for cycle sequencing are listed in the Appendix (section 14.5).

The cycle sequencing reaction was carried out with an initial denaturing step at 96ºC for 5 min. Twenty five cycles were repeated, in which each cycle consisted of another denaturing step at 95ºC for 30 s, followed by a primer annealing temperature of 50ºC for 15 s, and an elongation step set at 60ºC for 4 min. Cycle sequencing was carried out on the PCR Thermal Cycler (Hybaid, USA).

Following cycle sequencing, the entire 20µl volume of cycle sequencing product was cleaned up by ethanol precipitation. The procedure detailed in Current Protocols in

Human Genetics (Dracopoli et al. 1998) (Appendix 14.6) was followed, using sodium acetate (1.5M, pH>8, 250µM EDTA) as the monovalent cation solution.

Analysis of Sequencing

DNA sequences were analysed using the ABI PRISM® DNA Sequencing Analysis Software, version 3.7 (Applied Biosystems, USA). Electropherograms were examined visually for variations using the BioEdit Sequence Alignment Editor® version 7.0.0 (Isis Pharmaceuticals Inc. USA). Using this program, sequences were aligned to *CA4* genomic DNA (refseq: ENST00000300900) and mRNA (refseq: CCDS11624) sequences, which had been reannotated via EnsEMBL (http://www.ensembl.org/Homo_sapiens) using Annotv version 9. Multiple sequence alignments were performed using the ClustalW multiple sequence alignment tool (Thompson et al. 1997).

Variants that were discovered by sequence analysis were characterised as either reported or novel, based on information obtained from the Retina International Mutation Database (http://www.retina-international.org/sci-news/mutation.htm), or from the scientific literature. The mutation nomenclature guidelines of the Human Genome Variation Society (HGVS) based on coding DNA, as reported in den Dunnen et al. (2001), were followed in order to describe nucleotide changes. Where single nucleotide polymorphisms (SNPs) were discovered, the rs Reference SNP cluster numbers were used as opposed to ss numbers. SNP minor allele frequency counts were based on the 1000 Genome phase 1 genotype data from 629 individuals that was released in the 08-04-2010 dataset, as reported on the NCBI website (www.ncbi.nlm.nih.gov/projects/SNP/).

All novel variants were investigated to determine whether nucleotide changes resulted in amino acid changes. In cases where amino acid changes occurred, the University of Leicester Amino Acid Structure tutorial website (http://www.le.ac.uk/ by/ teach/ biochemweb/ tutorials/ aminoacidstruct.html) was used to study amino acid structures, and to determine the effect to the protein when the change of a particular amino acid resulted.

Where nucleotide changes occurred in intronic regions, splice prediction analysis was carried out. The online splice prediction tools at the Karolinska Institute (http://mordor.cgb.ki.se/cgi-bin/CONSITE/consite) and the Berkley Drosophila Genome Project (http://www.fruitfly.org/seq_tools/splice) were used to determine whether the variant would cause any splicing errors.

2.3. CFTR mutation (ΔF508) screen in RP17 R14W cohort

Due to a published report (Fanjul et al. 2002) in which targeting of CAIV to the plasma membrane was found to be compromised in CFPAC-1 pancreatic cells expressing the mutant ΔF508 cystic fibrosis transmembrane (CFTR) protein, a CFTR mutation screen was carried out on 52 members of the RP17 cohort.

2.3.1. Primer verification

Primers from Araujo et al. (2005) were used in this study. Primer pairs for amplification of the region of CFTR in which the ΔF508 mutation is found were analysed with regards to melting temperature and GC content (Primer3 v.0.4.0 http://frodo.wi.mit.edu/). In order to analyse the potential of primers to dimerize or form hairpin loops, they were analysed using the web-based OligoAnalyzer program (http://www.idtdna.com/analyzer/Applications/OligoAnalyzer). The positions of the primers on the CFTR region to which they anneal are depicted on the annotated sequence in the Appendix (section 14.7). Primers were fluorescently tagged at the 5' end for size detection using genotyping software. The primer sequences, sizes, and melting temperatures are listed in the Appendix (section 14.8).

2.3.2. Polymerase chain reaction

PCR for the CFTR amplicon was initially prepared using the standard reaction mixture detailed previously (section 2.2.4.1). Temperature gradient PCR reactions were set up in order to experimentally determine the most stringent annealing temperature for each primer pair. PCR was performed using temperature gradients of up to 12°C, with the primer melting temperature predicted from *in silico* analyses using the OligoAnalyzer

program being used to approximate the temperature at the middle of the gradient. The amplification was carried out under conditions described in section 2.1.3, and an annealing temperature of 64°C was selected. Due to the presence of a second, non-specific band on agarose electrophoresis gels after PCR amplification, a $MgCl_2$ titration was carried out at final concentrations of 4 to 9.0 mM. The titration showed that $MgCl_2$ at 9 mM resulted in the highest yield of specific PCR product, and this concentration was therefore used for amplification of CFTR.

PCR reactions were performed on the PCR Thermal Cycler apparatus GeneAmp® 9700 PCR System (Applied Biosystems, USA).

2.3.3. Agarose gel electrophoresis

The products of PCR were resolved by electrophoresis on 2% agarose gels as described in section 2.2.4.2.

2.3.4. Genotyping on the ABI Genetic Analyzer

In order to perform a sensitive size-quantification of the PCR products generated from amplification with the selected primers, genotyping was performed. PCR products were prepared in a 96-well microtitre plate in the following way: 1 µl CFTR PCR product, 4.5 µl HiDi formamide (Applied Biosystems, USA), and 0.2 µl of 500 ROX Size Standard™ (Applied Biosystems, USA).

Mixtures were denatured at 95°C for 2 min on a Hybaid Thermocycler, and immediately placed on ice prior to capillary-based electrophoresis on the ABI 3100 Genetic Analyser (Applied Biosystems, USA), followed by analysis using the GeneScan™ version 3.7 software (Applied Biosystems, USA).

3. Molecular study of RP17 phenotype

3.1. Plasmid Constructs

3.1.1. *CA4* constructs

All constructs used in this study were prepared according to standard techniques (Sambrook et al. 1989, pp 1.25-1.51).

WT and R14W mutant full-length human *CA4* cDNA sequences in the pCXN vector (*CA4*/pCXN) were a kind gift from Professor William S. Sly (St Louis School of Medicine, Missouri, USA). In order to construct *CA4*/pEGFPN-1 constructs, full-length *CA4* sequences were digested out of the pCXN mammalian expression vector using the *HindIII* and *SacII* restriction enzymes and cloned into the fluorescent pEGFP-N1 vector (Clontech, USA) at the *HindIII* (+622) and *SacII* (+649) sites using a 1:3 vector to insert molar ratio.

CA4 constructs (*CA4*/pEGSH) were generated by PCR amplification of the full-length *CA4* sequence using primers that contain cleavage sites for the restriction enzymes *Kpn1* and *Xho1*. PCR products were then loaded onto 2% agarose gels and subjected to electrophoresis at 100 V. After electrophoresis, PCR fragments corresponding to 500 bp (full length *CA4* and extra bases introduced by PCR primer, see Appendix (sections 14.1 and 14.2)) were excised from the agarose gel using the QIAquick Gel Extraction kit (Qiagen, Southern Cross Biotechnology, RSA) as per the manufacturer's instructions. The purified *CA4* fragment was then ligated into the pGEM-TEasy vector (Promega, Whitehead Scientific, RSA) via the T/A cloning site and then cleaved out of this construct using the *Kpn1* and *Xho1* restriction enzymes. The pEGSH construct was also digested using *Kpn1* and *Xho1*. The *CA4* fragment, flanked by *Kpn1* and *Xho1* sites, was then ligated into the digested pEGSH vector using a 1:3 vector to insert molar ratio. Competent *E.coli* DH5α bacterial cells were transformed with the ligation mixture and the *CA4*/pEGSH DNA extracted and purified by large-scale or small-scale plasmid preparation.

3.1.2. shRNA effector design

Due to the R14W mutation in CAIV being hypothesized to result in apoptosis of cells in which the protein is expressed, *in vitro* studies of RNAi were investigated as a means of therapy for the disease. In this dominantly inherited disease, it is the presence of the misfolded protein, and not its absence, which results in cell death (dominant negative effect). The objective was therefore to silence expression of the R14W mutant protein using shRNA, while allowing expression of the WT CAIV.

shRNAs were designed based on the expression vector system described by Brummelkamp and colleagues (2002). The design uses a DNA Pol III promoter, which drives expression of small transcripts that have a well-defined start site and a five-thymidine termination signal. In this case, the Pol III promoter from the pTZU6+1 vector was used for small transcript production (Lee et al. 2002). This promoter drives expression more strongly than the previously used Pol II promoters, and also has the advantage over another Pol III promoter, H1, in its being more efficient, constitutively expressed and longer lasting, both *in vitro* and *in vivo* (Mäkinen et al. 2006).

The shRNA effector sequences were designed with +/-19 nucleotides (nt) that match the target sequence representing the sense strand, followed by 19 nt of reverse complementary sequence that represents the antisense strand. This semi-palindromic sequence was interrupted by a short nine nt spacer/loop sequence. Finally the antisense sequence was followed by five thymidine residues which ultimately result in a two nt 3' overhang because termination site cleavage occurs after the second uracil (Baer et al. 1990). The thermodynamic properties of the transcript sequence predict the spontaneous formation of a short hairpin loop structure, which becomes the shRNA molecule. Cleavage of this double stranded shRNA product by Dicer has been shown to yield 21 and 22 nt sense and antisense products (Brummelkamp et al. 2002). In order to bias sense strand incorporation by RISC, functional asymmetry of the predicted duplex was induced by creating G:U mis-pairings, or "wobbles" at the 3' end of the anti-sense strand.

3.1.2.1. Mismatch placement

Using the sequence of the guide strand, three different shRNA constructs were designed that were complimentary to the mutant *CA4* transcript and therefore contained mismatches to the wild type allele. These mismatches (which consisted of a U to anneal to the mutant A instead of the wild type G at the relevant position) were placed at positions 15 and 16 in the first two constructs (base 1 was counted as the first base at the 5' end of the sense strand). In the third construct, the mismatch was placed at position 10, with a second mismatch (A) immediately 3' to the primary mismatch, at position 11 (Fig. 3.1), according to the methods of Miller et al. (2003) for increasing the binding of shRNA to a mutant target when WT and mutant genes differ by only a single nucleotide.

3.1.2.2. shRNA plasmid construction and cloning

Construction of shRNA-expressing vectors has been previously described (Castanotto et al. 2002) in which the pTZU6+1 vector is used as a template to create U6/shRNA cassettes. The previous method was modified by the use of a single PCR step. U6/shRNA cassettes (Fig. 3.2) were constructed as follows; A PCR cocktail of 200 µg of pTZU6+1 vector, 10 pmol U6 universal forward primer (Table), 10 pmol long reverse primer (Table), 0.2 mM dNTPs, 1 x GoTaq Buffer (Promega, Whitehead Scientific, RSA), and 2 units of GoTaq enzyme (Promega, Whitehead Scientific, RSA) was made up to a final volume of 25 µl with dH_2O. The cycling conditions were the same as those for standard PCR as indicated in the Appendix (section 14.3). PCR products were electrophoresed on a 2% agarose gel and the expected product size of 300 nt was excised under low ultra violet (UV) light and cleaned using the QIAquick Gel Extraction kit (Qiagen, Southern Cross Biotechnology, RSA) as per the manufacturer's instructions.

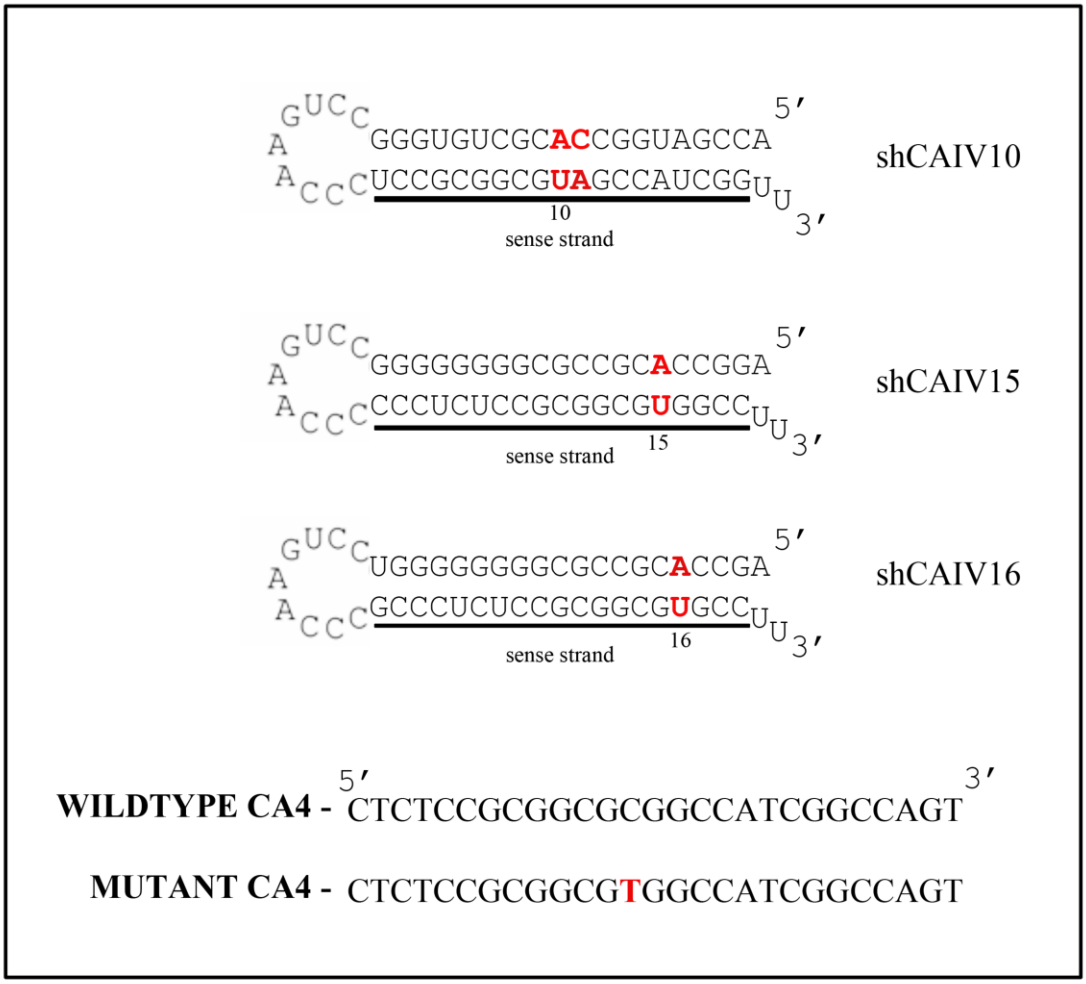

Figure 3.1. shCAIV molecule sequences shown as hairpin loops. Convention for the diagram follows Schwarz and colleagues (2006). Sequences of expected single mismatch sense/guide strands (underlined) processed from an shRNA format indicate the site of the mismatch to the C allele of the wild type CAIV. Sequence context of both the wild type and mutant targets are shown. The shRNAs were labelled according to the position of the primary mismatch relative to the 5' end of the guide strand.

The purified PCR products were quantified using a NanoDrop ND-1000 spectrophotometer (NanoDrop Technologies, Inqaba, RSA). A total of 100 ng of PCR product was ligated to the TA cloning vector pGEMTeasy (Promega, Whitehead Scientific, RSA) according to manufacturers' instructions, and incubated at 4^{o}C overnight. Competent DH5α E.coli cells were transformed with 10 µl of the ligation product and then plated on ampicillin selective agar plates. Blue/white screening was used to identify potentially positive clones.

White colonies were selected and inoculated into ampicillin selective medium. DNA was then extracted and purified using the kit (Qiagen, Southern Cross Biotechnology, RSA). To confirm the correct sequence, plasmid preparations were sequenced using both SP6 and T7 primers (Integrated DNA Technologies, Whitehead Scientific, RSA). It should be noted that some of the colonies representing the correct size fragment showed mismatches within the region of the U6/cassette. Correct sequences were confirmed by manual screening as well as using BioEdit (Tom Hall, Ibis Biosciences, USA). Plasmid integrity was verified by performing either *EcoRIII* or *NotI* (Promega, Whitehead Scientific, RSA) restriction endonuclease reactions and electrophoreses on a 2% agarose gel.

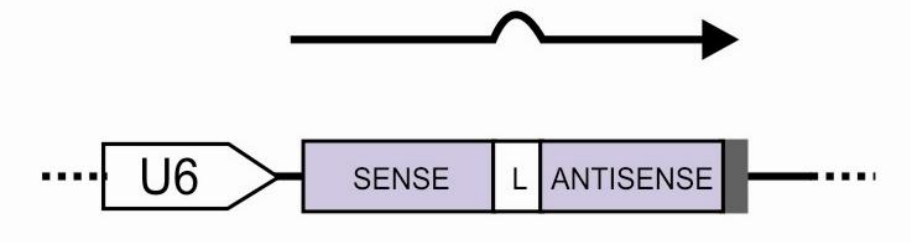

Figure 3.2. Schematic representation of the shRNA cassette. U6/shRNA expression plasmids were constructed using cassettes constructed as shown, where L indicates the 8-nucleotide spacer/loop.

3.1.2.3. Sequencing

DNA was sequenced to verify the presence of *CA4*/the shRNA effector sequence after subcloning. An initial cycle sequencing reaction was performed in a total volume of 20 µl consisting of 5 µl of the PCR product, 8 pmol of primer, 1 µl of the BigDye^{TM} termination mix (Applied Biosystems, RSA), 1 x BigDye^{TM} Buffer (Applied Biosystems, RSA), and distilled H_2O (dH_2O) to make up the final volume. The cycling conditions were performed on a Hybaid Touchdown Thermocycler (Appendix 14.5).

3.2. Cell culture

3.2.1. Maintenance of cell lines

SV40 transformed monkey kidney epithelium COS-7 cells (ATCC CRL-1651), human fibroblast epithelial HT-1080 cells (ATCC CCL-121), human embryonic endothelial kidney HEK-293 cells (ATCC CRL-157) and human kidney carcinoma RCC4 (+VHL) cells were used in this study. The first three cell lines are well known and commonly used for in vitro experiments, while the RCC4 cell line was used as a model of kidney cells that endogenously express CAIV protein.

Cells were cultured in Dulbecco's modified Eagle's medium (DMEM) (D7777-1L Sigma, USA) supplemented with 10% heat-inactivated fetal bovine serum, 100 U/ml penicillin and 100 µg/ml streptomycin. Cultures were maintained at 37°C in an atmosphere of 5% CO_2, and cells were passaged every two to four days.

3.2.2. Mycoplasma test

Cells grown on a coverslip in antibiotic-free media for 2-3 days were fixed in a 1:3 mixture of glacial acetic acid and methanol for 5 s, washed briefly with water to remove the fixing solution and then air-dried at room temperature (RT) for 5 min. Once dried, the DNA was stained with Hoechst 33258 (0.5 µg/ml) for 30 s, washed briefly with water to remove excess stain and then mounted on a slide with mounting fluid (Appendix, 14.12) at pH 5.5. The cells were viewed immediately by fluorescence microscopy under the DAPI filter. While only the nuclei of mycoplasma negative cells stained positive with Hoechst 33258, cells infected with mycoplasma showed staining in both the nucleus and cytoplasm. Cells found to be mycoplasma positive were not used for analyses.

3.2.3. Transient transfection assay

Cells were plated at a density of 1.5 x 10^5 cells/ml in 3.5 cm plates 1 day prior to transfection. For cell cycle analyses, cells were plated at a density of 4 x 10^5 cells/ml in 6 cm plates. Non-liposomal mediated gene transfer was performed using FuGENE®6 (Roche Applied Science, RSA) according to the manufacturer's instructions using 1 µg of

DNA for 3.5 cm plates and 2 µg for 6 cm plates. The DNA in transfection reactions consisted of either the full-length WT- or R14W *CA4* sequences cloned into pEGFP-N1 or full-length WT- or R14W *CA4* in pCXN vector. In the case of shRNA transfections, the transfected DNA was made up of equal amounts of full-length WT- or R14W CAIV in pCXN vector, and shCAIV construct. In experiments in which CAIV was silenced, a scrambled shRNA construct (shSCR) was used as a control (Appendix, 14.15). Cells were harvested either 24 h or 72 h after transfection.

3.3. Western blot analyses

Cells were plated at a density of 1.5 x 10^5 cells/ml and transfected as described previously. Either 24 or 72 h following transfection, cells were washed twice with 1 x phosphate-buffered saline (PBS) and then harvested and solubilized at 4°C with lysis buffer (40 mM Tris-HCl, 150 mM NaCl, 0.5% sodium deoxycholate, 1% Nonidet P40, 0.1% SDS and protease inhibitors). The lysate was then incubated on ice for 30 min and centrifuged at 12 000 rpm for 20 min at 4°C. Protein concentrations in lysates were determined using the BCA (bicinchoninic acid) protein assay kit (Thermo Scientific, USA) with bovine serum albumin as the standard. Two or 20 µg of protein extract were separated on a 12% SDS-PAGE gel under either non-reducing (no dithiothreitol (DTT) added and samples boiled for 2 min as opposed to 5 min) or reducing conditions and then transferred onto nitrocellulose Hybond-C membrane (Amersham, USA).

Following blocking for 1 h at room temperature, the membranes were probed with rabbit monoclonal anti-human primary antibodies: CAIV (1:5 000; gift from Professor William S. Sly, Saint Louis School of Medicine, Missouri, USA); BiP, PDI and GRP170 (1:1 000; These chaperone antibodies were a kind gift from Professor Gregory Blatch (Biomedical Biotechnology Research Unit, Rhodes University, Grahamstown) (originally obtained from Professor Richard Zimmerman, Medizinische Biochemie und Molekularbiologie, Universität des Saarlandes, Homburg, Germany). Immunoreactive bands were visualized with a horseradish peroxidase-conjugated secondary goat anti-rabbit serum (1:5 000) (Biorad, RSA) and detected with enhanced chemiluminescence (ECL) (Pierce, USA).

Rabbit polyclonal anti-p38 primary antibodies (1:5 000; Cell Signalling Technology Inc., USA) were used for normalisation.

3.4. Fluorescence-activated cell sorting

3.4.1 Cell cycle analysis

Cells were plated at a density of 4 x 10^5 cells/ml and transfected with either pCXN *CA4* or an shRNA construct. Either 24 or 72 h after transfection, cells were collected by trypsinisation, washed twice with cold 1 x PBS, and suspended in 2 ml of cold 1 x PBS. Cells were then counted with a haemocytometer (Neubauer, Germany) and fixed in 8 ml of 70% ice cold ethanol for a minimum of 30 min at -20ºC. Ethanol was removed by pelleting of fixed cells by centrifugation at 1 500 rpm for 5 min at RT. Cells were washed twice with 1 ml 1 x PBS and treated for 15 min at 37ºC in 1 x PBS supplemented with 50 µg/ml RNase A at a volume of 1 µl per 1 x 10^5 cells. At least 20 min before processing, cells were stained with propidium iodide (PI) solution (2 mM $MgCl_2$, 10 mM Pipes buffer, 0.1 M NaCl, 0.1% Triton X-100, 0.01 mg/ml PI) at a volume of 9 x that of the PBS/RNase A. Fluorescence-activated cell sorting (FACS) analysis was performed in a Beckman Coulter Cytomics FC500 flow cytometer (Beckman, USA) using the BD CellQuest™ Flow Cytometry Software (BD Biosciences, USA).

3.4.2. Apoptosis analysis

Cells were plated at a density of 4 x 10^5 cells/ml and transfected with either pCXN *CA4* or an shRNA construct. 72 h after transfection, cells were collected by trypsinization, and washed twice with cold 1 x PBS. Cells were harvested by centrifugation at 1 5000 rpm for 5 min and counted. The supernatant was discarded, and the pellet was resuspended in 1 x binding buffer at a density of 1 x 10^5 cells per ml. One hundred µl of the sample was transferred to a 10 ml culture tube, and incubated with Annexin V-FITC/Propidium Iodide (PI) (Sigma, USA) as per the manufacturer's instructions. Annexin V conjugated to FITC was used to quantitatively determine the percentage of cells in a population that are undergoing apoptosis and PI was used to stain all dead cells. Four hundred µl of 1 x binding buffer was added to each sample, and analysis was performed by FACS in a

Beckman Coulter Cytomics FC500 flow cytometer (Beckman, USA) using the BD CellQuest^{TM} Flow Cytometry Software (BD Biosciences, USA).

3.5. Fluorescence microscopy

Cells were plated onto glass coverslips at a density of 1.5 x 10^5 cells/ml. Cells were transfected (as previously described) 24 h after plating, and then processed either 24 h or 72 h after transfection.

Cells transfected with *CA4*/pCXN only or *CA4*/pCXN and shCAIV were fixed in ice-cold (-20°C) methanol or 4% paraformaldehyde at room temperature for 20 min and permeabilised in 0.2% Triton X-100 in 1 x PBS for 10 min. Cells were incubated overnight with rabbit monoclonal anti-human CAIV antibody at a dilution of 1:3 000 followed by incubation with Cy3 donkey anti-rabbit secondary antibody (Jackson ImmunoResearch Laboratories, Inc., USA). Cells were subsequently incubated in the dark for 10 min with 1 µg/ml 4',6-Diamidino-2-phenylindole (DAPI) in 1 x PBS, mounted on slides and visualized by fluorescence microscopy.

Cells transfected with *CA4*/pEGFP-N1 were incubated in a 1:10 000 dilution of ER-Tracker ^{TM} Blue-White DPX (E12353 Molecular Probes, Invitrogen, The Scientific Group-Adcock Ingram, SA) in 1 x Hank's Buffered Salt Solution (HBSS) for 30 min in order to specifically label the endoplasmic reticulum (ER). These cells were then viewed live in 1 x PBS.

3.6. Generation of stable cell lines

Following from analyses that involved transfected CAIV, COS-7 cells were stably transfected with the CAIV-expressing constructs in order to determine the effects of expression of the WT and mutant protein at levels that more closely represent those of the endogenously expressed protein.

Due to the observed apoptosis in cells in which R14W mutant CAIV is expressed, an Ecdysone inducible system (Agilent Technologies, USA) was used as a system which allowed control of the temporal expression of CAIV. The system is based on a synthetic ecdysone-inducible receptor and receptor recognition element that modulates expression of the gene of interest (*CA4*). In order to maintain tight control of the system, it consists of two components: the pERV3 receptor expression vector, and the pEGSH ecdysone inducible vector into which the gene of interest is cloned. Ponasterone A, an insect steroid hormone, was used as a dose-dependent inducer of the system.

The pERV3 vector encodes a synthetic receptor heterodimer composed of the ecdysone receptor (EcR) and the retinoid-X-receptor (RXR). These subunits are constitutively expressed using an internal ribosomal re-entry site (IRES), which allows expression of both from the same CMV promoter. This receptor heterodimer remains bound to a recognition element located upstream of a minimal promoter in the pEGSH inducible vector. The promoter remains transcriptionally silent until induction with Ponasterone A, which recruits co-activators to compete away a bound co-repressor, and thus instigate transcriptional activation of the gene of interest (Fig. 3.3).

3.6.1. Stable transfection with pERV3

To establish stable cell lines that could be induced to express either WT- or mutant CAIV the ecdysone system was utilised (Agilent technologies, USA). Briefly, COS-7 cells were plated on 3.5 cm dishes at a density of 1.5 x 10^5 cells/ml and transfected with 1 µg of the pERV3 receptor expression vector (Agilent technologies, USA). Individual clones were selected with 600 µg/ml G-418 antibiotic 48 h post transfection (as described below).

3.6.2. Drug selection of positive clones

To ensure that the stable cell lines were continuously expressing the desired plasmid, cells were treated with the appropriate antibiotic. G-418, a neomycin analogue, was used for the pERV3 vector and Hygromycin B for the pEGSH vector. To determine the effective concentration of antibiotic for each cell line, untransfected cells were seeded in

a 6-well plate so that cells were approximately 60% confluent on the first day of treatment. Cells were treated with concentrations of antibiotic ranging from 0 to 800 µg/ml, and monitored daily. The lowest concentration that resulted in complete cell death after approximately 10 days was selected. Following treatment of cells with antibiotic and monitoring of cell death, 600 µg/ml G418 antibiotic was selected as an optimal concentration to ensure death of cells not transfected with pERV3, and a 200 µg/ml Hygromycin B antibiotic concentration was used to selected against cells not transfected with pEGSH.

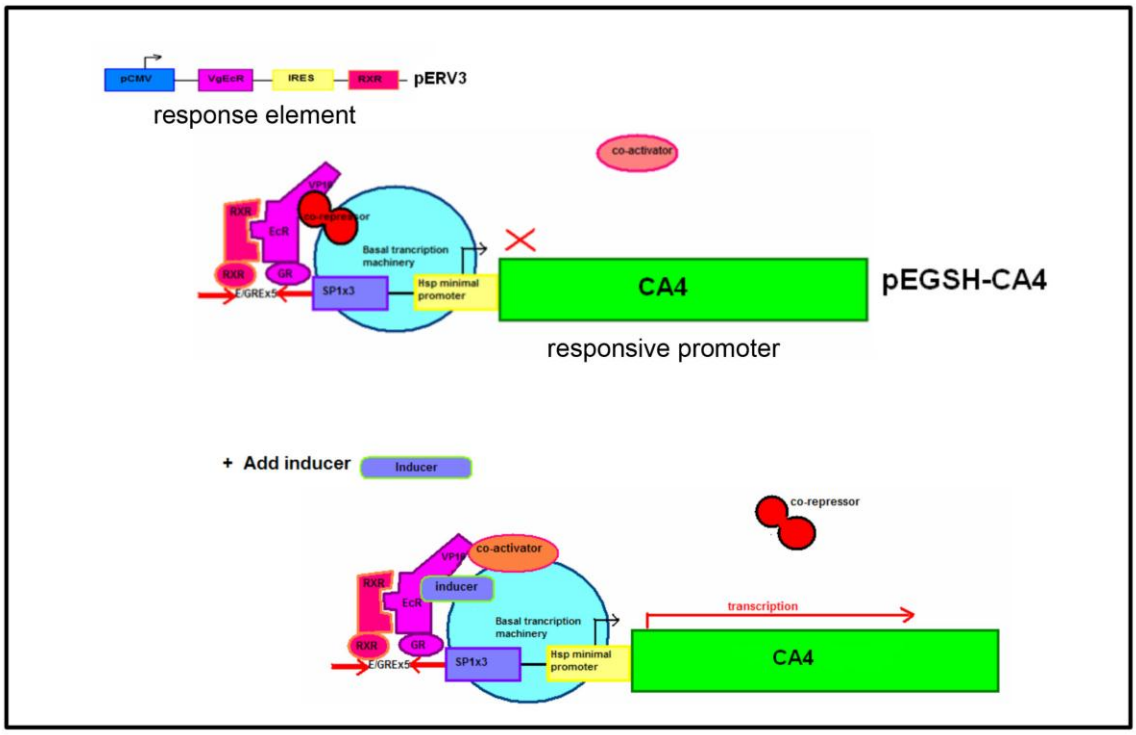

Figure 3.3. The ecdysone inducible system. The system consists of two vectors, the pERV3 response element, and the pEGSH vector containing the responsive promoter. While the response element constitutively expressed the heterodimeric subunit (EcR and RXR), the responsive promoter is transcriptionally silent. Upon binding of an inducer (Ponasterone A), a co-activator in recruited into a complex with the inducer and receptor heterodimer, and the promoter (shown in yellow) is activated to instigate transcription of the gene of interest (*CA4*).

3.6.3. Luciferase assay

A luciferase assay was carried out in order to determine which pERV3-expressing clones had highest expression of the receptor heterodimers. Stably transfected pERV3 cells were plated into 12-well dishes and transfected with 500 ng of the pEGSH-luc luciferase reporter plasmid (both from Agilent Technologies, USA). The vector pRL-TK, containing the thymidine kinase promoter, which drives the expression of a renilla reporter, was used as an internal control for transfection efficiency (50 ng per transfection). Cells were cultured for 24 h and then treated with Ponasterone A inducer (5 ng/ml) in order to induce expression of the pERV3 construct. Cells were cultured for a further 24 h after which cell extracts were harvested and assayed for firefly and renilla luciferase activity using the dual luciferase assay system (Promega, Madison, WI, USA) according to the manufacturer's instructions. Briefly, cells were lysed in 1 x lysis buffer (50 mM Tris-HCl pH 8, 150 mM NaCl, 0.5% sodium deoxycholate, 1% Nonidet P40, 0.1% SDS and protease inhibitors), cell lysates were frozen at -20ºC for at least 30 min, and then thawed. The lysate was then centrifuged at 13 000 rpm for 1 min at RT, and the supernatant was transferred to a fresh eppendorf. Ten µl of cell lysate was assayed immediately for reporter gene activity.

Luciferase activities were measured using the Luminoskan Ascent luminometer (Thermo Labsystems, Franklin, MA, USA). To normalise transfection efficiency, firefly luciferase values were divided by the renilla luciferase activity. All luciferase assays were performed in duplicate. pERV3 clones which showed the highest luciferase activity and the highest relative activity (i.e. induced/uninduced), were selected for stable transfection with the pEGSH vector containing the full-length *CA4* insert (either WT or mutant *CA4*).

3.6.4. Stable transfection with *CA4*/pEGSH

Once pERV3 clones were identified which showed high pERV3 expression, these clones were expanded and plated into 3.5 cm dishes for stable transfection. The pEGSH vector containing the full length human *CA4* cDNA was transfected into cells by non-liposomal mediated gene transfer using FuGENE®6 (Roche Applied Science, SA) according to the

manufacturer's instructions using 1 µg of DNA. As before, 600 µg/ml G418 antibiotic was added to the medium to add selective pressure in favour of pERV3 clones. In addition, 200 µg/ml Hygromycin B antibiotic was also added to medium to select for clones expressing the pEGSH-*CA4* construct. 14 days after antibiotic selection, surviving clones were picked, expanded, and assayed for CAIV expression (following induction with Ponasterone A) by western blotting using a rabbit monoclonal anti-human CAIV primary antibody. Clones that showed strong expression of CAIV protein upon induction were selected for use in further analyses.

3.7. Microarray analysis

Microarray analysis was carried out on RNA extracted from HT-1080 and HEK-293 cells transfected with either the pCXN-WT or pCXN-R14W mutant CAIV constructs. This analysis was performed in order to identify transcripts that are up- or down-regulated in either HT-1080 or HEK-293 cells, in response to the mutant CAIV protein. This would allow for the identification of candidate genes that are expressed in response to R14W mutant CAIV in HEK-293 cells, but not in HT-1080 cells. The Human Gene 1.0 ST Array (Affymetrix, USA) was used for the microarray analysis.

HT-1080 and HEK-293 cells were plated in 6 cm dishes at a density of 4 x 10^5 cells/ml and transfected with either the WT- or R14W mutant-CAIV pCXN construct (as described before). 24 h after transfection, RNA was isolated using the High Pure RNA Isolation Kit (Roche Applied Science, SA) as per the manufacturer's instructions. Briefly, cells were washed twice with 1 x PBS and then lysed in 200 µl PBS and 400 µl Lysis Buffer. The cell lysate was then vortexed and filtered, before being treated with DNase 1. The extract was then washed with Wash Buffers, and RNA eluted into sterile, nuclease-free water.

RNA concentration was determined using a NanoDrop ND-1000 spectrophotometer (NanoDrop Technologies, Inqaba, RSA), and the quality of RNA was verified by electrophoresis on a 1% agarose gel. The Bioanalyser Nano Assay (Agilent

Technologies, USA) was also used to assess the integrity of samples. The 260/230 ratio for RNA extracted from HT-1080 cells expressing WT CAIV was slightly less than the acceptable ratio of 1.5 (1.46), indicating the presence of contaminants. This sample was therefore purified by ethanol purification. Following this, all samples were then found to have integrity and purity within the acceptable ranges (260/280 between 1.8 and 2.0, 260/230 of more than 1.5, and a RNA integrity number between 7.0 and 10.0) (Fig. 3.4 and 3.5).

Samples were labelled using the Ambion WT Expression Kit (Ambion Inc., USA) according to manufacturer's instructions. A control RNA sample was included in order to monitor assay performance. As a standard, and to ensure that sufficient labelled target was used for hydridisation to the Human Gene ST Array, 200 ng of RNA was used for cDNA synthesis. Following cDNA synthesis, *in vitro* transcription was carried out in order to generate antisense RNA (cRNA). This was then cleaned up and first strand cDNA synthesis was carried out, followed by cRNA hydrolysis. For labelling, 5.5 µg of sense strand cDNA was fragmented, assessed on the Agilent Bioanalyser (Agilent Technologies, USA) for complete fragmentation, and subsequently end-labelled. Targets were then hybridised to the Human Gene ST Array for 17 hours. After hybridisation, the arrays were washed and stained using the GeneChip Fluidics Station 450, and scanned using the GeneChip Scanner 3000 7G (Affymetrix, USA).

Preliminary analysis was carried out using the Affymetrix Expression Console software in order to verify the high quality of the data and identify outliers. All samples fell within the acceptable ranges and were further analysed using bioinformatics software. The data was extracted from the Affymetrix platform into 4 .CEL files, which were normalised using Partek Genomic Suite (PGS), and annotated (Fig. 3.6).

(a)

Sample ID	Date	Conc. (ng/ul)	A260	A280	260/280	260/230
Control RNA	2011/07/07	136.13	3.403	1.794	1.9	2.1
HT1080 MUT CAW	2011/07/07	347.71	8.693	4.332	2.01	1.87
HT1080 WT	2011/07/07	355.2	8.88	4.626	1.92	1.46*
HEK 293 WT CAW	2011/07/07	357.31	8.933	4.515	1.98	1.88
HEK 293 MUT	2011/07/07	309.73	7.743	3.911	1.98	1.7

(b)

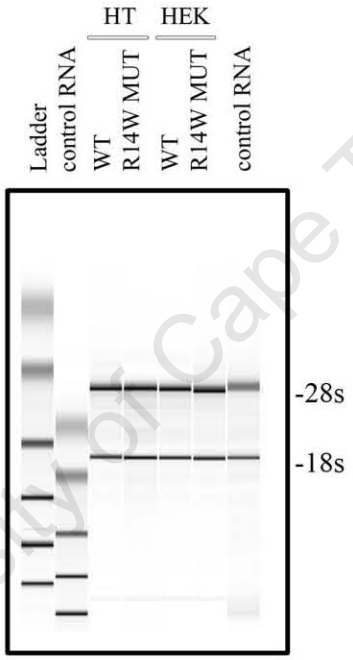

(c)

Sample ID	RIN Value	Comment
Control RNA (nano ladder)	N/A	Expected profile
HT MUT CAW	9.4	Pass
HT WT CAW	9.7	Pass
HEK 293 WT CAW	8.8	Pass
HEK 293 MUT CAW	9.6	Pass

Figure 3.4. Extraction of RNA from HT-1080 and HEK-293 cells expressing WT- and R14W mutant CAIV. RNA was harvested from HT-1080 and HEK-293 cells transfected with WT- or R14W CAIV in pCXN vector. Quantity of RNA was analysed using a NanoDrop spectrophotometer (a), while quality and integrity was assessed by electrophoresis on a 1% agarose gel (b). The Bioanalyser Nano Assay was used to determine RNA integrity (c).

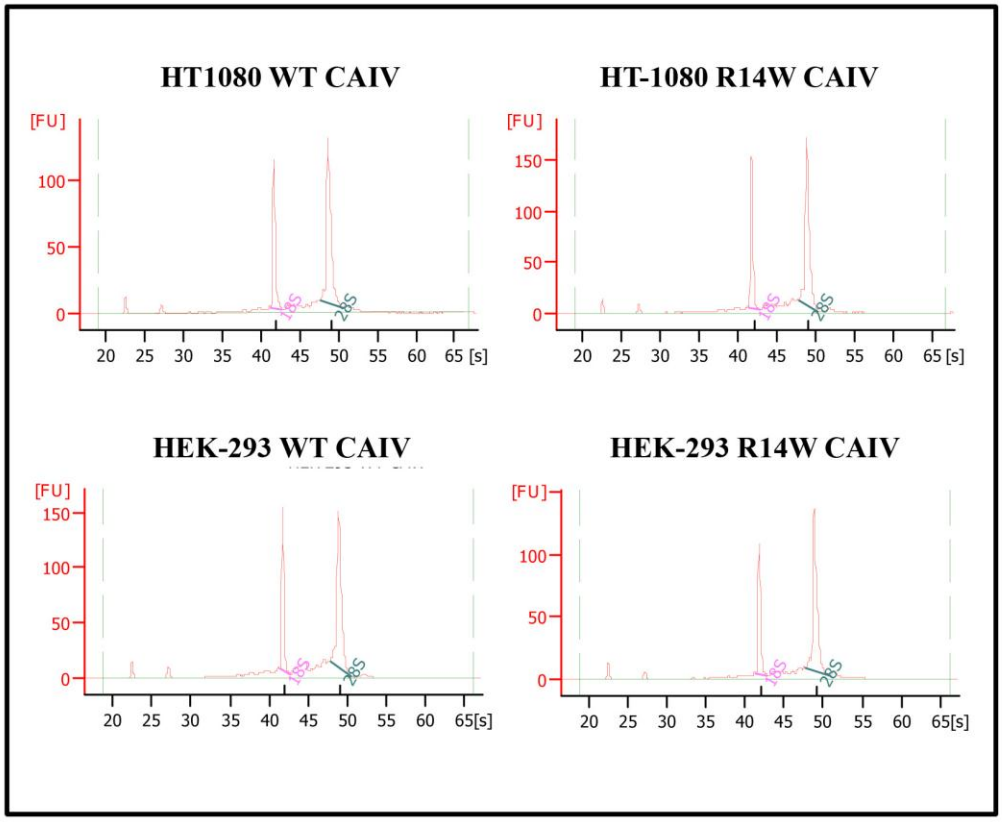

Figure 3.5. Bioanalyzer analysis of RNA from HT-1080 and HEK-293 cells expressing WT- and R14W mutant CAIV. RNA was harvested from HT-1080 and HEK-293 cells transfected with WT- or R14W mutant CAIV in pCXN vector. Quantity of RNA was analysed by Agilent 2100 Bioanalyzer Nano Assay. The y-axis denotes fluorescence while the x-axis denotes time in seconds. The presence of two clear peaks in all electropherograms indicate high quality, pure, eukaryotic total RNA.

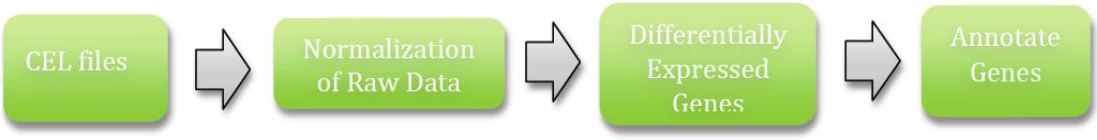

Figure 3.6. Flow diagram showing sequence of bioinformatics steps involved in the analysis of microarray data. Data from the Human Gene 1.0 ST Array was extracted as .CEL files, which was then normalised using PGS, compiled into a list of differentially expressed genes, and annotated.

The robust multichip normalisation (RMA) method (Irrizarry et al. 2002) was used to normalise data, and .CEL files were subjected to a 1-way ANOVA (analysis of variance) to compare the influence of factors being investigated. This allowed a list of differentially

expressed genes to be drawn up with associated error rates, where a gene was considered differentially expressed if the fold change was 1.5 or higher.

3.8. Immunoprecipitation of CAIV and mass spectrometry

Immunoprecipitation (IP) was carried out on the protein harvested from HT-1080 and HEK-293 cells transfected with the WT- or R14W mutant-CAIV protein. This was performed in order to isolate the CAIV expressed in these cells, as well as any CAIV-bound proteins. IP involves the use of A/G sepharose beads to isolate a protein of interest. Briefly, an antibody for the protein of interest is incubated with the cell extract, so that the antibody specifically binds to the relevant protein. Protein A/G sepharose beads, which bind to the antibody, are then added to the mixture. The beads are then spun out of solution with the antibody-protein complex attached in order to isolate the protein of interest from the rest of the sample. The beads are then released from the protein, which can be further analysed using a variety of methods.

Cells were plated in 6 cm dishes at a density of 4 x 10^5 cells/ml and transfected with either the WT- or R14W mutant-CAIV pCXN construct (as described before). 24 h after transfection, cells were washed twice with 1 x PBS and then harvested and solubilized at 4°C with lysis buffer (50 mM Tris-HCl pH 8, 150 mM NaCl, 0.5% sodium deoxycholate, 1% Nonidet P40, 0.1% SDS and protease inhibitors including sodium orthovanadate and sodium fluoride). The lysate was incubated on ice for 30 min with rolling, and cellular debris was removed by centrifugation at 12 000 rpm for 20 min at 4°C and the supernatant transferred to pre-cooled tubes. To pre-clear samples, A/G protein sepharose beads (Santa Cruz Biotechnology, USA) were added to the supernatant at a ratio of 40 µl beads per 1 ml supernatant, followed by incubation for 1 h at 4ºC with rolling. Following pre-clearing, the lysate was centrifuged at 2 000 rpm for 10 min at 4ºC and the supernatant transferred to fresh pre-cooled tubes. The protein concentrations in lysates were determined using the BCA (bicinchoninic acid) protein assay kit (Thermo Scientific, USA) with bovine serum albumin as the standard. Once protein concentration was determined, 300 µg of lysate was transferred to a fresh pre-cooled tube, and made up

to 1 ml with lysis buffer. Rabbit monoclonal anti-human CAIV antibody (1:1 000) was then added to the lysate and the samples incubated O/N at 4ºC with rolling.

The next day, 20 µl of A/G sepharose beads were added to the lysates and the samples incubated for 1 h at 4ºC with rolling. In order to dissociate beads from the protein-Ig complexes, a modified Filter Aided Sample (FASP) method was used. Samples were mixed with 500 µl lysis solution (5% SDS, 100mM Tris/HCl pH 7.6, 0.1M DTT) and DNA was sheared by sonification. The samples were then incubated at 95ºC for 5 min, before being clarified by centrifugation at 13 800 rpm for 5 min. The supernatant was removed and placed into a filter unit (Millipore cat no. 42410) with 200 µl of UA solution (8 M urea (Sigma, U5128) in 0.1M Tris/HCl pH 8.5. One ml per sample), before being centrifuged at 10 000 rpm for 15 min. Flow-through was discarded and 100 µl IAA solution (0.05 M iodoacetamide in UA. 0.1 ml per sample) was added to samples. Tubes were mixed at 600 rpm in a thermo mixer for 1 min and incubated for a further 20 min, after which filter units were again centrifuged at 10 000 rpm for 15 min. One hundred µl of IAA solution was again added to filter units and samples were centrifuged at 10 000 rpm for 15 min. This step was repeated twice and centrifugations steps were repeated with 100 µl ABC solution (0.05 M NH_4HCO_3 in dH_20. 0.25 ml per sample). Samples were then placed in 40 µl ABC with trypsin (enzyme to protein ratio of 1:100) and incubated in a wet chamber at 37ºC for 24 h. Filter units were transfered to new collection tubes and centrifuged at 10 000 rpm for 10 min. Forty µl ABC was again added to tubes and filter units centrifuged at 10 000 rpm for 10 min. Samples were then acidified with CF_3COOH and the filtrate desalted.

To confirm isolation of CAIV immune-complexes, 5 µl of the isolated protein was also resolved by 12% SDS-PAGE for western blot analyses with anti-human CAIV antibody (1:5 000). Once successful IP of CAIV was confirmed, 50 µg of the sample was sent to the Proteomics Laboratory at the Central Analytical Facility of the University of Stellenbosch for mass spectrometry analysis in order to identify proteins bound to CAIV.

During this process, a co-precipitate of a UV light-absorbing matrix and a biomolecule (the proteins of interest) is irradiated by a nanosecond laser pulse. Most of the laser energy is absorbed by the matrix, but a fraction of it ionizes the biomolecule, which is accelerated in an electric field through a flight tube. Depending on their mass to charge ratio, different molecules are accelerated through the tube at different speeds, and reach a detector at different times. Each molecule in a sample therefore yields a distinct signal, and the method can be used for the characterisation and detection of a wide range of molecules. Mass spectrometry can identify proteins from 400 to 350 000 Da, and can detect molecules at extremely low quantities (10^{-15} to 10^{-18} mole) with an accuracy of 0.1 to 0.01%.

Prior to analysis, the protein concentration of each sample to be analysed is determined using the NanoDrop ND-1000 spectrophotometer (NanoDrop Technologies, Inqaba, RSA). One hundred μg aliquots of sample are removed and subjected to trypsin digestion overnight. Samples are then subjected to HPLC analysis and data acquisition, and analysed with regards to sequence assignment and database interrogation using the ProteinPilot software programme (Applied Biosystems, USA).

The results from the IP/mass spectrometry were expected to confirm some of those obtained by microarray analysis.

Results

Genetics of RP17

4. Characterisation of the UCT RP17 cohort

The complete UCT RP17 cohort consists of 6 families, which together have 185 members listed on the Human Genetics database. Of these, 63 individuals have the R14W CAIV mutation. RP17 symptoms and age of onset were previously believed to follow those of other types of adRP. However, data generated by Rebello et al. (2004) implies that this phenotype is distinct from that of other autosomal dominant forms of RP. Specifically, in RP17 the primary location of cell death is in choriocapillaris cells as opposed to rod and cone cells in the retina. A considerable variation of the RP17 phenotype from that of adRP will have important implications for the diagnosis, management, and approaches to therapy for RP17. This study therefore sought to characterise the phenotype of RP17 patients by examining family and medical records of individuals within the cohort. Characterisation was performed based on age of onset of RP symptoms, severity of phenotype and disease progression, penetrance of disease symptoms, and inheritance patterns. Details for some individuals did not include a comprehensive list of these parameters, therefore characterisation of the cohort was based on the data that was availale at the time of the study.

All individuals catalogued on the database, and those who are mutation positive (highlighted in blue), are detailed in Tables 4.1a, b and c. Table 4.1d is a summarised list all of the individuals in the cohort, and shows the total number of individuals within each family, as well as the total numbers of affected individuals. Figures 4.1a, b and c, show examples of pedigrees of the RP17 families, which demonstrate the autosomal dominant inheritance pattern of the disease. Patients were initially tested for the R14W CAIV mutation based on having a family history of RP17 or of an unknown dominant form of RP, or due to the results of ocular examination, visual field testing, or an electroretinogram.

DNA number	Phenotype	Result	DNA number	Phenotype	Result
RPD 8.1ELO	AFFECTED	Positive	RPD 8.33STA	SPOUSE	
RPD 8.2GEO	SPOUSE		RPD 8.34HEN	SPOUSE	
RPD 8.3CYR	AFFECTED	Positive	RPD 8.35LOL	AT RISK	Negative
RPD 8.4MCL	SPOUSE		RPD 8.36FRA	AFFECTED	Positive
RPD 8.5VIV	AFFECTED	Positive	RPD 8.37MAG	AT RISK	Negative
RPD 8.6ECD	SPOUSE		RPD 8.38LAM	UNAFFECTED	Negative
RPD 8.7CAR	AT RISK	Negative	RPD 8.39AND	UNAFFECTED	Negative
RPD 8.8MIC	AT RISK	Negative	RPD 8.40WIL	AT RISK	Negative
RPD 8.9DJN	AT RISK	Negative	RPD 8.41CHA	UNAFFECTED	Negative
RPD 8.10SHI	AT RISK	Negative	RPD 8.42JOH	AT RISK	
RPD 8.11RON	AFFECTED	Positive	RPD 8.43LIN	AFFECTED	Positive
RPD 8.12ANG	AT RISK	Negative	RPD 8.44VDL	AT RISK	Negative
RPD 8.13LPB	AFFECTED	Positive	RPD 8.45ESM	UNAFFECTED	Negative
RPD 8.14HMB	AFFECTED	Positive	RPD 8.46HAN	AT RISK	Negative
RPD 8.15AJB	AT RISK	Positive	RPD 8.47MER	AT RISK	Negative
RPD 8.16JFF	SPOUSE		RPD 8.48AND	AT RISK	
RPD 8.17BJH	AFFECTED	Positive	RPD 8.49RUD	AFFECTED	Positive
RPD 8.18HJR	AFFECTED	Positive	RPD 8.50PET	SPOUSE	
RPD 8.19GER	SPOUSE		RPD 8.51CAR	AT RISK	Negative
RPD 8.20NEL	SPOUSE		RPD 8.52MCG	AT RISK	Negative
RPD 8.21MAR	SPOUSE		RPD 8.53WIM	SPOUSE	
RPD 8.22BEN	AT RISK		RPD 8.54LZ	AFFECTED	Positive
RPD 8.23LOU	SPOUSE		RPD 8.55WIL	SPOUSE	
RPD 8.24WIL	AFFECTED	Positive	RPD 8.56ELW	AT RISK	Negative
RPD 8.25BEN	AT RISK	Negative	RPD 8.57GRE	SPOUSE	
RPD 8.26ESM	SPOUSE		RPD 8.58MAR	AFFECTED	Positive
RPD 8.27WIL	UNAFFECTED	Negative	RPD 8.59AND	AT RISK	Negative
RPD 8.28WAN	UNAFFECTED	Negative	RPD 8.60MAR	SPOUSE	
RPD 8.29ISA	AFFECTED	Positive	RPD 8.61WIL	AT RISK	Negative
RPD 8.30WIE	AFFECTED	Positive	RPD 8.62WIL	QUERY	Negative
RPD 8.31KAT	AT RISK	Negative	RPD 8.63SUS	SPOUSE	
RPD 8.32LEV	AFFECTED	Positive	RPD 8.64ADR	QUERY	Negative

Table 4.1a. List of RP17 cohort showing both affected and unaffected family members. Individuals RPD 8.1 to RPD 8.61 are shown. Affected patients, who are positive for the R14W mutation, are highlighted in blue.

DNA number	Phenotype	Result	DNA number	Phenotype	Result
RPD 8.65LMB	SPOUSE		RPD 19.7ERN	UNAFFECTED	Negative
RPD 8.68KAR	AT RISK	Negative	RPD 19.8MEL	SPOUSE	
RPD 8.78STE	AFFECTED	Positive	RPD 19.9ENR	AT RISK	Positive
RPD 8.79ANN	SPOUSE		RPD 19.10EVE	AT RISK	Negative
RPD 8.80JAN	AFFECTED	Positive	RPD 19.11SAL	AT RISK	Negative
RPD 8.81MAR	AT RISK	Negative	RPD 19.12CHR	AT RISK	Negative
RPD 8.82DIE	SPOUSE		RPD 19.13BAS	AT RISK	Negative
RPD 8.83SUS	AT RISK	Negative	RPD 19.14MAG	SPOUSE	
RPD 8.84SAL	UNAFFECTED	Negative	RPD 19.15THE	SPOUSE	
RPD 8.85BAR	SPOUSE		RPD 19.16CRA	AT RISK	Negative
RPD 8.86GRE	AFFECTED	Positive	RPD 19.17ANG	AT RISK	Negative
RPD 8.87MAD	AT RISK	Positive	RPD 19.18VER	AFFECTED	Positive
RPD 8.88NAD	AT RISK	Negative	RPD 19.19DAN	SPOUSE	
RPD 8.89NEL	AT RISK	Negative	RPD 19.20AND	AFFECTED	Positive
RPD 8.90LOM	AT RISK	Negative	RPD 19.21JCA	AFFECTED	Positive
RPD 8.91JOE	AT RISK	Negative	RPD 19.22DIA	AFFECTED	Positive
RPD 8.92NOK	AT RISK	Negative	RPD 19.23SAS	AT RISK	Negative
RPD 8.93JAM	AFFECTED	Positive	RPD 19.24NEI	AT RISK	Negative
RPD 8.94MIE	AFFECTED	Positive	RPD 19.25ANE	SPOUSE	
RPD 8.95JER	AT RISK	Negative	RPD 19.26PET	AFFECTED	Positive
RPD 17.1DOR	AFFECTED	Positive	RPD 19.27VER	AT RISK	Negative
RPD 17.2HEA	SPOUSE		RPD 19.28MAR	AT RISK	Negative
RPD 17.3LOR	AT RISK	Negative	RPD 19.29NIG	AT RISK	Negative
RPD 17.4MIC	AFFECTED	Positive	RPD 19.30PRI	SPOUSE	
RPD 17.5WIL	SPOUSE		RPD 19.31ROG	AT RISK	Negative
RPD 17.6KEV	AFFECTED	Positive	RPD 19.32NAT	AT RISK	Negative
RPD 19.1MER	AFFECTED	Positive	RPD 19.33NAT	AT RISK?	Positive
RPD 19.2MAU	AFFECTED	Positive	RPD 19.34PEN	AFFECTED	Positive
RPD 19.3RON	AFFECTED	Inconclusive	RPD 19.35LOR	UNAFFECTED	Negative
RPD 19.4GAR	AT RISK		RPD 19.36CYN	UNAFFECTED	Negative
RPD 19.5HAR	AT RISK	Negative	RPD 19.37FRE	UNAFFECTED	Negative
RPD 19.6CIL	AT RISK	Negative	RPD 19.38CSM	UNAFFECTED	Negative

Table 4.1b. List of RP17 cohort showing both affected and unaffected family members. Individuals RPD 8.65 to RPD 19.38 are shown. Affected patients, who are positive for the R14W mutation, are highlighted in blue.

DNA number	Phenotype	Result	DNA number	Phenotype	Result
RPD 19.39RON	UNAFFECTED	Negative	RPD 61.22SHA	AT RISK	Positive
RPD 19.40JAS	AT RISK	Negative	RPD 61.23DYL	AFFECTED?	Positive
RPD 19.41RIT	AT RISK		RPD 61.24NEV	AT RISK	Negative
RPD 19.42JOS	AT RISK	Negative	RPD 61.25SER	AT RISK	Negative
RPD 19.43MIC	AFFECTED	Positive	RPD 61.26NEI	UNAFFECTED	Negative
RPD 19.44NIC	AFFECTED	Positive	RPD 61.27FIO	SPOUSE	
RPD 19.45DY_	AFFECTED	Positive	RPD 61.28ALM	AFFECTED	Positive
RPD 19.46SYL	AFFECTED	Positive	RPD 61.29JUL	AFFECTED	Positive
RPD 19.47LAU	AT RISK	Positive	RPD 61.30MAS	AT RISK	Negative
RPD 19.48VIC	AFFECTED	Positive	RPD 61.1JOH	AFFECTED	Positive
RPD 19.49NA_	AT RISK	Negative	RPD 61.2PAU	SPOUSE	
RPD 19.50DAR	AT RISK	Positive	RPD 61.3JAM	AFFECTED	Positive
RPD 61.1EUG	AT RISK	Negative	RPD 61.4ERI	SPOUSE	
RPD 61.2CAR	UNAFFECTED	Negative	RPD 61.5JOA	AFFECTED	Positive
RPD 61.3ALL	UNAFFECTED	Negative	RPD 61.6MIC	SPOUSE	
RPD 61.4ALX	UNAFFECTED	Negative	RPD 61.7PAM	AT RISK	Negative
RPD 61.5MAN	UNAFFECTED	Negative	RPD 61.8GAR	AT RISK	Negative
RPD 61.6GEO	UNAFFECTED	Negative	RPD 61.9CHI	AT RISK	Positive
RPD 61.7PEN	SPOUSE		RPD 61.10PAT	AT RISK	Negative
RPD 61.8PNY	SPOUSE		RPD 61.11JAF	AFFECTED	Positive
RPD 61.9KAR	AFFECTED	Positive	RPD 61.12ROB	AT RISK	Positive
RPD 61.10LIN	SPOUSE		RPD 61.13LEE	AT RISK	Positive
RPD 61.11JEA	AFFECTED?	Positive	RPD 913.1COR	AFFECTED	Positive
RPD 61.12NIC	AT RISK	Negative	RPD 913.2GER	AT RISK	
RPD 61.13AMO	AFFECTED	Positive	RPD 913.3JAC	AFFECTED	Positive
RPD 61.14NIC	AFFECTED	Positive			
RPD 61.15ANT	AFFECTED	Positive			
RPD 61.16CAR	AT RISK	Negative			
RPD 61.17JEA	AT RISK				
RPD 61.18LIN	AT RISK				
RPD 61.19DA_	UNAFFECTED	Negative			
RPD 61.20MIC	AFFECTED	Positive			
RPD 61.21MAR	SPOUSE				

Table 4.1c. List of RP17 cohort showing both affected and unaffected family members. Individuals RPD 19.39 to RPD 913.4 are shown. Affected patients, who are positive for the R14W mutation, are highlighted in blue.

Family number	Individuals on database	Affected individuals
RPD8	84	24
RPD17	6	3
RPD19	50	17
RPD61	29	10
RPD81	13	7
RPD913	3	2
TOTAL	185	63

Table 4.1d. Summary of RP17 cohort showing both affected and unaffected family members. The six families have a total of 185 individuals on the database, and 63 of these are affected.

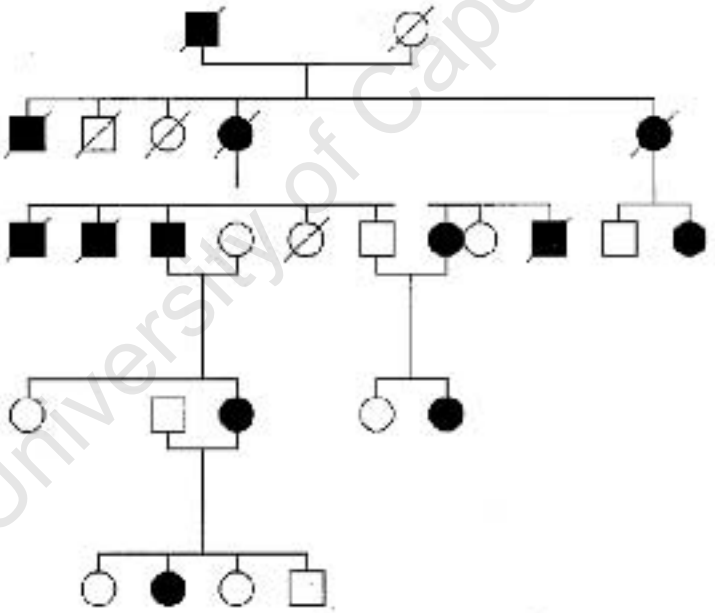

Figure 4.1a. RP17 family RPD8. Family RPD8 is an extremely large family, with 84 members included on the database. This pedigree shows a branch of that family, and clearly demonstrates the autosomal dominant nature of RP17. All generations are affected by RP, with the numbers of males and female members affected being comparable.

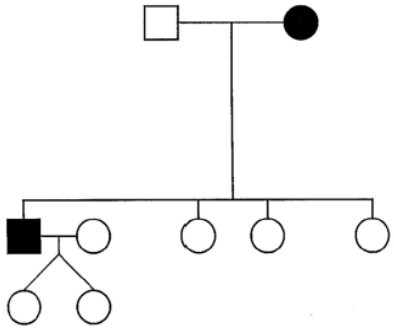

Figure 4.1b. RP17 family RPD17. Family RPD17 is a smaller family, with only 9 members, 6 of whom are included on the database. This pedigree shows members of the family.

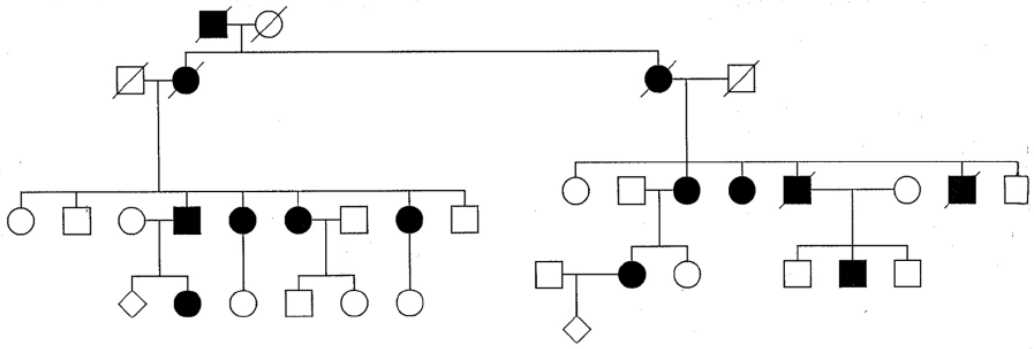

Figure 4.1c. RP17 family RPD19. Family RPD19, like RPD8, is a lage family, with 50 members included on the database. This pedigree shows a branch of that family, and clearly demonstrates the autosomal dominant nature of inheritance of RP17. As with Figures 4.1a and b, all generations are affected by RP.

While the age of onset of RP symptoms in affected individuals generally ranges from the late teens to the early twenties, in the RP17 cohort the age of onset starts as early as 7 years old to as late as 40 years of age (Table 4.2.). The RP17 cohort shows that patients with the R14W CAIV mutation display slightly more variable ages of onset than what is typical of individuals with adRP. For example, while the typical age of onset for adRP is in the mid-twenties (Daiger et al. 2007), 23% of the RP17 cohort started to display symptoms when they were under the age of 20 years. Most RP17 patients display symptoms of the disease at 20 years of age (the mode), with the mean age of onset being approximately 25 (24.63) years of age. The mutation shows complete age-related

penetrance in this cohort, although there appears to be a great deal of variation in the severity of the symptoms and their rate of progression over time.

Further characterisation of RP17 symptoms reveals variability even within families. For example, individual 34 in family RPD19 has an age of onset of 7 years, while individual 33 in the same family started to experience symptoms at 39 years of age (Table 4.2). In general, RP17 patients appear to have an earlier age of onset than that reported for other forms of adRP (Daiger et al. 2007), with many individuals experiencing symptoms by the age of 20 years or younger. The early age of onset of RP17 symptoms may suggest that retinal cell death occurs more promptly due to the collapse of the choriocapillaris layer. This would mean that therapeutic intervention in RP17 is required sooner than with other forms of RP, in order to prevent or delay retinal cell death.

Patient	Age of onset (yrs)
RPD8.11RON	16
RPD8.1ELO	20
RPD8.29ISA	20
RPD8.8.30WIE	20
RPD8.32LEV	40
RPD8.36FRA	30
RPD8.3CYR	25
RPD8.43LIN	39
RPD8.54LIZ	25
RPD8.58MAR	30
RPD8.78STE	20
RPD8.80JAN	27
RPD17.1DOR	26
RPD17.4MIC	18
RPD17.6KEV	17
RPD19.1MER	28
RPD19.20AND	16
RPD19.22DIA	20
RPD19.26PET	29
RPD19.33NAT	39
RPD19.34PEN	7
RPD19.43MIC	20
RPD19.44NIC	26
RPD61.15ANT	34
RPD81.11JAF	30
RPD81.1LEE	30
RPD81.5JAM	15
RPD81.9CHL	15

Table 4.2. Ages of onset of RP of selected members of the UCT RP17 cohort. The table shows that members of the cohort have ages of onset of symptoms of RP from as early as 7 years of age, to as old as 40 years of age. Most members display symptoms between the ages of 15 and 25 years.

5. Screening of the adRP cohort for *CA4* gene mutations

Following the identification of the R14W CAIV mutation by Rebello et al. (2004), the UCT Division of Human Genetics adRP cohort was only screened for the C>T mutation in the *CA4* gene. However, three novel additional mutations in the *CA4* gene were subsequently identified as being associated with RP17 (Alvarez et al. 2007; Yang et al. 2005). The current study therefore screened individuals in the UCT adRP cohort for these and other mutations in the entire coding region of the *CA4* gene. An additional motivation for this screen was that individuals who had previously tested negative for the C>T mutation in the *CA4* gene, could be informed that they may potentially develop RP17 and they could therefore be better managed.

In order to perform mutation detection analysis across the *CA4* gene, seven amplicons from 56 patient samples (Table 5.1) were screened. Amplicons 1a3-2, 2, 3/4, 5/6 and 7 were screened by dHPLC. Amplicons 1a3-1 and 1b, which required too many dHPLC methods to be analysed using this approach, were screened using sequencing analysis. Results for screening of *CA4* have been grouped into amplicons that showed no variants when screened by dHPLC (section 5.1), amplicons that showed dHPLC profile variants (section 5.2), and those amplicons that were screened by sequencing only (section 5.3).

5.1. Amplicons with no variant dHPLC profiles

Of the five amplicons screened by dHPLC, only amplicon 3/4 showed no variants in the 56 samples analysed. Figure 5.1 depicts the elution profile of amplicon 3/4 for four DNA samples (a), which, when compared to control samples (b), show no variation in elution profile at a temperature of 61.4°C. Amplicon 3/4 was also analysed by dHPLC at 62°C, and no changes were seen in the elution profiles of the 56 samples for this temperature either.

Patient number	Patient identifier	Patient number	Patient identifier
1.	RPD1.1FAT	28.	RPD207.1MAR
2.	RPD16.35CAV	30.	RPD334.5MKH
3.	RPD18.11SAL	31.	RPD348.1NOE
4.	RPD23.1ABD	32.	RPD368.2ANN
5.	RPD29.1KAA	33.	RPD391.1PHI
5a.	RPD41.13ZUK	34.	RPD399.1MTH
6.	RPD48.5EST	35.	RPD401.3
7.	RPD50.3DOL	36.	RPD402.2GIO
8.	RPD55.15LUK	37.	RPD436.2GAN
9.	RPD65.3GRA	38.	RPD439.1NIC
10.	RPD73.3THO	39.	RPD442.1ELI
11.	RPD76.1KTH	40.	RPD453.1MUS
12.	RPD78.1MJS	41.	RPD493.1465.1PHA
13.	RPD84.3JAC	42.	RPD493.1PAU
14.	RPD86.10NIC	43.	RPD498.1NIE
15.	RPD85.3SAN	44.	RPD501.1AND
16.	RPD89.6DOR	45.	RPD540.1BAN
17.	RPD93.4UDO	46.	RPD542.1LIZ
18.	RPD94.6CEC	47.	RPD468.1CYN
19.	RPD95.2EPH	48.	RPD737.5ANN
20.	RPD112.4HEA	49.	RPD906.1RIA
21.	RPD118.2ARL	53.	RPD987.1JUL
22.	RPD147.1JOH	54.	RPD989.1MAL
23.	RPD162.3CHR	56.	RPD1001.2MLA
24.	RPD191.1AUD	57.	RPD1002.1AND
25.	RPD194.2GEO	58.	RPD1005.1VIR
26.	RPD193.5MAR	60.	RPD1018.1TSH
27.	RPD195.3CHR	61.	RPD1107.2BIA

Table 5.1. CA4 screen cohort. The cohort for the screening of the CA4 gene for mutations, included 56 patients with dominant RP, in whom causal mutations had as yet not been identified. Note that although the patients are numbered up to 61, the cohort also includes 5a, while patient numbers 29, 50, 51, and 52, 55 and 59 were not included in the study.

dHPLC screening of amplicon 2 at 61.5°C and 62.2°C revealed variant profiles in six samples (6, 10, 22, 25, 41 and 56) (Fig. 5.2a). When these samples were sequenced (Fig. 5.2b), the variation was shown to be due to spurious changes in the dHPLC profiles, and not actual nucleotide sequence changes. Similar results were obtained for the screening of exon 7 at 61.4°C and 62.4°C. One sample showed variant profiles at both these temperatures (Fig. 5.3a). However, when this sample was sequenced (Fig. 5.3b), no sequence changes compared to the reference sequence were observed.

(a)

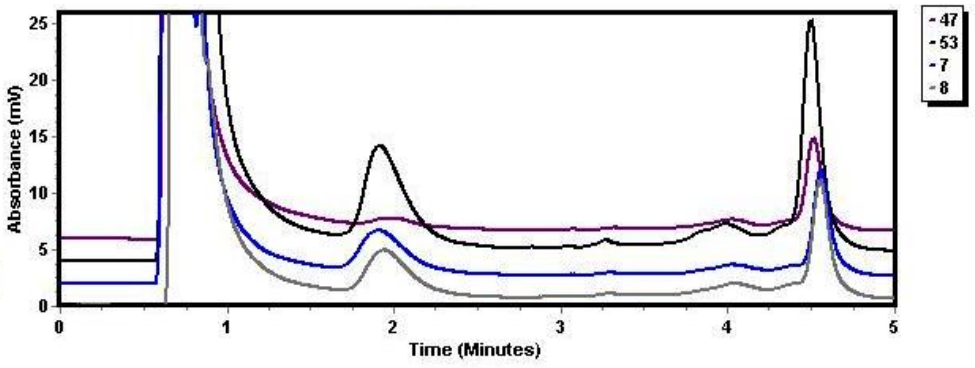

(b)

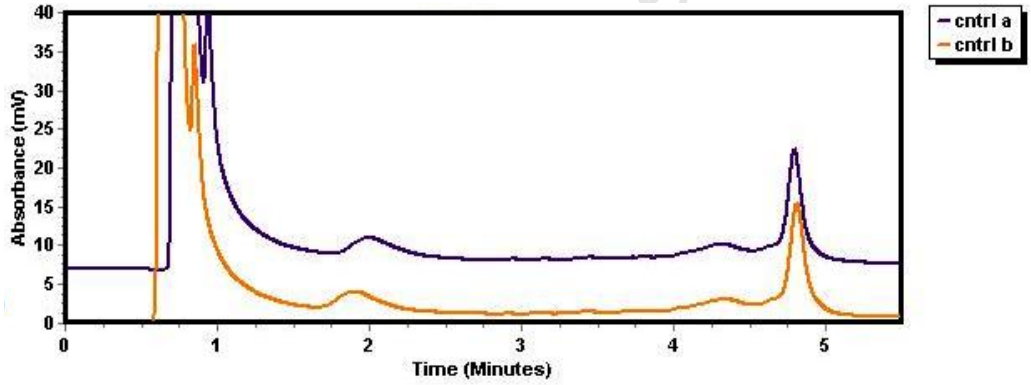

Figure 5.1. No samples showed variation in the elution profile of amplicon 3/4. A dHPLC chromatogram showing the elution profile of amplicon 3/4. (a) All samples in the cohort (samples 8, 7, 53 and 47 are shown in (a) displayed identical peaks to that of the control peak (b); indicating that no variants existed. These results were observed at both 61.4°C and 62.0°C.

The false positive results observed in amplicons 2 and 7 are likely due to incomplete optimisation of the dHPLC, because this method has been reported to be very reliable, with a less-than 1% error rate (Buyse and Roa, 2003; Crépin et al. 2006; Fasano et al. 2005; Liu et al. 1998). The 56 samples analysed were therefore considered to contain no nucleotide changes from the wild type/control sequence in amplicons 2, 3/4, and 7.

(a)

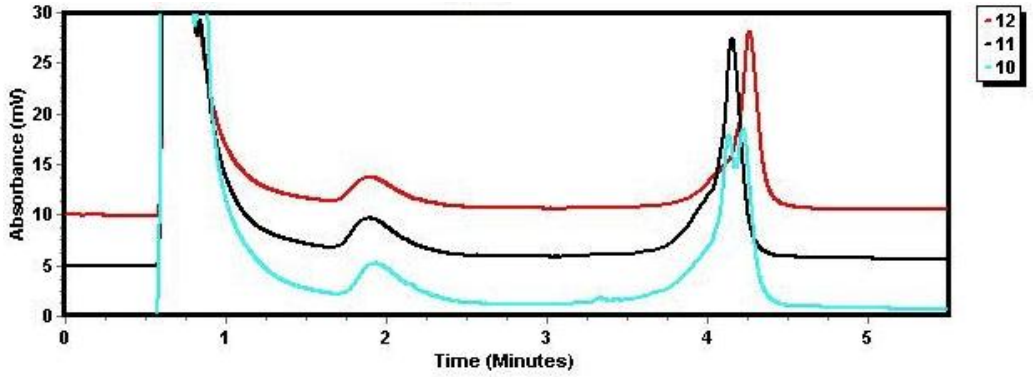

Figure 5.2a. Six samples displayed variant elution profiles of amplicon 2. dHPLC analysis of amplicon 2 at 61.5°C (shown) and 62.5°C identified six samples (number 6, 22, 25, 42 and 56 as well as 10, which is shown here) with variant profiles compared to those of normal samples (11 and 12) .

(b)

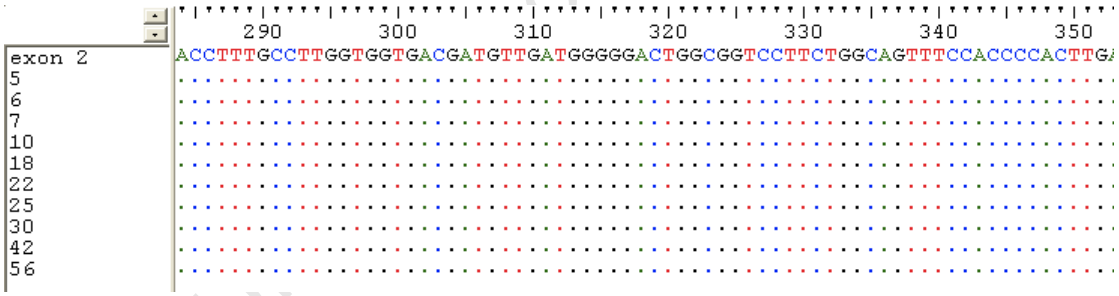

Figure 5.2.b Sequencing showed the variant elution profiles in amplicon 2 to be due to spurious changes. When six samples showing variant elution profiles were sequenced, no actual sequence changes compared to normal samples (5, 7, 18, and 30) were observed.

(a)

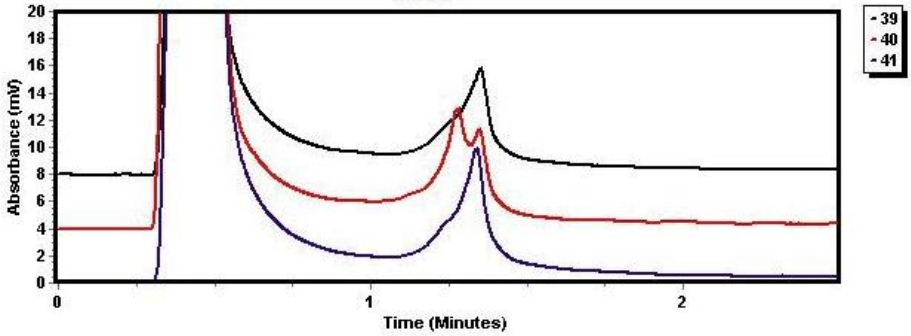

(b)

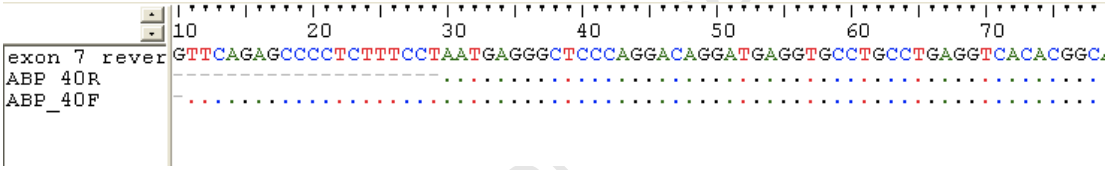

Figure 5.3. A variant elution profile in exon 7 of one sample was due to spurious changes. (a) dHPLC analysis of exon 7 at 61.4°C and 62.4°C (shown) identified one sample (number 40) with a variant profile compared to those of normal samples (39 and 41). When this sample was sequenced (b), no actual sequence changes compared to the reference sequence (exon 7 reverse, top sequence) were observed.

5.2. Amplicons that showed dHPLC profile variants

Upon performing dHPLC on exon 1a3-2 of the cohort, variants in the elution profile of eleven samples (18, 32, 33, 35, 36, 40, 42, 43, 48, 56 and 60) were detected. Nine of these samples (18, 32, 33, 40, 42, 43, 48, 56 and 60) showed variant profiles at 65.8°C, while eight showed variant profiles at 66.8°C (18, 32, 35, 36, 42, 43, 48 and 60). Among the variant elution profiles, two common variant patterns were observed at each temperature (Fig. 5.4a and b). However, due to the irregular shape of the control and wild type peaks ((28 and 47 in (a), and 18 and 20 in (b)), and the relatively short elution time of the DNA (x-axis), all eleven samples were sequenced.

All eleven samples with variant amplicon 1a3-2 dHPLC profiles were sequenced (Fig. 5.4c). Results revealed a heterozygous c.-316G>C nucleotide change in the 5'UTR region of the gene of only one of the samples (number 40) (Fig. 5.4d). This change was found upstream of the promoter, and had not been previously reported.

(a)

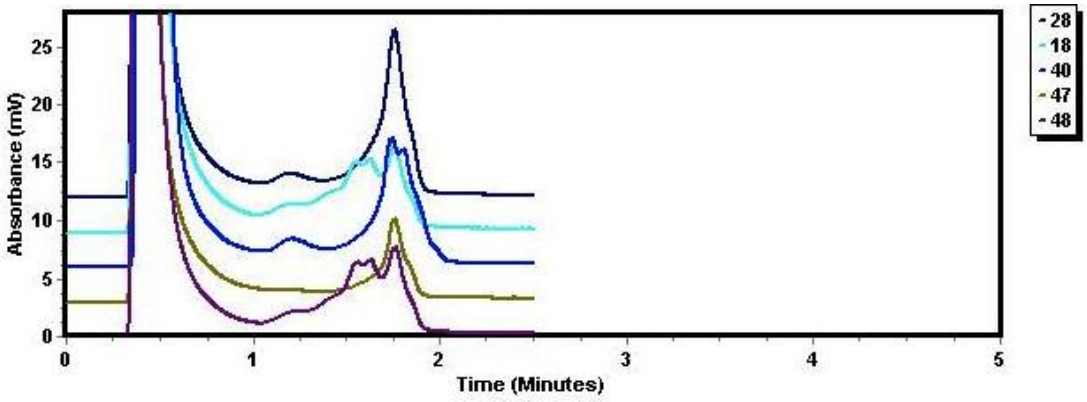

(b)

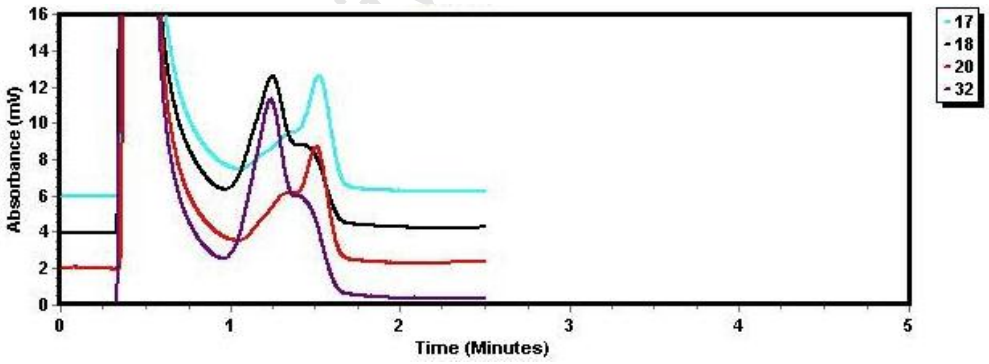

Figure 5.4a and b. Eleven samples showed variant dHPLC elution profiles in amplicon 1a3-2. dHPLC analysis of exon 1a3-2 identified eleven samples (samples 18, 32, 33, 35, 36, 40, 42, 43, 48, 56 and 60) with variant profiles compared to those of normal samples. (a) Nine of the samples (32, 33, 42, 43, 56 and 60 as well as 18, 40 and 48 which are shown) showed variant profiles at 65.8°C compared to normal samples (28 and 47). (b) Eight samples (35, 36, 42, 43, 48 and 60 as well as 18 and 32 which are shown) showed variant profiles at 66.8°C compared to normal samples (17 and 20). Note that two types of variant profiles from the normal profile were observed at each temperature.

(c)

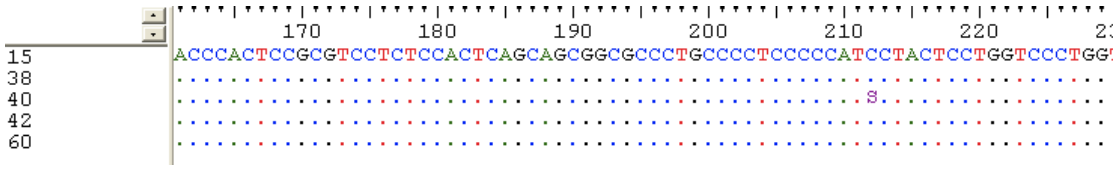

(d)

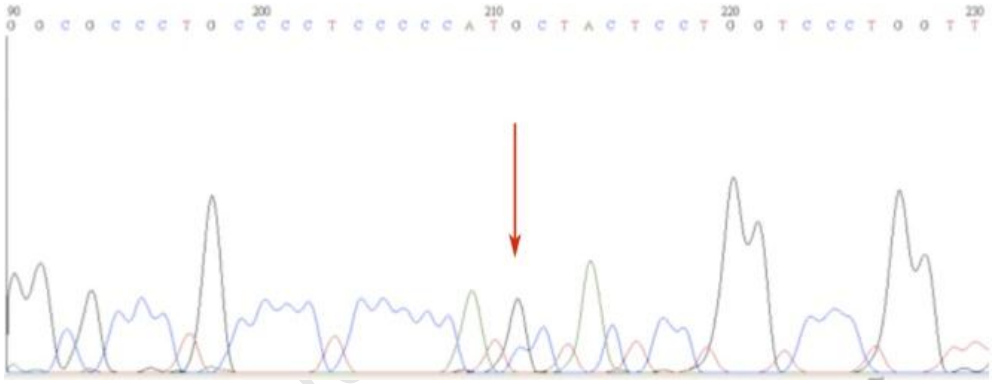

Figure 5.4c and d. Sequencing of eleven samples with variant dHPLC elution profiles in amplicon 1a3-2 revealed a G>C nucleotide change in one sample only. When all eleven samples with variant profiles were sequenced (only 40, 42, and 60 are shown) (c), a heterozygous G>C change, compared to normal samples 15 and 30, was discovered in sample 40 (red arrow) (d).

Screening of amplicon 5/6 by dHPLC analysis revealed four samples (20, 33, 40 and 45) to have variant profiles at both 61.4°C and 62.5°C (Fig. 5.5a). While all of these samples shared a common variant profile, when they were sequenced only sample 20 was shown to have a sequence that varied from the wild type sequence (Fig. 5.5b). This heterozygous G>A nucleotide change in sample 20 was identified as a reported single nucleotide polymorphism (SNP), rs 117704637. The nucleotide substitution (c.700G>A) has a minor

allele frequency of 0.006/5 and results in a missense amino acid change (Val234Ile) that is reported to have no clinical significance.

(a)

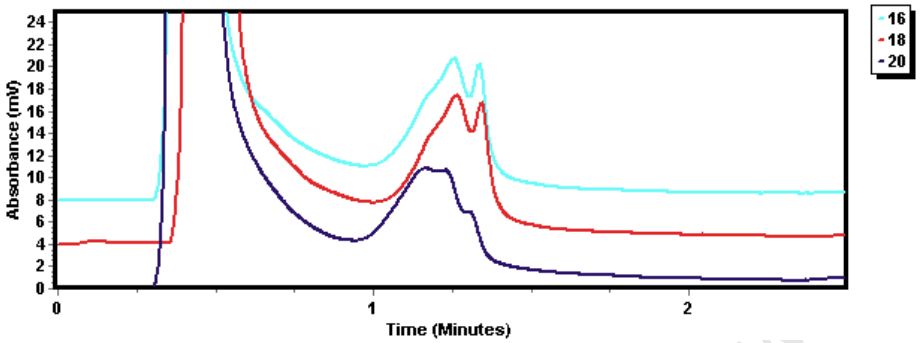

(b)

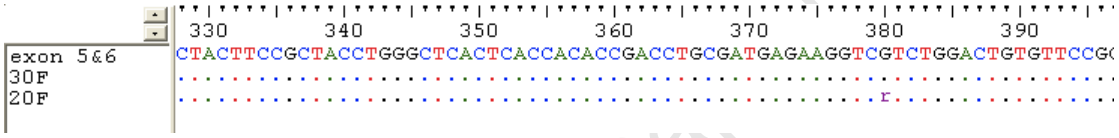

(c)

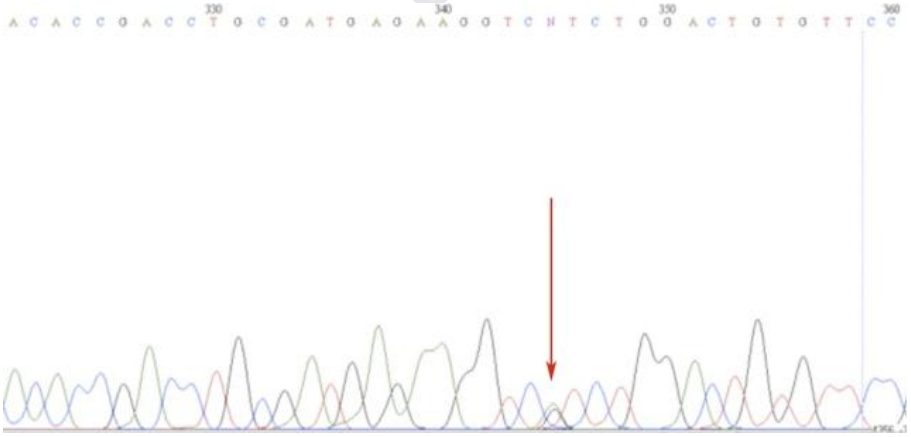

Figure 5.5. Four samples showed variant dHPLC elution profiles in amplicon 5/6. dHPLC analysis of amplicon 5/6 identified four samples (samples 20, 33, 40 and 45) with variant profiles compared to those of normal samples (16 and 18). All four samples showed these variant profiles at temperatures of 61.4 and 62.5 (shown). When the four samples with variant profiles were sequenced (only 20 and 30 are shown) (b) only one of them showed a sequence variant. (c) The variant observed during dHPLC analysis of amplicon 5/6 revealed a heterozygous G>A change compared to the reference sequence, in sample 20 (red arrow). Further analysis showed this change to be a previously-reported SNP.

5.3. Amplicons screened by sequencing only

Due to the difficulty in screening exons 1a3-1 and 1b using dHPLC analysis, these two amplicons were screened by sequencing only. Results from sequencing of exon 1a3-1 revealed three common nucleotide changes, namely G>T, G>C and C>G. The G>T nucleotide change was observed in fourteen samples (5a, 8, 17, 18, 28, 32, 33, 40, 42, 43, 44, 48, 56 and 57) (Fig. 5.6a). This variant (c.58+72G>T) was identified as a reported SNP (rs 58771049) that has a minor allele frequency of 0.117/147. While samples 18 and 48 had the T allele only at this position, the rest of the samples were heterozygous. The high frequency of the SNP in this cohort (14 out of 56 patients) compared to the general population is interesting, and may indeed be linked to a disease causing mutation, or may merely be due to shared inheritance of a common haplotype.

Two samples (8 and 56) were heterozygous for a G>C nucleotide change (Fig. 5.6b) at position c.-24. Analysis of this variant revealed it to be a reported SNP (rs 345191) with a minor allele frequency of 0.18/23. The third nucleotide change identified during analysis of exon 1a3-1 was a homozygous C>G change identified in samples 3 and 8 (Fig. 5.6c). This 5'UTR variant, at position c.-161 had not been described previously. The nucleotide change was analysed using the online splice prediction tools at the Karolinska Institute (http://mordor.cgb.ki.se/cgi-bin/CONSITE/consite) and the Berkley Drosophila Genome Project (http://www.fruitfly.org/ seq_tools/splice). The sequence containing the change was also analysed for changes in transcription factor binding sites using the online TESS (transcription element search system) tool (Shug and Overton, 1997; http://www.cbil.upenn.edu/cgi-bin/tess/tess). Using these analyses, no changes in splicing or in the binding sites were predicted. These nucleotide changes were therefore not predicted to be behind the RP phenotype in these patients.

(a)

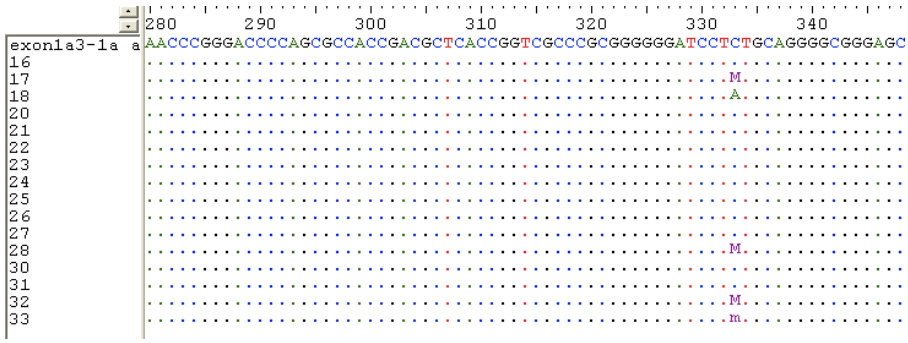

(b)

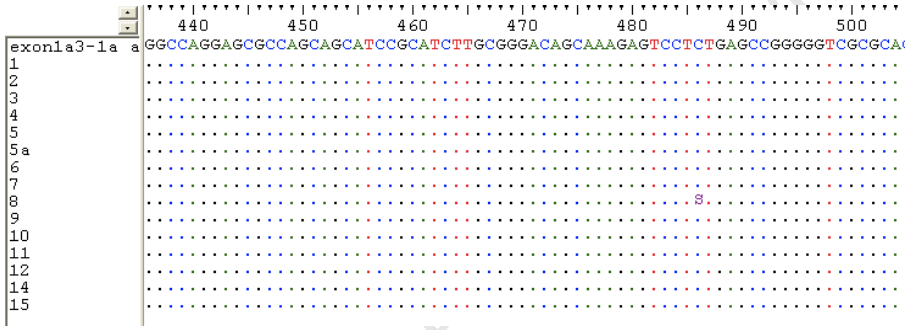

(c)

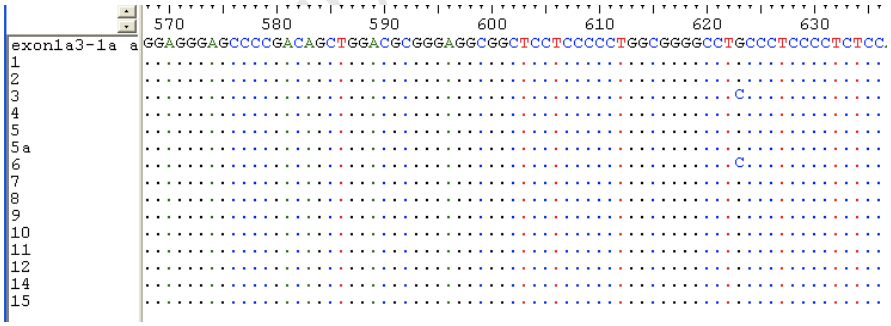

Figure 5.6 Sequencing of exon 1a3-1 revealed three nucleotide changes. (a) Fourteen samples (samples 5a, 8, 17, 18, 28, 32, 33, 40, 42, 43, 44, 48, 56 and 57) showed G>T nucleotide changes at position c.58+72 compared to the reference sequence (top sequence). Samples 18 and 48 (not shown) had only the T allele at this position, while the other samples were heterozygous. (b) Two samples (8 and 56) showed heterozygous G>C nucleotide changes at position c.-24 compared to the reference sequence. Note that the sequences shown are on reverse strands. (c) A third nucleotide change at position c.-161 was identified during analysis of exon 1a3-1. This homozygous variant was identified in two samples (3 and 8). Note that the sequences shown are on reverse strands.

Sequencing of exon 1b revealed that three samples shared a common variant. In these three samples (31, 33 and 37), an unreported A>C nucleotide change was discovered at position c.59-46 (Fig. 5.7). Since the change occurred in a non-coding (intronic) region, the nucleotide substitution was analysed using the same prediction tools as described above. Using these analyses, no changes in splicing or in transcription factor binding sites were predicted. As with the 5'UTR amplicon 1a3-1 variant, this nucleotide change was also therefore not predicted to be behind the RP phenotype.

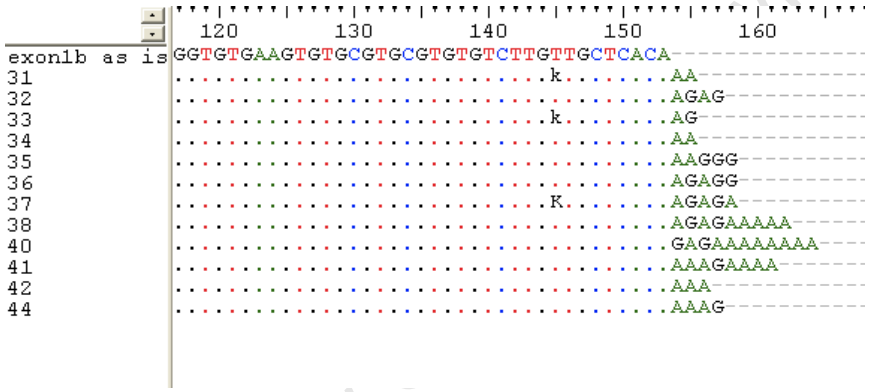

Figure 5.7. Sequencing of exon 1b revealed a nucleotide change in three samples. Samples 31, 33 and 37 showed A>C nucleotide changes at position c.59-46 compared to the reference sequence (top sequence).

The results of the mutation screen of *CA4* in the adRP cohort have been summarised in a table below (Table 5.2).

Table 5.2. *CA4* screen summarised results

Exon	Nucleotide change	Reported/Novel	Disease causing?
1a3-1	c.58+72 G>T	Reported (rs58771049)	No
1a3-1	c.-24 G>C	Reported (rs345191)	No
1a3-1	c.-161 A>C	Novel	Not predicted to be
1a3-2	c.-316 G>C	Novel	Not predicted to be
1b	c.59-46 A>C	Novel	Not predicted to be
5/6	c.700 G>A	Reported (rs117704637)	No

6. Cystic Fibrosis Transmembrane conductance Regulator mutation (ΔF508) screen in the RP17 cohort

A report published by Fanjul et al. (2002) studied the relationship between the Cystic Fibrosis Transmembrane conductance Regulator (CFTR) protein and CAIV in a human pancreatic duct cell line. The results of their study showed that in cells expressing a mutated (ΔF508) CFTR protein, CAIV was not transported to the plasma membrane. The current study therefore sought to determine what possible effect a combination of the mutant CFTR would have on an individual with the R14W CAIV mutation. Fifty-two patients in the UCT RP17 cohort were therefore screened for the ΔF508 mutation in the CFTR gene (Fig. 6.1). Size-based genotyping was carried out by DNA sequencing using fluorescently-labelled primers, and the records of mutation positive individuals were analysed for lung or pancreatic phenotypes associated with cystic fibrosis.

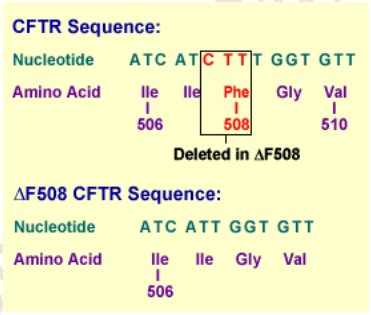

Figure 6.1. Region of the CFTR gene containing the ΔF508 mutation. The three base-pair (CTT) deletion in the CFTR gene results in the deletion of a phenylalanine residue at position 508.

The results of the screen revealed that one patient had a heterozygous ΔF508 mutation (Table 6.1). This was evidenced by the generation of a 90 bp as opposed to a 93 bp (as expected) fragment when the region was amplified by PCR, and the 3 bp deletion on one allele could clearly be seen during genotyping analysis (Fig. 6.2).

When the records of patient RPD8.80JAN were analysed there was no evidence of a lung, pancreatic, or more extreme ocular phenotype than would be expected. There was also no evidence of an aggravated retinal phenotype (for example, an earlier age of onset than expected, or rapid progression of the disease). In fact, records showed that for patient

RPD8.80JAN, age of onset of RP symptoms was 24 years (which is near the average age for adRP, and above that of many other patients in the cohort). The patient had reported night blindness, but unaffected day vision, at the time of testing (1995). In attempting to track the inheritance of the CFTR mutation, samples from family members of patient RPD8.80JAN were also examined. Of two siblings, only one was tested and results were negative. The father who had RP and was included in this cohort (RPD8.7STE), tested negative for the CFTR deletion. The CFTR mutation must therefore have been passed to this patient on the maternal allele. Samples had not been collected from the mother of patient RPD8.80JAN since she tested negative for the R14W CAIV mutation and her DNA was therefore not catalogued on the database.

Patient number	Patient identifier	CFTR genotyping result (ΔF508 mutation)
1.	RPD8.1FLO	NEGATIVE
2.	RPD8.5VIV	NEGATIVE
3.	RPD8.11RON	NEGATIVE
4.	RPD8.13LPB	NEGATIVE
5.	RPD8.14FMB	NEGATIVE
6.	RPD8.15AJB	NEGATIVE
7	RPD8.17BJH	NEGATIVE
8.	RPD8.18LDB	NEGATIVE
9.	RPD8.24WIL	NEGATIVE
10	RPD8.29ISA	NEGATIVE
11	RPD8.33WIE	NEGATIVE
12	RPD8.32LEV	NEGATIVE
13	RPD8.39FRA	NEGATIVE
14	RPD8.43LIN	NEGATIVE
15	RPD8.49RUD	NEGATIVE
16	RPD8.54LIZ	NEGATIVE
17	RPD8.58MAR	NEGATIVE
18	RPD8.78STE	NEGATIVE
19	RPD8.83JAN	POSITIVE
20	RPD8.85CRF	NEGATIVE
21	RPD8.93JAM	NEGATIVE
22	RPD8.94MIL	NEGATIVE
23	RPD17.1DOK	NEGATIVE
24	RPD17.4MIC	NEGATIVE
25	RPD17.5KEV	NEGATIVE
26	RPD18.1MER	NEGATIVE
27	RPD18.2MAU	NEGATIVE
28	RPD18.9ENR	NEGATIVE
29	RPD18.18VER	NEGATIVE
30	RPD18.20AND	NEGATIVE
31	RPD18.21JOA	NEGATIVE
32	RPD18.22DIA	NEGATIVE
33	RPD18.26PET	NEGATIVE
34	RPD18.33NAT	NEGATIVE
35	RPD18.34PEN	NEGATIVE
36	RPD18.45DYL	NEGATIVE
37	RPD18.50DAR	NEGATIVE
38	RPD61.9KAR	NEGATIVE
39	RPD61.11JEA	NEGATIVE
40	RPD61.13AMO	NEGATIVE
41	RPD61.16CAR	NEGATIVE
42	RPD61.20MIC	NEGATIVE
43	RPD61.22SHA	NEGATIVE
44	RPD61.28ALM	NEGATIVE
45	RPD61.29JUL	NEGATIVE
46	RPD81.1JOH	NEGATIVE
47	RPD81.3JAM	NEGATIVE
48	RPD81.5JOA	NEGATIVE
49	RPD81.9CHI	NEGATIVE
50	RPD81.11JAF	NEGATIVE
51	RPD81.12ROB	NEGATIVE
52	RPD81.13LEE	NEGATIVE

Table 6.1. Results from CFTR ΔF508 mutation screen in RP17 cohort. 52 patients from the RP17 cohort (with the R334W mutation + CAIV) were screened for the 3 bp deletion in the CFTR gene that results in the ΔF508 mutation in the protein. PCR was performed in order to amplify the region of the CFTR gene, and samples were screened by genotyping using fluorescently-labelled primers.

(a) WT CFTR DNA

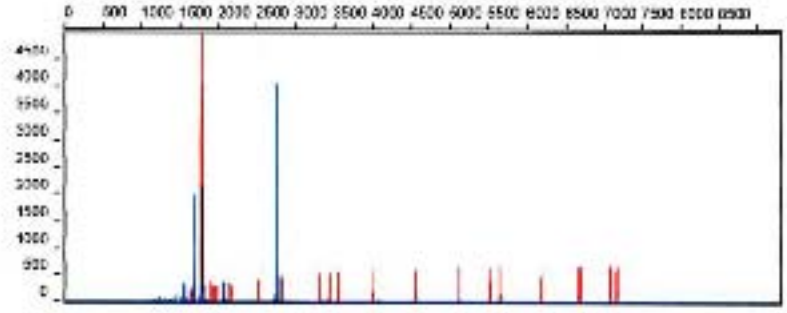

(b) Homozygous CFTR ΔF508 mutant

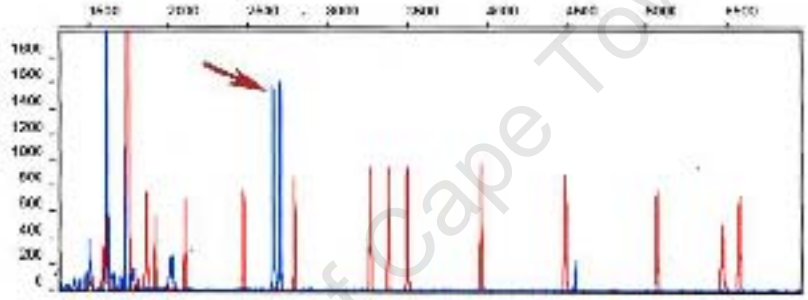

(c)

7B, 1	18	7.09	92.95	4061	37952	2660
8B, 1	2	7.18	92.91	4816	45169	2692
9B, 1	34	7.14	92.91	3771	35294	2678
10B, 1	10	7.07	92.95	2711	25103	2652
11B, 1	26	7.00	92.93	3071	27981	2625
12B, 1	42	7.04	92.89	3049	28110	2641
13B, 1	19	7.09	89.76	1586	15336	2657
13B, 2	19	7.19	92.92	1607	15281	2696

Figure 6.2. Genotyping analysis on the region of the CFTR gene carrying the ΔF508 mutation. Electropherograms from genotyping of a region of the CFTR gene in samples from the RP17 cohort. (a) Most samples are homozygous for the wildtype sequence,as shown by the presence of 2 overlapping peaks corresponding to 93 bp. (b) One sample displayed a second peak prior the the 93 bp peak (red arrow), which corresponds to a fragment of 90 bp. This sample therefore likely has the 3 bp deletion in CFTR which causes the ΔF508 mutation in the protein. A chart showing the sizes of fragments confirms that the 3 bp deletion results in a 90 bp fragment (red arrow), as opposed to the 93 bp WT fragment. Red signals in the electropherograms represent size standards. The sizes of fragments are automatically determined by comparison with an internal standard DNA ladder, GS-.000.

7. Molecular study of RP17 phenotype

The first sections of this study have sought to define and characterise the effects of the R14W mutation at the phenotypic and genotypic level. The results showed that there is significant variation in the age of onset of symptoms of RP17. Furthermore, the age of onset for many RP17 patients is earlier than that for other dominant forms of RP (Daiger et al. 2007). This study also explored the idea of a CAIV/CFTR metabolon and investigated the possible effects of a compound CAIV/CFTR mutation. Interestingly, the patient in whom a compound mutation was found, did not show any worsened ocular (or any other) phenotype. A genetic screen on patients in the adRP cohort was also performed, and did not identify any novel CAIV mutations. The next section of this study further investigated the molecular mechanisms which underlie the RP17 disease phenotype.

As mentioned in Chapter 1, previous research attempting to define the underlying cause of disease in RP17 has been controversial. Specifically, while most research has shown apoptosis to be the cause of cell death in RP17 (Bonapace et al. 2007; Datta et al. 2008; Datta et al. 2010; Rebello et al. 2004), the molecular mechanisms leading to this apoptosis have yet to be conclusively identified. In this section, three different cell lines (COS-7, HEK-293 and HT-1080 cells) were transiently transfected with the WT- or R14W mutant-CAIV, and used as cell models in which to identify the molecular mechanisms that lead to the death of cells expressing the R14W mutant protein.

7.1 Expression of R14W mutant CAIV in COS-7 cells leads to cell cycle arrests

Previous reports suggested that the R14W mutation in CAIV may be causative of RP17 by inducing ER-stress and apoptosis (Bonapace et al. 2007; Datta et al. 2008; Rebello et al. 2004). To further explore this, FACS analysis was used to determine whether cells expressing the R14W mutation undergo cell cycle arrest, which, if not reversed or corrected, has been shown to lead to apoptosis (Pham et al. 2003; Weinberg, 2005). Briefly, COS-7 and HEK-293 cells were transiently transfected with the pCXN

expression vector encoding either WT- or R14W CAIV and their cell cycle profiles were analysed 72 h later.

Results showed that while the COS-7 cells expressing WT CAIV have a cell cycle profile typical of normal dividing cells (Fig. 7.1a and b), ectopic expression of R14W mutant CAIV in these cells resulted in an S and G2/M cell cycle arrest (Fig. 7.1c). In contrast to COS-7 cells, HEK-293 cells expressing either the WT- or R14W mutant-CAIV, displayed comparable cell cycle profiles and had similar numbers of cells at S and G2/M (Fig. 7.1d, e and f). These results showed that whereas expression of the R14W mutant CAIV protein in COS-7 cells induced cellular stress that triggered cell cycle arrests, it had no effect on the HEK-293 cells. It is particulary interesting to note that HEK-293 cells are of kidney origin, and that RP17 patients show no kidney phenotype. The HEK-293 cell line may therefore provide an ideal system in which to elucidate the molecular mechanisms behind the lack of an RP17 kidney phenotype. HT-1080 cells could not be analysed by cell cycle analysis because they exhibit polyploidy, making it difficult to study their profile (Fig. 7.1g).

7.2. Expression of R14W mutant CAIV induces apoptosis in COS-7 and HT-1080 cells

Since FACS analysis showed that expression of R14W CAIV causes cell cycle arrest in COS-7, but not HEK-293 cells, futher analyses were conducted to determine the effect of the mutant CAIV protein on apoptosis. To this end, COS-7, HT-1080 and HEK-293 cells were transfected with the same expression constructs used in section 7.1, and stained with propidium iodide (PI) and Annexin V-FITC for flow cytometry. Annexin V is an impermeable dye that binds to phosphatidylserine on the cell membrane when cells undergo apoptosis. Apoptotic cells were measured by positive staining for both PI and FITC.

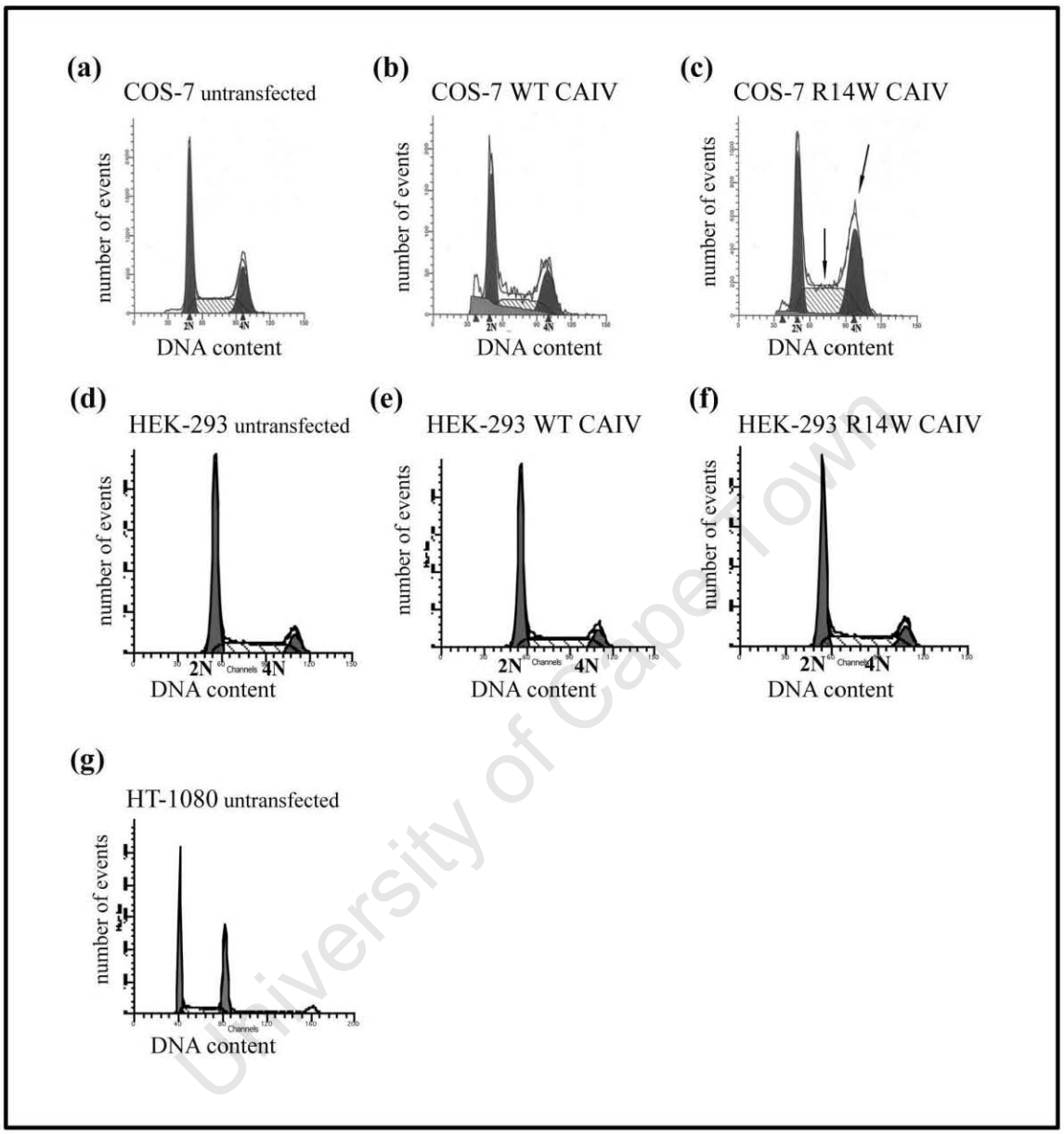

Figure 7.1. Expression of R14W mutant CAIV in COS-7 cells, but not HEK-293 cells, leads to S and G2/M phase cell cycle arrests. The cell cycle status of untransfected cells (a, d) or cells transfected with WT CAIV (b, e) or R14W MUT CAIV (c, f) was determined by measuring their DNA content using fluorescence-activated cell sorting analyses. Peaks at 2N and 4N DNA content represent the number of cells in the G1 and G2/M phases, respectively. The hatched areas represent the number of cells in S-phase. Light gray shaded areas along the x-axis represent cellular debris. Arrows in (c) point to S and G2/M cell cycle arrests. The effect of the R14W mutant CAIV protein on the cell cycle of HT-1080 cells (g) was not analysed due to the irregular profile of these polyploid cells, which made the study of HT-1080 cell cycles difficult.

The results for the COS-7 cells showed that whereas 20.7% of R14W mutant CAIV transfected cells underwent apoptosis, this was the case for only 5.8% of cells expressing the WT protein (Fig. 7.2a and b). Similarly, HT-1080 cells expressing the R14W mutant

CAIV (Fig. 7.2d) showed a 17.43% increase in the number of apoptotic cells compared to cells expressing the WT protein (0%) (Fig. 7.2c). In contrast, the numbers of HEK-293 cells that stained positive for FITC and PI were similar for cells expressing either the WT- or the R14W mutant CAIV protein (Fig. 7.2e and f). When the numbers of Annexin V-FITC/PI positive cells transfected with the R14W CAIV construct were compared to cells expressing WT CAIV protein it was shown that at least 3.5 times more COS-7, and 17 times more HT-1080 cells underwent apoptosis (Fig. 7.2g). Consistent with the cell cycle analyses shown in Figure 7.1, the number of apoptotic HEK-293 cells expressing either WT- or R14W mutant was comparable (Fig. 7.2g). These results again showed that HEK-293 cells, in contrast to COS-7 and HT-1080 cells, do not display adverse effects when expressing the R14W mutant CAIV protein in contrast to the WT CAIV.

7.3. R14W mutant CAIV protein is not processed to its mature form in COS-7 and HT-1080 cells

Taken together, the above results in COS-7 and HT-1080 cells provided additional evidence that expression of the R14W mutant CAIV protein causes apoptosis, which begged the question as to how this occurs, and why HEK-293 cells are able to tolerate the mutant form of CAIV. The mature CAIV protein results from post-translational processing which includes the formation of two disulphide linkages that compact the protein. As a result, mature CAIV migrates as a single 35 kDa band under non-reducing SDS-PAGE conditions, whereas the misfolded precursor protein migrates at 37 kDa (Rebello et al. 2004; Stams et al. 1996). It was previously hypothesised that expression of the R14W mutant CAIV protein in the COS-7 cells induced apoptosis due to improper post-translational processing and folding. To test this hypothesis in this study, protein from cells transfected with either WT- or R14W mutant-CAIV expression vectors was analysed by western blot analyses under reducing and non-reducing conditions.

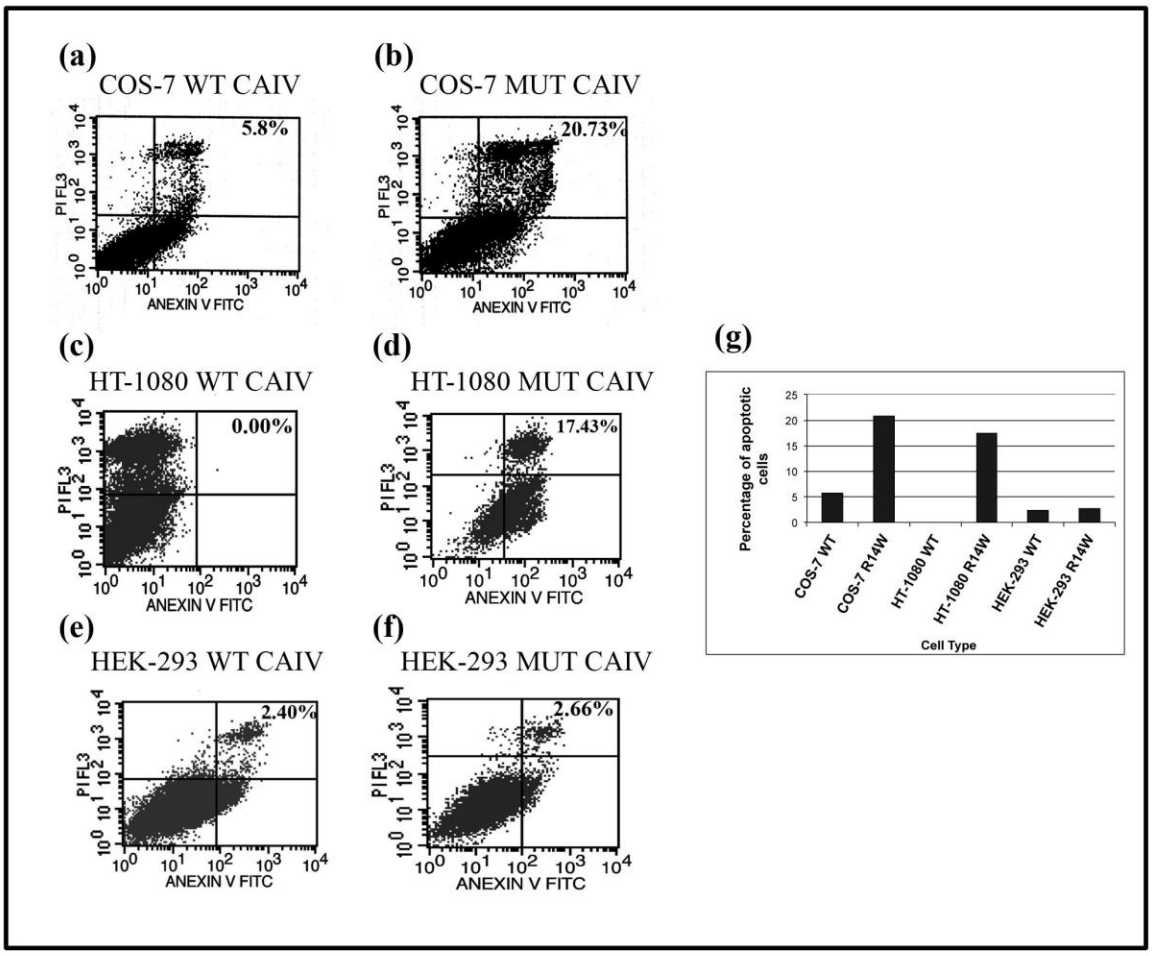

Figure 7.2. Expression of R14W mutant CAIV induces apoptosis in COS-7 and HT-1080 cells. (a, b) COS-7, (c, d) HT-1080 and (e, f) HEK-293 cells expressing either WT- or R14W mutant CAIV were stained with Annexin V-FITC and propidium iodide (PI) in order to quantify apoptosis by flow cytometry. In the histograms, values indicate the percentages of cells that stain positive for FITC/PI that are undergoing apoptosis (upper right-hand quadrant). The graph (g) shows the percentages of FITC/PI positive cells transfected with the R14W mutant CAIV compared to FITC/PI positive cells expressing WT CAIV for each cell line.

Results for COS-7 cells showed that while the R14W mutant protein migrated as a diffuse bandthe WT CAIV protein migrated as a single compact band that corresponds with the mature form of CAIV (Fig. 7.3a). The same results were obtained when these experiments were performed in the HT-1080 cells (Fig. 7.3a). To confirm that the difference in mobility of WT- and R14W mutant-CAIV protein is indeed due to disulphide bond formation, protein samples were also analysed by western blotting using reducing conditions. As seen in Figure 7.3b, the WT- and R14W mutant-CAIV protein migrated at the same rate under these conditions. These results thus provide support for

the hypothesis that the R14W mutation prevents the accurate processing and complete folding of the CAIV protein. Interestingly, and in line with the flow cytometry findings, the HEK-293 cells were able to process the WT- and R14W mutant-CAIV equally efficiently, as evidenced by the respective proteins migrating as single integral bands (Fig. 7.3a).

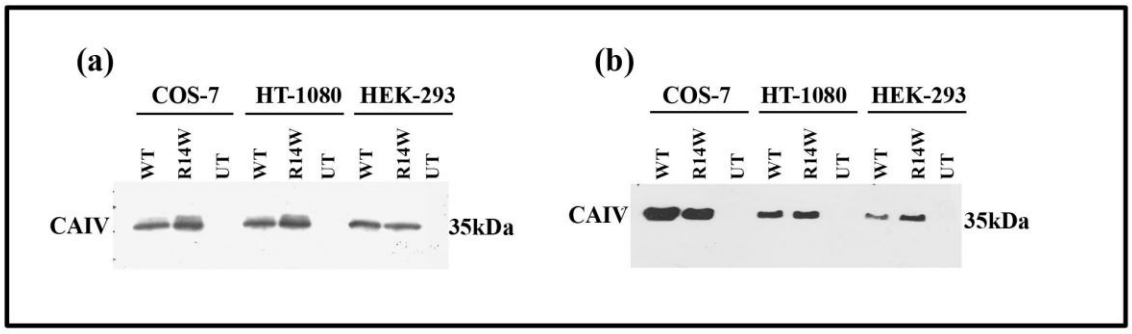

Figure 7.3. R14W mutant CAIV is not processed to its mature form in COS-7 and HT-1080 cells. Western blot analyses under non-reducing (a) and reducing (b) conditions were used to compare expression of CAIV from total protein (2µg) isolated from COS-7, HT-1080 and HEK-293 cells transfected with WT- or R14W MUT CAIV. Protein blots were probed with an antibody specific for CAIV and the protein detected by chemiluminescence. The retarded mobility of CAIV under non-reducing conditions in (a) is a measure of the immature protein.

7.4. R14W mutant CAIV forms ER-associated aggregates in COS-7 and HT-1080 cells

To further elucidate the mechanism by which the R14W mutant CAIV induced apoptosis, the hypothesis that it was due to the ER-retention of the misfolded and incompletely processed protein was tested. The subcellular localisation of transfected WT- and R14W mutant-CAIV protein in COS-7, HT-1080 and HEK-293 cells was therefore investigated by immunofluorescence. As expected, fluorescent imaging of all cells expressing the WT CAIV revealed that the protein was distributed throughout the cytoplasm and in particular along the plasma membrane (Fig. 7.4a). In contrast, in COS-7 and HT-1080 cells, the R14W mutant CAIV protein aggregated in regions around the cell nucleus where the rough ER is located (Fig. 7.4a). Interestingly, expression of R14W CAIV in HEK-293 cells resulted in subcellular localisation similar to that of the WT CAIV. Importantly, when COS-7 cells were transfected with WT- or R14W mutant-GFP-tagged CAIV

followed by staining with an ER-tracker dye and analysed by immunofluorescence, only the GFP-tagged R14W mutant CAIV protein co-localized with the ER (Fig. 7.4b). These results confirm that the R14W mutant CAIV protein is indeed retained in the ER in COS-7 cells, and that HEK-293 cells have the capacity to fold and process the R14W mutant form of CAIV.

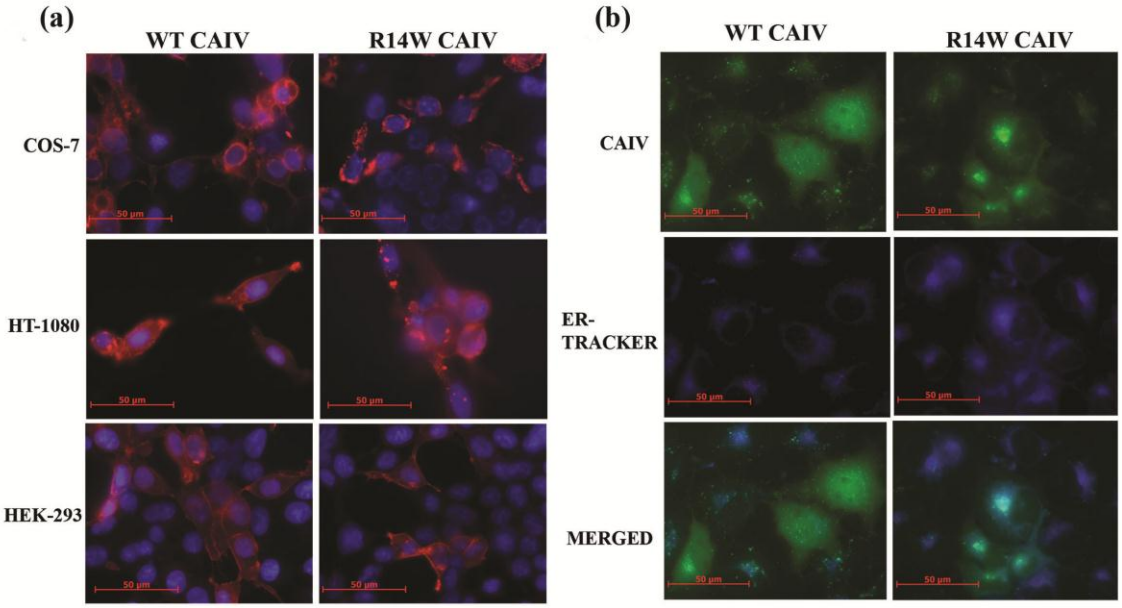

Figure 7.4. The R14W mutant CAIV protein forms endoplasmic reticulum (ER)-associated aggregates in COS-7 cells. (a) R14W mutant CAIV aggregates in a region corresponding to the ER in COS-7 and HT-1080 cells. COS-7, HT-1080 and HEK-293 cells expressing either pCXN-WT or pCXN-R14W CAIV were analysed by immunohistochemistry to determine the cellular localisation of WT- or R14W mutant CAIV protein. Cells were fixed, permeabilised, and treated with anti-CAIV antibody, followed by Cy3-conjugated secondary antibody, and visualised by fluorescence microscopy for DAPI (blue nuclear stain) and CAIV (red stain). **(b) The R14W mutant CAIV protein co-localises with the ER in COS-7 cells.** In order to determine whether R14W CAIV is retained in the ER, COS-7 cells were transfected with either pEGFPN1-WT CAIV or pEGFPN1-R14W CAIV and incubated in medium containing an ER-tracker dye. Live cells were visualised by flourescence microscopy and the green stain shows localisation of WT - and R14W CAIV protein while the ER stains blue. Scale bars represents 50µm.

The results from sections 7.1 to 7.4 provide a model for how expression of the R14W mutant CAIV protein causes apoptosis in cells in which it is expressed. They show that in COS-7 and HT-1080 cells the protein is incompletely processed and folded within the ER, leading to its retention in this organelle instead of progressing along the protein-folding pathway. The results also show that these cells expressing R14W mutant CAIV undergo cell cycle arrest, and it is likely that apoptosis results as a cause of cells remaining in a prolonged state of ERAD, UPR, and cell cycle arrest as a result of the misfolded protein.

7.5. COS-7 cells that stably express CAIV show similar effects to transiently-transfected cells

Experiments described above consistently showed that expression of R14W mutant CAIV in COS-7 cells elicits a response that leads to ER stress induced apoptosis as has been hypothesised to occur in RP17 patients. However, these results were obtained using transient transfections, which generally lead to much higher levels of protein compared to endogenous levels. To therefore exclude the possibility that the previously observed results were due to abnormal levels of CAIV protein, COS-7 cells were stably transfected with WT- and R14W mutant-CAIV. Since expression of R14W mutant CAIV has been shown to cause apoptosis, the ecdysone system was used to specifically generate stable, but inducible, CAIV cell lines (Materials and Methods, section 3.6). Briefly, COS-7 cells were stably transfected with the pERV3 construct and 600 μg/ml G418 antibiotic was added to medium to select for pERV3-expressing clones. The pERV3 vector encodes a receptor heterodimer composed of the ecdysone receptor (EcR) and the retinoid-X-receptor (RXR). This receptor heterodimer remains bound to a recognition element upstream of a promoter in the pEGSH inducible vector, keeping it transcriptionally silent until induction with Ponasterone A. Clones expressing pERV3 were isolated and expanded, and expression of receptor heterodimers was investigated using luciferase assays with a pEGSH-luc construct. Clones 3 and 5 showed the highest relative luciferase activity (i.e. induced/uninduced) (Fig. 7.5) and were therefore selelcted for stable transfection with the pEGSH vector containing the full-length WT- or R14W mutant *CA4* cDNA.

As previously described, 200 μg/ml Hygromycin B antibiotic was then used to select for clones expressing the pEGSH-*CA4* construct. Positive clones were selected and expanded, and CAIV protein expression induced with Ponasterone A. Western blot experiments revealed that WT clones 2, 3 and 4 and MUT clones 5 and 6 showed strong induction of CAIV protein (Fig. 7.6) and were therefore selected for further analyses.

(a)

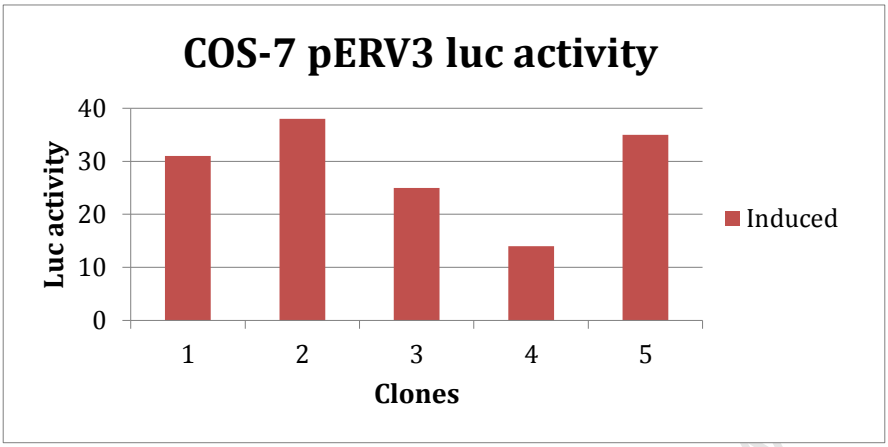

(b)

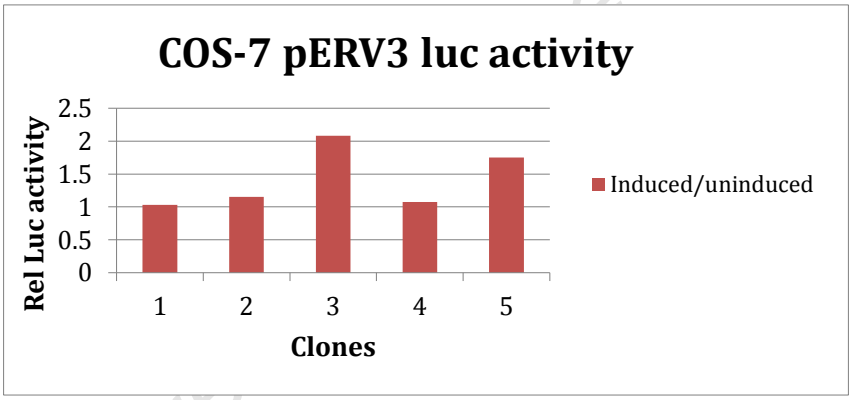

Figure 7.5. Luciferase assays carried out to select COS-7 pERV3 clones with the highest expression of the pERV3 response elements. COS-7 pERV3 clones were transiently transfected with a pEGSH-luc vector and expression of luciferase induced with Ponasterone A. The clones that showed both the highest luciferase activity (a) and the highest relative luciferase activity (b) were selected for stable transfection with pEGSH-*CA4*.

7.5.1. Stably-expressed R14W mutant CAIV is misfolded and retained in the ER of COS-7 cells

In order to investigate folding and processing of CAIV in COS-7 cells stably expressing WT- and R14W mutant-CAIV, protein extracts were analysed by western blot analysis. More specifically, this was carried out to determine whether stably expressed R14W

mutant CAIV is incompletely processed, as was observed in COS-7 cells that were transiently expressing the protein. COS-7 cells were induced to express CAIV with 5 ng/ml Ponasterone A 24 h after plating, and cells were harvested 20 h later for western blot analysis (under non-reducing conditions) using an anti-CAIV antibody.

Results, shown in Figure 7.6, were consistent with those observed for the transiently transfected protein shown in section 7.3. While WT CAIV was predominantly present as a single band of 35 kDa in size, an additional ~37 kDa band, representing unfolded precursor protein, was observed for R14W mutant CAIV. In all samples, an additional fast-migrating band (indicated by an asterisk) was observed which is presumed to be due to non-specific binding of the CAIV antibody to another carbonic anhydrase. Interestingly, as opposed to transiently expressed CAIV, of which 2 µg was loaded onto acrylamide gels, 20 µg of the stably expressed protein was loaded in order for the protein to be detectable. This indicated that the stably integrated protein was present at lower levels than that of the transiently-expressed CAIV. These results confirmed that stably transfected protein is present at lower levels that may mimic more closely the levels of endogenous protein expressed, for example, in the choriocapillaris cells.

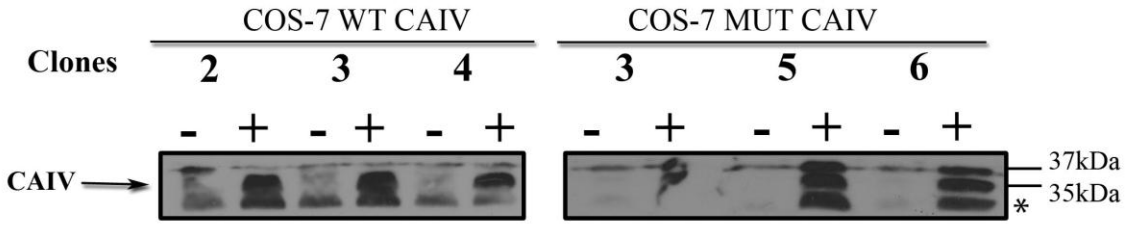

Figure 7.6. R14W CAIV is incompletely processed in COS-7 cells which stably express the mutant protein. Western blot analyses were used to show expression of of WT- and R14W mutant CAIV from total protein (20 µg) isolated from COS-7 cells which were induced to express the stably transfected protein. (-) cells are uninduced, while (+) cells have been treated with the Ponasterone A inducer. Protein blots were probed with antibodies for CAIV and detected by chemiluminescence. A low-moecular weight band (asterisk) indicates non-specific antibody binding.

It was next investigated whether stably expressed R14W mutant CAIV is retained within the endoplasmic reticulum as had been observed with the transiently expressed mutant protein. Briefly, cells were plated as before onto glass coverslips, induced with Ponasterone A 24 h after plating, and processed for immunofluorescence 20 h after induction.

Results from immunofluorescence studies with WT clone 2 and MUT clone 5 are shown in Fig. 7.7. While the stably expressed WT CAIV was present throughout the cell cytoplasm, the R14W mutant form of the protein showed perinuclear localisation. An ER-tracker dye could not be used to verify localisation of R14W mutant CAIV, as the stain cannot be used on cells that have been permeabilised and fixed. However, based on previous experiments (section 7.4), this perinuclear localisation is believed to indicate ER retention. It must be noted that the WT form of the protein was not found along the cell membrane as was observed with transiently expressed WT CAIV, perhaps due to the lower levels of the stably expressed protein.

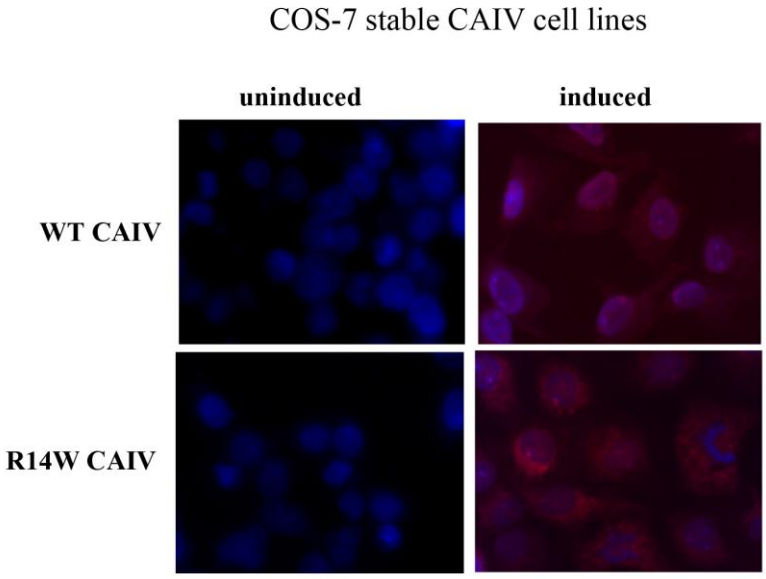

Figure 7.7. Stably expressed R14W mutant CAIV forms aggregates in COS-7 cells. COS-7 cells stably expressing either WT or R14W mutant CAIV were analysed by immunohistochemistry to determine the cellular localisation of the CAIV protein. Cells were fixed, permeabilised, and treated with anti-CAIV antibody, followed by Cy3-conjugated secondary antibody and visualised by fluorescence microscopy for DAPI (blue nuclear stain) and CAIV (red stain).

Taken together, the above results confirmed that the results obtained for the transient transfections were not due to abnormally high levels of transfected CAIV protein, but were as a result of the R14W mutation.

8. Short hairpin (shRNA) silencing of CAIV

Previous studies on RP17 (Bonapace et al. 2004; Datta et al. 2008) have suggested the use of carbonic anhydrase inhibitors as therapy for the disease. These molecules have historically been used in the treatment of cystoid macular oedema, which is associated with RP. The toxicity of and resistance to the treatment over time (Grover et al. 2005; Melo et al. 2007; Ozdemir et al. 2005; Saraiva et al. 2003) however, have repudiated the use of CA inhibitors, and necessitated research into other forms of therapy. Furthermore, the specific use of CA inhibitors to treat macular oedema in RP17 patients has resulted in no improvement in vision (Professor Ari Ziskind, personal communication, 2010), supporting the need for the development of other therapies such as RNAi.

This study therefore considered the possibility that allele-specific silencing of the R14W mutant CAIV could be achieved by RNAi. This is a cellular mechanism of gene silencing in which a short strand of introduced RNA is used to target a complementary strand of mRNA for degradation (Boudreau et al. 2008). While siRNA was popular in the early 2000s, shRNA has been shown to achieve longer lasting knockdown of gene expression with much smaller amounts of RNAi required (Yu et al. 2002; Rao et al. 2009).

8.1. Allele-specific shRNA silencing of CAIV

To explore the use of allele-specific shRNA as a putative therapy for RP17, three different shCAIV constructs, referred to as constructs 10, 15 and 16, were designed (Fig. 3.1). These constructs were transiently co-transfected with pCXN expression vectors encoding either the WT- or R14W mutant-CAIV, into COS-7, HT-1080, and HEK-293 cell lines. To control for off target effects, a scrambled control shRNA (shSCR) was included in all experiments and the efficacy of knockdown for each of the three shCAIV constructs was monitored by western blotting using an anti-CAIV antibody (Fig. 8.1 a, b

and c). Densitometric readings for each band are compared to each other in a bar graph as part of Figure 8.1.

The results obtained for COS-7 cells (Fig. 8.1a) showed that 24 h after co-transfection with shCAIV construct 15, protein levels of R14W mutant CAIV were undetectable compared to cells co-transfected with WT CAIV or the shSCR construts. These results suggested that shCAIV construct 15 is effective and specific for knockdown of R14W mutant CAIV. In contrast, knockdown of R14W mutant CAIV by construct 16 was marginal. Surprisingly, construct 10 was efficient in reducing levels of WT CAIV, but led to an increase in expression of the R14W mutant CAIV protein. Based on these results construct 15, from here on referred to as shCAIV15, was used in further analyses to examine the effects of knockdown of R14W mutant CAIV in COS-7 cells.

In HT-1080 cells (Fig. 8.1b), transfections with all three constructs resulted in complete knockdown of the R14W mutant CAIV protein. Unfortunately, compared to the shSCR control, expression of all three constructs also caused significant knockdown of WT CAIV. While constructs 15 and 16 were excluded from further experiments with HT-1080 cells, construct 10 (shCAIV10) was used to analyse the effect of knocking down R14W mutant CAIV in these cells, because slightly more WT CAIV protein expression was maintained in its presence compared to the other two constructs.

The shRNA knockdown of CAIV protein in HEK-293 cells with all three constructs as shown in Figure 8.1c, led to different levels of knockdown of WT- and R14W mutant-CAIV proteins. Interestingly, while constructs 10 and 15 were more efficient at knocking down R14W mutant CAIV compared to WT CAIV, the opposite was observed for construct 16. Silencing with shCAIV16 showed complete knockdown of WT CAIV, with very little effect on mutant CAIV. The highest preservation of WT CAIV protein levels was observed with construct 10 (shCAIV10) and therefore this construct was used in further analyses in HEK-293 cells.

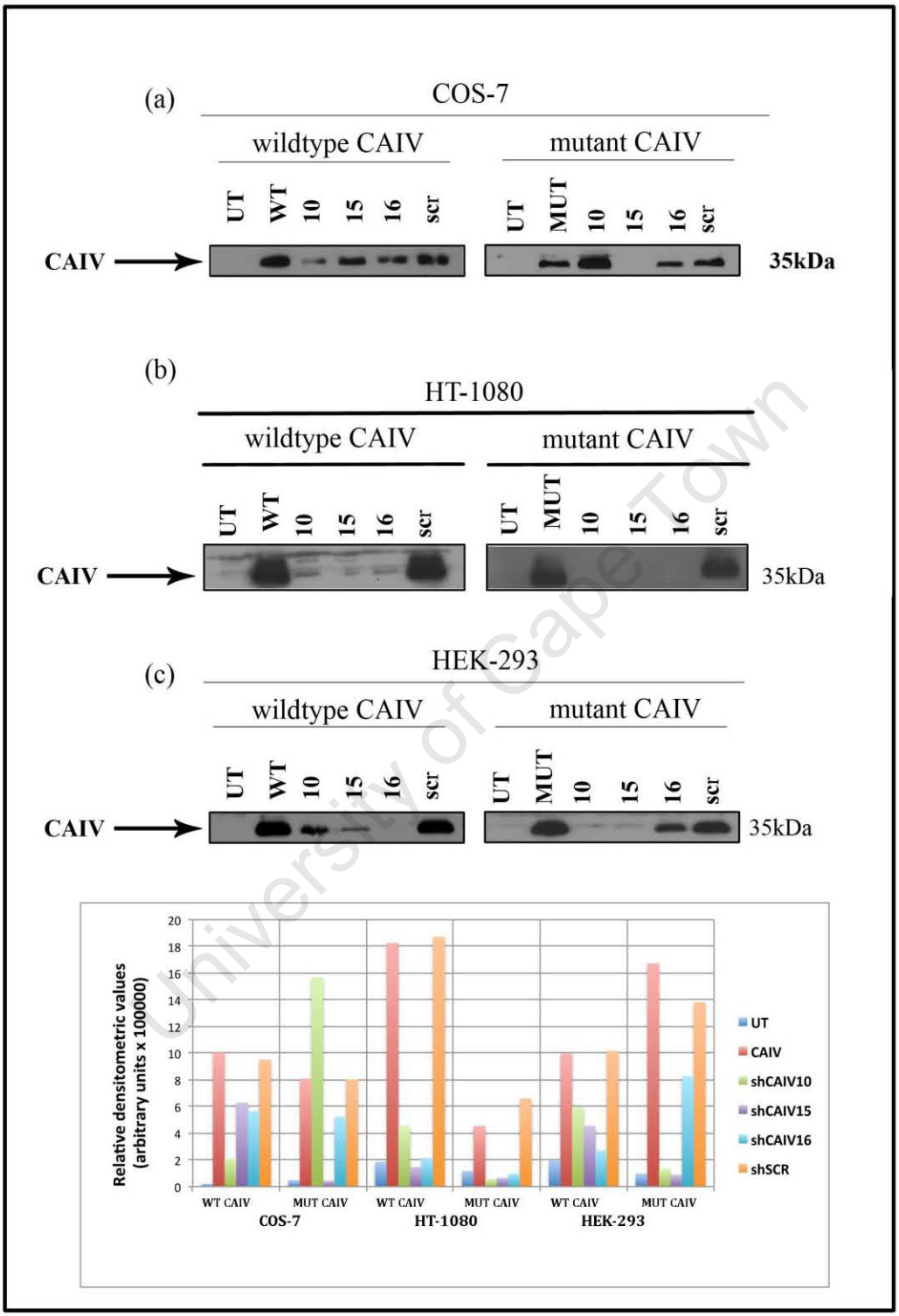

Figure. 8.1. Allele-specific shRNA silences expression of R14W mutant, but not wildtype CAIV. Western blot analyses were used to compare expression of CAIV from total protein (2 µg) isolated from COS-7, HT-1080 and HEK-293 cells transfected with pCXN-WT CAIV or pCXN-R14W CAIV and three different shCAIV constructs (numbered 10, 15, and 16) or a scrambled shRNA (scr). Protein blots were probed with an antibody specific for CAIV and CAIV protein was detected by chemiluminescence. The bar graph in the lower section of the figure compares the intensity of bands in each blot to each other, based on the reading for the background.

It is worth noting that in these HEK-293 cells (and to a lesser degree in HT-1080 cells) shCAIV10, which was the construct designed using the methods of Miller et al. (2003), was most successful in allele-specific knockdown of CAIV. While shCAIV15 and shCAIV16 were designed with a single mismatch (corresponding to the R14W mutation), shCAIV10 had this mismatch, as well as another adjacent mismatch, further decreasing its specificity to the WT mRNA sequence for CAIV.

8.2. Silencing of R14W mutant CAIV prevents the formation of mutant protein aggregates in COS-7 and HT-1080 cells

Previous work from this study analysed the effect of the R14W mutation in CAIV, and showed that the mutant protein aggregates in the ER of cells (section 7.4). Our results from section 7, as well as the results from other published studies (Rebello et al. 2004, Bonapace et al. 2007) suggest that this accumulation of protein in the ER is responsible for cells undergoing the unfolded protein response (UPR) (Rebello et al. 2004), and ultimately leads to cell cycle arrest and apoptosis.

We therefore sought to determine whether silencing of R14W mutant-CAIV using allele specific shCAIV constructs could eliminate enough of the mutant CAIV protein to prevent the formation of aggregates. To this end, COS-7, HT-1080, and HEK-293 cells were transiently transfected with the pCXN vector expressing WT- or R14W-mutant CAIV and shCAIV constructs (shCAIV15 for COS-7 cells and shCAIV10 for HT-1080 cells and HEK-293 cells), and visualised using fluorescence microscopy. As previously shown, WT CAIV protein was localised throughout the cytoplasm and along the plasma membrane in COS-7 cells, while the R14W mutant protein formed aggregates in the ER (Fig. 8.2). As expected, shCAIV15 silenced expression of R14W mutant CAIV, and abrogated the formation of perinuclear aggregates in COS-7 cells (Fig. 8.2). In findings consistent with western blot experiments (section 8.1), expression of shCAIV15 in COS-7 cells had no significant effect on silencing of WT CAIV. Results from fluorescence microscopy also confirmed the specificity of the shCAIV15 construct on silencing of

R14W mutant CAIV, and showed that expression of the shSCR construct had no effect on the subcellular localisation of either WT- or R14W mutant-CAIV (Fig. 8.2).

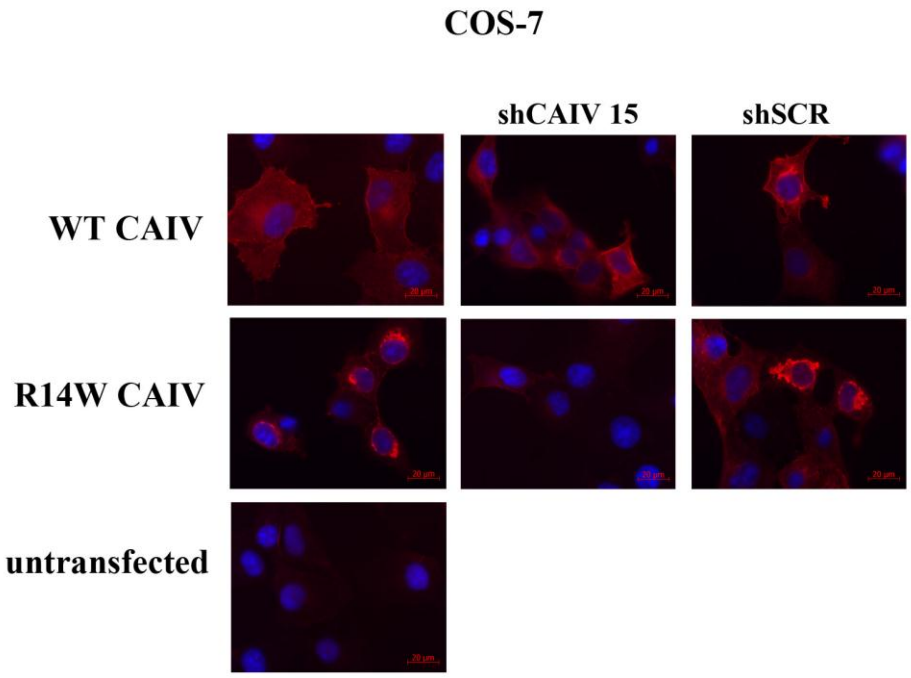

Figure 8.2. Silencing of R14W mutant CAIV prevents the formation of mutant protein aggregates in COS-7 cells. COS-7 cells expressing either WT CAIV or R14W CAIV and shCAIV15 or shSCR were analysed by immunohistochemistry to determine the cellular localisation of WT- and R14W mutant CAIV protein. Cells were fixed, permeabilised, and treated with anti-CAIV antibody, followed by Cy3-conjugated secondary antibody and visualised by fluorescence microscopy for DAPI (blue nuclear stain) and CAIV (red stain). Scale bars represent 20µm.

Transfection of shCAIV10 into HT-1080 cells expressing R14W CAIV also resulted in silencing of the mutant protein (Fig. 8.3). As shown previously, transfecting shCAIV10 into HT-1080 cells expressing WT CAIV protein did not result in significant silencing of the WT CAIV protein, but was highly specific to the R14W mutant CAIV. As was the case with experiments in COS-7 cells, shSCR constructs were included as a control to exclude off target effects (Fig. 8.3). Transfections with the shSCR construct also showed, as with previous localisation experiments, that the expression of shRNA in cells did not have an adverse effect on subcellular localisation of CAIV protein.

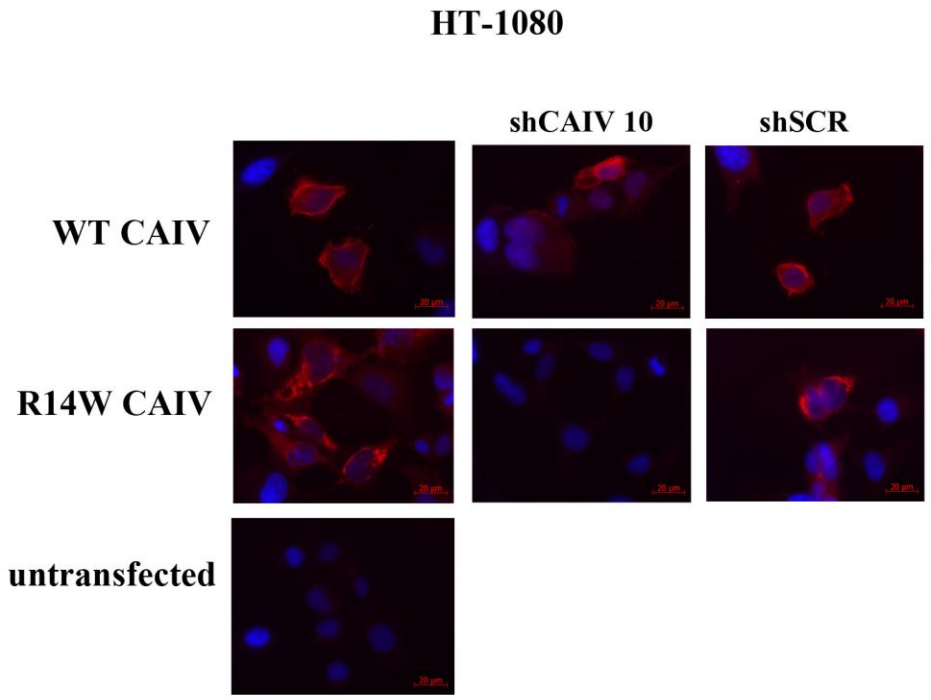

Figure 8.3. Silencing of R14W mutant CAIV prevents the formation of mutant protein aggregates in HT-1080 cells. HT-1080 cells expressing either WT CAIV or R14W CAIV and shCAIV10 or shSCR were analysed by immunohistochemistry to determine the cellular localisation of WT- and R14W mutant CAIV protein. Cells were fixed, permeabilised, and treated with anti-CAIV antibody, followed by Cy3-conjugated secondary antibody and visualised by fluorescence microscopy for DAPI (blue nuclear stain) and CAIV (red stain). Scale bars represent 20μm.

The previous sections had shown that HEK-293 cells have the ability to fold and transport R14W mutant CAIV correctly (section 7.4, Fig. 7.4) and it was therefore next investigated whether the shRNA would impact adversely on trafficking of R14W mutant protein. As expected, shCAIV10 silenced expression of the R14W mutant, but did not silence expression or have an effect on the trafficking of the WT protein (Fig. 8.4). Expression of the shSCR construct did not result in silencing of either WT- or R14W mutant-CAIV, and had no effect on the subcellular localisation of the protein (Fig. 8.4). The results in HEK-293 cells were in keeping with previous results which showed that they are able to transport the R14W mutant form of the protein to the cell membrane.

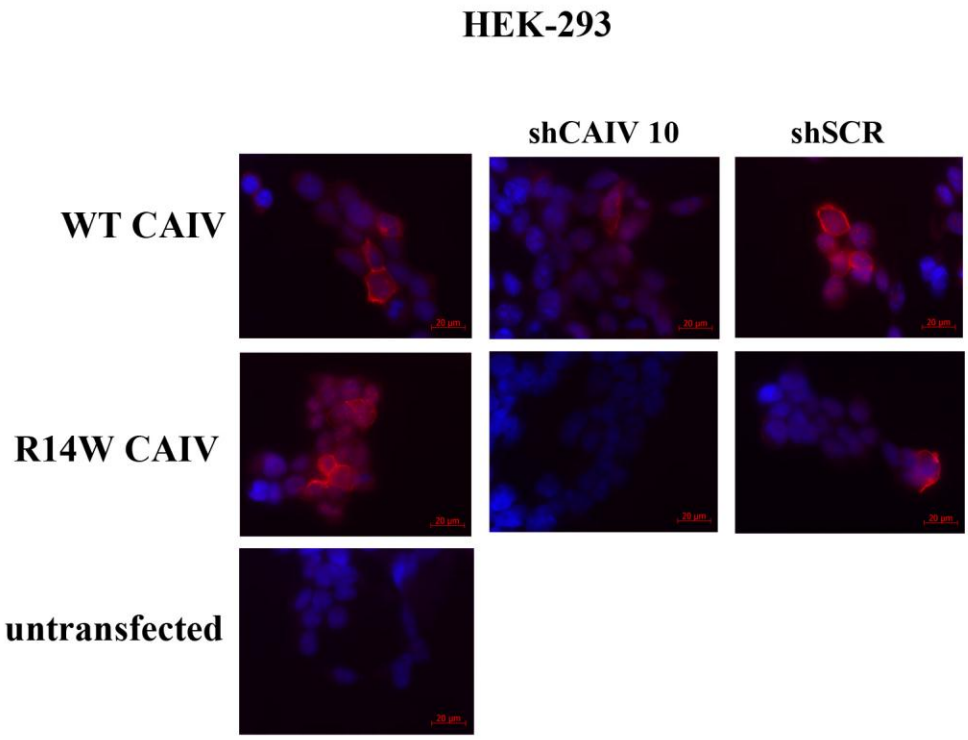

Figure. 8.4. shCAIV does not affect trafficking of WT CAIV protein in HEK-293 cells. HEK-293 cells expressing either WT CAIV or R14W CAIV and shCAIV10 or shSCR were analysed by immunohistochemistry to determine the cellular localisation of WT- and R14W mutant CAIV protein. Cells were fixed, permeabilised, and treated with anti-CAIV antibody, followed by Cy3-conjugated secondary antibody and visualised by fluorescence microscopy for DAPI (blue nuclear stain) and CAIV (red stain). Scale bars represent 20µm.

In summary, results from this section show that the shCAIV constructs were specific for R14W mutant CAIV and this was confirmed by results obtained for the shSCR constructs. These results were from both sections 8.1 and 8.2 are particularly important because they show, for the first time, that it is possible to silence expression of the R14W CAIV mutant protein, but not the WT form, using shRNA constructs. This suggests that allele-specific shRNA is a feasible approach to examine in the development of therapy for RP17.

8.3. Silencing of R14W mutant CAIV prevents S and G2/M cell cycle arrests in COS-7 cells

We have previously shown (section 7.1) that expression of the R14W mutant CAIV protein causes COS-7 cells to undergo S and G2/M cell cycle arrests. To determine whether silencing of the R14W mutant CAIV would prevent these cell cycle arrests, cells were co-transfected with either WT- or R14W mutant-CAIV and with shCAIV constructs and processed for flow cytometry 24 h after transfection.

As expected, untransfected COS-7 cells and those expressing WT CAIV showed a cell cycle profile similar to that of normal dividing cells (Fig. 8.5a and g). Similar to previous data, ectopic expression of R14W mutant CAIV resulted in a drastic S phase cell cycle arrest (Fig. 8.5d) rather than the S and G2/M cell cycle arrests observed previously (section 7.1, Fig. 7.1c). It is however important to note that unlike previous experiments in which cells were processed 72 h post-transfection, in this set of experiments cells were processed 24 h post-transfection because differential processing of R14W mutant-CAIV was already evident at this time point (Fig. 8.6). Therefore cells were also processed 24 h after transfection for the analyses in sections 8.3 to 11. It is conceivable that 72 h of expression of R14W mutant CAIV as opposed to 24 h triggers an additional cell cycle checkpoint arrest such as G2/M, nevertheless, the expression of shCAIV15 in COS-7 cells abrogated the S phase arrest induced by transfected mutant CAIV (Fig. 8.5e). Interestingly, in these experiments, the scrambled shRNA also reduced the S-phase arrest in cells expressing the R14W mutant CAIV, although a small G2/M arrest was experienced by these cells (Fig. 8.5f). This effect of the shSCR on cells expressing the R14W mutant CAIV protein will be discussed later (section 13.2). As shown in Figure 8.5b and c, the shCAIV15 and shSCR respectively, had no effect on the cell cycle of COS-7 cells expressing the WT CAIV protein.

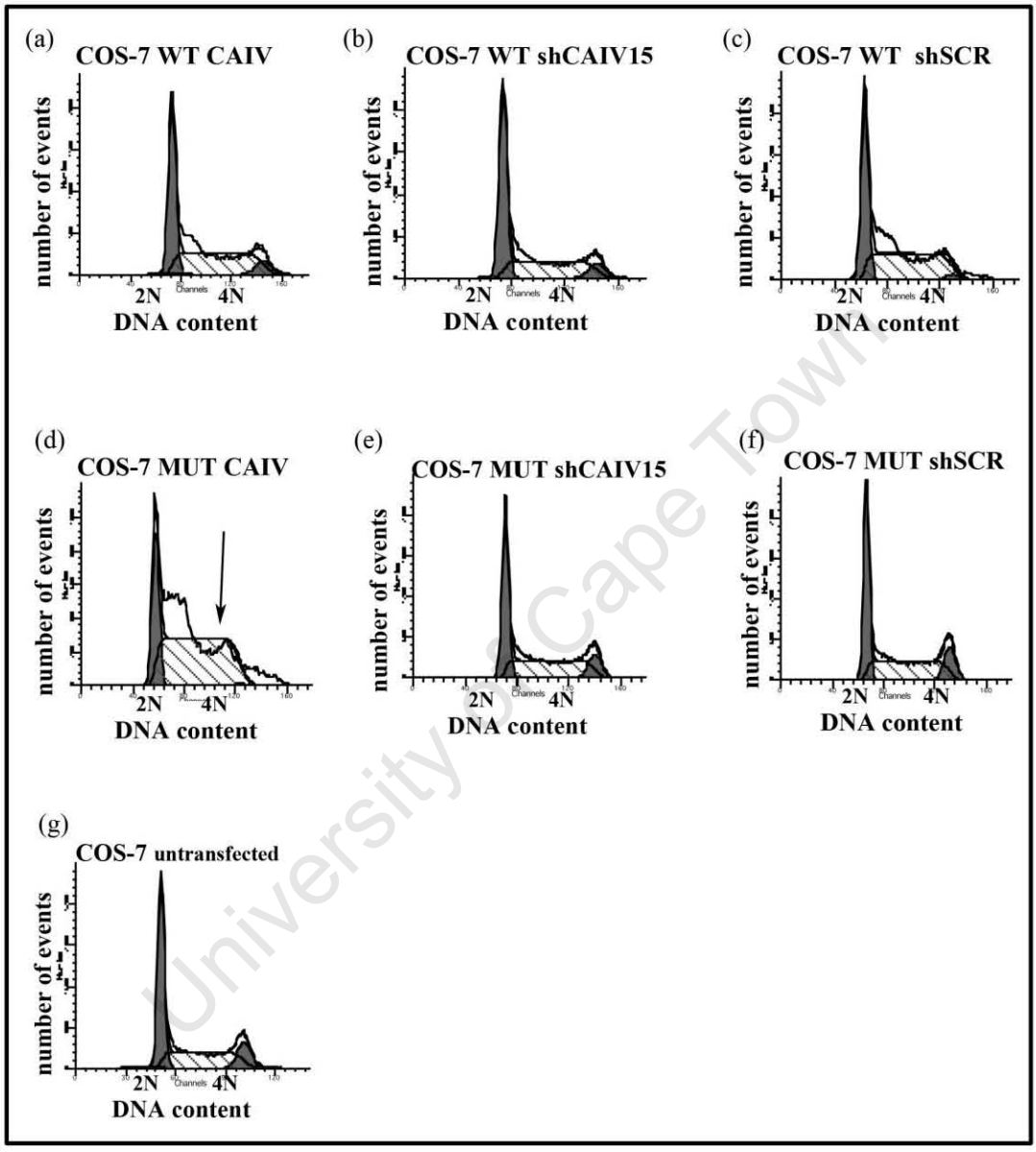

Figure 8.5. Silencing of R14W mutant CAIV prevents COS-7 cells from undergoing S phase cell cycle arrest. The cell cycle status of untransfected cells (g) or cells transfected with WT CAIV (a, b and c) or R14W mutant CAIV (d, e and f) and shCAIV15 (b and e) or shSCR (c and f) was determined by measuring their DNA content using fluorescence-activated cell sorting analysis. Peaks at 2N and 4N DNA content represent the number of cells in G1 and G2/M phases respectively and the hatched areas represent the number of cells in S-phase. The arrow in (d) points to an S phase cell cycle arrest.

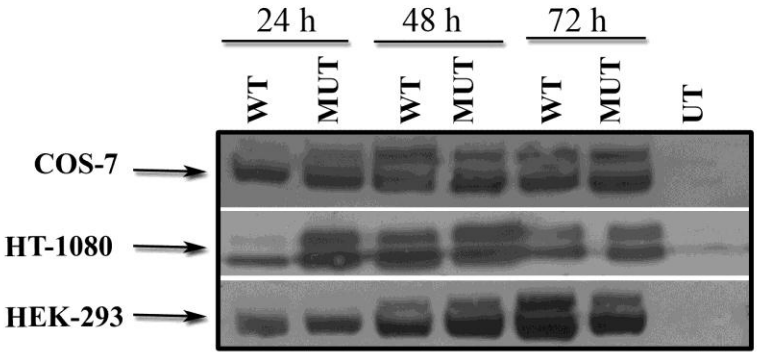

Figure. 8.6. Time point analysis of CAIV expression reveals differential expression between WT and R14W CAIV at 24 h. Western blot analyses were used to compare expression of CAIV from total protein (2 μg) isolated from COS-7, HT-1080 and HEK-293 cells transfected with WT- or R14W mutant CAIV. Protein blots were probed with antibodies specific for CAIV and the protein was detected by chemiluminescence.

Earlier work has shown that HEK-293 cells expressing either the WT- or R14W mutant-CAIV do not undergo cell cycle arrests (section 7.1, Fig. 7.1, d, e and f). It was, however, attractive to determine whether expression of shCAIV10 would have any effect on the cell cycle in this cell line. Indeed, the results show that cells co-transfected with either WT- or R14W mutant-CAIV and either shCAIV10 (Fig. 8.7b and e) or an shSCR (Fig. 8.7c and f), exhibited a normal cell cycle profile. These results confirmed that HEK-293 cells expressing the R14W mutant CAIV do not undergo cell cycle arrest, and furthermore, that the shCAIV/shSCR does not have any adverse effects on cell cycle in HEK-293 cells.

Note that as with previous sections on FACS analysis, HT-1080 cells were not included in these analyses as we had shown (section 7.1, Fig. 7.1g) that they exhibit polyploidy, making it challenging to accurately compare cell cycle profile changes in this cell type.

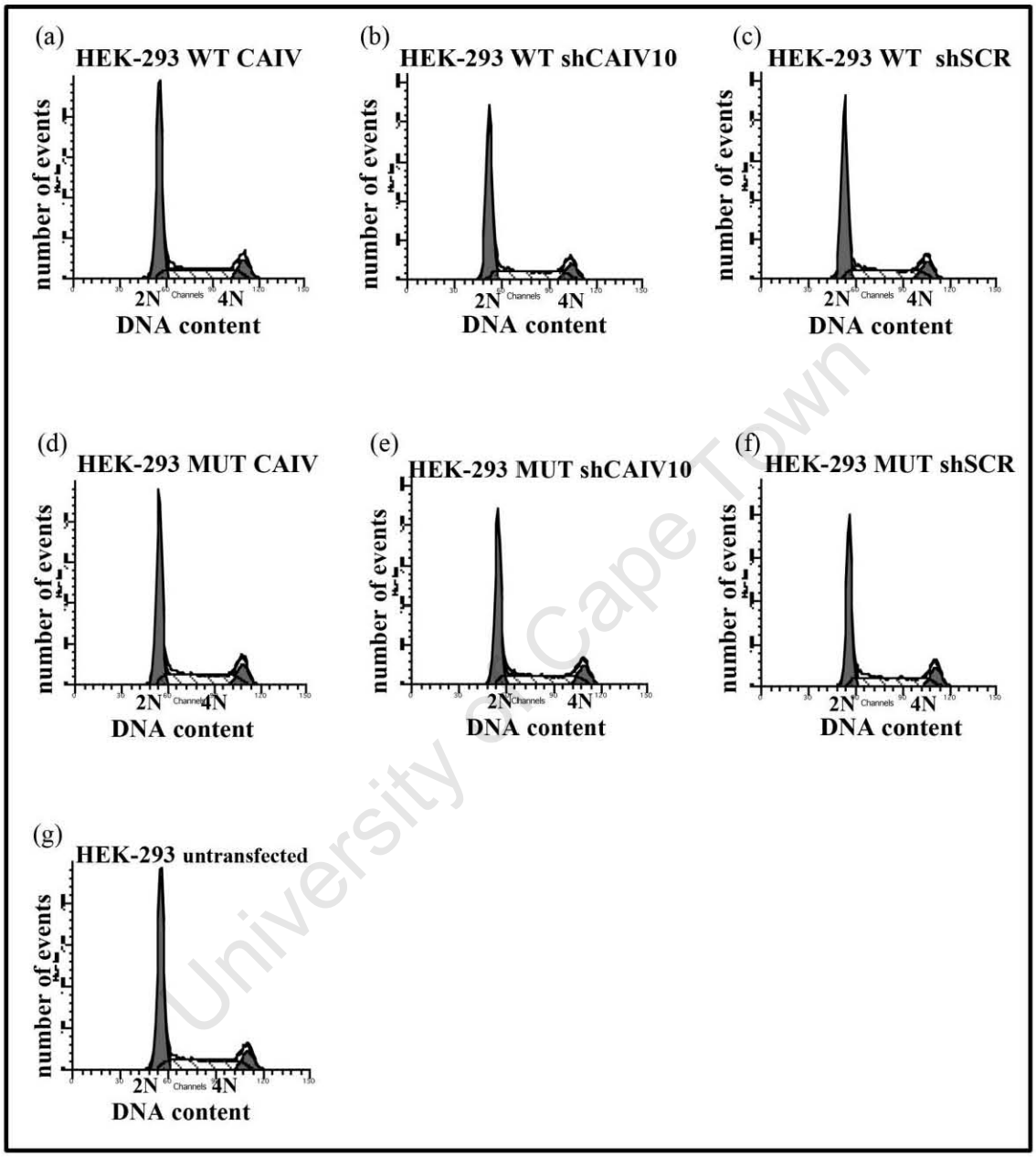

Figure 8.7. shCAIV has no adverse effect on the cell cycle of HEK-293 cells expressing WT or R14W mutant CAIV. The cell cycle status of untransfected cells (g) or cells transfected with WT CAIV (a, b and c) or R14W CAIV (d, e and f) and shCAIV10 (b and e) or shSCR (c and f) was determined by measuring their DNA content using fluorescence-activated cell sorting analyses. Peaks at 2N and 4N DNA content represent the number of cells in G1 and G2/M phases respectively.

8.4. Silencing of R14W mutant CAIV protects COS-7 and HT-1080 cells from undergoing apoptosis

Since the allele-specific silencing of R14W mutant CAIV was shown to prevent COS-7 cells from undergoing cell cycle arrests, the effect of knockdown of the mutant protein on apoptosis was determined. To this end, COS-7 and HT-1080 and HEK-293 cells were co-transfected with WT- or R14W mutant-CAIV, and the shCAIV constructs, or shSCR. These cells were then harvested 24 h after transfection and co-stained for Annexin V and propidium iodide (PI) before being analysed by flow cytometry as described previously.

As expected, compared to 0% of cells expressing WT protein undergoing apoptosis, 10% of the COS-7 R14W mutant-CAIV expressing cell population was apoptotic (Fig. 8.8d). Expression of shCAIV15 in COS-7 cells expressing R14W mutant CAIV rescued these cells from undergoing apoptosis (Fig. 8.8e). However, in keeping with previous data for the cell cycle profile (Fig. 8.8f), the shSCR also reduced the number of cells undergoing apoptosis, but with less efficiency than shCAIV15 (Fig. 8.8f). Consistent with previous experiments (section 7.2), COS-7 cells expressing WT CAIV and untransfected COS-7 cells had a negligible number of cells undergoing apoptosis (Fig. 8.8a and g) and this result was unaffected by the expression of either shCAIV15 or shSCR (Fig. 8.8b and c). A histogram (Fig. 8.8h) shows a graphical representation of these results. The results showing that silencing of R14W mutant CAIV prevents cells from undergoing apoptosis also support the hypothesis that expression of this R14W mutant protein induces apoptosis in these cells. It is worth pointing out that in this set of experiments the actual numbers of cells undergoing apoptosis were lower than that described in section 7.2 for the reasons explained previously (section 8.2).

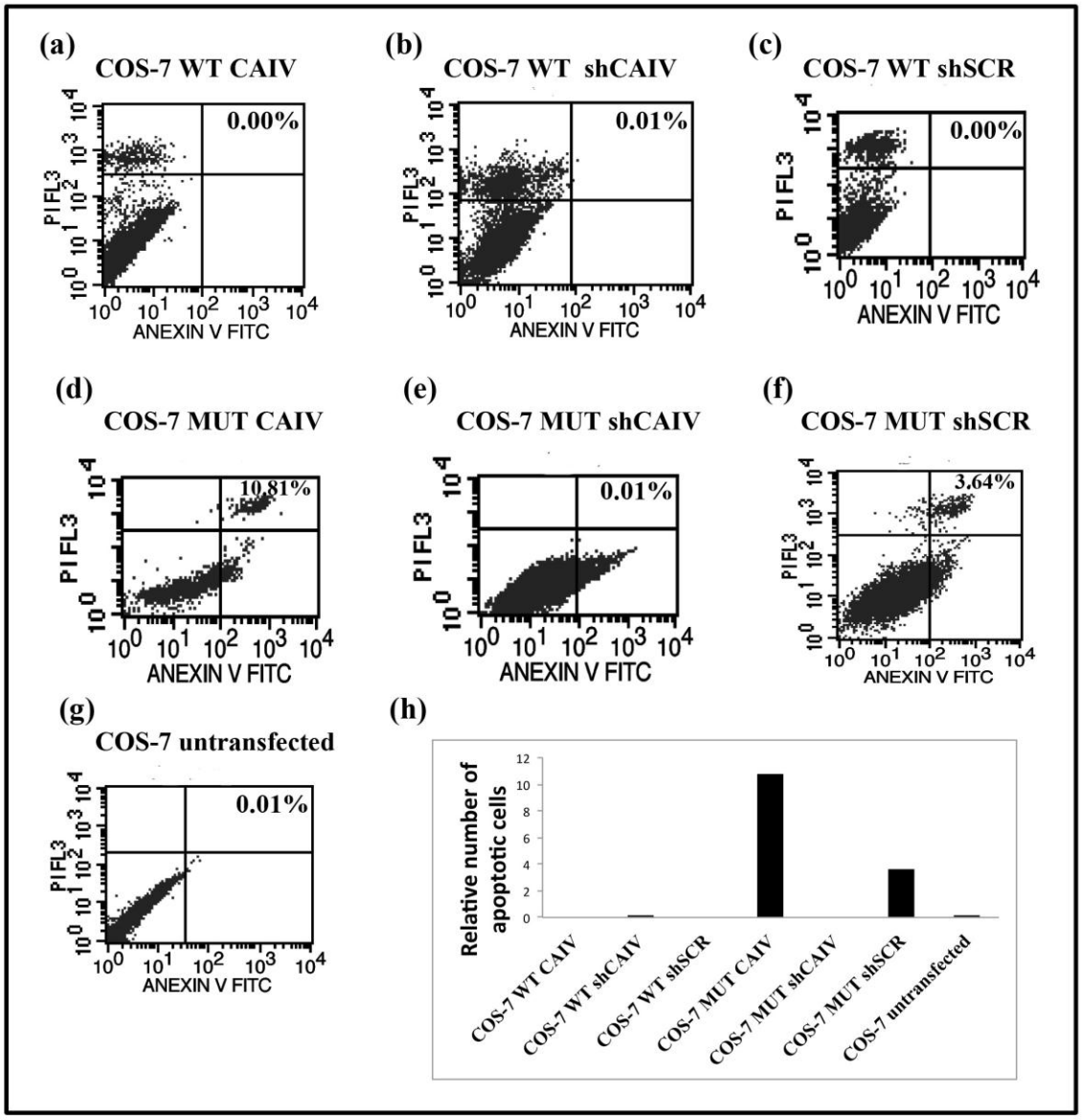

Figure 8.8. Silencing of R14W mutant CAIV prevents COS-7 cells from undergoing apoptosis. COS-7 cells expressing either WT CAIV or R14W CAIV and shCAIV15 or shSCR were stained with Annexin V-FITC and propidium iodide (PI) in order to quantify apoptosis by flow cytometry. In the histogram, the columns indicate the percentages of cells that stain positive for FITC/PI and that are undergoing apoptosis (upper right-hand quadrant).

Apoptosis analyses for the expression of WT- and R14W mutant-CAIV in HT-1080 cells showed similar results as were previously observed (Fig. 7.2 c and d). Compared to cells expressing WT CAIV, there was an increase in the number of apoptotic cells when the R14W mutant CAIV was expressed (Fig. 8.9a and d). When these R14W CAIV-expressing cells were transfected with shCAIV10 (Fig. 8.9e), there was a decrease in the

number of cells undergoing apoptosis compared to cells expressing either R14W mutant CAIV only, or cells expressing the shSCR construct (Fig. 8.9d and f). Interestingly, and in contrast with experiments in COS-7 cells, expression of the shCAIV in HT-1080 cells expressing WT CAIV resulted in an increase in the numbers of cells undergoing apoptosis (Fig. 8.9b). In addition, expression of the shSCR constructs in HT-1080 cells expressing either WT- or R14W mutant-CAIV resulted in an increase in the number of apoptotic cells (Fig. 8.9c and f). Figure 8.9h is a graphic representation of the above results. The difference in the responses of COS-7 and HT-1080 cells to expression of the shRNA constructs emphasises the need to take cell type-specific differences into account when establishing cell culture models for disease. These results will be discussed further in section 13.2.

In light of the adverse effects of the shCAIV10 and shSCR on HT-1080 cell viability and apoptotic profile, these constructs were also tested on HEK-293 cells expressing the WT- and R14W mutant-CAIV. While the apoptotic profiles of HEK-293 cells expressing the WT- and R14W mutant-CAIV were comparable (Fig. 8.10a and d), a slight increase in the numbers of cells undergoing apoptosis was observed when cells were co-transfected with shCAIV10 (Fig. 8.10b and e), and an even larger increase with the shSCR construct (Fig. 8.10c and f). These results were surprising because earlier results showed that the shCAIV10 and shSCR had no adverse effects on HEK-293 cell cycle progression (Fig. 8.7), and they will be discussed in section 13.2.

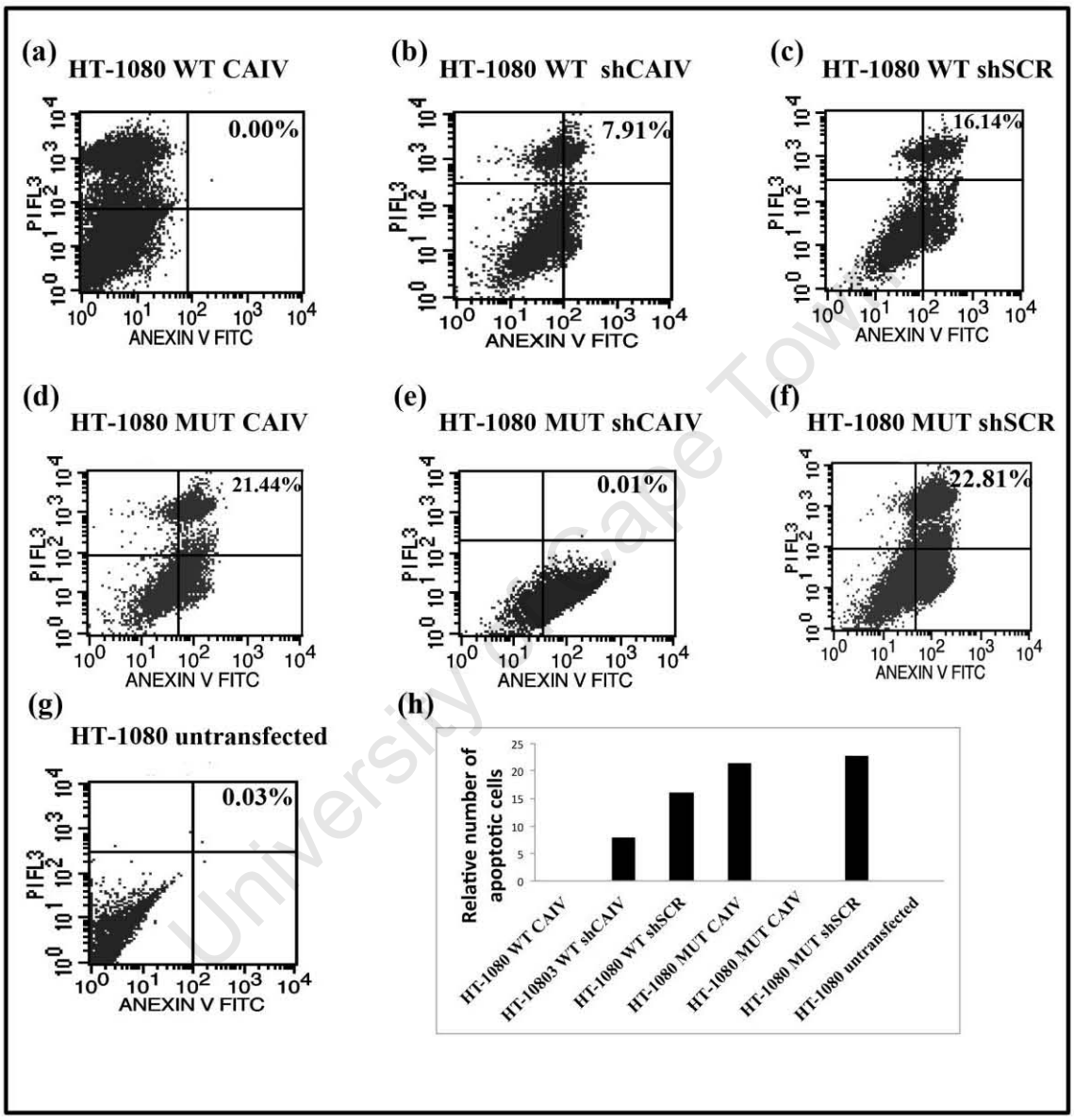

Figure 8.9. Silencing of R14W mutant CAIV prevents HT-1080 cells from undergoing apoptosis. HT-1080 cells expressing either WT CAIV or R14W mutant CAIV and shCAIV10 or shSCR were stained Annexinv V-FITC and propidium iodide (PI) in order to quantify apoptosis by flow cytometry. In the histogram, the columns indicate the percentages of cells that stain positive for FITC/PI and that are undergoing apoptosis (upper right-hand quadrant).

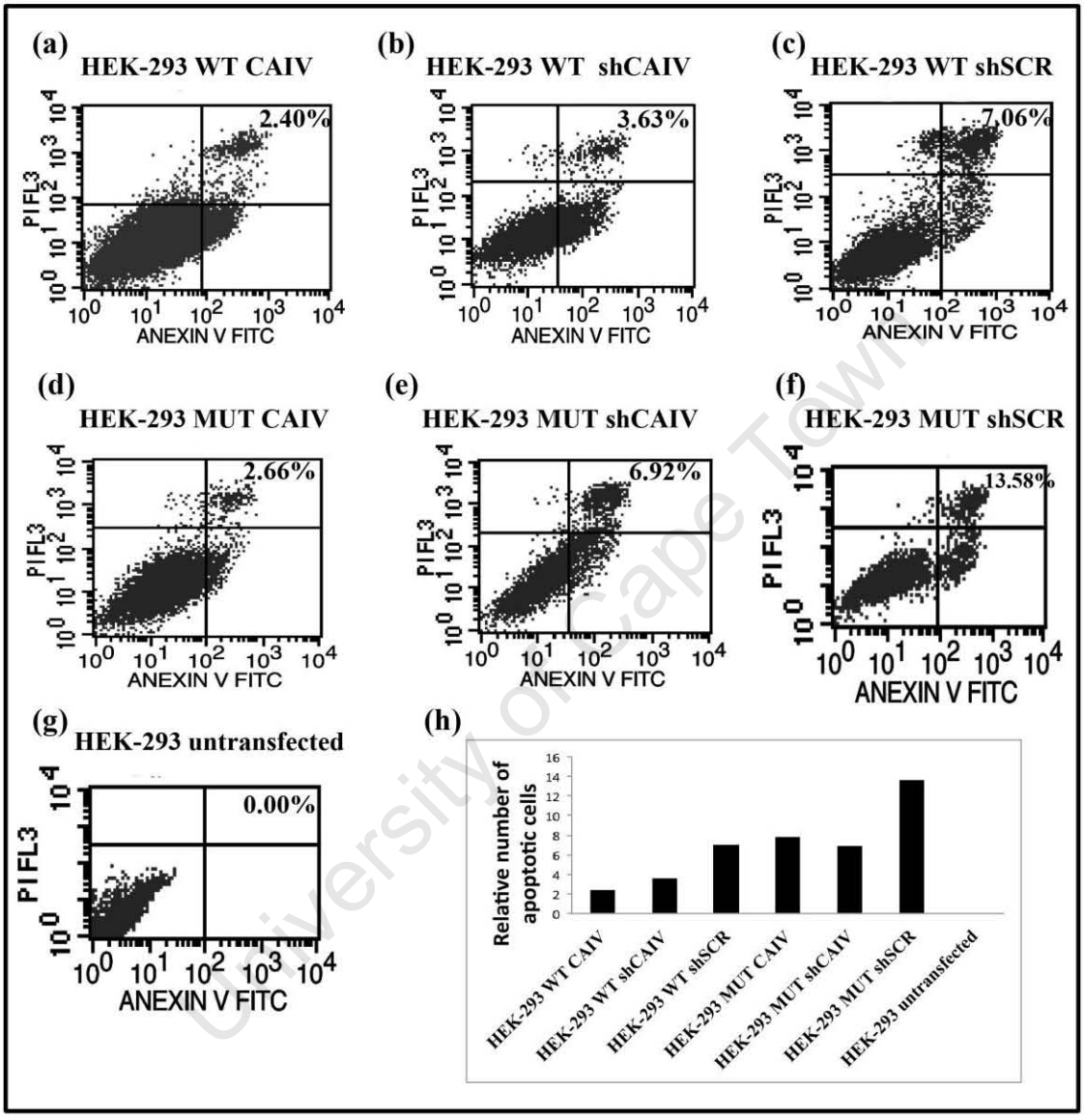

Figure 8.10. shCAIV has an effect on the percentage of HEK-293 cells undergoing apoptosis. HEK-293 cells expressing either WT- or R14W mutant CAIV and shCAIV10 or shSCR were stained with Annexin V-FITC and propidium iodide (PI) in order to quantify apoptosis by flow cytometry. In the histograms, the columns indicte the percentages of cells that stain positive for FITC/PI and that are undergoing apoptosis (upper right-hand quadrant). Note that in (b) and (e), the vertical Annexin V threshold line has been moved automatically by the CellQuest programme in an attempt to place populations of cells into specific quadrants.

9. Comparison of expression levels of ER-specific chaperones BiP, GRP170, and PDI

The initial part of this study examined the molecular mechanisms behind cell death in cells in which the R14W mutant CAIV was being ectopically expressed. Our results not only revealed the precise molecular mechanism behind the death of cells expressing R14W mutant CAIV; but also highlighted an interesting phenomenon in HEK-293 cells. These cells, in contrast to COS-7 and HT-1080 cells, were able to correctly fold, process, and traffic R14W mutant CAIV. In doing so, HEK-293 cells expressing the mutant protein did not undergo cell cycle arrest and apoptosis.

These results in the kidney-derived HEK-293 cells (Graham et al. 1977; Shaw et al. 2002), together with the findings that RP17 patients have no kidney phenotype despite strong expression of the protein in the proximal renal tubules (Rebello et al. 2004), suggest that kidney cells may possess intrinsic properties which allow them to fold and process R14W mutant CAIV protein. If this were the case, then identifying factors responsible may provide additional therapeutic avenues. To this end, this section of the study sought to identify chaperone proteins that are differentially expressed in HEK-293 cells expressing R14W CAIV compared to COS-7 and HT-1080 cells expressing this mutant protein.

9.1. Varying levels of ER-specific chaperones observed in untransfected COS-7, HT-1080 and HEK-293 cells

As an initial investigation, levels of chaperone proteins that have been shown to play a key role in ER-specific folding namely BiP, GRP170 and PDI, were examined. Western blotting with antibodies to these three chaperones was performed to compare the levels of chaperones in untransfected cells to cells transfected with either WT- or R14W-mutant CAIV. RCC4 (+VHL) kidney-carcinoma cells, which endogenously express CAIV, were included in these analyses as an additional kidney-derived cell line.

Results showed that the COS-7, HT-1080 and RCC4 cells had comparable levels of BiP and PDI (a bubble in the COS-7 BiP lane has caused distortion of the band). The levels of GRP170, however, appeared to be comparatively high in COS-7 cells, with HEK-293 cells expressing the lowest levels of this chaperone. Interestingly, HEK-293 cells appeared to have lower levels of all three ER-chaperones tested and indeed had undetectable levels of BiP (Fig. 9.1). When comparing the two kidney cell lines, the higher levels of all three chaperones in RCC4 cells compared to HEK-293 cells was also noteworthy. p38 was used as a loading control in this experiment, and densitometric analysis was also performed in order to analyse band intensity relative to p38.

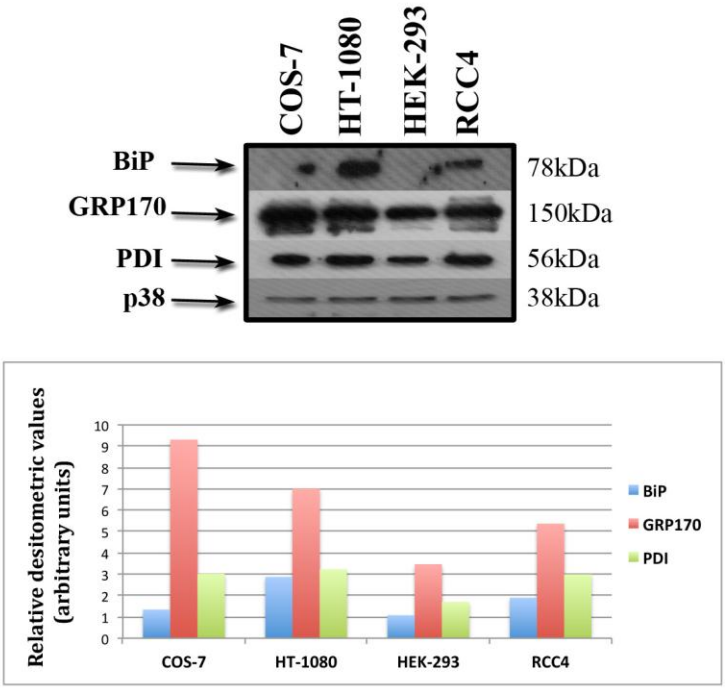

Figure 9.1. Levels of ER-specific chaperones vary in untransfected COS-7, HT-1080 and HEK-293 cells. Western blot analyses were used to compare expression of CAIV from total protein (20 µg) isolated from COS-7, HT-1080 and HEK-293 cells. Protein blots were probed with antibodies specific for BiP, GRP170 and PDI and detected by chemiluminescence. p38 was used as a loading control, and densitometric analysis of the western blot used to compare chaperone bands relative to p38.

9.2. Levels of ER chaperones change in response to expression of either WT- or R14W mutant-CAIV

We next wanted to determine whether expression of the ER-chaperones BiP, GRP170 and PDI is altered in cells transfected with WT- or R14W mutant-CAIV. Because COS-7, HT-1080 and HEK-293 cells expressed different levels of transfected CAIV, the levels of BiP, GRP170 and PDI were compared for the different constructs within each cell line by western blot analysis. In order to control for loading, densitometric analysis of bands was performed (shown as bar graphs, Fig. 9.2) as well as staining of membranes with Ponceau S (Appendix, section 14.16, Figure 14.7).

Expression of the three chaperones in transfected cells was expressed in relation to chaperone levels in untransfected cells for each cell type (i.e. fold change). Figure 9.2 shows that in all three cell types, levels of BiP were higher in cells transfected with R14W mutant CAIV compared to levels in WT CAIV-expressing cells. Interestingly, although the levels of BiP in HEK-293 cells followed this pattern, the levels were higher in transfected cells compared to untransfected cells than the increases in levels of the chaperone in transfected COS-7 and HT-1080 cells (Fig 9.2). Levels of GRP170 in COS-7 and HEK-293 cells were higher in cells transfected with R14W mutant CAIV compared to levels in cells transfected with WT CAIV (Fig 9.2). In contrast, levels of GRP170 remained constant in HT-1080 cells transfected with either form of CAIV. When levels of PDI were compared, it was interesting to note that levels of the chaperones remained constant in COS-7 cells transfected with WT- or R14W mutant-CAIV. In contrast, levels of PDI were increased in HT-1080 cells transfected with R14W mutant CAIV compared to cells transfected with the WT form of the protein, while the opposite change in levels was observed in HEK-293 cells.

In summary, results from sections 9.1 and 9.2 did not reveal any obvious link between levels of the three ER chaperones tested, and the differential responses of COS-7, HT-1080 and HEK-293 cells to R14W mutant CAIV. For example, while COS-7 and HT-1080 cells transfected with R14W mutant protein display the same phenotype, the

expression profile of the chaperones tested in these cell types were different under the same conditions. Another interesting observation was that COS-7, HT-1080 and HEK-293 cells have different endogenous levels of BiP, GRP170 and PDI. Furthermore, compared to untransfected COS-7 and HT-1080 cells, untransfected HEK-293 cells were shown to have lower levels of these chaperones.

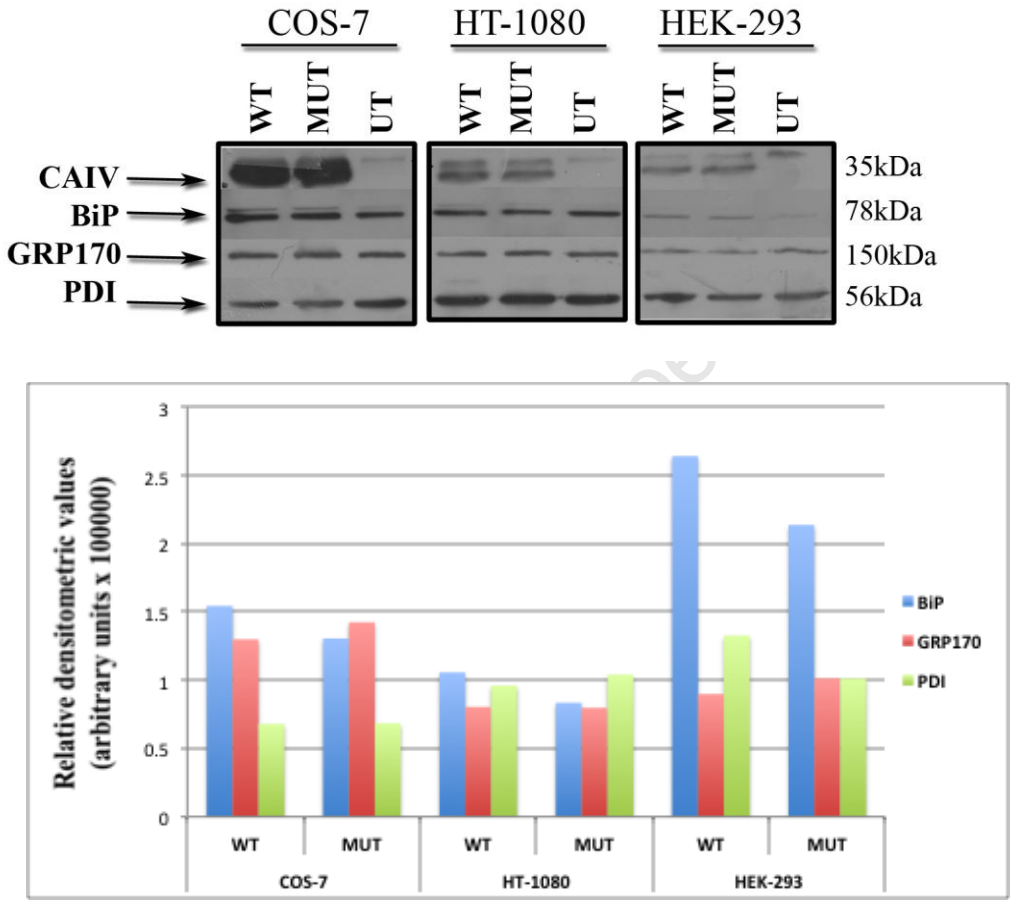

Figure 9.2. Levels of ER-specific chaperones vary in response to expression of either WT- or R14W CAIV in transfected cells. Western blot analyses were used to compare expression of CAIV from total protein (20 µg) isolated from untransfected COS-7, HT-1080 and HEK-293 cells or cells transfected with WT- or R14W mutant CAIV. Protein blots were probed with antibodies specific for CAIV, BiP, GRP170 and PDI and the proteins detected by chemiluminescence. The bar graph shows the results of densitometric analysis which was performed against the autoradiograph background in order to control for differences in protein loading.

9.3. Levels of ER chaperones change in response to shCAIV in HT-1080 cells expressing the WT- and R14W mutant-CAIV protein

The above investigations excluded a potential role for the ER chaperones BiP, GRP170 and PDI in mediating the different phenotypes between COS-7 and HT-1080, and HEK-293 cells expressing R14W mutant CAIV. However, results from allele-specific silencing of this protein using shRNA raised the question of the effect of shCAIV on the levels of these vital chaperones. This was considered significant precisely because the RP17 phenotype arises due to the accumulation of misfolded protein in the ER. Consequently, it is important that therapeutic interventions using shCAIV do not interfere with the normal protein folding machinery when trying to treat this disease. To this end, the levels of BiP, GRP170 and PDI in HT-1080 cells were examined in response to shCAIV. Analysis of western blot results showed that compared to untransfected HT-1080 cells, levels of the BiP chaperone were decreased in response to co-transfection with R14W mutant CAIV and shCAIV10. In contrast, levels of GRP170 were increased drastically in cells co-transfected with WT CAIV and shCAIV10 (Fig. 9.3).

These results again suggested that levels of ER-specific chaperones vary considerably between cell lines, and in response to transfections with CAIV or shRNA constructs. While the results did not show a clear correlation in any of the cell lines between levels of chaperone and WT- or R14W mutant-CAIV or shRNA, it can still nevertheless not be excluded that changes in these chaperone levels may still a minor role to play, albeit along with other proteins, in the cell's specific response to WT- or R14W mutant-CAIV.

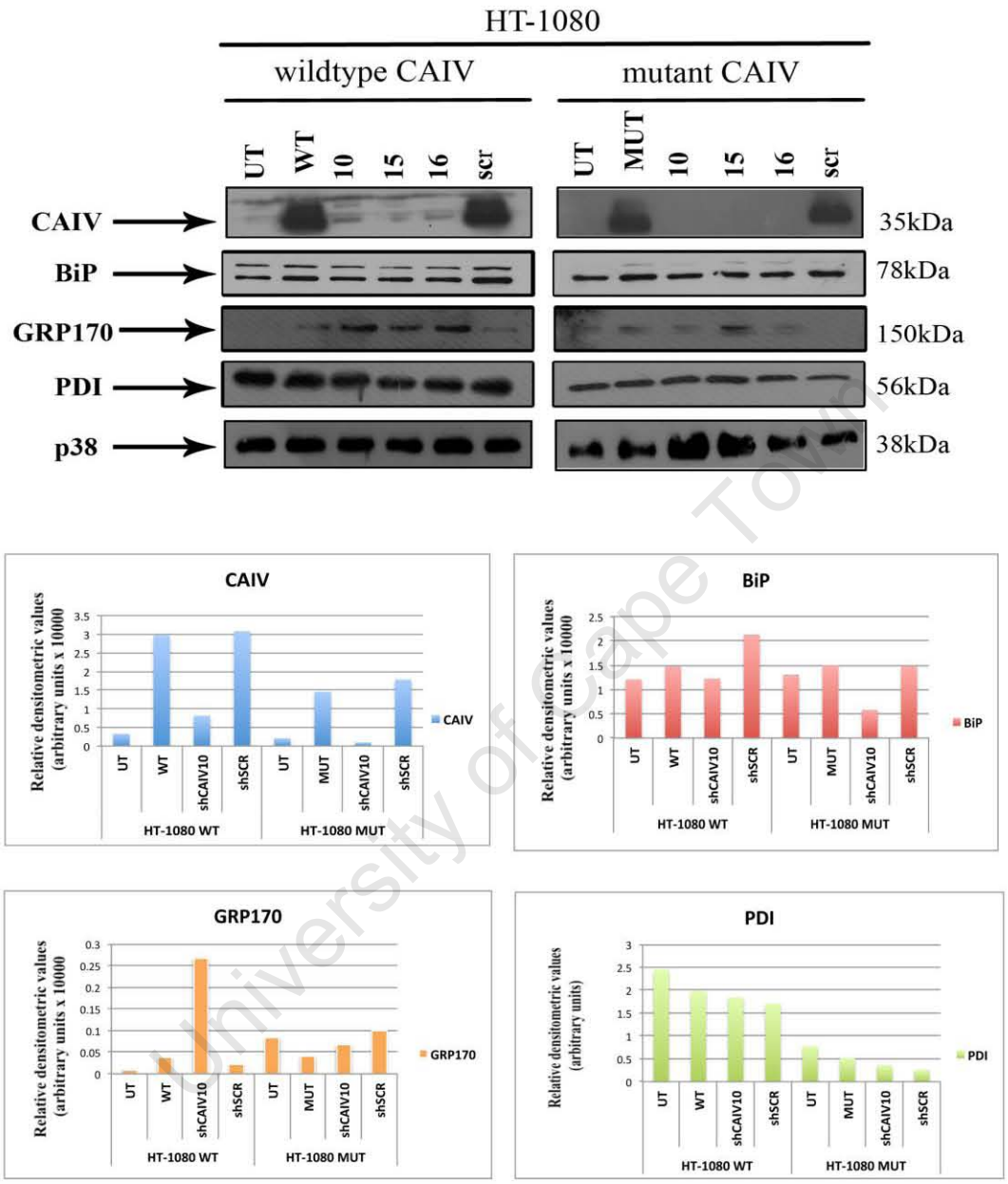

Figure 9.3. Levels of ER-specific chaperones change in response to shCAIV10 in HT-1080 cells. Western blot analyses were used to compare expression of CAIV from total protein (20 µg) isolated from untransfected HT-1080 cells or cells transfected with either WT- or R14W mutant CAIV in pCXN and shCAIV constructs (10, 15, 16) or a scrambled shRNA construct (scr). Protein blots were then probed with antibodies specific for CAIV, BiP, GRP170 and PDI and the proteins detected by chemiluminescence. p38 was used as a loading control. Bar graphs show the results of densitometric analysis performed to measure the intensity of bands relative to p38. Since only shCAIV 10 was used in experiments that analysed the effects of knockdown of R14W mutant CAIV, bar graphs from densitometric analyses only compare the results of shCAIV10 knockdown (and not that done with the other shCAIV constructs) on levels of the three ER-specific chaperones.

10. Analysis of mRNA transcript levels in HT-1080 and HEK-293 cells expressing WT- and R14W mutant-CAIV protein

The results from sections 7.2 to 7.4 which showed that unlike HT-1080 cells, HEK-293 cells are able to fold and process R14W mutant CAIV, suggested that there may be cell type-specific factors expressed in this cell type which facilitate folding/processing, and thereby protect HEK-293 cells from R14W CAIV-induced apoptosis.

To explore this hypothesis, microarray experiments were carried out as a preliminary pilot study to compare gene expression in the human-derived HT-1080 and HEK-293 cells transfected with WT- and R14W mutant-CAIV, respectively. This was done by isolating RNA from the respective cell lines transfected with either WT- or R14W mutant-CAIV expression constructs, and hybridising it to a Human Gene 1.0 ST Array (Affymetrix, USA). This work allowed for observing genome-wide gene expression in the different cell lines, and to determine which genes, if any, account for the ability of HEK-293 cells expressing R14W CAIV to evade apoptosis. It is worth reiterating that this aspect of the study included only the human cell lines, HT-1080 and HEK-293, in order to limit the number of observed variables. COS-7 cells, which were also used in the earlier research, were not used in this part of the study because of the likely additional variables/gene expression patterns owing to their non-human (i.e. monkey) origin.

Briefly, HT-1080 and HEK-293 cells were plated, transfected, and harvested, and RNA extracted from cells expressing the WT- and R14W mutant-CAIV protein as per the protocol described in section 3.7. RNA quality and purity was assessed using a NanoDrop ND-1000 spectrophotometer (NanoDrop Technologies, Inqaba, RSA) and Agilent 2100 Bioanalyzer Nano Assay (Agilent Technologies, USA). The purity of RNA was confirmed by electrophoresis on a 1% agarose gel as described in section 3.8. All samples met the required criteria for microarray analysis, which was performed at the Centre for Proteomics and Genomic Research (CPGR) as per the Affymetrix recommended protocol using the GeneChip Human Gene 1.0 ST Array (Affymetrix, USA).

Data was analysed using the Affymetrix Genotyping Console Software Version 2.0 (Affymetrix, USA) as well as Partek Genomics Suite version 6.4 (Partek Inc, USA), using all of the default settings.

Preliminary analysis of data from the microarray experiment using a 2-fold variance as a cut-off value as is commonly used (Huang et al. 2008; Steinhoff and Vingron, 2006; Yang et al. 2002) showed that ten genes were differentially expressed between HEK-293 cells transfected with WT- and R14W mutant-CAIV, fifteen between HT-1080 cells transfected with WT- and R14W mutant-CAIV, and only one each between HT-1080 and HEK-293 cells transfected with WT CAIV or R14W mutant CAIV (Table 10.1). These differentially expressed genes included transcripts for the cerebellar degeneration protein, phospholipase A2, zinc finger protein 847, two ambiguous RNA transcripts, and small nuclear RNAs U5A and U5D. While these initial results were interesting in showing that there were more differentially expressed transcripts within each cell line in response to WT- or R14W mutant-CAIV than between cell lines, the total number of transcripts returned from the data obtained, using this cut-off value, was too low.

Table 10.1. Exon expression in HEK-293 and HT-1080 cells transfected with wildtype (WT) and R14W mutant (MUT) CAIV. Transcript expression was compared by microarray analysis. Using a 2-fold variance cut-off value, few genes were found to be differentially expressed.

Cell types compared	Differentially expressed genes (2-fold)
HEK-293 WT **vs** HEK-293 MUT	10
HT-1080 WT **vs** HT-1080 R14W MUT	15
HEK-293 WT **vs** HT-1080 WT	1
HEK-293 MUT **vs** HT-1080 MUT	1

The low number of transcripts and the unlikelihood of these transcripts being involved in the different responses of HEK-293 cells and HT-1080 cells to R14W mutant CAIV expression, as well as the inability to cluster transcripts into functionally relevant groups, prompted the use of a less-stringent 1.5-fold variance in expression as a cut-off value. The use of a 1.5-fold cut-off value is accepted as still being significant, and has been used in other studies, including those by McCarthy and Smythe (2009) and Wu (2008). A

Venn diagram in Figure 10.2 shows the numbers of differentially expressed transcripts obtained from each comparison using a 1.5-fold cut-off value.

It is important to note that when comparing levels of transfected CAIV, both HT-1080 and HEK-293 cells had the same levels of expressed WT- and R14W mutant transcript (1.00-fold). Altogether, 33 297 probe sets were analysed, of which 11 149 were control background probes, leaving 22 148 transcripts to be analysed for differential expression. A one-way analysis of variance (1-way ANOVA) statistical analysis model (Kerr et al. 2000) was used to normalise data. Before exploring the gene list obtained from microarray analysis, the data was checked for adherence to the seven criteria of a "good" gene list as described by Huang et al. (2008). Namely, it should contain (1) a high number of important marker genes, (2) a reasonable number of genes (within the hundreds to thousands), (3) a high number that pass statistical thresholds, (4) a notable portion of genes being involved in interesting biological processes as opposed to randomly spread throughout all processes, (5) the data should show high enrichment for certain biological processes, (6) be reproducible, and (7) be able to be confirmed by other experiments. Data obtained from the current study met at least six of these criteria (1-6), and was therefore deemed fit for functional analysis.

The Database for Annotation, Visualization and Integrated Discovery tool (DAVID) version 6.7 (accessed August to December 2011) (Huang et al. 2008) was utilised in order to cluster data according to functionality, and to highlight important processes that the differentially expressed genes may be involved in. An example of a DAVID functional annotation clustering report is shown in Figure 10.1. The DAVID was selected instead of similar tools (e.g GoMiner, GOstat and GoToolBox), due to it being unique in its expanded backend annotation database, advanced modular enrichment algorithms, and enhanced exploratory ability in data mining (Huang et al. 2008). In order to investigate responses to WT- and R14W mutant-CAIV, genome-wide exon expression was compared between HEK-293 cells and HT-1080 cells transfected with WT- and R14W mutant-CAIV. Results from comparisons were then analysed in order to determine

whether these transcripts could explain the differences in response to expression of R14W mutant CAIV between HEK-293 and HT-1080 cells.

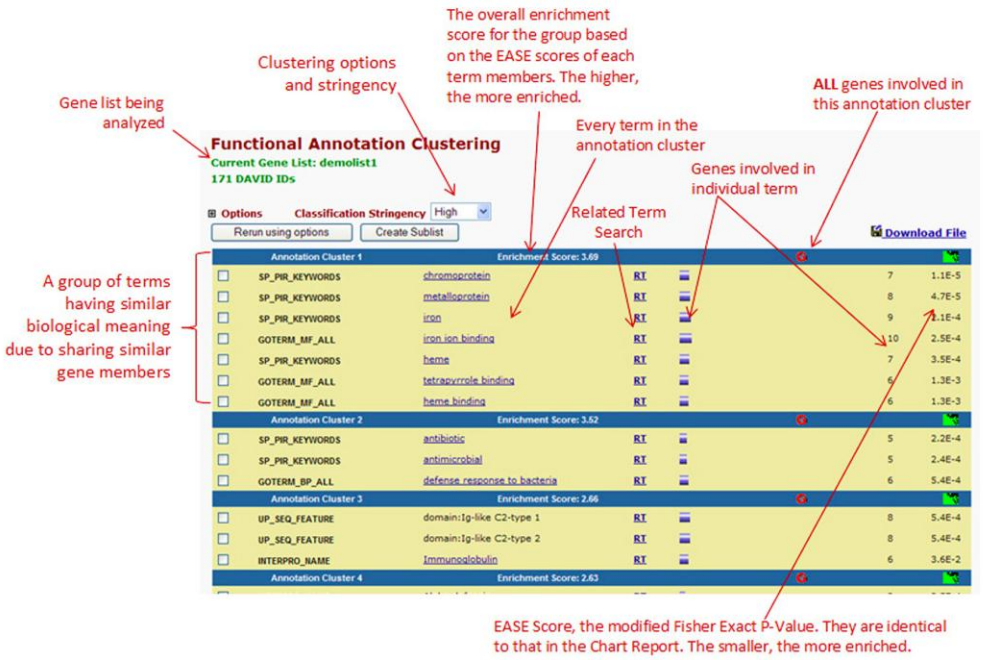

Figure 10.1. Example of a DAVID functional annotation clustering report. The report displays similar annotations together with the view that similar annotations should similar gene members. The report shows each term included in each cluster, as well as the enrichment scores, and allows the exploration of genes involved in each individual term.

10.1. Transcripts differentially expressed between HEK-293 and HT-1080 cells expressing R14W mutant CAIV

Following the results of section 7, in which HEK-293 cells were shown to be able to fold and process R14W mutant CAIV while COS-7 and HT-1080 cells were not, transcripts from HEK-293 cells and HT-1080 cells transfected with R14W mutant CAIV were compared. Differentially expressed transcripts between the two cell types were analysed in order to determine whether they might plausibly be responsible for the ability of HEK-293 cells to fold and process the R14W mutant protein and evade apoptosis, while HT-1080 cells respond negatively to the mutant protein.

Selection of transcripts with a 1.5-fold or higher difference in expression between HEK-293 and HT-1080 cells transfected with R14W mutant CAIV identified a total of 71 transcripts (Fig. 10.2).

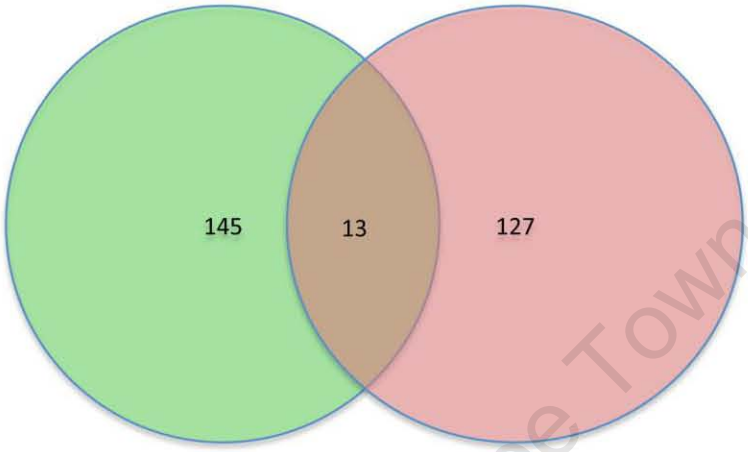

Data Set	Transcripts
HEK MUT vs HEK WT	158
HT MUT vs HT WT	140
HEK MUT vs HEK WT and HT MUT vs HT WT	13

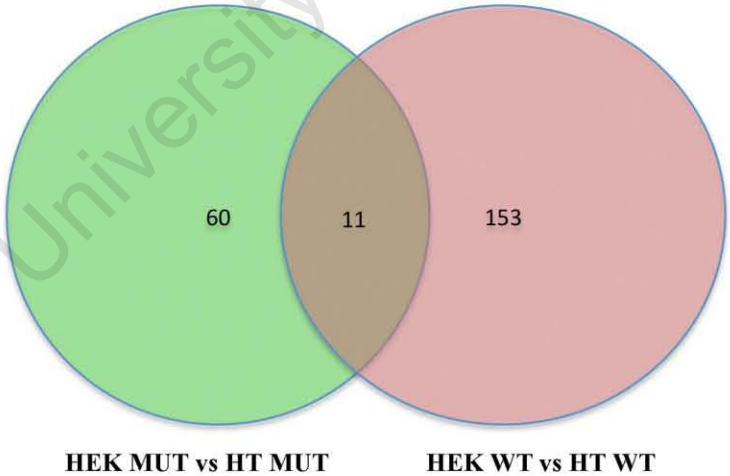

Data Set	Transcripts
HEK MUT vs HT MUT	71
HEK WT vs HT WT	164
HEK MUT vs HT MUT and HEK WT vs HT WT	11

Figure 10.2. Venn diagram showing the numbers of transcripts differentially expressed between HEK-293 and HT-1080 cells transfected with WT- and R14W mutant-CAIV.

Thirty nine of these transcripts were down-regulated in HEK-293 cells compared to HT-1080 cells. Performing a functional annotation clustering of these 39 transcripts using DAVID resulted in 6 clusters being returned, with group enrichment scores of 1.16 to 0.34 (based on EASE scores determined by modified Fisher Exact P-values). These group enrichment scores reflect the biological significance of gene groups to allow their ranking in terms of importance or relevance. Performing the same clustering on the 32 transcripts up-regulated in HEK-293 cells compared to HT-1080 cells transfected with R14W mutant CAIV returned 3 clusters with group enrichment scores of 2.61 to 0.08. When performing functional annotation clustering in DAVID, higher group enrichment scores are better than lower scores. Many of the transcripts that were differentially expressed in WT- and R14W mutant-CAIV-transfected cells will appear in more than one cluster, according to their GO (gene ontology) terms, however, the sections below will identify and characterise the most relevant and interesting transcripts, based on the group which most accurately describes their function in relation to the aims of this study.

Transcripts that were down-regulated in HEK-293 cells compared to HT-1080 cells expressing the mutant protein included some involved in signal transduction like the gamma aminobutyric acid (GABA) A receptor alpha 6 (Peran et al. 2004) or glycine receptor beta (Chen, et al. 2004) proteins that act as ion channels. Other transcripts that were identified as being down-regulated in HEK-293 cells include zinc finger proteins 284, 542 and 701 and other general transcription factors. Zinc finger proteins are involved in transcriptional regulation, can bind both DNA and protein, and belong to the kreuppel C2H2-type zinc-finger protein family (Brayer and Segal, 2008). In conjunction with their transcriptional regulator roles, zinc finger proteins are also involved in processes linked to cancer and tumour invasion, as well as cellular stress responses (Comijin et al. 2001; Davletova et al. 2005; Desjarlais et al. 1992). Mutations in the genes for these proteins have been shown to be involved in neuronal abnormalities (Hirata et al. 2006), neurodegeneration (Doran et al. 2006) and skeletal and craniofacial abnormalities (Momeni et al. 2000). Due to their ubiquitous nature and varying roles, it is difficult to draw a correlation between the down-regulation of zinc finger proteins in

HEK-293 cells and their ability to fold and process R14W mutant CAIV. The comparatively lower levels in HEK-293 cells expressing R14W mutant CAIV may merely indicate that HEK-293 cells are undergoing lower levels of cellular stress than HT-1080 cells transfected with mutant CAIV, and therefore do not need up-regulation of zinc finger proteins to initiate stress responses.

The only apoptosis-related protein that was identified as being down-regulated in HEK-293 cells compared to HT-1080 cells transfected with R14W mutant CAIV was rhomboid domain containing 1 (RHBDD1), a peptidase that modulates apoptosis through BCL-2 interacting killer protein (BIK). Knock-down of RHBDD1 in HEK-293 cells has been shown to enhance apoptosis (Wang et al. 2008). The down-regulation of RHBDD1 in HEK-293 cells by 1.82 fold compared to HT-1080 cells, suggests that HEK-293 cells expressing R14W mutant CAIV ought to display increased apoptosis compared to HT-1080 cells expressing the mutant protein. This is contradictory to results from section 7.2 which show that HEK-293 cells transfected with R14W mutant CAIV do not undergo apoptosis. However, further investigation into RHBDD1 showed that it has a number of substrates, including apoptosis regulators BCL-2 (B-cell lymphoma 2) and BCL-xl (B-cell lymphoma extra large). While BCL-2 has both apoptosis suppressor and activator activities under different conditions, BCL-xl acts as an apoptosis suppressor, particularly when co-expressed with BCL-2 (Chinnadurai et al. 2008). Although transcripts for these proteins could not be identified on the list returned by microarray, comparison of levels of BCL-2-related protein A1 (BCL2A1) and BCL-2 athanogene 2 (BAG2) was carried out. HEK-293 cells transfected with R14W mutant CAIV had higher levels of expression of BCL2A1 and BAG2 (by at least 1.3 fold) than HEK-293 cells expressing WT CAIV, or HT-1080 cells expressing either form of CAIV. HEK-293 cells transfected with WT CAIV had lower levels of the two than HT-1080 cells. The effect of RHBDD1, BCL-2 and related proteins on apoptosis appears to be complex, but thess protein may well be involved in signalling pathways with determine under what conditions HEK-293 cells undergo apoptosis.

The 32 transcripts that were up-regulated in HEK-293 cells transfected with R14W mutant CAIV compared to HT-1080 cells transfected with mutant CAIV similarly did not yield any obvious candidates responsible for the ability of HEK-293 cells to fold and process R14W mutant CAIV and evade apoptosis. Transcripts that were identified as being differentially expressed included olfactory receptors (family 1, 4, 11 and 52) as well as another G protein coupled receptor (number 32). The third cluster that these transcripts were related to included metal ion binding proteins like placental alkaline phosphatase, hephaestin-like protein 1, and ret finger protein-like 2.

As evidenced from the results above, the analysis of transcripts that were differentially expressed between HEK-293 and HT-1080 cells transfected with R14W mutant CAIV did not reveal the up-regulation of any proteins related to protein folding or processing in HEK-293 cells. Most proteins that were differentially expressed (either up- or down-regulated) related to transcriptional regulation, and therefore this comparison did not yield any obvious proteins that may be directly responsible for the ability of HEK-293 cells to fold and process R14W mutant CAIV and evade apoptosis.

Since these comparisons did not reveal proteins that could be directly related to the ability of HEK-293 cells to fold and process R14W mutant CAIV, transcripts that were differentially expressed between HEK-293 and HT-1080 cells transfected with WT CAIV were next examined to investigate the intrinsic differences in expression between the two cell types.

10.2. Transcripts differentially expressed between HEK-293 and HT-1080 cells expressing WT CAIV

Selection of transcripts with a 1.5-fold or higher difference in expression between HEK-293 and HT-1080 cells transfected with WT CAIV identified a total of 164 transcripts (Figure 10.2).

102 of these transcripts were down-regulated in HEK-293 cells compared to HT-1080 cells. A functional annotation clustering of these transcripts resulted in 23 clusters being returned. These clusters had group enrichment scores of 1.98 to 0.02. Clustering of the 62 transcripts that were up-regulated in HEK-293 cells compared to HT-1080 cells transfected with WT CAIV returned 12 clusters with group enrichment scores of 3.53 to 0.05.

A large majority of the transcripts that were down-regulated in HEK-293 cells expressing WT CAIV compared to HT-1080 cells included those involved in chemical homeostasis, cell-cell signalling, cell adhesion and blood vessel development. Most of the proteins translated from these transcripts are involved in wound healing, an essential function of fibroblast cells, from which HT-1080s are derived. There were also a number of receptors (endothelin receptor type A, olfactory receptor families 2 and 7) that presumably also have specific roles in HT-1080 cell signalling and homeostasis. There were four apoptosis-related genes found to be down-regulated in HEK-293 cells (CD24 molecule, STE20-related kinase adaptor beta, neurofilament (light polypeptide) and thrombospondin 1), however, the proteins encoded by these genes have very indirect involvement with apoptosis, and are unlikely to be associated with the response of HEK-293 cells to R14W mutant CAIV. When comparing HEK-293 cells to HT-1080 cells transfected with WT CAIV, some of the terms included in clusters with lower enrichment scores also included genes for a number of transmembrane proteins, as well as some zinc finger proteins (181, 204 and 847).

Included in the 62 transcripts that were up-regulated in HEK-293 cells compared to HT-1080 cells transfected with WT CAIV, were both olfactory (family 1, 2 and 52) and taste receptors (type 2, members 43 and 46). There were also a number of metal ion binding proteins (zinc finger protein 570 and phospholipase A2 group X) and other transcriptional regulators (mediator complex subunit 10) which are not anticipated to play a direct role in the folding and processing of CAIV in HEK-293 cells.

The transcript for PR domain containing 9 (PRDM9) was also up-regulated in HEK-293 cells transfected with WT CAIV. PRDM9 is a histone methyltransferase that is essential for progression into mitosis and plays a role in transcriptional regulation during the early stages (prophase) of mitosis (Baudat et al. 2010). Higher expression of this protein in HEK-293 cells may force cells to progress into mitosis and avoid S or G2/M cell cycle arrest despite expression of R14W mutant CAIV, although the lack of other phenotypic differences in HEK-293 cells suggests that their ability to avoid cell cycle arrest and apoptosis is more closely linked to their ability to fold and process R14W mutant CAIV.

Two proteins involved in protein folding were also up-regulated in HEK-293 cells transfected with WT CAIV. Heat shock 70kDa protein 4-like (Hspa4l, also referred to as APG-1) is a chaperone that belongs to the HSP110 family and acts as the cytosolic equivalent to GRP170 (Kampinga et al. 2009). Like GRP170, it has been proposed to have a role as a nucleotide exchange factor for HSP70 chaperones (Dragovic et al. 2006; Polier et al. 2008). A study on Hspa4l expression found that knockout mice displayed an increased incidence of male infertility and developed hydronephrosis (a back-up of urine in the kidney). Examination of these mice found that infertility was due to increased apoptosis in developing germ cells in male, but not female mice (Held et al. 2006). In addition to being up-regulated in HEK-293 cells transfected with WT CAIV compared to HT-1080 cells (by 1.52 fold), Hspa4l was also down-regulated in HEK-293 cells transfected with R14W mutant CAIV compared to WT CAIV-expressing HEK-293 cells (by 1.49 fold) and WT CAIV-expressing HT-1080 cells (by 1.4 fold). While a knockdown of Hspa4l is detrimental, up-regulation of Hspa4l has also been related to the presence of denatured proteins, and instigation of the stress response via HSP70 (Mivechi et al. 2011).. However, the role of Hspa4l in cytosolic-specific protein folding decreases the likelihood that this chaperone is directly involved in the differential folding of R14W mutant CAIV in HEK-293 cells compared to HT-1080 cells.

The endoplasmic reticulum and golgi intermediate compartment and golgi 3 (Ergic3) protein which was also up-regulated in WT CAIV-transfected HEK-293 cells plays an

important role in transport of proteins between the endoplasmic reticulum and golgi. This protein forms clusters that carry out anterograde and retrograde sorting between the ER and Golgi, and therefore also plays a role in the concentration, folding, and quality control of newly-synthesised proteins (Appenzeller-Herzog and Hauri, 2006). Higher expression of Ergic3 in HEK-293 cells (by 1.6 fold) may therefore endow them with a higher folding, processing and protein transport capacity than HT-1080 cells under normal cellular conditions. It is interesting to note, however, that expression of Ergic3 was not up-regulated in HEK-293 cells transfected with R14W mutant CAIV (in fact expression was decreased by 1.2-fold), making this protein an unlikely candidate to explain how HEK-293 cells are able to fold and process the mutant protein.

Since comparisons between HEK-293 cells and HT-1080 cells did not yield proteins which could clearly explain the ability of HEK-293 cells to fold and process R14W mutant CAIV while HT-1080 cells could not, this study next compared gene expression within cell lines.

10.3. Transcripts differentially expressed in HEK-293 cells expressing R14W mutant CAIV protein compared to WT CAIV

Selection of transcripts with a 1.5-fold or higher difference in expression between HEK-293 cells transfected with WT- or R14W mutant-CAIV identified 158 transcripts that were differentially expressed (Fig. 10.2).

There were 109 transcripts down-regulated in HEK-293 cells transfected with R14W mutant CAIV compared to cells transfected with the WT CAIV construct. Performing a functional annotation clustering of these 109 transcripts resulted in 15 clusters being returned, with group enrichment scores of 3.92 to 0.01. Performing the same clustering on the 49 transcripts up-regulated in HEK-293 cells transfected with R14W mutant CAIV compared to WT CAIV, resulted in 7 clusters with group enrichment scores of 0.82 to 0.09.

In order to avoid redundancy and to categorise transcripts in groups that are relevant to this study (i.e. those that may be involved in some way in protein expression, folding and processing, cell cycle regulation and apoptosis), the transcripts identified as being differentially expressed are listed under four categories: metal ion binding proteins and transcription factors, signalling pathway proteins, membrane components, and cell cycle and apoptosis regulators.

Metal ion binding proteins and transcription factors

By far the highest scoring group of transcripts differentially expressed between HEK-293 cells expressing WT- and R14W mutant-CAIV was a cluster related to metal ion binding, which included many transcription factors, co-factors, and other proteins associated with the nucleus. Included in this group were 13 zinc finger proteins (234, 284, 382, 383, 415, 440, 441, 443, 493, 506, 542, 578, and 846).

Some members of this ubiquitous group were found to be down-regulated up to 2.17 fold in HEK-293 cells transfected with R14W mutant CAIV compared to HEK-293 cells transfected with WT CAIV.

Other metal ion binding proteins that had trancripts down-regulated in R14W mutant HEK-293 cells compared to WT CAIV HEK-293 cells include activating transcription factor 7 interacting protein 2 (Atf7ip2), a transcription factor recruiter that couples transcription factors to general transcription apparatus (Ichimura et al. 2005) and PCF11, a component of pre-mRNA cleavage complex II and negative elongation factor (de Vries et al. 2000). Both of these transcriptional regulators are expressed ubiquitously however, and are unlikely to have a direct response on the ability of HEK-293 cells to fold and process R14W mutant CAIV protein.

An interesting transcript that was down-regulated in R14W mutant CAIV-expressing HEK-293 cells compared to WT CAIV-expressing cells was that for centrosomal protein 290kDa (CEP290). CEP290 is a DNA and nuclear matrix-associated protein that has also

been shown to have a critical function in ciliary transport in the eye. Mutations in the CEP290 gene which lead to loss of function of the protein have been linked to renal cyst formation (Sayer et al. 2006) and Leber Congenital Amaurosis, a congenital form of RP (den Hollander et al. 2006). Interestingly, as well as being separately involved in renal and visual systems, mutations in CEP290 have also been associated with syndromes such as Joubert symdrome, Senior Loken syndrome and nephronophthisis (Sayer et al. 2006; Gorden et al. 2008), which are characterised by both retinal degeneration and renal failure. While CEP290 was expressed at 1.51 times lower levels in R14W mutant CAIV-expressing HEK-293 cells compared to WT CAIV cells, its indirect role in transcriptional regulation (let alone protein folding, cell cycle regulation, or apoptosis) means that although this protein has interesting links to the study, it is unlikely to be directly involved in the HEK-293 cells' ability to fold and process R14W mutant CAIV.

Signalling pathway proteins

A number of genes for olfactory receptors and taste receptors were differentially expressed in HEK-293 cells expressing WT- and R14W mutant-CAIV. While olfactory receptors from families 7, 8 and 13 were down-regulated in HEK-293 cells expressing R14W mutant CAIV, some members from families 4 and 5 were up-regulated. Taste receptor proteins type 2, members 9 and 43 were also down-regulated in HEK-293 cells expressing the mutant CAIV. An endothelium-derived vasoconstrictor peptide, called endothelin 1 (Horstmeyer et al. 2005) was also included in the group of proteins down-regulated in R14W mutant CAIV-expressing HEK-293 cells, as well as frizzy-related protein, a cell growth and differentiation factor expressed in specific cell types (Loughlin et al. 2004). As with the proteins involved in transcriptional regulation, those involved in signalling pathways seem to be involved in normal cell type-specific functions, and not likely to be directly responsible for the ability of HEK-293 cells to fold and process R14W mutant CAIV and evade apoptosis.

Cell cycle and apoptosis regulators

The next group of transcripts that were differentially expressed in HEK-293 cells expressing WT- and R14W mutant-CAIV included cell cycle regulators and controllers of apoptosis. While these transcripts fell into distinct groups during clustering, since this study aimed to identify the factor(s) that protect HEK-293 cells expressing R14W mutant CAIV from undergoing apoptosis which occurs via cell cycle arrest, they are discussed together.

Transcripts for cell cycle regulators that are down-regulated in R14W mutant CAIV-expressing HEK-293 cells include G1 to S phase transition 2 (GSPT2), which is involved in cell cycle progression and in termination of translation (Zhouravleva et al. 2006). MutS homologue 4, another protein which was down-regulated in R14W mutant CAIV cells, has been shown to play a role in cell cycle regulation in some cell types in response to radiation (Davis et al. 1998). However, this protein's specific role is in the segregation of homologous chromosomes during meiosis 1 (Santucci-Darmanin et al. 2000), and its differential expression is therefore unlikely to be directly related to the ability to fold and process R14W mutant CAIV.

Levels of the transcript for the Wee1 homologue protein that is a checkpoint regulator were increased in HEK-293 cells expressing the mutant protein. Wee1 is a tyrosine kinase that maintains mitotic timing by phosphorylating CDK1/cyclin B1 kinase to keep it in an inactive state. Wee1 is present in high levels during the S and G2 phases of the cell cycle (Heald et al. 1993; McGowan et al. 1995). When cells need to progress into mitosis, Wee1 levels decrease. The increase in levels of Wee1 would be expected to cause an increase in the number of cells at the S and G2 phases of the cell cycle. However, this was not observed in experiments in section 7.1, where HEK-293 cells had relatively few cells at the S and G2 phase, and did not undergo cell cycle arrest in response to R14W mutant CAIV. Interestingly, the activity of Wee1 has been shown to depend heavily on activation by HSP90, a cytosolic chaperone which plays a key role in

protein folding, response to stress, and cell-cycle regulation (Aligue et al. 1994; Goes, 2001; Wiech et al. 1992), possibly linking Wee1 activity to these cellular processes.

Some of the transcripts down-regulated in R14W mutant CAIV-expressing HEK-293 cells encode proteins involved in the regulation of apoptosis. One of these proteins was baculoviral IAP (inhibitor of apoptosis) repeat-containing 3, an inhibitor of apoptosis (Hu and Yang, 2003). Surprisingly, WD repeat domain 92, an apoptosis promoter (Saeki et al. 2006), was also included in the same cluster. Again, due to the apparent ambiguity in the association of apoptosis-related proteins with HEK-293 cells expressing WT CAIV, these proteins were not considered to be directly involved in response to expression of CAIV. There were no transcripts involved in apoptosis that were up-regulated in HEK-293 cells expressing R14W mutant CAIV compared to HEK-293 cells expressing the WT protein.

Membrane components

The last group of transcripts that are down-regulated in R14W mutant-expressing HEK-293 cells encode proteins that form part of the plasma membrane of cells. Being involved in signalling and embedded in the plasma membrane, the olfactory and taste receptors described above were also clustered in both these groups, along with components of the signal peptidase complex and solute carrier (SLC) proteins.

The signal peptidase complex proteins sec11c and signal peptide peptidase-like 2A (SPPL2A) were down-regulated in HEK-293 cells expressing R14W mutant CAIV compared to cells expressing the WT protein. The former protein was also down-regulated in HEK-293 cells transfected with R14W mutant CAIV compared to HT-1080 cells (1.4-fold). Sec11c is a component of the microsomal signal peptidase complex and acts to remove the signal peptide from translated proteins as they enter the ER lumen (Böhni et al. 1988). Like sec11c, SPPL2A also functions as an intramembrane protease, but this protein also plays a role in regulating immunity and preventing disease (Martin et al. 2009). The higher expression of these proteins in HT-1080 cells may be in order to

cleave and process other proteins that are translated as part of the stress response to the unfolded mutant CAIV.

The solute carrier proteins down-regulated in R14W mutant CAIV-expressing HEK-293 cells include SLC family 45 member 4 (SLC45A4) and SLC organic anion transporter family member 4C1 (SLCO4C1). These transcripts were expressed at levels 1.57 and 1.64 less in R14W mutant CAIV HEK-293 cells compared to WT CAIV-expressing cells. While not much has been published on SLC45A4, SLCO4C1 has been associated with organic anion transport in epithelial cells, and in particular, in cells of the proximal renal tubules (Mikkaichi et al. 2004). The down-regulation of these anion transporters in cells transfected with R14W mutant CAIV may be as a result of decreased metabolic activities as these cells direct their activities towards mutant CAIV folding. It is interesting to note that other organic anion transporter transcript families (13, 27, 32 among others) were expressed at similar levels between HEK-293 cells and HT-1080 cells transfected with WT- and R14W mutant-CAIV.

The large number of zinc finger proteins that were down-regulated in R14W mutant CAIV-expressing HEK-293 cells is intriguing, particularly in light of the high enrichment scores and levels of differential expression. It is possible that these zinc finger proteins may play a part in the down-regulation of transcription of cell cycle arrest- and apoptosis-promoting genes, in response to expression of R14W mutant CAIV. Conversely, they may up-regulate expression of genes involved in protein folding and processing in response to the mutant protein. The levels of these genes which are regulated by the zinc finger protein may not increase/decrease by as much as the 1.5-fold threshold used in this study, but may nevertheless be changed enough to elicit the response of HEK-293 cells to expression of R14W mutant CAIV which was observed in sections 7 and 8.

Interestingly, there were no readily identifiable chaperone proteins that were differentially expressed between HEK-293 cells transfected with R14W mutant CAIV or the WT protein. When microarray results were examined, most members of the HSP70

family (which includes BiP and GRP170) were expressed at similar levels (ie. at the same levels or up to 1.2 fold difference) in R14W mutant- and WT CAIV-expressing HEK-293 cells. This result was not surprising however, since western blot experiments on levels of these chaperones had shown no significant difference in expression within cell lines. Apart from sec11c, comparison of transcripts that were down-regulated in R14W mutant CAIV-expressing HEK-293 cells compared to WT CAIV-expressing HEK-293 cells revealed few proteins that may have been involved in differential processing of WT- and R14W mutant-CAIV in HEK-293 cells. Therefore, this study next examined transcripts that were differentially expressed between HT-1080 cells expressing WT- and R14W mutant-CAIV.

10.4. Transcripts differentially expressed in HT-1080 cells expressing R14W mutant CAIV protein compared to WT CAIV

Selection of transcripts with a 1.5-fold or higher difference in expression between HT-1080 cells transfected with WT- or R14W mutant-CAIV identified 140 transcripts that were differentially expressed (Fig. 10.2).

Ninety one of these transcripts were down-regulated in HT-1080 cells transfected with R14W mutant CAIV compared to cells transfected with the WT CAIV construct. Performing a functional annotation clustering of these 91 transcripts using DAVID resulted in 13 clusters being returned. These clusters had group enrichment scores of 1.36 to 0.02. Performing the same clustering on the 49 transcripts up-regulated in HT-1080 cells transfected with R14W mutant CAIV compared to WT CAIV, resulted in 6 clusters with group enrichment scores of 0.98 to 0.09. Transcripts that were identified as being differentially expressed between HT-1080 cells transfected with WT- and R14W mutant-CAIV were listed under categories that included transcripts relevant to the study, as explained in section 10.1. The three categories include cell cycle and apoptosis regulators, co-chaperones, and metal ion binding proteins and transcription factors.

Cell cycle and apoptosis regulators

Many transcripts that were differentially expressed in HT-1080 cells transfected with WT- and R14W mutant-CAIV relate to cell cycle regulation and initiation of apoptosis.

Included in this group were transcripts that were down-regulated in HT-1080 cells transfected with R14W mutant CAIV. Among these were mitotic checkpoint regulator 'mitotic arrest deficient-like 1' (MAD2l1), a protein that regulates cell cycle and may protect cells from undergoing apoptosis (Fung et al. 2005; Michel et al. 2004). HT-1080 cells transfected with R14W mutant CAIV expressed over 1.75 times less MAD2l1 than cells transfected with WT CAIV, and severe repression of MAD2l1 levels has been shown to result in mitotic failure. Other cell cycle-related transcripts that were down-regulated in R14W mutant CAIV HT-1080 cells were anaphase promoting complex subunit 1 (ANAPC1), which controls progression of cells from mitosis through to the G1 phase of the cell cycle (Grossberger et al. 1999) and protein phosphatase 1 catalytic subunit beta isoform (PPP1CB) which regulates the G1 to S phase transition of the cell cycle (Park et al. 2011). PPP1CB has been shown to interact with protein phosphatase 1 regulatory (inhibitory) subunit 15A (PPP1R15A), an apoptosis-related protein that was down-regulated in HT-1080 cells expressing R14W mutant CAIV compared to cells expressing the WT protein. PPP1R15A prevents cells from undergoing apoptosis by facilitating the recovery of the cell from ER stress (by reversing the shutting down of protein synthesis initiated by stress) (Tsaytler et al. 2011). Another apoptosis inhibitor, baculoviral IAP (inhibitor of apoptosis) repeat-containing 3 (Hu and Yang, 2003) was also found to be down-regulated in HT-1080 cells expressing R14W mutant CAIV.

The down-regulation of these cell cycle regulators and apoptosis inhibitors is aligned with the results in section 7 that show that HT-1080 cells expressing R14W mutant CAIV protein undergo apoptosis. As explained in section 7.1, HT-1080 cells were not analysed by FACS analysis, and therefore the effect of the mutant CAIV protein on HT-1080 cell cycle has not been determined. However, the negative effect of R14W mutant CAIV on

cell cycle regulators as determined by microarray analysis, does suggest that expression of R14W mutant CAIV in HT-1080 cells has an effect on cell cycle progression.

Co-chaperones

One co-chaperone was identified as being down-regulated in HT-1080 cells expressing R14W mutant CAIV compared to HT-1080 cells expressing the WT CAIV protein. Small glutamine-rich tetratricopeptide repeat (TPR)-containing beta protein (SGTB) binds directly to HSP70 and HSP90, and modulates these chaperones' ATPase activity (Winnefeld et al. 2003). Interestingly, SGTB depletion in cells has been shown to cause mitotic arrest and lead to cell death (Winnefeld et al. 2003). Due to its role in protein folding, cell cycle and cell death, SGTB may be a candidate protein to introduce to HT-1080 cells transfected with R14W mutant CAIV, to encourage these cells to fold and process the mutant protein.

Metal ion binding proteins and transcription factors

As observed in experiments comparing transcripts differentially expressed in HEK-293 cells transfected with R14W mutant or WT CAIV, metal ion binding proteins were also found to be differentially expressed in HT-1080 cells. Zinc finger proteins 181, 204, 26, 397, 826 and 847 were all found to be down-regulated in HT-1080 cells transfected with R14W mutant CAIV compared to cells transfected with the WT protein. As mentioned in section 10.2, these proteins are involved in transcriptional regulation, and can bind both DNA and protein (Brayer and Segal, 2008). Their down-regulation in mutant CAIV cells may indicate an indirect involvement in the inability of these cells to fold and process R14W mutant CAIV. Down-regulation of these zinc proteins may up-regulate genes involved in cell cycle arrest or apoptosis or down-regulate genes involved in protein folding or cell survival.

Similarly, zinc finger CCHC domain containing 17 protein was found to be up-regulated in HT-1080 cells transfected with R14W mutant CAIV compared to HT-1080 cells expressing the WT protein. Up-regulation of this protein may conversely down-regulate

genes involved in cell cycle arrest or apoptosis or up-regulate genes involved in protein folding or cell survival.

10.5 Combined comparisons

Comparisons between HEK-293 and HT-1080 cells transfected with WT- or R14W mutant-CAIV was carried out to identify shared transcripts that are differentially expressed between the two cell types. This experiment thus identified genes that were either up- or down-regulated in both HEK-293 and HT-1080 cells transfected with mutant CAIV compared to both cell types expressing the WT form of CAIV.

Examining proteins that are differentially-expressed in both HEK-293 and HT-1080 cells transfected with R14W mutant CAIV identified 13 transcripts that are up- or down-regulated (Table 10.2). Eleven of these genes were down-regulated, while 2 were up-regulated in all cells transfected with the mutant protein. Included in the group of genes that were down-regulated is replication factor C, a five-subunit protein that is required for replication and repair of DNA (Green et al. 2000). Its down-regulation in cells expressing mutant CAIV may be a response of cells to shut down some aspects of regulation while coping with the presence of the mutant CAIV. Small nuclear RNA (snRNA) U5A and U5D were also down-regulated in R14W mutant CAIV-expressing cells. These RNAs act as active components of the spliceosome and play a role in pre-mRNA splicing (Chabot et al. 1985; Sontheimer and Steitz, 1993). While snRNA U5A was down-regulated more in HEK-293 mutant cells that HT-1080 cells, U5D was down-regulated less (Table 10.2), making it difficult to explain the down-regulation of these molecules in the context of this study.

Small nucleolar RNA (snoRNA) H/ACA box 9 was up-regulated in cells transfected with R14W mutant CAIV. snoRNAs are involved in the processing and transport of pre-ribosomal RNAs which will eventually participate in global protein translation within the cell (Ganot et al. 1997; Li et al. 2005). Their up-regulation in cells expressing mutant

CAIV may therefore indicate the instigation of translation of proteins which will aid in managing the R14W mutant CAIV.

Other transcripts which were differentially expressed in all cells transfected with R14W mutant CAIV are detailed in Table 10.2, and have not been discussed further due to the unlikelihood of them being directly (or even indirectly) responsible for the ability of HEK-293 cells to fold and process R14W mutant CAIV.

When the 11 transcripts that were differentially expressed in all HEK-293 cells compared to all HT-1080 cells were analysed, there were also no obvious candidates that would explain the ability of HEK-293 cells to fold and process R14W mutant CAIV. All of the transcripts' up- or down-regulation could be explained by cell-type specificity (Table 10.3). It was interesting to note that a transcript called Hypothetical LOC644714 appeared in both lists (Table 10.2 and 10.3). Expression of this transcript was down-regulated in both HEK-293 and HT-1080 cells transfected with R14W mutant CAIV, but to a lesser degree in HEK-293 cells. An investigation into this transcript however showed it to be a cell type specific protein present in keratinocytes and hair follicles (Hafner et al, 2010; Shin et al. 2010).

Again, when comparing multiple expression experiments, it was interesting to note the up-regulation of Hspa4l in HEK-293 cells transfected with WT CAIV vs. HT-1080 cells. As mentioned, this protein was also down-regulated in HEK-293 cells transfected with R14W mutant CAIV compared to HT-1080 cells, although only by 1.4 fold. Although this protein did not appear in Table 10.3, this difference in expression is notable, particularly in light of the role of this protein family in ER-specific protein folding and preventing apoptosis (Beere et al. 2000). The protein being present at higher levels in HEK-293 under "normal" conditions, allowing HEK-293 cells greater "native" folding capability, may explain changes in the levels of Hspa4l. Levels may increase in HT-1080 cells in response to the mutant CAIV as these cells try to fold the mutant protein, and then experience ER-stress. The rise in Hspa4l may be in an attempt to prevent cell death

as a result of the misfolded CAIV. HEK-293 cells would not experience an increase in HSP70-4l, as their ability to fold the mutant CAIV protein would prevent them from undergoing ER-stress. Puzzlingly, the many other HSP70-like transcripts which were detected by microarray showed very little difference in expression between HEK-293 and HT-1080 cells transfected with WT- or R14W mutant-CAIV.

Table 10.2. Transcripts differentially expressed in all cells transfected with R14W mutant CAIV compared to WT cells

Transcript name	Up/down-regulated in all MUT cells	Fold variance	
		HEK MUT vs HEK WT	HT MUT vs HT WT
Replication factor C (activator 1) 1	Down	2.36	1.68
Small nuclear RNA U5A	Down	2.35	1.72
Zinc finger protein 847	Down	2.09	3.48
Small nuclear RNA U5D	Down	2.05	2.33
AT rich interactive domain 4B	Down	1.88	1.57
(RBP1-like) Arrestin domain containing 3	Down	1.81	1.85
AT rich interactive domain 4A (RBP1-like)	Down	1.64	1.51
Interferon-induced protein with tetratricopeptide repeats	Down	1.60	1.94
Small Cajal body-specific RNA 9	Down	1.58	1.58
Hypothetical protein LOC644714	Down	1.55	2.11
KIAA1370	Down	1.51	1.61
Small nucleolar RNA, H/ACA box 9	Up	1.52	1.68
Crystallin, zeta (quinone reductase)	Up	1.60	1.52

Table 10.3. Transcripts differentially expressed in HEK-293 cells compared to HT-1080 cells

Transcript name	Up/down-regulated in all HEK cells	Fold variance	
		HEK MUT vs HT MUT	HEK WT vs HT WT
Cerebellar degeneration-related protein 1	Down	3.37	3.1
Melanoma antigen family C, 2	Down	1.98	1.97
Endothelin receptor type A	Down	1.7	1.59
RNA binding motif protein 23	Down	1.66	1.64
Glycine receptor, beta	Down	1.60	1.54
Hypothetical LOC644714	Both	1.51 Up	2.28 Down
Glutathione S-transferase theta pseudogene 1	Up	1.61	1.54
MicroRNA 34a	Both	1.64 Up	1.51 Down
Pregnancy specific beta-1-glycoprotein 2	Both	1.66 Up	1.79 Down
Zinc finger protein 737	Up	1.91	1.83

As a last measure to identify any proteins responsible for the ability of HEK-293 cells to fold and process R14W mutant CAIV, the entire list of transcripts identified by microarray was probed for terms related to ER-specific protein folding and protein processing (e.g. endoplasmic reticulum, folding, chaperone, co-chaperone etc.). This search identified many transcripts for chaperones, including members of the HSP70 family, as well as proteins like the stress-associated endoplasmic reticulum protein family 2 (SERP2), endoplasmic reticulum-golgi intermediate compartment 1 (ERGIC1), endoplasmic reticulum chaperone SIL1 homologue, and endoplasmic reticulum to nucleus signalling 1. None of these transcripts showed significant differences in expression between HEK-293 and HT-1080 cells transfected with WT- or R14W mutant-CAIV. Interestingly however, activating transcription factor (ATF6), an ER stress-related protein (Malhotra, 2007) was down-regulated in HEK-293 cells transfected with R14W mutant CAIV (by at least 1.1 fold) compared to HT-1080 cells transfected with either form of the CAIV protein, confirming that compared to HEK-293 cells, HT-1080 cells undergo more ER stress in response to expression of R14W mutant CAIV.

This investigation into gene expression in HEK-293 and HT-1080 cells transfected with WT- and R14W mutant-CAIV revealed a number of transcripts which may aid in the folding and processing of R14W mutant CAIV in HEK-293 cells, or in the response of HT-1080 cells to the mutant protein. Intriguingly, the analysis showed that there were more genes differentially expressed within each cell line in response to WT- or R14W mutant-CAIV, than when comparing cell types to each other. In order to further investigate the folding and processing of CAIV in HEK-293 and HT-1080 cells, mass spectrometry was carried out on protein extracts from both cell types transfected with WT- and R14W mutant-CAIV.

11. Identification of proteins involved in the processing of CAIV by mass spectrometry

As mentioned in sections 8 and 9, this study sought not only to determine the molecular mechanisms behind RP17, but also to investigate possible methods of neutralising the molecular pathology caused by R14W mutant protein (which may have implications in providing therapy for the disease).

The observation that HEK-293 cells were able to correctly fold R14W mutant CAIV indicated that there may be proteins expressed in these cells that allow for the processing of the mutant protein and the evasion of cell death. These cellular processes and proteins may be expressed either endogenously under normal circumstances or in response to expression of the mutant CAIV protein. Section 9 examined the expression of three ER-chaperones in an attempt to determine whether any of these proteins may be responsible for the ability of HEK-239 cells to fold R14W mutant CAIV. This was followed by section 10, in which microarray analyses were used to examine the up- or down-regulation globally, of proteins that may be responsible for the ability of HEK-293 cells to fold and process R14W mutant CAIV. Since none of the proteins identified in these sections were recognised as being differentially expressed in HEK-293 cells in a manner which would account for the folding of R14W CAIV, another approach was undertaken to in an attempt to identify proteins that may have been assisting in folding. Mass spectrometry analysis was used to identify proteins that bind to CAIV in HEK-293 cells, but not in HT-1080 cells. As this analysis followed microarray analysis, some of the results were expected to confirm some of the transcripts that were differentially expressed between HT-1080 and HEK-293 cells. As with the microarray analyses, this study was carried out as an exploratory study. The mass spectrometry, however, followed a more targeted approach in which only proteins bound to CAIV were included in the analysis. The list of CAIV-associated proteins was therefore expected to be much shorter than that obtained from microarray analysis, during which global expression was measured.

As with chapter 10, protein expression was only analysed using extracts from HT-1080 and HEK-293 cells. HT-1080 and HEK-293 were transfected with either WT- or R14W mutant-CAIV and protein extracts harvested (Fig. 11.1a) CAIV protein (as well as proteins bound to CAIV) was then isolated using immunoprecipitation (IP) with an anti-CAIV antibody or a non-specific IgG antibody. Western blotting analysis using the same anti-CAIV antibody showed that the procedure resulted in the isolation and purification of CAIV and CAIV-complexed proteins (Fig. 11.1b and c). After IP, the purified samples were sent to the Proteomics Laboratory at the Central Analytical Facility of the University of Stellenbosch. Here, the samples were analysed by mass spectrometry in order to identify proteins that were bound to CAIV.

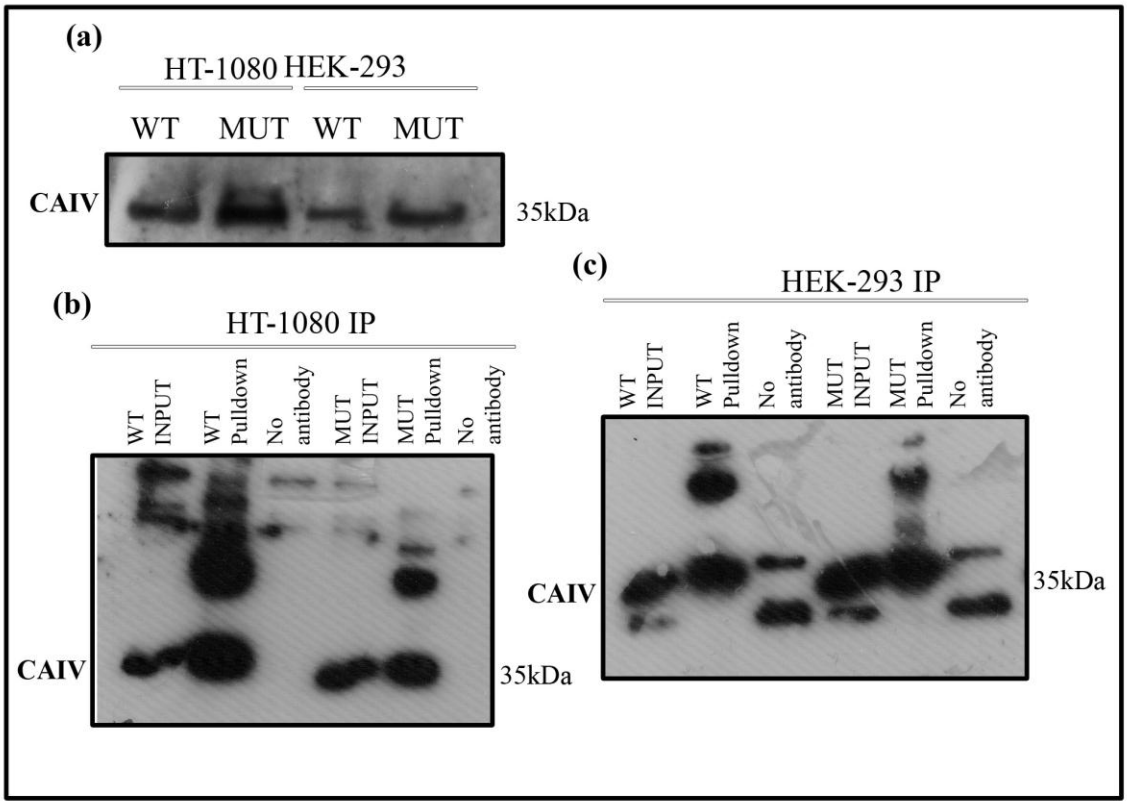

Figure. 11.1. Immunoprecipitation pull down of CAIV. (a) HT-1080 and HEK-293 cells transfected with WT- or R14W CAIV in pCXN vector show comparable levels of CAIV protein expression. Western blot analyses were used to compare expression of CAIV from total protein (2 µg) isolated from HT-1080 and HEK-293 cells transfected with WT- or R14W mutant CAIV. Anti-CAIV antibody was then used to isolate and purify CAIV protein from HT-1080 **(b)** and HEK-293 **(c)** cellular extracts. Protein blots (including the IP pull down blot) were probed with antibodies specific for CAIV.

11.1. Identification of proteins bound to WT- and R14W mutant-CAIV in HEK-293 cells

Specific attention was directed toward the proteins bound to WT- and R14W mutant-CAIV in HEK-293 cells, in order to identify proteins that may allow this cell type to fold and process mutant CAIV and evade cell cycle arrest and apoptosis. Mass spectrometry on proteins bound to CAIV in HEK-293 cells showed that there were differences in the proteins that bound to the WT- and R14W mutant form of CAIV.

Analysis of proteins bound to CAIV in HEK-293 cells produced a list of 88 proteins that were bound to the R14W mutant CAIV, while 72 were bound to the WT protein. A list of the different proteins bound to WT- and R14W mutant-CAIV in HEK-293 cells is detailed in the Appendix, with proteins of interest highlighted in yellow (section 14.16).

An examination of the list of proteins associated with R14W CAIV in HEK-293 cells reveals some of the proteins that may aid HEK-293 cells in folding R14W mutant CAIV. One of these proteins is DNAJ (subfamily C member 2) (DNAJC2, also referred to as Zrf1, Zrf2 or zuotin), the cytosolic HSP40 co-chaperone that is responsible for assisting in protein folding and modulating the activity of HSP70 chaperones (Kampinga et al. 2009; Li and Lee, 2006). Interestingly, when levels of DNAJC2 transcript were compared by microarray, HEK-293 cells transfected with R14W mutant CAIV had slightly lower levels (1.2 fold) than those transfected with the WT protein. HEK-293 cells transfected with WT CAIV and HT-1080 cells transfected with either form of CAIV expressed similar levels (maximum of 1.17 fold difference in expression). DNAJ stimulates HSP70 proteins within the ER and also remains bound to HSP70s as they fold newly synthesized proteins (Qiu et al. 2006). Although it is tempting to relate binding of DNAJC2 to R14W mutant CAIV to the processing of this protein in HEK-293 cells, the cytosolic location of this chaperone makes its involvement in differential processing of R14W mutant CAIV by HEK-293 cells unlikely.

A number of proteins in, and associated with, the HSP70 family of chaperones were bound to CAIV in HEK-293 and HT-1080 cells expressing the WT, but not the R14W mutant form of CAIV (HSPA9, HSPA13). This finding may further support the role of these and other HSP70s in the normal processing of the CAIV protein.

Isoforms of the sodium bicarbonate exchanger family were also bound to CAIV in HEK-293 cells expressing the R14W mutant protein, supporting the observations of Yang et al. (2005), who proposed that CAIV forms a membrane complex with the NBC1 bicarbonate exchanger protein. However, this was not the case in HT-1080 cells expressing CAIV, which did not have any bicarbonate exchangers bound to the protein. These results, along with those from section 7, further invalidate the hypothesis that cell death in R14W mutant CAIV-expressing cells is caused by a disrupted CAIV/NBC1 metabolon.

Another protein which was bound to R14W mutant CAIV in HEK-293 cells is isoform 2 of S phase cyclin A-associated protein in the endoplasmic reticulum (Scraper). Scraper is located in the endoplasmic reticulum and interacts with cyclin A to activate the G1/S phase transition of the cell cycle (Tsang et al. 2007). This protein may help to encourage HEK-293 cells to progress through the cell cycle normally, although the reason behind its binding to R14W mutant CAIV is unclear.

As with microarray experiments, various zinc finger proteins (287, 406, 518A, 609) were identified as being present in HEK-293 expressing the WT- and R14W mutant-CAIV. This may again indicate their activity in the transcriptional regulation of other genes in response to the presence of WT- or mutant CAIV, or their role as metallothioneins that transfer the zinc ion to CAIV, and thus enhance the activity of the enzyme (Li et al. 1980).

Mass spectrometry, like microarray analyses, identified a number of candidate proteins that may aid in folding and processing of R14W mutant CAIV in HEK-293 cells. Most notably in these studies, however, was the observation that many of the proteins that were found to be up- or down-regulated (as shown by microarray analyses), or bound to CAIV

(as shown by mass spectrometry) did not show an obvious link to CAIV processing. These results highlight the complexity of cellular responses, and emphasise that any biological response carried out by a cell is not brought about by a single protein, and is more likely to be underlined by a myriad of smaller changes at the transcriptional level.

Discussion

The extensive genetic heterogeneity that underlies even the dominant retinal disorders, is illustrative of the very disparate molecular pathologies which underlie this group of diseases. The research presented here sought to focus intensively on the RP17 form of adRP, ranging from genetic screening of members of the adRP cohort for *CA4* gene mutations, to examining the phenomenon of a CAIV metabolon. This study also investigated the molecular pathogenesis underlying RP17, and used the results to explore a number of proof of principle options for therapy for the disease.

Investigating the molecular mechanisms that lead to the RP17 phenotype was one of the key aims of the study. While a clear link between the CAIV R14W mutation and phenotype in South African RP17 families has been established, several confounding factors have called for a further investigation into this disease. Firstly, while the first group to identify the R14W CAIV mutation in RP17 described protein misfolding and apoptosis as the molecular mechanisms behind disease (Rebello et al. 2004), alternative pathogenic mechanisms have been suggested for the same mutations. A study by Yang et al. (2005) proposed a change in pH buffering due to dysfunction of CAIV as the cause of RP17. Additional studies on the disease have supported the hypotheses of either one of the two groups (Alvarez et al. 2007; Bonapace et al. 2004; Rebello et al. 2004; Sun et al. 2008; Yang et al. 2005). Furthermore, while the link between with R14W mutation in CAIV has been clearly established in the South African RP17 cohort, a northern Swedish study reported a 4% incidence of the R14W CAIV mutation in a background population that did not manifest any obvious phenotype. This was in contrast with studies on the South African and Chinese cohorts (Alvarez et al. 2007; Rebello et al. 2004), which showed 100% penetrance of the RP17 phenotype. Lastly, until recently, the RP17 cohort in South Africa had not been studied in any great detail in order to clearly describe and define the RP17 phenotype.

This study therefore sought to characterise the RP17 phenotype, at both the genetic and molecular (functional) level, as well as to use these observations to propose possible methods to explore molecular techniques as proof of priciple for the development of therapy to treat or prevent the disease.

12. Genetics of RP17

An investigation of the RP17 cohort showed the ages of onset of disease to be similar to that typically expected for patients with dominant forms of RP (i.e. onset of symptoms during teenage years with severe visual impairment at 30-40 years of age) (Daiger et al. 2007; Shintani et al. 2009). While most patients experienced symptoms in their early twenties, outliers experienced symptoms as early as 7 years of age, or as late as 40 years of age. That RP17 may manifest so early in life is an important consideration when attempting to prevent the disease phenotype in mutation-positive individuals. Furthermore, an earlier onset will mean that loss of vision will occur earlier than is typically expected, and therapeutic interventions, which work best when there are some surviving photoreceptors in the retina (Jacobson et al. 2005), will have to be undertaken as soon as is possible in RP17 patients.

Further confounding the issue of defining the RP17 phenotype, was the report that some individuals in a northern Swedish cohort who had the R14W mutation did not show the RP phenotype at all (Köhn et al. 2008). This report detected the mutation when screening a number of genes for mutations linked to Bothnia Dystrophy. When an individual was found with the mutation but who was completely asymptomatic for RP, screening on the background population, found the SNP at a frequency of 4% in this region.

This degree of variation and apparent lack of penetrance of the disease has been described for other forms of adRP (Berson et al. 1969; Rivolta et al. 2002), and may be explained by the different pathology of RP17 when compared to other forms of RP (e.g. RP1, McWilliam et al. 1989). While most dominant forms of RP have the photoreceptors in the retina as the primary site of insult, in RP17 the initial endogenous insult is in the

supporting choriocapillaris. This may mean that unique genes and proteins that determine choriocapillaris survival and are not expressed in photoreceptors, may affect the onset and progression of RP17 specifically. For example, a recent study showed the importance of a mitochondrial membrane protein, Ucp2, in the clearing of apoptotic cells from surrounding tissue by phagocytes (Park et al. 2011). It was shown both *in vitro* and *in vivo* that mice that were deficient in the protein were unable to clear apoptotic cells, and suffered significant defects in the thymus and testes. The expression of analogous proteins to Ucp2 in the choriocapillaris may similarly affect the clearance of apoptotic cells in this layer, and impact on survival of this tissue. thereby explaining in principle the differences in penetrance of such diseases between individuals and potentially between populations.

In a longitudinal ophthalmological investigation of the RP17 cohort (unpublished data), Ramesar et al. studied the eyes and phenotypes of 21 patients with RP17, and found a "unique chorioretinal phenotype" in these patients that differs from those with classical autosomal dominant RP. In the older patients within the cohort, choroidal atrophy approximated to choroideremia. Collapse of the choriocapillaris has been linked to atrophy of the RPE layer and retinal degeneration in a study by Deutman (1983), who called the disease "choriocapillaritis", or acute multifocal ischaemic choroidopathy (AMIC). His study provided a link between defects in the choriocapillaris, and the downstream effects on the retina.

Support for RP17 being considered separately to typical RP, could also be gained from the results from retinal examinations and fluorescein angiography. The procedure involves application of sodium fluorescein into the eye, which stains the blood vessels and can be used to observe the retinal vasculature (Hayreh, 1974). Results from the unpublished Ramesar study on the pathology of RP17 showed extensive hyperfluorescence in some areas of the retina upon diffusion with fluorescein. This was believed to have indicated capillary leakage and abnormal vasculature in this layer of the eye. If the pattern of degeneration shows some evidence of non-proliferative or

proliferative retinopathy as may be observed in diabetes (in which retinal blood vessels are primarily affected) and not RP (Lahdenranta et al. 2001), a case may be made for RP17 to be considered separately from other types of RP. For example, retinopathy may be treated at the non-proliferative stage by laser therapy in order to prevent leakage of already-damaged blood vessels into surrounding layers, and in the case of RP17, gene or protein therapy could be used at the same time to prevent continued cell death in this layer. The observations of this and other studies point to the possible role of ophthalmologists whose observations might in some instances indicate alternative molecular pathologies of disease even within the adRPs. This in turn might lead to a faster identification of the underlying mutations, and have implications both in terms of management of the disease, and in attempts to develop treatment and therapy.

Screening of the adRP cohort for mutations in the coding regions of the *CA4* gene was carried out in order to determine whether any of these individuals had the R14W mutation, or any further mutations.

Screening of 56 individuals from the adRP cohort revealed that one patient (RPD453.1MUS) had a heterozygous c.-316G>C nucleotide change in the 5'UTR. Another two patients (RPD18.11SAL and RPD55.15LUK) shared a homozygous c.-161C>G change in the 5'UTR, while three (RPD348.1NOE, RPD391.1PHI, and RPD436.2GAN) had an A>C nucleotide change upstream of exon 1b at position c.59-46. None of these variants had been previously reported, and they were all therefore analysed using the online splice prediction tools at the Karolinska Institute (http://mordor.cgb.ki.se/cgi-bin/CONSITE/consite) and the Berkley Drosophila Genome Project (http://www.fruitfly.org/ seq_tools/splice). The sequences were also analysed for changes in transcription factor binding sites using the online TESS (transcription element search system) tool (http://www.cbil.upenn.edu/cgi-bin/tess/tess; Shug and Overton, 1997). Using the above software, no changes in splicing or to transcription factor binding sites were predicted.

While the available software did not report any of the novel substitutions as having the potential to affect splicing or transcription factor binding, it must be noted that a screen of the full genomic sequence of *CA4* using the TESS tool did not return any of the transcription factors shown to bind to *CA4*. Using the Ingenuity Pathway Analysis software tool (Ingenuity Systems Inc., USA) both HTT (huntingtin) and ATN1 (atrophin1) were returned as transcription factors that bind to CAIV (Fig. 12.1). The discrepancy questions the utility of this software, and how large the database of TESS transcription factors may be. This is especially important since one of the CAIV mutations linked to RP17 has been identified in the 3'UTR (+59G>A, Yang et al. 2005), and studies such as that by Wray (2007) have highlighted the importance of the 5'- and 3' regulatory regions in phenotypic variations. Nevertheless, HTT and ATN have been shown to bind CAIV in the nervous system only (Kaltenbach et al. 2007), and nucleotide substitutions which affect their binding are therefore not likely to have a direct effect with regards to RP17 and the visual system.

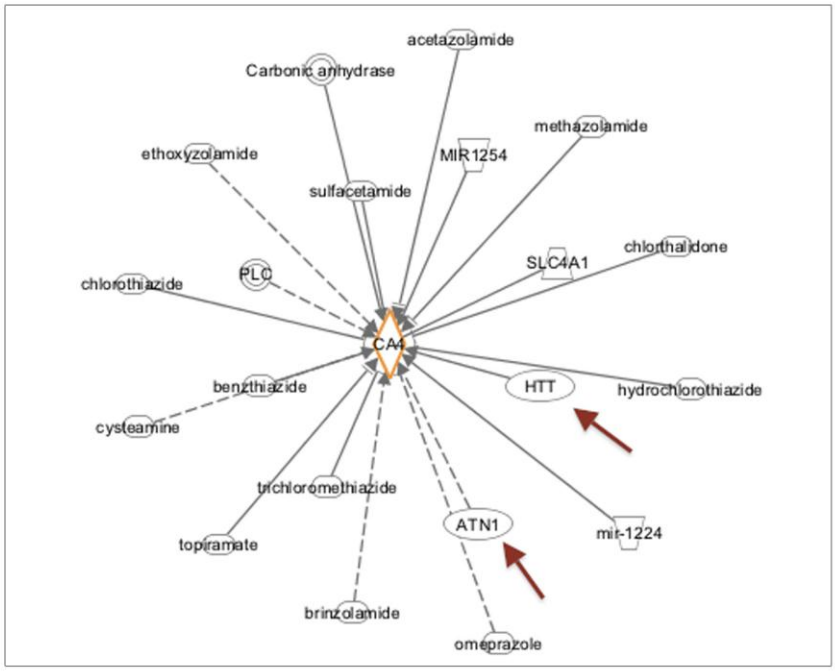

Figure 12.1. An interaction network between CAIV and other molecules. A CAIV network diagram generated using the Ingenuity Pathway Analysis software shows that the protein interacts with transcription factors HTT and ATN1, as well as inhibitors like acetazolamide and methazolamide.

In order to thoroughly examine the effect of nucleotide substitutions upstream or downstream of the *CA4* gene or within the intronic regions, a broader range of software programmes may need to be used in an effort to obtain a more up to date and complete picture of the behaviour and interactions of the normal protein, and the possible effects of sequence changes.

A screen by genotyping was carried out on the ΔF508-containing region of the CFTR gene in order to determine whether any individuals in the RP17 cohort (i.e. CAIV R14W mutation carriers) had the additional 3 bp deletion in the CFTR. The screen was based on a study which linked mistrafficking of CAIV with the ΔF508 mutation in the CFTR gene (Fanjul et al. 2002). The hypothesis was that if CAIV and CFTR normally interact in a metabolon (as suggested by Fanjul et al. 2002), mutations in both of these proteins in the same individual should result in a lung or pancreatic (where CFTR is expressed) phenotype in addition to RP17.

Genotyping showed one individual (RPD8.80JAN) to be heterozygous for the CFTR ΔF508 mutation. A family analysis revealed that the father of this individual, who was also a member of the RP17 cohort (RPD8.7STE), did not have the 3 bp deletion, and it was therefore presumed to have been inherited *in cis* on the maternal allele (we did not have access to a DNA sample for this individual to confirm this). It was therefore inferred that individual RPD8.80JAN was the first in the family to have both the CFTR and CAIV mutations, and the "metabolon phenotype" could not be explored in other members of the same family.

Phenotypic characterisation of patient RPD8.80JAN (at 24 years of age) did not reveal any lung or pancreatic phenotype, or indeed a more severe ocular phenotype for RP than expected. This may have been due to the heterozygous nature of the CFTR mutation, and it may be of more value to find a homozygous ΔF508 mutation carrier with a heterozygous mutation in CAIV, and determine if the CAIV mutation impacts on the

severity of cystic fibrosis in this case. It may also be useful to look *in vivo* at CAIV mutations in conjunction with mutations in other interacting proteins such as AE1 or NBC1, and also determine whether there is an aggravated phenotype (ocular, renal or otherwise) in these individuals. Research by Fanjul et al. (2002) and Alvarez et al. (2003) on a pancreatic transport metabolon suggest that CFTR may target CAIV to the plasma membrane, where it forms a complex with NBC1 in this organ. In addition, recent experiments on CFTR-deficient mice revealed an altered gene expression profile and an accumulation of mucus in the small bowel and colon. Treatment of CFTR-deficient mice with a synthetic peroxisome proliferator-activated receptor γ (PPAR γ) ligand that up-regulates CAIV expression, resulted in partial rescue of these symptoms (Harmon et al. 2010). These findings all point further towards some interaction between CAIV and CFTR, although this is likely to be tissue specific, and the effect of a disruption of this interaction on organs other than the pancreas has still not been determined.

Based on their studies in HEK-293 cells, Yang et al. (2005) attributed the disruption of a CAIV/NBC1 complex to the RP17 phenotype. However, based on the results of the present study, where these cells did not display the misfolding phenotype in response to the mutant CAIV protein, it is unlikely that this interaction is critical to cell survival, at least in the case of HEK-293 (and possibly other kidney-derived) cells. Nevertheless, studies such as the one undertaken in this research, are always challenging, as their success depends on finding individuals who have mutations in both genes, then examining the phenotype and trying to link the two, as opposed to linking a phenotype to a mutation as is done in classical genetics.

13. Molecular study of RP17 phenotype

In an effort to understand the molecular mechanisms underlying RP17, a functional study of the R14W CAIV mutation was carried out in three different cell types, COS-7, HT-1080, and HEK-293 cells. The study was carried out to investigate the mode of cell death in RP17 in light of the opposing models proposed by Rebello et al. (2004) and Yang et al. (2005). The results from cell cycle analysis, western blot analysis, and protein

localisation experiments provide compelling evidence to support the hypothesis suggested by Rebello et al. (2004). Firstly, COS-7 cells expressing a transfected R14W mutant CAIV experienced S and G2/M cell cycle arrests and apoptosis. Secondly, western blot analysis showed that whereas the WT CAIV protein is predominantly present in its mature form, the turnover of precursor to mature enzyme is impeded in the R14W mutant CAIV. These results suggest that the R14W mutation affects correct folding of CAIV, which explains the retention of the mutant peptide in the ER, as observed by fluorescence microscopy.

Following from the results in transiently transfected cells, COS-7 cells were also stably transfected with constructs expressing either the WT- or the R14W mutant CAIV protein. This was to determine whether expression of both forms of CAIV at levels that more closely mimic endogenous levels, would yield the same results as observed in COS-7 cells that transiently express the protein.

COS-7 cells stably expressing R14W mutant CAIV were not able to process the protein in the same way as the WT CAIV, and the protein formed aggregates, as was observed during the transient transfection experiments. These results may typify the response in endogenous systems, which express CAIV at lower levels, but over more prolonged periods, than the transiently-transfected cell models. They may also suggest that choriocapillaris cells cannot fold and process endogenous R14W mutant CAIV efficiently, and that the accumulation of mutant protein in cells over time eventually causes cell death. The results from experiments with stably-expressed R14W mutant CAIV which show lower expression of the protein may also help to further explain the progressive nature of RP17, and the delay of symptoms until the second decade of life. The delay in RP17 symptoms may also be explained by the activation or de-activation of signalling pathways in response to R14W mutant CAIV. Some such pathways were hinted at during microarray analysis of HEK-293 and HT-1080 cells transfected with WT- and R14W mutant-CAIV.

Microarray analysis was carried out on cell lines expressing CAIV in an attempt to explain the unexpected observation that HEK-293 cells were able to process, fold and traffic the R14W mutant CAIV comparably to the WT protein. This finding was significant, especially as they did not undergo a cell cycle block and apoptosis. This data raised the interesting possibility that different cell types may have different mechanism(s) for processing the CAIV protein to its mature form and that some cells have mechanisms of bypassing the deleterious effect of the R14W mutation. In the case of HEK-293 cells, this lack of phenotype may be explained by the ability to fold and process R14W mutant CAIV more efficiently than other cell types, allowing it to be exported from the ER and transported to the plasma membrane. To some extent, this initial exploratory section of the study was undertaken to find clues that would help to investigate the "holy grail"of genetics; the issue of penetrance vs. non penetrance.

Interestingly, it was studies of WT- and R14W mutant-CAIV expression in HEK-293 cells that led Yang et al. (2005) to propose that the death of choriocapillaris cells was due to disruption of a CAIV/NBC1 interaction. Results from mass spectrometry analysis of proteins bound to WT- and R14W mutant-CAIV in HEK-293 and HT-1080 cells showed that NBC1 is not bound to the protein in HT-1080 cells. Since these cells do undergo cell cycle arrest and apoptosis in response to mutant CAIV, it is therefore even more unlikely that the death of cells is due to a disruption of this metabolon. It is possible that Yang et al. (2005) did not observe misfolding of R14W mutant CAIV in HEK-293 cells due to the ability of this cell type to fold the mutant protein, as was observed in the present study.

This differential processing of a mutant protein by different cell types may also explain the lack of ‘penetrance’ of the pathogenic effect of mutant CAIV in different tissues, where it is known to be expressed and functional. This is relevant particularly in view of the earlier findings that although CAIV is strongly expressed in the renal tubules, RP17 patients show no discernable kidney phenotype (Rebello et al. 2004; Yang et al. 2005). This phenomenon has previously been attributed to the high metabolic activity of the retina, and possible lower tolerance of retinal tissue to metabolic imbalance. It has also

been suggested, when considering the "CAIV haploinsufficiency" model of disease in RP17, that other carbonic anhydrase isozymes in renal tissue may functionally compensate for CAIV or counter its deleterious effect (Alvarez et al. 2007; Yang et al. 2005). Results from microarray analyses showed that HEK-293 cells transfected with R14W mutant CAIV expressed 1.2 fold less CAII than WT cells and 1.15 fold less than HT-1080 cells transfected with R14W mutant CAIV. CAIV and CAXIV, another isozyme that has been shown to compensate for CAIV (Alvarez et al. 2005; Shah et al. 2005), was expressed at similar levels in all cells. This lack of up-regulation of carbonic anhydrase isozymes in HEK-293 cells which do not undergo cell cycle arrest and apoptosis may invalidate the argument that other CAs compensate for CAIV in its absence, and that haploinsufficiency of the protein causes cell death in RP17.

It is also possible that the detrimental effect of the R14W mutation is not seen in renal tissue because the endothelial cells in the proximal tubules express specific chaperones that allow them to correctly fold R14W mutant CAIV, and therefore evade apoptosis. This is an interesting possibility in light of reports that show that the null CAIV mouse experiences no visual phenotype (Ogilvie et al. 2007; Trifunovic et al. 2008) and that transgenic mice expressing R14W CAIV also have no retinal phenotype, but both experience progressive renal damage, which is enhanced by haploinsufficiency of an ER co-chaperone ($p58^{IPK}$) (Datta et al. 2010; Ogilvie et al. 2007). Protein folding agents like $p58^{IPK}$ could aid in folding in the human kidneys and mouse choriocapillaris, and explain the lack of phenotype in these tissues, despite strong expression of the mutant CAIV protein. Co-chaperones Hspa4l and DNAJ, and anti-apoptotic proteins BCL2A1 and BAG2, identified by microarray analysis, may act in similar ways to aid in HEK-293 cell folding of R14W mutant CAIV, thereby preventing apoptosis.

Also supporting the case of cell-specific responses to particular mutations is an earlier study by Datta et al. (2007), which showed that a signal sequence mutation in the human preproparathyroid hormone (PPTH) that leads to hypoparathyroidism causes apoptosis of HEK-293 cells. In this case, application of 4-phenylbutyric acid as a chemical chaperone

rescued cells from undergoing apoptosis. These studies by Datta et al. and others provide additional evidence for cell-specific differences in CAIV processing, and further suggest that these differences in responses to the mutant protein may also be species-specific. The observations of this study on the molecular mechanisms underlying RP17, taken in conjunction with earlier studies, also highlight the need for cautious interpretation when using cell and/or animal models for human diseases.

Once the molecular mechanisms underlying cell death in RP17 had been elucidated, further experiments were undertaken with the view to exploring means of therapy for the disease. Since protein misfolding and aggregation of the mutant R14W CAIV in affected cells had been identified as the primary cause of cell death, allele-specific shRNA was used to reduce expression of the mutant protein in an effort to show proof of principle of the selective silencing of the mutant allele in RP17. This approach was identified as being particularly relevant because previous work in this study had uncovered that it was not a haploinsufficiency of CAIV, but rather the dominant negative molecular pathology caused by the mutant protein, that lead to cell death.

Three different shRNA constructs were designed against mutant CAIV mRNA, and the efficacy of knockdown of each of the three was measured. Interestingly, shCAIV10, which had an additional mismatch to the one against the normal WT CAIV mRNA, caused almost complete knockdown of R14W mutant CAIV, with the highest remaining levels of WT protein, in HT-1080 and HEK-293 cells. The approach that uses two mismatches to the WT and only one to the mutant, was designed by Miller et al. (2004) and was not found to be an effective method of allele–specific knockdown by Scholefield et al. (2009) in their experiments. The effectiveness of shCAIV15 as opposed to shCAIV10 in the allele-specific knockdown of R14W mutant CAIV in COS-7 cells was surprising, and as with the initial studies on the molecular mechanisms of disease, highlights the importance of understanding that results may be cell-type specific, when drawing conclusions from experiments using cell models.

The results from protein expression studies using shRNA were confirmed by fluorescence microscopy, which again showed that the shCAIV constructs specifically silenced the R14W mutant form of CAIV. As expected, shCAIV15, when applied to COS-7 cells expressing the R14W mutant CAIV protein, was able to rescue these cells from undergoing cell cycle arrest. Remarkably, COS-7 cells expressing the R14W mutant CAIV, that were also transfected with the non-specific shSCR constructs, also did not undergo cell cycle arrest. This finding may be explained by the shSCR affecting non-specific silencing of R14W mutant CAIV. However, western blot analyses and immunofluorescence studies clearly showed that the scrambled sequence (Appendix, section 14.15) does not decrease expression of either the R14W mutant or the WT CAIV protein. Therefore, it is more likely that the scrambled sequence may be activating some of the signalling and transcription pathways of cell cycle regulators (cyclins, E2F, CDKs etc.) which play a part in ensuring that the cell cycle progresses smoothly, even through abnormal conditions such as ER stress and the UPR (Persengiev et al. 2004). This effect of the shSCR on COS-7 cells was also reproduced during apoptosis analyses, where the scrambled construct prevented COS-7 cells expressing R14W CAIV from undergoing apoptosis to some degree.

In contrast to the favourable effects of the shSCR on COS-7 cells, the construct increased apoptosis in HT-1080 and HEK-293 cells. The shCAIV10 constructs expressed in these cells also had an adverse effect, and increased the numbers of cells undergoing apoptosis. These results may have been due to non-specific silencing by shCAIV10 of proteins which are responsible for preventing apoptosis (a BLAST search showed part of the sequence to hybridise weakly to a putative microRNA sequence), or to the activation of pathways and regulators as mentioned above, combined with an increased sensitivity of these two cell types to increased or decreased protein levels, compared to COS-7 cells. Adverse effects to shRNA have indeed been well documented (Bridge et al. 2003), with the interferon response in particular being induced, and leading to lethality in some cases (Cao et al. 2005; Grimm et al.; Martin et al. 2011). Interestingly, studies on the lethality of shRNA have shown transcripts expressed from U6 promoters, though more effective,

to cause more severe detrimental effects than those expressed from the H1 promoter (Cao et al. 2005; Pebernard and Iggo, 2004). A balance therefore needs to be reached between the efficiency, length and stability of silencing, and the potential lethal effects of the shRNA.

The results from experiments with shCAIV again highlight the relevance of cell-type specific effects, a phenomenon that has been well documented, including cell-specific responses to molecules that affect cell viability or cause apoptosis (Haupt et al. 1996; Pollman et al. 1999). In the application of therapy, this would mean that more research would have to be done to select a cell model that better approximates choriocapillaris cells in its responses to shRNA, and this cell type would have to be used to assess the effect of silencing therapy on cell cycle progression and apoptosis.

The results from section 7 that showed that HEK-293 cells did not experience the adverse effects that R14W mutant CAIV protein had on COS-7 and HT-1080 cells, suggested that these cells may be able to fold, or better able to tolerate the misfolding of proteins in the ER. Levels of the ER-specific chaperones BiP, GRP170 and PDI were therefore investigated in the three cell lines in order to determine whether they were responsible for the ability of HEK-293 cells to fold and process R14W mutant CAIV. The result that untransfected COS-7 cells had elevated levels of GRP170 compared to the other cell types was noteworthy, as levels of this chaperone were expected to be present at higher levels in HEK-293 cells. The increased levels may be species-specific and due to COS-7 cells being of monkey origin while the other cell types are human, or indicate that these cells have a higher "basal" stress level than HT-1080 and HEK-293 cells (GRP170 is also a stress-induced protein). Also of great interest was the lower expression of all three chaperones (BiP in particular), in untransfected HEK-293 cells. The ability of these cells to fold and process R14W mutant CAIV would suggest increased levels of these or other chaperones in HEK-293 cells, however, like many other heat shock proteins, cell type-specific chaperone levels may be important (Nollen and Morimoto, 2002), and HEK-293

cells may require lower levels of a particular chaperone to exert an effect equal to or more than, that experienced by COS-7 and HT-1080 cells.

When levels of the three chaperones were tested in transfected cells, it was found that BiP levels increased in COS-7 cells in response to expression of either the WT- or R14W mutant form of CAIV. Increases in the levels of BiP were greater in WT CAIV-expressing cells compared to COS-7 cells expressing R14W mutant CAIV. A study by Gorbatyuk et al. (2010) showed that overexpression of BiP in HeLa (cervix carcinoma) cell and rat models of P23H RHO misfolding had no effect on processing and transport of the mutant RHO protein. However, delivery of BiP to rats by adeno-associated viral (AAV) vectors alleviated ER stress by reducing levels of active ATF6, elF2α. and CHOP. This resulted in a decrease in apoptosis and an increase in photoreceptor cell survival. The lower levels of BiP in COS-7 cells expressing R14W mutant CAIV and the lower levels of ATF6 in HEK-293 cells expressing the mutant protein, may hint at a role for this pathway in encouraging folding and processing of R14W mutant CAIV. This is supported by the comparatively higher levels of BiP in transfected HEK-293 cells (which are able to fold and process R14W mutant CAIV) compared to levels in transfected COS-7 and HT-1080 cells. Increasing levels of BiP may reduce levels of active ATF6, preventing cells expressing mutant CAIV from undergoing apoptosis.

Results from transfections with shCAIV in HEK-293 and HT-1080 cells expressing CAIV showed fluctuations in the levels of the chaperones tested in response to the shRNA. These fluctuations show that shCAIV may impact on the levels of important chaperones within the cell, and highlight the need to monitor off-target effects when considering this potential method of therapy for RP17.

The experiments with levels of BiP, GRP170 and PDI did not conclusively show that these proteins are involved in the ability of HEK-293 cells to fold and process R14W mutant CAIV. Expression of a mutant protein can have many effects on the cell, which elicit responses in the ER, effects on transcription and translation, impact the cell cycle,

or result in apoptosis (Liu and Kaufman, 2003). Therefore, it is not unreasonable to propose that proteins involved in more than one, or in fact all of these processes, may impact the the response of HEK-293 cells to mutant CAIV. Therefore, in order to expand our investigation into the effects of R14W mutant CAIV, microarray analysis on cells expressing the WT and R14W mutant form of the protein was carried out.

Microarray analysis identified a number of proteins involved in signalling pathways and transcriptional regulation that were differentially expressed in HEK-293 and HT-1080 cells transfected with WT- or R14W mutant-CAIV. The finding that expression of zinc finger proteins is differentially regulated in cells in response to CAIV was a particularly unexpected one. These proteins are ubiquitously expressed in a range of cell types (Desjarlais et al. 1992; Zeng et al. 1991), but it was interesting to find that even within cell types, the family of zinc finger protein expressed was dependant on whether it was in response to the WT- or R14W mutant-CAIV. The zinc finger proteins are mostly involved in transcriptional regulation, however, their activity can be extended to include the donation of a zinc ion to metalloenzymes like CAIV, as is the case with metallothioneins (Huang et al. 2001; Li et al. 1980). An investigation into the role of zinc in carbonic anhydrases reveals the importance of this ion both in the activity of the enzyme, and in its folding (Cox and Lendon, 2000). A study on the activity of CAVI showed that treatment with zinc increases synthesis and secretion of the protein. The suggestion was that the presence of zinc stimulated *CA6* gene activity (Henkin et al. 1999).

The microarray results that show that zinc finger proteins were differentially expressed in response to CAIV may imply a feedback loop between CAIV and the zinc finger proteins. In HEK-293 cells particularly, this up- or down-regulation of the zinc finger proteins may lead to transcriptional activation of other genes which help the cell to fold and process R14W mutant CAIV. While both cell types expressed zinc finger proteins, HEK-293 cells may be more sensitive to levels of these proteins than HT-1080 cells. The importance of zinc in the observed responses of HEK-293 cells may also be underpinned

by the observation that in HEK-293 cells, there was an increase in the expression of RNA transcripts of genes related to olfactory processes. Activation of these genes has been shown to be particularly responsive to zinc (Hirata, 2006; Mackay-Sim and Dreosti, 1989; Smith, 1938; Tsai and Reed, 1997). It is therefore possible that pathways activated by zinc ions, zinc bound by CAIV, or zinc finger proteins, may play a part in determining the response of HEK-293 cells to R14W mutant CAIV.

This link between zinc-related transcriptional activation and HEK-293 responses to CAIV, may also underlie the up-regulation of genes involved in cell cycle progression (e.g. Wee1) and inhibition of apoptosis (e.g. baculoviral IAP) in HEK-293 cells expressing the R14W mutant CAIV protein.

It must be noted that microarray analysis of transcripts expressed in HEK-293 cells showed expression of some genes associated with neuronal tissue (e.g. calneuron 1, neuronal growth regulator). This finding has been reported in a previous study (Shaw et al. 2002), where it was reported the adenoviral vectors used to immortalise cell lines may preferentially transform neuronal lines. However, kidney specific transcripts were also observed in HEK-293 cells (e.g. kidney associated antigen, fetal kidney cadherin 6), highlighting the possibility that HEK-293 cells may be contaminated with cells of neuronal origin, rather than be of neuronal origin themselves.

The finding that many genes that were differentially expressed between cells expressing WT- and R14W mutant-CAIV are involved in cell cycle and apoptosis was particularly relevant to this study due to the results which showed that R14W mutant CAIV causes cell cycle arrest and apoptosis in COS-7 and HT-1080 cells. Differentially expressed genes involved in cell cycle included the mitotic checkpoint regulator MAD2l1, as well as GSPT2, PRDM9 and PPP1CB. PPP1R15A, and another apoptosis related protein, RHBDD1, was also differentially expressed.

Microarray analysis also identified some differentially expressed genes whose products are involved in protein folding and processing within the cell. These included Sec11c, Ergic3, SPPL2A, SGTB and Hspa4l. While the Sec11c protein is an ER-associated component of the signal peptidase complex that acts to remove the signal peptide from proteins as they enter the ER lumen (Böhni et al. 1988), the other proteins act in the folding and transport of translated peptides. Due to the location of the R14W mutation in the signal sequence of CAIV, and the hypothesis that the mutation effects removal of the signal sequence from the protein during processing in the ER, all of these proteins may be considered as candidate genes to introduce into cells expressing the R14W mutant CAIV, to determine whether up-regulation can facilitate correct cleavage and folding of the protein.

Another candidate for functional studies that serve to correct the folding of R14W mutant CAIV *in vitro* may be the DNAJ protein. Althought transcripts of this gene were found to be down-regulated in cells expressing the R14W mutant CAIV, mass spectrometry analyses showed that it was bound to CAIV in HEK-293 cells expressing the mutant protein. DNAJ facilitates the activity of HSP70 proteins such as BiP (Li and Lee, 2006), which aid in the ER-associated folding of cytosol and secretory proteins (Mayer and Bukau, 2005). Levels of BAG2, another co-chaperone of HSP70, were found to be elevated in cells expressing the R14W mutant form of CAIV. This protein regulates the activity of HSP70 (Arndt et al. 2005; Dai, 2006) and the degradation of misfolded proteins, by binding in a complex with HSP70 and CHIP, a ubiquitin ligase (Dai et al. 2005). Its up-regulation may provide another regulatory mechanism to control the degradation of R14W mutant CAIV in HEK-293 cells so that the protein can be folded properly. The association between HSP70 protein levels and HEK-293 cells was demonstrated previously during western blotting experiments with chaperone proteins, where levels of BiP, an HSP70 family protein, were found to be increased in HEK-293 cells expressing WT- and R14W mutant-CAIV. It may well be that DNAJ, when bound to R14W mutant CAIV in HEK-293 cells, helps to stimulate binding of BiP to fold the

protein and act in concert with other co-chaperones like BAG2, to prevent unwanted degradation.

Finally, one more protein that was bound to CAIV in HEK-293 cells, and may be further investigated for its ability to prevent COS-7 and HT-1080 cells from undergoing cell cycle arrest, is Scraper. This ER-specific protein interacts with cyclin A to activate the G1/S phase transition of the cell cycle (Tsang et al. 2007). This protein may act in close proximity to CAIV as opposed to directly binding to the protein, and could prevent HEK-293 cells expressing R14W mutant CAIV from undergoing cell cycle arrest.

Efforts to prevent apoptosis caused by ER stress may be directed at three different responses. These include (i) Decreasing the amount of misfolded R14W CAIV in an attempt to restore ER homeostasis, (ii) attenuating the activation of ER stress sensors, and (iii) modulating the activity of ER stress transducers, and therefore interfering with the interaction network responsible for implementation of the ER stress responses (Griciuc et al., 2011). This study addressed all three of these responses in an attempt to explore the principle of therapy for RP17. While shCAIV was used to silence R14W mutant CAIV, chaperones were also investigated for their ablity to fold and process the mutant protein. In order to address (ii) and (iii), expression of proteins also associated with ER stress, cell cycle arrest, and apoptosis were explored in HEK-293 and HT-1080 cells using microarray analysis and mass spectrometry.

The present study identified a number of methods to consider (shCAIV and chaperones, or interference with cell cycle and apoptosis activators) in attempting to neutralise the pathogenecity caused by for RP17. However, before genetic or proteomic interventions are considered for therapy, the delivery of these molecules to the target cells needs to be addressed. During the treatment of a congenital form of arRP called Leber's Congenital Amaurosis, subretinal delivery of AAV vectors containing correct copies of the RPE65 gene proved to be successful in restoring vision (Bainbridge et al. 2008). In the case of RP17, because a number of mutations have now been associated with the disease,

suppression of both WT- and mutant-CAIV expressed in the choriocapillaris, followed by replacement of the protein, may be the most sensible option for therapy. This method has proved successful in the RHO RP mouse model, in which AAV vectors were also used for delivery (Millington-Ward et al. 2009; Smith et al. 2009). These vectors have shown high targeting frequencies, can be used for a wide variety of genes and proteins, and other molecules, and show low toxicity to cells (Khan et al. 2010). The advantages over other constructs are therefore clear, and AAVs should seriously be considered for the delivery of therapy for RP17.

In order to specifically target the choriocapillaris, the delivery of therapy to this layer specifically, would have to be achieved. This could be done by physical delivery to the pars plana of the retina (although this may cause holes in the macula or retina, which could lead to bleeding in these tissues). Targeted delivery may also be achieved through the use of cell-type specific binding of molecules to the choriocapillaris cells. Similar methods have been described by McNamara et al. (2006) in their use of aptamer-siRNA chimeras able to bind specifically to prostate cancer cells and tumour vascular endothelium. Molema (2005) emphasised the importance of targeting endothelial cells in a report on cancer therapy. While these studies targeted cells with the intention to cause cell death, the same principles may be applied in the targeting of molecules to choriocapillaris endothelium, in an effort to prevent cells from undergoing apoptosis.

Conclusion

This study examines the genetics of RP17 and identifies the R14W mutation as the only one likely to cause the disease in the South African cohort. It also characterises the phenotype in terms of age of onset and severity of phenotype, and confirms that age of onset in RP17 is similar to that observed in other autosomal dominant forms of RP. A screen of the dominant UCT adRP cohort for other CAIV mutations showed no other significant variants.

Using cell biology techniques, the present study also reveals the molecular mechanisms underlying the RP17 phenotype. It provides an explanation for how the R14W mutant CAIV induces apoptosis in cells of the choriocapillaris, but not kidneys, of RP17 patients and opens up exciting possibilities of approaches that could be employed in the therapy of, or treatment for, RP17. It also addresses and describes two possible mechanisms of RP17 therapy to explore: allele-specific shRNA, and molecular chaperones and chaperone-like proteins. Microarray analysis and mass spectrometry highlight some proteins that may be used in an effort to prevent cells expressing the R14W mutant form of CAIV from misfolding the protein and undergoing cell cycle arrest and apoptosis. While suggesting how these interventions could be best utilised in the treatment of RP17, the results also bring up important issues, e.g. whether responses to CAIV protein are due to the inherent presence of particular proteins within the cell, or as a result of transfection with WT- or R14W mutant-CAIV protein. Many of the results, particularly from microarray experiments, also emphasise the importance of levels of proteins expressed, the different sensitivity of different cell types, and show that in some cases, knockdown of proteins may be as destructive as over-expression. Therefore, as well as investigating and proposing mechanisms of disease and modes of therapy for RP17, this study also highlights some limitations when using conventional disease models, and emphasises the importance of using the most appropriate cell and animal models during investigations into this and other diseases.

References

Acland GM et al. (2001) Gene therapy restores vision in a canine model of childhood blindness. Baseline 28:92-95

Aligue R, Akhavan-niak H, Russell PA (1994) Role for Hsp9O in cell cycle control: Weel tyrosine kinase activity requires interaction with Hsp9O. EMBO J 13:6099-6106

Altschul SF, Gish W, Miller W, Myers EW, Lipman DJ (1990) Basic Local Alignment Search Tool. J Mol Biol 215:403-410

Alvarez L, Fanjul M, Carter N, Hollande E (2001) Carbonic anhydrase II associated with plasma membrane in a human pancreatic duct cell line (CAPAN-1). J Histochem Cytochem 49:1045-1053

Alvarez BV, Loiselle FB, Supuran CT, Schwartz GJ, Casey JR (2003) Direct extracellular interaction between carbonic anhydrase IV and the human NBC1 sodium/bicarbonate co-transporter. Biochem 42:12321-12329

Alvarez BV, Vilas GL, Casey JR (2005) Metabolon disruption: a mechanism that regulates bicarbonate transport. EMBO J 24:2499-24511

Alvarez BV et al. (2007a) Identification and characterization of a novel mutation in the carbonic anhydrase IV gene that causes retinitis pigmentosa. Invest Ophthalmol Vis Sci 48:3459-3468

Alvarez BV, Gilmour GS, Mema SC, Martin BT, Shull GE, Casey JR, Sauve Y (2007b) Blindness caused by deficiency in AE3 choride/bicarbonate exchanger. PLOS One 2:e839 doi:10.1371/journal.pone.0000839

Amaral MD (2004) CFTR and Chaperones: Processing and Degradation. J Mol Neurosci 23:41-48

Ameres SL, Martinez J (2007) Molecular Basis for Target RNA Recognition and Cleavage by Human RISC. Mol Biotech 130:101-112

Andréasson C, Rampelt H, Fiaux J, Druffel-Augustin S, Bukau B (2010) The endoplasmic reticulum Grp170 acts as a nucleotide exchange factor of Hsp70 via a mechanism similar to that of the cytosolic Hsp110. J Biol Chem 285:12445-12453

Anelli T, Sitia R (2008) Protein quality control in the early secretory pathway. EMBO J 27:315-327

Anfinsen CB (1973) Principles that govern the folding of protein chains. Science 181:223-23

Appenzeller-Herzog C, Hauri H (2006) The ER-Golgi intermediate compartment (ERGIC): in search of its identity and function. J Cell Sci. 119:2173-2183

Araújo FGD (2005) Prevalence of ΔF508, G551D, G542X, and R553X mutations among cystic fibrosis patients in the North of Brazil. Blood 38:11-15

Arndt V, Daniel C, Nastainczyk W, Alberti S (2005) BAG-2 Acts as an Inhibitor of the Chaperone-associated Ubiquitin Ligase CHIP. Mol Biol Cell 16:5891-5900

Baba T et al. (2009) Maturation of the fetal human choriocapillaris. Invest Ophthalmol Vis Sci 50:3503-3511

Baer M, Nilsen TW, Costigan C, Altman S (1990) Structure and transcription of a human gene for H1 RNA, the RNA component of human RNase P. Nucl Acids Res 18:97-103

Bainbridge SS et al. (2008) Effect of Gene Therapy on Visual Function in Leber Congenital Amaurosis. N Eng J Med 358:2231-2239

Baker AH, Zaltsman AB, George SJ, Newby AC (1998) Divergent effects of tissue inhibitor of metalloproteinase-1, -2, or -3 overexpression on rat vascular smooth muscle cell invasion, proliferation, and death in vitro. TIMP-3 promotes apoptosis. J Clin Invest 101:1478-1487

Bardien-Kruger S et al. (1999) Refinement of the RP17 locus for autosomal dominant retinitis pigmentosa: construction of a YAC contig and investigation of the candidate gene retinal fascin. Eur J Hum Genet 7:332-338

Bardien S, Ramesar R, Bhattacharya S, Greenberg J (1997) Retinitis pigmentosa locus on 17q (RP17): fine localization to 17q22 and exclusion of the PDEG and TIMP2 genes. Hum Genet 101:13-17

Barral JM, Broadley SA, Schaffar G, Hartl FU (2004) Roles of molecular chaperones in protein misfolding diseases. Seminars in cell and developmental biology 15:17-29

Baudat F, Buad J, Grey C, Fledel-Alon A, Ober C, Przeworski M, Coop G, de Massy B (2010) PRDM9 is a major determinant of meiotic recombination hotspots in humans and mice. Science 327:836-840

Beckmann RP, Mizzen LE, Welch WJ (1990) Interaction of Hsp 70 with newly synthesized proteins: implications for protein folding and assembly. Science 248:850-854

Beere HM et al. (2000) Heat-shock protein 70 inhibits apoptosis by preventing recruitment of procaspase-9 to the Apaf-1 apoptosome. Natl Cell Biol 2:469-475

Beneteau C et al. (2011) Microtriplication of 11q24.1: a highly recognisable phenotype with short stature, distinctive facial features, keratoconus, overweight, and intellectual disability. J Med Genet doi:10.1136/jmedgenet-2011-100008

Bergt JM (1992) Toward rules relating zinc finger protein sequences and DNA. Biophysics 89:7345-7349

Bernstein E, Caudy AA, Hammond SM, Hannon GJ (2001) Role for a bidentate ribonuclease in the initiation step of RNA interference. Nature 409:363-366

Berson EL (1996) Retinitis pigmentosa: Unfolding its mystery. Proc Natl Acad Sci USA 93:4526-4528

Berson EL, Rosner B, Sandberg MA, Hayes KC, Nicholson BW, Weigel-DiFranco C, Willett W (1993) A Randomized Trial of Vitamin A and Vitamin E Supplementation for Retinitis Pigmentosa . Arch Ophthalmol 111:761-772

Berson EL, Rosner B, Sandberg MA, Hayes KC, Nicholson BW, Weigel-DiFranco C, Willett W (1993) Vitamin A Supplementation for Retinitis Pigmentosa. Arch Ophthalmol 111:1456-1458

Berson EL, Rosner B, Sandberg MA, Weigel-DiFranco C, Moser A, Brockhurst RJ, Hayes KC, Johnson CA, Anderson EJ, Gaudio AR, Willett WC, Ernst J. Schaefer. Clinical Trial of Docosahexaenoic Acid in Patients With Retinitis Pigmentosa Receiving Vitamin A Treatment. Arch Ophthalmol. 2004;122(9):1297-1305.

Blaauwgeers HGT et al. (1999) Polarized Vascular Endothelial Growth Factor Secretion by Human Retinal Pigment Epithelium and Localization of Vascular Endothelial Growth Factor Receptors on the Inner Choriocapillaris: Evidence for a Trophic Paracrine Relation. Am J Pathol 155:421-428

Böhni PC, Deshaies RJ, Schekman RW(1998) Sec11 is Required for Signal Peptide Processing and Yeast Cell Growth. Cell 106:1035-1042

Bonapace G, Waheed A, Shah GN, Sly WS (2004) Chemical chaperones protect from effects of apoptosis-inducing mutation in carbonic anhydrase IV identified in retinitis pigmentosa 17. Proc Natl Acad Sci USA 101:12300-12305

Boron WF (2010) Evaluating the role of carbonic anhydrases in the transport of HCO_3^--related species. Biochimica Et Biophysica Acta 1804:410-421

Boudreau RL, Martins I, Davidson BL (2008) Artificial MicroRNAs as siRNA Shuttles: Improved Safety as Compared to shRNAs In vitro and In vivo. Mol Ther 17:169–175

Bradbury J (2003) Chaperones: keeping a close eye on protein folding. Lancet 361:1194-1195

Breyer KJ, Segal DJ (2008) Keep your fingers off my DNA: Protein-protein interactions mediated by C2H2 zinc finger domains. Cell Biochem and Biophys 50:111-131

Bridge AJ, Pebernard S, Ducraux A, Nicoulaz A, Iggo R (2003) Induction of an interferon response by RNAi vectors in mammalian cells. Nat Genet 34:263-264

Brown D, Zhu XINL, Sly WS (1990) Localization of membrane-associated carbonic anhydrase type IV in kidney epithelial cells. Cell Biol 87:7457-7461

Browning C, Gray T, Amoaku WM (2005) Isolation, culture, and characterisation of human macular inner choroidal microvascular endothelial cells. Br J Ophthalmol 89:1343-1347

Brummelkamp TR, Bernards R, Agami R (2002) A System for Stable Expression of Short Interfering RNAs in Mammalian Cells. Science 296:550-553

Buchholz DE, Hikita ST, Rowland TJ, Friedrich AM, Hinman CR, Johnson LV, Clegg DO (2009) Derivation of Functional Retinal Pigmented Epithelium from Induced Pluripotent Stem Cells. Stem Cells. 27:2427–2434

Buyse IM, Roa BB (2003) Liquid Chromatography and Sequence Analyses for MECP2 Mutations in Rett Syndrome. Methods 217:119-130

Cai H, Wang CC, Tsou CL (1994) Chaperone-like activity of protein disulfide isomerase in the refolding of a protein with no disulfide bonds. J Biol Chem 269:24550-24552

Cajo GC et al. (2006) The role of the DIF motif of the DnaJ (Hsp40) co-chaperone in the regulation of the DnaK (Hsp70) chaperone cycle. J Biol Chem 281:12436-44

Cao W, Hunter R, Strnatka D, McQueen CA, Erickson RP (2005) DNA constructs designed to produce short hairpin, interfering RNAs in transgenic mice sometimes show early lethality and an interferon response. Pediatrics 46:217-225

Carter ND, Fryer A, Grant AG, Hume R, Strange RG, Wistrand PJ (1990). Membrane specific carbonic anhydrase (CAIV) expression in human tissues. Biochimica et Biophysica Acta – Biomembranes. 1026:113-116

Cashman SM, Binkley EA (2005) Towards mutation-independent silencing of genes involved in retinal degeneration by RNA interference. Gene Ther 12:1223-1228

Castanotto D et al. (2002) Functional siRNA expression from transfected PCR products . RNA 8:1454-1460

Cavallotti C, Corrado BG, Feher J (2005) The human choriocapillaris: evidence for an intrinsic regulation of the endothelium? J Anat 206:243-247

Chabot B, Black DL, LeMaster DM, Steitz JA (1985) The 3' splice site of pre-messenger RNA is recognised by a small nuclear ribonucleoprotein. Science 230:1344-1349

Chadderton N et al. (2009) Improved retinal function in a mouse model of dominant retinitis pigmentosa following AAV-delivered gene therapy. Mol Therapy: J Am Soc Gene Ther 17:593-539

Chapple JP et al. (2001) Unfolding retinal dystrophies: a role for molecular chaperones? Trends in Mol Med 7:414-421

Chaudhuri TK, Paul S (2006) Protein-misfolding diseases and chaperone-based therapeutic approaches. FEBS J 273:1331-1349

Chen C, Dillon GH, Huang R (2004) Molecular determinants of proton modulation of glycine receptors. J Biol Chem 279:876-883

Chinnadurai G, Vijayalingam S, Rashmi R (2008) BIK- the founding member of the BH3-only family proteins: mechanisms of cell death and role in cancer and pathogenic processes. Oncogene 27:S20-S29

Choi Y, Yeo S, Hong Y, Kim S, Lim S (2011) Changes of gene expression profiles in the cervical spinal cord by acupuncture in an MPTP-intoxicated mouse model. Gene 481:7-16

Cideciyan AV (2010) Leber congenital amaurosis due to RPE65 mutations and its treatment with gene therapy. Progress in retinal and eye research doi:10.1016/j.preteyeres.2010.04.002

Clemens JC, Ursuliak Z, Clemens KK, Price JV, Dixon JE (1996) J Biol Chem 271:17002–17005

Clemson CM et al. (2011) Therapeutic potential of valproic acid for retinitis pigmentosa. Br J Ohpthalmol 95:89-93

Comijn J, Berx G, Vermassen P, Verschueren K, van Grunsven L, Bruyneel E, Mareel M, Huylebroeck D, and van Roy F (2001). The two-handed E box binding zinc finger protein SIP1 downregulates E-cadherin and induces invasion. Mol Cell 7:1267–1278

Cox EH, McLendon GL (2000) Zinc-dependent protein folding. Curr Opin Chem Biol 4:162-165

Crépin M et al. (2006) Evaluation of denaturing high performance liquid chromatography for the mutational analysis of the MEN1 gene. J Mol Endocrin 36:369-76

Dai Q (2006) The cochaperone and ubiquitin ligase CHIP in protein quality control. PhD Dissertation, University of North Carolina at Chapel Hill

Dai Q et al. Regulation of the cytoplasmic quality control protein degradation pathway by BAG2. J Biol Chem 280:38673-38681

Datta R, Waheed A, Bonapace G, Shah GN, Sly WS (2009) Pathogenesis of retinitis pigmentosa associated with apoptosis-inducing mutations in carbonic anhydrase IV. Proc Natl Acad Sci USA 106:3437-3442

Datta R et al. (2010) Progressive renal injury from transgenic expression of human carbonic anhydrase IV folding mutants is enhanced by deficiency of p58IPK. Proc Natl Acad Sci USA 107:6448-6452

Davis TW et al. (1998) Defective Expression of the DNA mismatch repair protein, MLH1, alters G2-M cell cycle checkpoint arrest following ionizing radiation. Cancer Res 58:767-778

Davletova S, Schlauch K, Coutu J, Mittler R (2005) The Zinc-Finger Protein Zat12 Plays a Central Role in Reactive Oxygen and Abiotic Stress Signaling in Arabidopsis. Plant Physiol 139:847-856

Dejneka NS, Bennett J (2001) Gene therapy and retinitis pigmentosa: advances and future challenges. BioEssays 23:662–668

Demirci FYK, Chang MH, Mah TS, Romero MF, Gorin MB (2006) Proximal renal tubular acidosis and ocular pathology: a novel missense mutation in the gene (SLC4A4) for sodium bicarbonate cotransporter protein (NBCe1). Mol Vis 12:324-330

den Hollander AI et al. (2006) Mutations in the CEP290 (NPHP6) gene are a frequent casue of Leber congenital amaurosis. Am J Hum Genet 79:556-561

Deng S, Zhou H, Xiong R, Lu Y, Yan D, Xing T, Dong L, Tang E, Yang H (2007) Over-expression of genes and proteins of ubiquitin specific peptidases (USPs) and proteasome subunits (PSs) in breast cancer tissue observed by the methods of RFDD-PCR and proteomics. Breast Cancer Research And Treatment 104:21-30

Denton M (1999) The inverted retina: maladaptation or pre-adaptation. Origins and Design 37:19-22

Deutman AF (1983) Acute multifocal ischaemic choroidopathy and the choriocapillaris. Intl Ophthalmol 6:155-160

de Vries H, Ruegsegger U, Hubner W, Friedlein A, Langen H, Keller W (2000) Human pre-mRNA cleavage factor II(m) contains homologs of yeast proteins and bridges two other cleavage factors. EMBO J 19:5895-5904

Dinour D et al. (2004) A novel missense mutation in the sodium bicarbonate cotransporter (NBCe1/SLC4A4) causes proximal tubular acidosis and glaucoma through ion transport defects. J Biol Chem 279:52238-52246

Doran B, Gherbesi N, Hendricks G, Flavell RA, Davis RJ, Gangwani L (2006) Deficiency of the zinc finger protein ZPR1 causes neurodegeneration. Proc Natl Acad Sci 103:7471-7475

Dracopoli NC (ed.) (1998) Current Protocols in Human Genetics. John Wiley and Sons, New York 2:10.6.1–10.6.10

Dragovic Z, Broadley SA, Shomura Y, Bracher A, Ulrich Hartl F (2006) Molecular chaperones of the Hsp110 family act as nucleotide exchange factors of Hsp70s. EMBO J 25:2519-2528

Dryja TP, Li T (1995) Molecular genetics of retinitis pigmentosa. Hum Mol Genet. 4:1739-1743

Duckett CS et al. (1996) A conserved family of cellular genes related to the baculovirus iap gene and encoding apoptosis inhibitors. EMBO J 15:2685-2694

Dudek, J et al. (2009) Functions and pathologies of BiP and its interaction partners. Cell Mol Life Sci 66:1556-1569

Dunnen JD, Antonarakis S (2001) Nomenclature for the description of human sequence variations. Hum Genet 109:121-124

Elbashir SM, Harborth J, Lendeckel W, Yalcin A, Weber K, Tusch T (2001) Duplexes of 21-nucleotide RNAs mediate RNA interference in cultured mammalian cells. Nature 411:494-498

Elstner E, Müller C, Koshizuka K, Williamson EA, Park D, Asou H, Shintaku P, Said JW, Heber D, Koeffler HP (1998) Ligands for peroxisome proliferator-activated receptorγ and retinoic acid receptor inhibit growth and induce apoptosis of human breast cancer cells in vitro and in BNX mice. Proc Natl Acad Sci 95:8806-8811

Enzmann V, Yolcu E, Kaplan HJ, Ildstad ST (2009) Stem cells as tools in regenerative therapy for retinal degeneration. Arch Ophthalmol 127:563-571

Fanjul M (2002) Targeting of carbonic anhydrase IV to plasma membranes is altered in cultured human pancreatic duct cells expressing a mutated (ΔF508) CFTR. Eur J Cell Biol 81:437-447

Fasano T, Bocchi L, Pisciotta L, Bertolini S, Calandra S (2005) Denaturing high-performance liquid chromatography in the detection of ABCA1 gene mutations in familial HDL deficiency. J Lipid Rs 46:817-822

Fink AL (1999) Chaperone-mediated protein folding. Physiol Rev 79:425-49

Fire A, Xu S, Montgomery MK, Kostas SA, Driver SE, Mello CC (1998) Potent and specific genetic interference by double-stranded RNA in Caenorhabditis elegans. Nature 391:806-811

Fleming RE, Crouch EC, Ruzicka CA, Sly WS (1993) Pulmonary carbonic anhydrase IV: developmental regulation and cell-specific expression in the capillary endothelium. AJP - Lung Physiol 265:627-635

Fleming RE et al. (1995) Carbonic anhydrase IV expression in rat and human gastrointestinal tract: regional, cellular, and subcellular localization. J Clin Invest 96:2907-2913

Flower RW (1993) Extraction of choriocapillaris hemodynamic data from ICG fluorescence angiograms. Invest Ophthalmol Vis Sci 34:2720-2729

Fung MK, Han HY, Leung SC, Cheung HW, Cheung AL, Wong YC, Ling MT, Wang X (2005) MAD2 interacts with DNA repair proteins and negatively regulates DNA damage repair. J Mol Biol 381:24-34

Galy A, Roux MJ, Sahel JA, Léveillard T, Giangrande A (2005) Rhodopsin maturation defects induce photoreceptor death by apoptosis: a fly model for RhodopsinPro23His human retinitis pigmentosa. Hum Mol Genet 14:2547-2557

Ganot P, Caizergues-Ferrer M, Kiss T (1997) The family of box ACA small nucleolar RNAs is defined by an evolutionarily conserved secondary structure and ubiquitous sequence elements essential for RNA accumulation. Genes Dev 11:941-956

Gaur R (2006) RNA interference: a potential therapeutic tool for silencing splice isoforms linked to human diseases. BioTechniques 40:S15-S22

Gething M (1999) Role and regulation of the ER chaperone BiP. Seminars in Cell and Developmental Biology. 10:465-472

Goder V, Junne T, Spiess M (2004) Sec61p Contributes to Signal Sequence Orientation According to the Positive-Inside Rule. Mol Biol Cell 15:1470-1478

Goes FS, Martin J (2001) Hsp90 chaperone complexes are required for the activity and stability of yeast protein kinases Mik1, Wee1 and Swe1. Eur J Biochem 268:2281–2289

Gorbatyuk MS, Knox T, Lavail MM, Gorbatyuk OS, Noorwez SM (2010) Restoration of visual function in P23H rhodopsin transgenic rats by gene delivery of BiP/Grp78. Proc Natl Acad Sci 107:5961-5966

Gorden NT et al. (2008) CC2D2A is mutated in Joubert syndrome and interacts with the ciliopathy-associated basal body protein CEP290. Am J Hum Genet 83:559-571

Graham FL, Smiley J (1997) Characteristics of a Human Cell Line Transformed by DNA from Human Adenovirus Type 5. J Gen Virol 36:59-72

Green CM, Erdjument-Bromage H, Tempst P, Lowndes N.F (2000) A Novel Rad24 checkpoint protein complex closely related to replication factor C. Curr Biol 10:39-42

Griciuc A, Aron L, Ueffing M (2011) ER stress in retinal degeneration: a target for rational therapy? Trends Mol Med 17:442-451

Grimaldi CM, Cleary J, Dagtas AS, Moussai D, Diamond B (2002) Estrogen alters thresholds for B cell apoptosis and activation. J Clin Invest 109:1625-1633

Grimm D et al. (2006) Fatality in mice due to oversaturation of cellular microRNA/short hairpin RNA pathways. Nature 441:537-541

Grossberger R et al. (1999) Characterization of the DOC1/APC10 subunit of the yeast and the human anaphase-promoting complex. J Biol Chem 274:14500–14507

Grover S, Apushkin MA, Fishman GA (2006) Topical Dorzolamide for the Treatment of Cystoid Macular Edema in Patients With Retinitis Pigmentosa. Am J Ophthalmol 141:850-858

Guerriero CJ, Brodsky JL (2012) Protein folding and endoplasmic reticulum-associated degradation in human physiology. Physiol Rev 92:537-576

Guo S, Kemphues KJ (1995) Par-1 a Gene Required for Establishing Polarity in C . elegans Embryos , Encodes a Putative Ser / Thr Kinase That Is Asymmetrically Distributed. Cell 81:611-620

Hafner C, Martino E, Pitt E et al. (2010) FGFR3 mutation affects cell growth, apoptosis and attachment in keratinocytes. Exp Cell Res 316:2008-2016

Hageman GS (1991) Localization of Carbonic Anhydrase IV in a Specific Capillary Bed of the Human Eye. Proc Natl Acad Sci USA 88:2716-2720

Hammarström P (2009) Protein folding, misfolding and disease. FEBS letters 583:2579-2580

Hampton RY (2000) ER stress response: Getting the UPR hand on misfolded proteins. Current biology 10:518-521

Han J, Lee Y, Yeom K, Nam J, Heo I, Rhee J, Young Sohn S, Cho Y, Zhang B, Kim VN (2006) Molecular Basis for the Recognition of Primary microRNAs by the Drosha-DGCR8 Complex. Cell 125:887-901

Hartl FU, Hayer-Hartl M (2002) Molecular chaperones in the cytosol: from nascent chain to folded protein. Science 295:1852-1858

Hayreh SS (1974) Submacular choroidal vascular pattern: Experimental fluorescein fundus angiographic studies. Albrecht Von Graefes Arch Klin Exp Ophthalmol 192:181-96

Heald R, McLoughlin M, McKeon F (1993) Human wee1 maintains mitotic timing by protecting the nucleus from cytoplasmically activated cdc2 kinase. Cell 74:463-474

Held T et al. (2006) Hspa4l deficient mice display increased incidence of male infertility and hydronephrosis development. Mol Cell Biol 26:8099-8108

Henkin RI, Martin BM, Agarwal RP (1999) Efficacy of Exogenous Oral Zinc in Treatment of Patients with Carbonic Anhydrase VI Deficiency. Am J Med Sci 318:392

Hetz C (2012) The unfolded protein response: controlling cell fate decisions under ER stress and beyond. Mol Cell Biol. Doi:10.1038nrm3270

Hims MM, Diager SP, Inglehearn CF (2003) Retinitis pigmentosa:genes, proteins and prospects. Dev Ophthalmol 37:109-125

Hirata T et al. (2006) Zinc-finger gene Fez in the olfactory sensory neurons regulates development of the olfactory bulb non-cell-autonomously. Dev 133:1433-1443

Höhfeld J, Cyr DM, Patterson C (2001) From the cradle to the grave: molecular chaperones that may choose between folding and degradation. EMBO reports 2:885-890

Horstmeyer A, Licht C, Scherr G, Eckes B, Krieg T (2005) Signalling and regulation of collagen I synthesis by ET-1 and TGF-beta1. FEBS J. 272:6297-6309

Hsu CA et al. (1998) Retinoid induced apoptosis in leukemia cells through a retinoic acid nuclear receptor-independent pathway. Blood 89:4470-4479

Hu S, Yang X (2003) Cellular inhibitor of apoptosis 1 and 2 are ubiquitin ligases for the apoptosis inducer Smac/DIABLO. J Biol Chem 278:10055-10060

Huang Z, Liu F, Zheng Q, Yu W (2001) Zinc Transfer Kinetics of Metallothioneins and Their Fragments with Apo-carbonic Anhydrase. Chinese J Chem 19:462–467

Humphries MM, Rancourt D, Farrar GJ, Kenna P, Hazel M, Bush RA, Sieving PA, Sheils DM, McNally N, Creighton P (1997) Natl Genet 15:216–219

Ichimura T, Watanabe S, Sakamoto Y, Aoto T, Fujita N, Nakao M (2005) Transcriptional repression and heterochromatin formation MBD1 and MCAF/AM family proteins. J Biol Chem 280:13928-13935

Illing ME, Rajan RS, Bence NF, Kopito RR (2002) A rhodopsin mutant linked to autosomal dominant retinitis pigmentosa is prone to aggregate and interacts with the ubiquitin proteasome system. J Biol Chem 277:34150-34160

Jacobson SG et al. (2010) Normal central retinal function and structure preserved in retinitis pigmentosa. Invest Ophthalmol Vis Sci 51:1079-1085

Jeppesen P, Sanye-hajari J, Bek T (2007) Increased Blood Pressure Induces a Diameter Response of Retinal Arterioles that Increases with Decreasing. Invest Ophthalmol Vis Sci 48:328-331

Jin ZB et al. (2011) Modeling Retinal Degeneration Using Patient-Specific Induced Pluripotent Stem Cells. PLoS ONE 6, e17084

Kalloniatis R. (2004) Retinitis pigmentosa : understanding the clinical presentation, mechanisms and treatment options. Clin Exp Optom 84:65-80

Kaltenbach LS et al. (2007) Huntingtin Interacting Proteins Are Genetic Modifiers of Neurodegeneration PLoS Genet 3:e82 doi:10.1371/journal.pgen.0030082

Kampinga HH, Hageman J, Vos MJ, Kubota H, Tanguy RM, Bruford EA, Cheetham ME, Chen B, Hightower LE (2009) Guidelines for the nomenclature of the human heat shock proteins. Cell Stress and Chaperones 14:105-111

Kaufman RJ (2002) Orchestrating the unfolded protein response in health and disease. Perspective 110:1389-1398

Kerem BS, Rommens JM, Buchanan JA, Markiewicz D, Cox TK, Chakravarti A, Buchwald M, Tsui LC (1989) Identification of the cystic fibrosis gene: genetic analysis. Science 245:1073-1080

Kerr MK, Martin M, Chrchill GA (2000) Analysis of variances from gene expression microarray data. J Comput Biol 7:819-837

Khan IF et al. (2010) Engineering of Human Pluripotent Stem Cells by AAV-mediated Gene Targeting. Molecular Therapy 18:1192–1199

Kiilgaard JF, Prause JU, Prause M, Scherfig E, Nissen MH (2007) Proliferation of RPE Cells in the Periphery in In Vivo Studies in Pigs. Invest Ophthalmol Vis Sci 48:355-360

Kim PS et al. (2008) Defective protein folding and intracellular retention of thyroglobulin-R19K mutant as a cause of human congenital goiter. Mol Endocrinol 22:477-484

Köhn, L. et al. (2008) Carrier of R14W in carbonic anhydrase IV presents Bothnia dystrophy phenotype caused by two allelic mutations in RLBP1. Invest Ohpthalmol Vis Sci 49:3172-3177

Kong CS, Yu J, Minion FC, Rajan K (2011) Identification of biologically significant genes from combinatorial microarray data. ACS Comb. Sci. 13:562-572

Kosmaoglou M, Schwarz N, Bett JS, Cheetham ME (2008) Molecular chaperones and photoreceptor function. Progress in retinal and eye research 27:434-449

Lahdenranta J, Pasqualini R, Schlingemann RO, Hagedorn M, Stallcup WB, Bucana CD, Sidman RL, Arap W (2001) An anti-angiogenic state in mice and humans with retinal photoreceptor cell degeneration. Proc Nat Acad Sci 98:10368-10373

Laity JH, Lee BM, Wright PE (2001) Zinc finger proteins: new insights into structural and functional diversity, Curr Opin Struc Biol 11:39-46

Lee NS, Dohjima T, Bauer G, Li H, Li M, Ehsani A, Salvaterra P, Rossi J (2002) Expression of small interfering RNAs targeted against HIV-1 rev transcripts in human cells. Nat Biotech 20:500–505

Li TY, Kraker AJ, Shaw CF, Petering DH (1980) Ligand substitution reactions of metallothioneins with EDTA and apo-carbonic anhydrase. Proc Natl Acad Sci 77:6334-6338

Li J, Lee AS (2006) Stress Induction of GRP78/BiP and Its Role in Cancer. Curr Mol Med 6:45-54

Li X, Liu Y, Alvarez BV, Casey JR, Fliegel L (2006) A Novel Carbonic Anhydrase II Binding Site Regulates NHE1 Activity. Biochem 45:2414–2424

Li S, Zhou H, Luo Y, Zhang P, Qu L (2005) Identification and functional analysis of 20 box H/ACA small nucleolar RNAs (snoRNAs) from Schizosaccharomyces pombe. J Biol Chem 280:16446-16455

Lin JH et al. (2007) IRE1 signaling affects cell fate during the unfolded protein response. Science 318:944-949

Lin JH, Walter P, Yen TSB (2008) Endoplasmic reticulum stress in disease pathogenesis. Ann Rev Pathol 3:399-425

Liu CY, Kaufman RJ (2003) The unfolded protein response. J Cell Sci 116:1861-1862

Liu W, Smith DI, Rechtzigel KJ, Thibodeau SN, James CD (1998) Denaturing high performance liquid chromatography (DHPLC) used in the detection of germline and somatic mutations. Solutions 26:1396-1400

Loughlin J et al. (2004) Functional variants within the secreted frizzy-related protein 3 gene are associated with hip osteoarthritis in females. Proc Natl Acad Sci USA 101:9757-9762

Luheshi LM, Crowther DC, Dobson CM (2008) Protein misfolding and disease: from the test tube to the organism. Curr Opin Chem Biol 12:25-31

Mackay-Sim A, Dreosti IE. (1989) Olfactory function in zinc-deficient adult mice. Exp Brain Res 76:207-212

Makinen PI, Koponen JK, Karkkainen A, Malm TM, Pulkkinen KH, Koistinaho J, Turunen MP, Yla-Herttuala S (2006) Stable RNA interference: comparison of U6 and H1 promoters in endothelial cells and in mouse brain. J Gene Med 8:433–441

Malhotra JD, Kaufman RJ (2007) The endoplasmic reticulum and the unfolded protein response. Seminars in cell and developmental biology 18:716-31

Marneros AG et al. (2005) Vascular Endothelial Growth Factor Expression in the Retinal Pigment Epithelium Is Essential for Choriocapillaris Development and Visual Function. Am J Pathol 167:1451-1459

Martin L, Fluhrer R, Haass C (2009) Substrate requirements for SPPL2b-dependent regulated intramembrane proteolysis. J Biol Chem 284:5662-5670

Martin JN, Wolken N, Brown T, Dauer WT, Ehrlich ME, Gonzalez-Alegre P (2011) Lethal toxicity caused by expression of shRNA in the mouse striatum: implications for therapeutic design. Gene Ther 18:666–673

Martinez J, Patkaniowska A, Urlaub H, Lu R, Tuschl T (2002) Single-Stranded Antisense siRNAs Guide Target RNA Cleavage in RNAi. Cell 110:563-574

Mayer MP, Bukau B (2005) Hsp70 chaperones: Cellular functions and molecular mechanism. Cell Mol Life Sci 62:670-684

McCarthy DJ, Smythe GK (2009) Testing significance relative to a fold-change is a TREAT. Bioinformatics 25:756-771

McGowan CH, Russell P, Page S (1995) Cell cycle regulation of human WEE1. EMBO J 14:2166-2175

McNamara JO et al. (2006) Cell type-specific delivery of siRNAs with aptamer-siRNA chimeras. Nat Biotech 24:1005-1015

McWilliam P et al. (1989) Autosomal dominant retinitis pigmentosa (ADRP): Localization of an ADRP gene to the long arm of chromosome 3. Genomics 5:619-622

Melo GB, Farah ME, Aggio FB (2007) Intravitreal injection of bevacizumab for cystoid macular edema in retinitis pigmentosa. Acta Ophthalmologica Scandinavica. 85:461–463

Mendes HF, Cheetham ME (2008) Pharmacological manipulation of gain-of-function and dominant-negative mechanisms in rhodopsin retinitis pigmentosa. Hum Mol Genet. doi:10.1093/hmg/ddn202

Mendes HF, van der Spuy J, Chapple JP, Cheetham ME (2005) Mechanisms of cell death in rhodopsin retinitis pigmentosa: implications for therapy. Trends in Mol Med 11:177-185

Michel L, Diaz-Rodriguez E, Narayan G, Hernando E, Murty VV, Benezra R (2004) Complete loss of the tumor suppressor MAD2 causes premature cyclin B

degradation and mitotis failure in human somatic cells. Proc Natl Acad Sci USA 101:4459-4464

Mikkaichi T et al. (2004) Isolation and characterization of a digoxin transporter and its rat homologue expressed in the kidney. Proc Natl Acad Sci USA 101:3569-3574

Miller N (2004) The misfolding diseases unfold. Beremans Ltd

Miller VM et al. (2003) Allele-specific silencing of dominant disease genes. Proc Natl Acad Sci USA 100:7195-7200

Millington-Ward S et al. (2011) Suppression and replacement gene therapy for autosomal dominant disease in a murine model of dominant retinitis pigmentosa. Mol Ther : J Am Soc Gene Ther 19:642-9

Mivechi NF, Eroglu B, Moskofidis D (2011) Heat shock protein deficiencies as model systems for brain pathologies and cancer. US Pat 12/744866

Moiseyev G, Chen Y, Takahashi Y, Wu BX, Ma JX (2005) RPE65 is the isomerohydrolase in the retinoid visual cycle. Proc Natl Acad Sci USA 102:12413-12418

Molema G (2005) Design of vascular endothelium-specific drug-targeting strategies for the treatment of cancer. Acta Biochimica Polonica 52:301-310

Momeni P et al. (2000) Mutations in a new gene, encoding a zinc-finger protein, cause tricho-rhino-phalangeal syndrome type I. Nat Genet 24:71-74

Mori K (2009) Signalling Pathways in the Unfolded Protein Response: Development from Yeast to Mammals. J Biochem 146:743-750

Nagaia N, Hosokawab M, Itoharac S, Adachid E, Matsushitab T, Hosokawaa N, Nagata K (2007) Embryonic Lethality of Molecular Chaperone Hsp47 Knockout Mice Is Associated with Defects in Collagen Biosynthesis. J Biol Chem 150:1499-1506

Nakatsukasa K, Brodsky JL (2008) The recognition and retrotranslocation of misfolded proteins from the endoplasmic reticulum. Traffic 9:861-870

Napoli C, Lemieux C, Jorgensen R (1990) Introduction of a Chimeric Chalcone Synthase Gene into Petunia Results in Reversible Co-Suppression of Homologous Genes in trans. Plant Cell 2:279-289

Nishitoh H (2011) CHOP is a multifunctional transcription factor in the ER stress response. J Biochem 151:217-219

Nollen EAA, Morimoto RI (2002) Chaperoning signaling pathways: molecular chaperones as stress-sensing "heat shock" proteins. J Cell Sci 115:2809-2816

Noorwez SM et al. (2003) Pharmacological chaperone-mediated in vivo folding and stabilization of the P23H-opsin mutant associated with autosomal dominant retinitis pigmentosa. J Biol Chem 278:14442-14450

Noorwez SM et al. (2004) Retinoids assist the cellular folding of the autosomal dominant retinitis pigmentosa opsin mutant P23H. J Biol Chem 279: 16278-16284

Noorwez SM, Ostrov DA, McDowell JH, Krebs MP, Kaushal S (2008) A high-throughput screening method for small-molecule pharmacologic chaperones of misfolded rhodopsin. Invest Ophthalmol Vis Sci 49:3224-3230

Ogilvie JM et al. (2007) Carbonic anhydrase XIV deficiency produces a functional defect in the retinal light response. Proc Natl Acad Sci USA 104:8514-9

Ohno-Matsui K, Yoshida T, Uetama T, Mochizuki M, Morita I (2003) Vascular endothelial growth factor upregulates pigment epithelium-derived factor

expression via VEGFR-1 in human retinal pigment epithelial cells. Biochem Bioph Res Comm 303:962-967

Outeiro TF, Tetzlaff J (2007) Mechanisms of disease II: cellular protein quality control. Seminars in pediatric neurology 14:15-25

Ozdemir H, Karacorlu M, Karacorlu S (2005) Intravitreal triamcinolone acetonide for treatment of cystoid macular oedema in patients with retinitis pigmentosa. Acta Ophthalmologica Scandinavica 83:248–251

Pal-Bhadra M, Bhadra U, Birchler J (1997) A Co-suppression in Drosophila: gene silencing of Alcohol dehydrogenase by white-Adh transgenes is Polycomb dependent. Cell 90:479-490

Park D et al. (2011) Continued clearance of apoptotic cells critically depends on the phagocyte Ucp2 protein. Nature 477:220–224

Park J et al. (2011) Comparative gene expression analysis of somatic cell nuclear transfer-derived cloned pigs with normal and abnormal umbilibal cords. Biol Reprod 84:189-199

Parkkila S, Parkkila AK, Juvonen T, Rajaniemi H (1994) Distribution of the carbonic anhydrase isoenzymes I, II, and VI in the human alimentary tract. Gut 1994:646-650

Pebernard S, Iggo RD (2004) Determinants of interferon-stimulated gene induction by RNAi vectors. Diff erentiation 72:103–111

Peran M, Hooper H, Rayner SL, Stephenson FA, Salas R (2004) GABAA receptor alpha1 and alpha6 subunits mediate cell surface anchoring in cultured cells. Neurosci Lett 364:67-70

Persengiev SP, Zhu X, Green MR (2004) Nonspecific, concentration-dependent stimulation and repression of mammalian gene expression by small interfering RNAs (siRNAs). RNA 10:12-18

Pham LV, Tamayo AT, Yoshimura LC, Lo P, Ford RJ (2003) Inhibition of constitutive NF-kB activation in mantle cell lymphoma B cells leads to induction of cell cycle arrest and apoptosis. J Immunology 171:88-95

Phelan JK, Bok D (2000) A brief review of retinitis pigmentosa and the identified retinitis pigmentosa genes. Mol Vis 6:116-24

Polier S, Dragovic Z, Hartl FU, Bracher A (2008) Structural basis for the cooperation of Hsp70 and Hsp110 chaperones in protein folding. Cell 133:1068-1079

Pollman MJ, Naumovski L, Gibbons GH (1999) Vascular Cell Apoptosis: Cell Type–Specific Modulation by Transforming Growth Factor-ß1 in Endothelial Cells Versus Smooth Muscle Cells. Circulation. 1999:2019-2026

Purkerson JM, Kittelberger AM, Schwartz GJ (2007) Basolateral carbonic anhydrase IV in the proximal tubule is a glycosylphosphatidylinositol-anchored protein. Kidney Intl 71:407-416

Purkerson JM, Schwartz GJ (2005) Expression of membrane-associated carbonic anhydrase isoforms IV, IX, XII, and XIV in the rabbit: induction of CA IV and IX during maturation. Am J Physiol. 288:1256-1263

Pushkin A (2004) Molecular mechanism of kNBC1-carbonic anhydrase II interaction in proximal tubule cells. J Physiol 559:55-65

Qiu X, Shao Y, Miao S, Wang L (2006) The diversity of the DnaJ/Hsp40 family, the crucial partners for Hsp70 chaperones. Cell Mol Life Sci 63:2560-2570

Rao DD, Vorhies S, Senzer N, Nemunaitis J (2009) siRNA vs shRNA: similarities and differences. Adv Drug Deliv Rev 61:746-759

Ratcliff F, Harrison BD, Baulcombe DC (1997) A similarity between viral defense and gene silencing in plants. Science 276:1558-1560

Rebello G et al. (2004) Apoptosis-inducing signal sequence mutation in carbonic anhydrase IV identified in patients with the RP17 form of retinitis pigmentosa. Proc Natl Acad Sci 101:6617-6622

Reithmeier RAF (2001) A Membrane Metabolon Linking Carbonic Anhydrase with Chloride/Bicarbonate Anion Exchangers. Blood Cells, Molecules, and Diseases. 27:85-89

Rivolta C, Sharon D, DeAngelis MM, Dryja TP (2002) Retinitis pigmentosa and allied diseases: numerous diseases, genes, and inheritance patterns. Hum Mol Genet 11:1219-27

Saliba RS, Munro PMG, Luthert PJ, Cheetham ME (2002) The cellular fate of mutant rhodopsin: quality control, degradation and aggresome formation. J Cell Sci 115:2907-2918

Sambrook J (1989) Molecular Cloning: A laboratory manual.

Sankpal NV et al. (2009) Transcriptional Repression of Epithelial Cell Adhesion Molecule Contributes to p53 Control of Breast Cancer Invasion Transcriptional Repression of Epithelial Cell Adhesion Molecule Contributes to p53 Control of Breast Cancer Invasion. Cancer Res doi:10.1158/0008-5472.CAN-08-2708

Santucci-Darmanin S et al. (2000) MSH4 acts in conjunction with MLH1 during mammalian meiosis. FASEB J 14:1539-1547

Saraiva VS, Sallum JMF, Farah ME (2003) Treatment of cystoid macular edema related to retinitis pigmentosa with intravitreal triamcinolone acetonide. Ophthalmic surgery, lasers and imaging 34:398-400

Sauvé Y, Karan G, Yang Z, Li C, Hu J, Zhang K (2006) Treatment with Carbonic Anhydrase Inhibitors Depresses Electroretinogram Responsiveness in Mice. Adv Exp Med Biol 572:439-446

Sayer JA et al. (2006) The centrosomal protein nephrocystin-6 is mutated in Joubert syndrome and activates transcription factor ATF4. Natl Genet 38:674-681

Scholefield J et al. (2009) Design of RNAi hairpins for mutation-specific silencing of ataxin-7 and correction of a SCA7 phenotype. PloS one 4(9)e7232

Schröder M, Kaufman RJ (2005) ER stress and the unfolded protein response. Mut Res 569:29-63

Seaki M, Irie Y, Ni Li, Yoshida M, Itsuki Y, Kamisaki Y, Monda A (2006) WD40 repeat protein, promotes apoptosis induced by TNF-alpha. Biochem Biophys Res Commun 342:568-572

Shah GN et al. (2005) Carbonic anhydrase IV and XIV knockout mice: roles of the respective carbonic anhydrases in buffering the extracellular space in brain. Proc Natl Acad Sci USA 102:16771-16776

Shahidullah M, To CH, Pelis RM, Delamere NA (2009) Studies on bicarbonate transporters and carbonic anhydrase in porcine nonpigmented ciliary epithelium. Invest Ophthalmol Vis Sci 50:1791-1800

Shaw G, Morse S, Ararat M, Graham FL (2002) Preferential transformation of human neuronal cells by human adenoviruses and the origin of HEK 293 cells. The FASEB J 16:869-871

Shen X, Zhang K, Kaufman RJ (2004) The unfolded protein response – A stress signaling pathway of the endoplasmic reticulum. J Chem Neuroanat 28:79-92

Shin H et al. (2010) Identification of transcriptional targets of Wnt/β-catenin signalling in dermal papilla cells of human scalp hair follicles: EP2 is a novel transcriptional target of Wnt3a. J Derm Sci doi:10.1016/j.jdermsci.2010.02.011

Shinohara T, Mulhern ML, Madson CJ (2008) Silencing gene therapy for mutant membrane, secretory, and lipid proteins in retinitis pigmentosa (RP). Med Hypoth 70:378-380

Shintani K, Shechtman DL, Gurwood AS (2009) Review and update: current treatment trends for patients with retinitis pigmentosa. Optom 80:384-401

Shore G, Papa FR, Oakes SA (2011) Signalling cell death from the endoplasmic reticulum stress response. Curr Opin Cell Biol 3:143-149

Silke J, Vaux DL (2001) Two kinds of BIR-containing protein - inhibitors of apoptosis or required for mitosis. J Cell Sci 114:1821-1827

Silva JM, Li M, Chang K et al. (2005) Second-generation shRNA libraries covering the mouse and human genomes. Nat Genet 37:1281-1288

Smith SC et al. (2006) The Metastasis-Associated Gene CD24 Is Regulated by Ral GTPase and Is a Mediator of Cell Proliferation and Survival in Human Cancer and Survival in Human Cancer. Cancer Res doi:10.1158/0008-5472.CAN-05-3855

Sontheimer EJ, Steitz JA (1993) The U5 and U6 small nuclear RNAs as active site components of the spliceosome. Science 262:1989-1996

Stams T, Nair SK, Okuyama T, Waheed A, Sly WS, Christianson W (1996) Crystal structure of the secretory form of membrane-associated human carbonic anhydrase IV at 2.8-A resolution. Proc Natl Acad Sci USA 93:13589-13594

Steinhoff C, Vingron M (2006) Normalization and quantification of differential expression in gene expression microarrays. Briefings in bioinformatics 7:166-77

Sterling D, Alvarez BV, Casey JR (2002) The extracellular component of a transport metabolon. Extracellular loop 4 of the human AE1 Cl^-/HCO^{3-} exchanger binds carbonic anhydrase IV. J Biol Chem 277:25239-25246

Strauss O (2005) The retinal pigment epithelium in visual function. Physiol Rev 85:845-881

Sun XC, Li J, Cui M, Bonanno JA (2008) Role of Carbonic Anhydrase IV in Corneal Endothelial HCO_3^- Transport. Invest Ophthalmol Vis Sci 49:1048-1055

Sung C (1991) Functional Heterogeneity of Mutant Rhodopsins Responsible for Autosomal Dominant Retinitis Pigmentosa. Proc Natl Acad Sci USA 88:8840-8844

Suparan CT, Scozzafava A (2007) Carbonic anhydrases as targets for medicinal chemistry. Bioorg Med Chem 15:4336-4350

Svichar N et al. (2009) Carbonic anhydrases CA4 and CA14 both enhance AE3-mediated Cl^--HCO^{3-} exchange in hippocampal neurons. J Neurosci 29:3252-3258

Tam LCS et al. (2008) Therapeutic benefit derived from RNAi-mediated ablation of IMPDH1 transcripts in a murine model of autosomal dominant retinitis pigmentosa (RP10). Human molecular genetics 17:2084-2100

Thompson JD, Gibson TJ, Plewniak F, Jeanmougin F, Higgins DG (1997) The CLUSTAL_X Windows Interface: Flexible Strategies for Multiple Sequence Alignment Aided by Quality Analysis Tools. Nucl Acids Res 25:4876-4882

Tsai RY, Reed RR (1997) Cloning and functional characterization of Roaz, a zinc finger protein that interacts with O/E-1 to regulate gene expression: implications for olfactory neuronal development. J Neurosci 17:4159-4169

Tsang WY, Wang L, Chen Z, Sánchez I, Dynlacht BD (2007) SCAPER, a novel cyclin A–interacting protein that regulates cell cycle progression. J Cell Biol 178:621-633

Tsaytler P, Harding HP, Ron D, Bertolotti A (2011) Selective inhibition of a regulatory subunit of protein phosphatase 1 restores proteostasis. Science 332:91-94

Valencia-Sanchez MA, Liu J, Hannon GJ, Parker R (2006) Control of translation and mRNA degradation by miRNAs and siRNAs. Genes and Dev 20:515-524

Van der Krol A, Mur LA, Beld M, Mol JNM, Stuitje AR (1990) Flavonoid genes in petunia: Addition of a limited number of gene copies may lead to a suppression of gene expression. Plant Cell 2:291-299

Vince JW, Reithmeier RAF (2000) Identification of the Carbonic Anhydrase II Binding Site in the Cl-/HCO3- Anion Exchanger AE1. Biochem 39:5527–5533

Wang Q, Chen Q, Zhao K, Wang L, Wang L, Elias I Traboulsi (2001) Update on the molecular genetics of retinitis pigmentosa. Ophthal Genet 22:133-154

Wang J et al. (2009) Progressive aggregation despite chaperone associations of a mutant SOD1-YFP in transgenic mice that develop ALS. Proc Natl Acad Sci 106:1392-1397

Wang Y et al. (2008) A novel member of the Rhomboid family, RHBDD1, regulates BIK-mediated apoptosis. Cell Mol Life Sci 65:3822-3829

Wang F, Song W, Brancati, G, Segatori (2011) Inhibition of endoplasmic reticulum-associated degradation rescues native folding in loss of function protein misfolding diseases. J Biol Chem 286:43454-43464

Weinberg RA (2005) The retinoblastoma protein and cell cycle control. Cell 81:323-330

Went P, Dirnhofer S, Salvisberg T, Amin MB, Lim SD, Diener P, Moch H (2005) Expression of epithelial cell adhesion molecule (EpCam) in renal epithelial tumors. Am J Surgical Path 29:83-88

Wiech H, Buchner J, Zimmermann R, Jakob U (1992) Hsp90 chaperones protein folding in vitro. Nature 358:169-170

Winnefeld M, Rommelaere J, Cziepluch C (2004) The human small glutamine-rich TPR-containing protein is required for progress through cell division. Exp Cell Res 293:43-57

Wiseman RL, Powers ET, Buxbaum JN, Kelly JW, Balch WE (2007) An adaptable standard for protein export from the endoplasmic reticulum. Cell 131:809-821

Wistrand PJ, Schenholm M, Lönnerholm G (1986) Carbonic anhydrase isoenzymes CAI and CA II in the human eye. Invest Ophthalmol Vis Sci 27:419-428

Woessner JF (2001) That impish TIMP: the tissue inhibitor of metalloproteinases-3. J Clin Invest 108:2-3

Wray GA (2007) The evolutionary significance of cis-regulatory mutations. Nat Rev Genet 8:206-216

Wu F, Ivanov I, Xu R, Safe S (2009) Role of SP transcription factors in hormone-dependent modulation of genes in MCF-7 breast cancer cells: microarray and RNA interference studies. J Mol Endocrinol 42:19-33

Yang Y and Li X (2000) The IAP family: endogenous caspase inhibitors with multiple biological activities. Cell Res 10:169-177

Yang YH et al. (2002) Normalization for cDNA microarray data : a robust composite method addressing single and multiple slide systematic variation. Nat Genet 30:1-10

Yang, Z. et al. (2005) Mutant carbonic anhydrase 4 impairs pH regulation and causes retinal photoreceptor degeneration. Hum Mol Genet 14:255-265

Yau KW (1994) Phototransduction mechanism in retinal rods and cones. The Friedenwald Lecture. Invest Ophthalmol Vis Sci 35:9-32

Yu JY, DeRuiter SL, Turner DL (2002) RNA interference by expression of short-interfering RNAs and hairpin RNAs in mammalian cells. Proc Natl Acad Sci 99:6047–6052

Zeng J, Heuchel R, Schaffner W, Kägi JH (1991) Thionein (apometallothionein) can modulate DNA binding and transcription activation by zinc finger containing factor Sp1. FEBS letters 279:310-312

Zhouravleva G, Schepachev V, Petrova A, Tarasov O, Inge-Vechtomov S (2006) Evolution of translation termination factor eRF3: Is GSPT2 generated by retrotransposition of GSPT1's mRNA? IUBMB Life 58:199-202

Zhu XL, Sly WS (1990) Carbonic anhydrase IV from human lung: Purification, characterization, and comparison with membrane carbonic anhydrase from human kidney. J Biol Chem 265:8795-8801

Appendix

14.1. Annotated CA4 sequence

Key:
Miscellaneous features are highlighted in green
Start codon is highlighted in green
Stop codon is highlighted in red
Primer sequences are highlighted in purple> (forward), or <purple (reverse),
or underlined (if there are overlaps)
Exonic sequences are highlighted in Blue
Promoter portion 5' of Exon 1a is underlined

```
 LOCUS       AC025048         137921 bp    DNA  linear  PRI 19-JUL-2002
 Homo sapiens chromosome 17, clone CTD-2319I12,complete sequence.
 . . . . .
 97201 agagcaaaga cttgaactca gaacactggg ggcctctgca gagtaagagg aaggaggctg
 97261 gggctgctgg gctgggctct cccactcagg tggcctgggc tggcagcttt atgggccctg
 97321 taagtcgctg ggacatgtca gcactcattc cagctctaac gaccctaaat caggccttgt
 97381 cccctacagg taagcagggc cccaggtagt ctaaatagtg acaggtgact ggtttatggc
 97441 aggccaggac tggggtcagg gctggagata aggctgagaa tgttaagacc aggaacagga
 97501 agagagggcc actcaccctg tgtaaccttg aagttagaga tggcagatgg agcaggaacc
 97561 agtccaccac cccatcgcca atgtgcaggc tctgtggtgc ccataattaa gatgcaccca
 97621 taagagagtg tatagcttta ccccctcccgc attcctcaga ggggatgccc taccagggac
 97681 tcgttctcct cacccatctt tatggtccca aaatgcaccc agggcccccc tctctcctgg
 97741 ggggcctgaa tgcaatgaac tttaaagtgg atcattgatc aacagtccct taaccccacc
 97801 aaagtttccc aagcctctcc cctgctcatc agggggctgg ccagaggtca cagggactcc
 97861 ctgggggtgg tttttattcc caggaacagg cttcctcagt cctgaaaggg acatttttat
 97921 agccctgtga acacaaatgc actccccaga ataggctctg ggtgtggaat ccctcctgtg
 97981 gctgtcatgg tcgcaggctg gtgattacat tatacagtgg tgttgacaat agagccctaa
 98041 gcctggcatg gacacccccc cacctccctc ctgcctctct gtaggatcaa agctgctctg
 98101 tgaggctgtg tgatcctggg ccaggagcgg ggagtcagcc tcaaccctaa gcaaggagga
 98161 agcatctttg cctgaatcct tctgggggag gcaatccccc ttcagaagtc cctagcccag
 98221 gttcgaaggt cggtagggac tgagaggttg gcagcggatg gggagtggct aaaccagaaa
 98281 aaggggggctt cctgttgatg gattgatgga ggaggtccag gtccactgcc tggttccccg
                           dbSNP (rs345192 A/G)
 98341 tccctctccc gcaccccagc ctgagcttcc caaactccca cagaagcccc caccccatgt
 98401 gggacacaga ggacctgcag tagcaggagg gcacagctaa gagaggagac aagaggcagc
 98461 ttgggggcat gggggggacc ccatttcccc aaatgttgga gccgccctta agggaacttc
 98521 ccctggactc ctctggaggt cttgccagat gggagaacca ggggtccatt cagaccccag
 98581 tctcttctct tcccatctca tctctccacc tgggggggctc aaagaaccta gctcctcccc
 98641 tttgacccca tcagcttctc cctcaccgaa tcctcttaca atccatttct taattctgcc
 98701 ccatcaaccc tccctggtca tcacataaac accagcaagg gcagtagttt agggacagct
 98761 ttgctctgta ttcgaagaaa ggtctttggt ctgcttagaa attaagtttg gagcagcctg
 98821 ggaggaaata gaagagatga gacccagaga atcaatggcc actgccaaag agagatagga
 98881 gagcctttct gcggccactg attcaacaaa cggcatcaca cgcccctcag cctctcatct
 98941 cttcgaggcc atctccaccc ccacccccac ccccacccca aggccattcc aaggtcccat
 99001 tcaagaccac tgcgcagggg tggcgccaga atgatcaaag tcatcatggg gcactcatct
```

Exon 1a

```
 99061 ttgtgtgggt caagcacttt gt>ggtgtcgt gtccctgttc> ccaaaccagg gaccaggagt
```

Exon1a3-2R

```
Exon1a-R
 99121 aggatggggg aggggcaggg cgccgctgct gagtggagag gacgcggagt gggtgagggg
Promoter
 99181 gccttgcgca cagggcaaga ggtggccagg cagggcgggg gaccgggggag agcggaggat
Exon1a3-1R
                                          GC_signal
 99241 ttcag>atgag ggacagggga aggtggagag gggagggcag gccccgccag ggggaggagc
 99301 cgcctcccgc gtccagctgt cggggctccc tcccgtcgcg gctcc<gctat aaaacccagg
Exon1a3-2F
                                                    TATA_signal
 99361 ccggcaggat cgctgcaccc gcggcggcct cctcggtgcg cgacccccgg ctcagaggac
CA4mRNA-F
                                                          dbSNP
(rs345191 G/C)
 99421 tctttgctg>t cccgcaagat gcggatgctg ctggcgctcc tggccctctc cgcggcg<cgg
CA4E1awt-F
                          Start
Mutation(C→T)
 99481 ccatcggcca gtgcaggtga gctcccgggc tccggcccca ggtgcccctc ggcggtcccc
 99541 tccgtgcccc cagctcccgc ccctgcaggag gatccccccg cgggcgaccg gtgagcgtcg
                                    UCT SNP (G/T)
 99601 gtggcgctgg ggtcccgggt tgcgtgtgcg ccgggggccg cgagggtgcg ggaggactgg
                                                   dbSNP (rs345190 C/G)
 99661 gcagcgcgcg agcttgtgtg tgcacacgcg tgtcagcacc ggctgggggа gcgtgtgcac
 99721 gggtgtgcgc ggtgagggtg tgtgcgcgtg gcccggcga<g a<cga<gttggg agtccctgat
Exon1a2-F
 99781 aaggatgcgt ctcaggccgg gcgcgggtgc tccagcctga aatgccagca cgttgggagg
Exon1a-F
 99841 cagaggcggg tggatcacct gagcccagga gttcgagacc agcatggcca acatggtgaa
Exon1a3-1F
 99901 atcccatctc taccaaaaat acaaacatta gccggacgtg gtggcacacg cctgtaatcc
 99961 cagctactcg ggaggctgag gcccgagaat cgcttgaacc caggaggtgg aggttgcagt
100021 gagatcacgc cactgcactc cagcctggtg ctccgtttaa aaaaaaaaaa aaaaaaaaaa
100081 aaaaaaaaaa aaaaggatgc ttctcggacc cgcctcaacg cacgccttct tttctcaccc
100141 agcctcctcc gtctgcccgt gggtttccgt ccgtcccgct gggactcagc gctgggtgac
100201 tgccccgcgg ccagagcaag ggcggtctgg cagggtcctg gaagccgcgc ttcccacacg
100261 ggttccttgc ccctgagggt cgcaagctcc cctggcctcc ctaacctcca gcgctgaatt
100321 gggagcctgg cgggggcggg gggtgggggа cccggagccc caaggcctct gcggagccgg
100381 tctttccgga cagggtgatt ttcgtttaaa gattaatggt gaagccgagc tcttaattat
100441 tcctctaggt gggaggtggc aggaaaggca tgttaatatt tgataagaag ctaaaggcgc
100501 ttcaagcggc tgggcacagg gatccgatcc tggaggcacc ttctttgcaa ccccagaccc
100561 catcaccgga agacccccтc tgccagttct cagcccaacc acccctcgga tggttcttgg
100621 ggtccacgca ggctgaaacc tcctctccca agttaggtgc tccatcctca aagcggcgga
100681 gtgaggggtg aaggtgtcct ctgcacagag aggagccagc gtgtgccctt tgcagcaggg
100741 actggctgag ctgtcttaga gggtcgaggg gcaccttgca gcctctccac cgggcccctg
100801 ggagaagaaa gagaaaaagc agaatgtgga aacttttatt tgtagggttg gacattggaa
100861 acctactaag cagctagaaa gtagaaagag aaatgctttg cagttctggt gctttgtagc
100921 tgtgtggtct tgggtaagtc acttcctgtc ccatttgcaa aacaggtgtt gtcattctga
100981 cttcaggggt tttaagcgtt tgaataagat aatgggttta agtgattagt gcggtgcctg
101041 tgtggcacgt ggctggtgtg tcatatacca agtttatggg gctctccccc aagcctgggg
101101 ccagtgtcag gaatgtgtct cagctcaccc ctcacacaag ctgctatccc ctttagtgcc
101161 aaggctttct gactgggacc tgccttccat tcatcttatg gaggactcaa gctgagaagg
101221 gaccaggttg catatggcga cccccagagc atctctgtcc attgagacaa gaggccgggt
101281 gaggatattt ggtccccttc agagccccag acccctggcc gggagcgact gagactttgc
101341 ccaggaaaca cttgggttgt gctgagctgt ttttcaggat tatcccctgt ccctcagagg
101401 gggaggtggg gtgagcaagg tccattagag aggcttcttc agccatcttg aaataagggg
101461 gaggggtggc aggtcagtca gtgtgggggg cagtagctgg gtgacaggcg actgactttc
101521 ggtctctaac ctctggtcag ggtggatgga ctaggtagga tgtggcgctg gacaccgaga
101581 cctctgggta ggtagcccct ctccttccca agccctcttg ggagtggcct gagtcagtgg
```

101641 gctggtactt acctgcaagg gtggccctct cattcaacga agacaggaac ctgagtggtg
101701 ggtgctcctg ccaccagcac cccaccctca tccaccgaca tggacctgac ccctggcctt
101761 gacctcacca ccattatgtt ttcctggctg ctgcttcctg aagaaggtag ttacaagtgc
101821 gttcagccaa gcaggtcaaa agtctccatg attaagacag tggatcacag gtcaccacta
101881 caaacctagg agctgcggcc agagccaggg aagaccaaat tcctaagaaa agctaagcct
101941 ggaccagatg ggccccaggg aggctgtgag gcgagttaca gggggctcca ccctttgcag
102001 ctggctcttg gggatgctgg ctgaagggag gcttctcctg gaatggctgc ccccgggccc
102061 tccagtcaga gaagaggcca gcccaatctt caaaacccct tcctccttca agacctctgc
102121 gggtggggac atgggatgat tatggcaagg aactgtcatg gtgcaaatgc cctctgattt
102181 attatctcct tagtcaccag cactgggaat ttggtggctg cacctgtcag aggcgtttga
dbSNP (rs345189 T/C)
102241 accagagtga ctccattttg ggtgagagct aggaaaatga ggccgagatt tgctgggctg
102301 cattatcaga aagtcaggca tttctagcct ctagatgttt gcagttaagg gaacaaatta
102361 ataatattta ctacacagac ccagacttgg gaaggtccag atactccgat atctggagag
102421 caaaggcatt cctaattttg ctttaaaaat aataatgttg gctgggcacg gtggctcaca
102481 cctgtaatcc cagcactttg ggaggccgag gcgggtggat catttgaggt caggagttcg
102541 agaccagcct ggtcaacatg gtgaaaccct gtctctacta aaaatacaaa gattagctgg
102601 gcatggtggt acatgcctgt aatcccagtt actcaggagg ctgaggcagg agaattgctt
102661 gaaactggga agtggaggtt gcagtgagcc aagagcccac actgccctc cagcctgggc
102721 aacagagcga gactctatct caataataat aataatatca attcttggat aatgtagtaa
102781 ttaagaaaat taatccttta tcacaaaccc ttgtagcaga gcacatgtcc ccatatatac
102841 aacgcattga atgcattcct tccttctctg acttttggga atgtcctact ctgtctatgg
102901 agtagctgtc ctttcaccac tgtactttct taataaacgt gcttttcctt tgcactgcag
102961 actcaacctg aattctctct tgtgcaagat ccaagaaccc tctcttgggg tctggatcgg
dbSNP (rs345188 A/G)
103021 gacccctttc ctgtaacatg ccttctgtca gaggaagatt atgggactca gaatgtcaga
103081 taactcccct gtggagactg agcaaaggca gagcgggagc tggaggcttc ggagctctgc
103141 cccactgctg gggtggcgag tggccactgc cctctgcaga atccacccac atgggggtgg
103201 ttcaggtgca gcaactccca gggacagcag agccctgccc ggggctgggg atgggccatc
103261 agggggagga cactgcagct ctgaaaaagg cgatgccagc agggaaggag aggcagtgat
103321 cagggcaggg aaactccaaa gcccaaagca gctcttcgtg gccagttagt tttcctgggg
103381 atgctccctc atggctcctt ccccatcctg tccccactcc ggggactcta ccctggctta
103441 gactacaaga agatgggact gtgggggcag cccaggcaag aagggagagg gtggatgagc
103501 tcagagacct cagctttggc tgagtgggaa ccgtgctttt cttaggaatt tcctcatctt
103561 gatttctttc caagtcactt catttctctc ctctctcggc ccctccttgg ctttggccat
103621 ctgctcccaa aaggaggcca tggggtgggt gggaggggtg ggggggaggg aaggagttgt
103681 cgatgggatt ttactaagtg ccaagccgcc tgaaacctca tttaatcctc cccaaggccc
103741 tatgaggtgg gtatgtttgt ctcatgttac agatgataca actgaggctc agagagctta
103801 agggacttgc ccccaaaccc atctaagccc cctgagcggc tcagccagaa ttccaagctc
103861 tggatgagat gttgtgttcg ccctgctggt gcagcctttt aaaaaaatta atagacttta
103921 tttttagagc aattttaggc tcacataaaa attcagcagg aagtacagag ggttcccata
103981 ggccccttctg ccctgcatgc actttccccc cttattaaca tcttgcatcc atgtgggaca
104041 tttgaggtgc agccttttt tcagagatgc tgggttctat tgccctgagg cagagccctc
104101 agcctgtccc cagagatcag gactgtgcgg ttgaggggca ggggaggaag cctggctgct
104161 ttcctcctag cgggagctgt gagacgctag ccaagaaggg atcttagtaa cacagggtga
104221 gacattctgg ggaggggccg cctaatctcc tccctcatct tggatctggg aaggctgccc
104281 ggttgaacct gactctattg tcccaggagc ggaggctggg ccaagtcctc ctcttctcct
104341 ctcaccagcc tcttttccag gtttggggtg ggggaggtaa gcgcggagga ggctgctggt
104401 gaccaaagga tggagtatcc aagccagccc catgttagag atgagtggcc tcagagggct
104461 tccctggagg gccagtggct gcttggcctg gccctgcctg gggaacagag ccctatgcca
104521 gctgacctgt tgatcagccc ctgcttggtt ttcaattgag tctcttttttc tgggccctca
104581 atcctgctgc caggaacact ccatcccagc ccaagagggg ctccaacccc aggggtaggc

Exon 1b

104641 ccagcctctg atcctcctgt gtgtgtgagc aacaagacac acg>cacgcac acttcacacc
Exon1b-R
104701 cttcctctct gctccagagt cacactggtg ctacgaggtt caagccgagt cctccaacta
104761 cccctgcttg ggtgagtaca gccagtccag ggg<actgctc tttgtgcatg gtgggcacca
Exon1b-F
104821 cgcaagccga aatggagacc ccggaagagt gggaagggga ggggtgatgg tggcttccca
104881 ggcagatatc agttcccagc atacacacac acacacacac acacacactc tctctctctc
104941 tctcacacac acacacacac agatatacaa acacacacac tcacacagaa acacacacac

105001 aacacacaca caagcacaca ctcaaacact cacactcaca catgcacaca cacactcaca
105061 ctcacacaaa cccacactca ctcacacaca caaacacaca ctcacactct cctgtcctgg
105121 tgctcaggga ccagggagca tagagtgacc tgagtcttca ctggcacctg ctgtcatcga
105181 gagggcatgt tccctgtgga ataaatcggt agcagcatta aaggaagaaa ggcgttttgc
105241 tgtttcccat aataaaacgg ggagttgttt ctatcccagt gacacccctt gcagggtgcc
105301 tgagtgatgg tcctttacgc ttttatttga atgctgacca attcgaatgc aaaccctgca
105361 gtctgctgtg ttttggtgac tgagcagtgc tgcccgctcc tgaccctggc ccacctggtg
105421 ttggggtcac cagggttcgg ggaaccagct cctccagggt tactcctctc cctcccattc
105481 ctcagatgat gctcagcgcc cttcatcagc agccccccg ggggtcccac tccacagttt
105541 ccaaagccct ctccatccac ctcctttaaa ctctctgaca tcccagggaa gcggattatc
dbSNP (rs345187 A/G)
105601 tctgcagttc ccattttaca tttgggaaac ccagggcttg gagaggccat gtgcaccacc
105661 tcatgaagtt gtccctaccc cggagctcac agtcaacagt tggcaaccct gttcccaccc
105721 tgttccacac tggggctaga ctccccagcc ttgcatgtat gtttctgtgg aggaggagga
105781 ggagggccca gggagggcga gagtggagtt cggagctgag catccctgca gcacagcctt
Exon 2
105841 caggccaccc caaagcgttt ctgtgtgg>ga actgagtggg tgggcctgac ttcagtgggg
Exon2-R
105901 tggtgggggc tacaccttgg tgccaggcac ccgactctca gcccaccttc tctccctgct
105961 cagtgccagt caagtggggt ggaaactgcc agaaggaccg ccagtccccc atcaacatcg
106021 tcaccaccaa ggcaaaggtg gacaaaaaac tgggacgctt cttcttctct ggctacgata
106081 agaagcaaac gtggactgtc caaaataacg ggcactcagg tgggctggat ggaggcccca
106141 ggcaggcctg ggcacccgag ttccccaagg actgagagga tggggctcct cccaggaggg
106201 tgtgccagac ccaggcccat ctgtgctgtg aggtggctga aaatcccatg ggggaggaca
106261 gcttccagga ggagagagca ctctagtatg ttttcgttac t<tttgtcaga ccagtctggg
Exon2-F
106321 atgtgggggc aggaaacgtt ccaggaagaa ggacatgtgc aaaggcgcgg aggcatggaa
106381 cagctcggcg tgttcagagg actgccagga gctctgtgtg gaggaaggac agacagtgaa
106441 gccaggcaga gcccaagcaa ggcccagggg cagctgggct ggggcccaag ggcagatcac
106501 ccaggcctga ggagtttgga cattaccccg aggacaccag ggcaccacag aggaggtgga
106561 cgcagaggag gcaccaggac agagctgcag tttggggcag tggagggtgc aggagagggg
106621 gaggcaggca gggagaccaa ggaggaggcc agggaaaggt ccggggctgt cccaccctgt
106681 cccaccccgc gccacccctg caggccagaa ccagagctca tgaaggttgg gaggcaggag
Exon 3
106741 acaatgtccc atctgggtga agctgggatg aagagcta>ga ggaggctgag ggaggctggt
Exon3n4-R
106801 tcgaggactc tgccccttct gtgctcccag tgatgatgtt gctggagaac aaggccagca
106861 tttctggagg aggactgcct gccccatacc aggccaaaca gttgcacctg cactggtccg
106921 acttgccata taagggctcg gagcacagcc tcgatgggga gcactttgcc atggaggtga
106981 gggccccttc ccgactggga ccttgtctgg gctctgggcg cgcacctgcc ttgggcaagg
Exon 4

Consensus sequences have been identified as necessary but not sufficient for splicing. In vertebrates, these sequences are
(the slash identifies the exon-intron or intron-exon junction):
C(orA)AG/GTA(orG)AGT "donor" splice site
T(orC)nNC(orT)AG/G "acceptor" splice site.
A third sequence, which in yeast is TACTAAC , is necessary within the intron sequence.

107041 agggtagtcc aggcccttca taggtcccct tttcacccct ccaccccgac cagatgcaca
107101 tagtacatga gaaagagaag gggacatcga ggaatgtgaa agaggcccag gaccctgaag
107161 acgaaattgc ggtgctggcc tttctggtgg aggtgggact cccatccccc acttcccggg
107221 gaacccgggg ctgagagctt cttcttagga <ttcagagacc tgggactcca gcgaggcagg
Exon3n4-F
107281 agggggcggg gagactccaa cttccgcctc tgtttctggg gttgcatgtc cccgggccag
107341 gtggggagcc cagagcctca atcccagaag ctgcctggcc ttccgcccc agatcgggag
dbSNP (rs345186 C/T)
Exon 5
107401 aatgaactgg ccaccaccac tggctcctg cagactttct caagacc>ctt ccctcccttt
Exon5n6-R

107461 ccaggctgga acccaggtga acgagggctt ccagccactg gtggaggcac tgtctaatat
107521 ccccaaacct ggtgagtcag gatgggggag aagggcttgg ggtgaggggg gggattcctc
107581 ccacaaagga aggggtgggt gtgcggggag ctgggctctc agagtgcagg ggaagagggg
Exon 6
107641 ctccttctcc caccctcact gacagtgtcc tctgccccta tctcagagat gagcactacg
107701 atggcagaga gcagcctgtt ggacctgctc cccaaggagg agaaactgag gcactacttc
107761 cgctacctgg gctcactcac cacaccgacc tgcgatgaga aggtcgtctg gacttgttc
dbSNP (2229178 T/G)
107821 cgggagccca ttcagcttca cagagaacag gtgcacaggg cctggggcag ggcatgggct
107881 cccactgcct ggctccccag aaa<ttatccc tctgtctgcc ctcagaggtc cctcaggata
Exon5n6-F
107941 caggtgggga gcccaggtaa ctgaagtccg ttgttaatca tcgacattca ctgaagacag
108001 gcaagaaaag cctgagctgt tccatcacca gattgggggc tagacaggag gcaggggaag
108061 gtggagtcat tcagaaaatg gtgctggggt ttctatcatg aacgaggctc tggggagaca
108121 gcagtgagcc caaaggaccc aaatccctac ccttgcactg ctttcattcc aaaacagtgg
108181 ttctcaaagt gcggcccctg gaccagtgga gtcaacatca tcactggggg aatttgttag
108241 aaatgctaat cctcagagct actgaatcag gaactctggg ggtggagccc aggcatctgg
108301 ggcccaacaa gcccgccccc cagctgatgc taacgcatgc tcaagtttga gaggccacagt
108361 cctgtagtaa gagtgacaag agaagcaggc attgcgggcc ccctggggtg tgagtgaaag
108421 gaagccaatg ggcacttagc cttcacccat gccacgcacc tcatttacat cccctattct
Exon 7
108481 tatcatcttc acgaccacct tgagagccag gggttcagag cccctctttc ct>aatgaggg
Exon7-R
108541 ctcccaggac aggatgaggt gcctgcctga ggtcacacgg cagggagtgc agctcccct
108601 gccccgacct gctgagcccc atcacttccg cagatcctgg cattctctca gaagctgtac
108661 tacgacaagg aacagacagt gagcatgaag gacaatgtca ggcccctgca gcagctgggg
108721 cagcgcacgg tgataaagtc cggggccccg ggtcggccgc tgccctgggc cctgcctgcc
108781 ctgctgggcc ccatgctggc ctgcctgctg gccggcttcc tgcgatgatg gctcacttct Stop
dbSNP (rs1803230
C/A)
108841 gcacgcagcc tctctgttgc ctcag<ctctc caagttccag gcttccggtc cttagccttc
CA4mRNA-R
dbSNP (rs2229179 - G/A)
108901 ccaggtggga ctttaggcat gattaaaata tggacatatt tttggagaaa cctttctcaa
polyA signal polyA cleavage site
108961 gtgtgtttt<t agccttccac aactacccca ccctgtcccc ctccacccac ccctgttcct
Exon7-F
109021 cctgttccag ggcgggggct ttaaggccag gagatttctc ccaagcaggt accaccaggt
109081 gtccccactc ccgttctatg tgaattccgt gtctataccc cactcccttc taccaggacc
109141 tggaccttgg agagatgctg aaggcatctt ggagcttcat cacagcggaa gctagaggag
109201 ttccaatctg atctcttcat catatagagg gggaaactga ggctgagaaa gacaaggttg
109261 gggccgggca tagtgattca cgcctgtaat cctggcacgt tgcgaggcag aggcacgtga
109321 atcacttgag ccctggagtt caagaccagc ctaggcaaca tggtgaagcc ctgtctctat
109381 aaaaaataca aaaattaacc aggtgtggtg gtgcacacct gtagtcccag ctactcagga
109441 ggttgaggca ggaggattgc ttgaacccag gaggcgaagg ttgcagtgag ctgagattgt
109501 gccactgcac tccagcctgg gcaacagagc gagagagaag aggctgcttg gctggctgga
109561 ggccatatac tgaggctagg gcagagccga ctgcatgacg gcagccccag ccctgtgcgt
109621 tctcccctgt gctaggggtg aaagggtgtc atgtgtgggg atggcctagg caaggtgggc
109681 gaaaggaagt tcatttgttt gctcaaaaat ttattgagcg tttatgctct aggcactggg
109741 gatatggcag agaataaaag acaaaaatgc ctgccctcct ggagttcaca gtctagtgga
109801 gagacagccc ataaatgaag caggcatgtt gtctaataga tcgggaggca gtgagtgcat
109861 gggagaaaga gaattcaggg caggggccg ggcgcagtgg ctcatgcctg taattccagc
109921 actttgggaa gccgaggcgg gcagatcacc tgaggtcagg ggtttgagac cagcctggcc
109981 aacgtggcga aacaccgtct ttactaaaaa tacaaaaatt agctgggcat ggtggcgggt
110041 gccggtaatt cagctattca ggaggctgag gcaggagaat tgaggcagag tttgcagtaa
110101 gccaagattg aaccactgca ctccaacctg ggtgacagag agagactctg tctcaaaaaa
110161 aaaaaaaaag agagaattca gggcagggaa ggtgggaagc cctgggggaa ggggcggctg
110221 ggaggaggcc agagatggag gcctctggag actgcaaatg ttgaggtgcg gcagggaggg

14.2. CA4 primers

Name	Size	TM (°C)	Sequence
Exon1a3-1F	558	54	ccttatcagggactcccaac
Exon1a3-1R		53	ggagagcggaggatttcag
Exon1a3-2F	301	50	cggcctgggttttatagc
Exon1a3-2R		52	gtgtgggtcaagcactttgt
Exon1b-F	150	52	caccatgcacaaagagcagt
Exon1b-R		52	tgtgagcaacaagacacacg
Exon2-F	473	52	atcccagactggtctgacaaa
Exon2-R		51	ccaaagcgtttctgtgtgg
Exon3n4-F	513	54	tggagtcccaggtctctgaa
Exon3n4-R		52	tgaagctgggatgaagagcta
Exon5n6-F	497	54	gagggcagacagagggataa
Exon5n6-R		54	cctgcagactttctcaagacc
Exon7-F	477	54	ggggtagttgtggaaggcta
Exon7-R		54	gttcagagcccctctttcct

14.3. PCR standard reaction mixture

Reagent	Final concentration	Volume
DNA	200 µg/µl	1 µl
Forward primer	20 pmol/µl	0.5 µl
Reverse primer	20 pmol/µl	0.5 µl
dNTPs	20 µM	1 µl
GoTaq Buffer	1 X	5 µl
GoTaq	1 U/µl	0.1 µl
Sterile distilled water	-	16.9 µl
Total		25 µl

14.4. Generuler^{TM} 100 bp DNA Ladder Plus

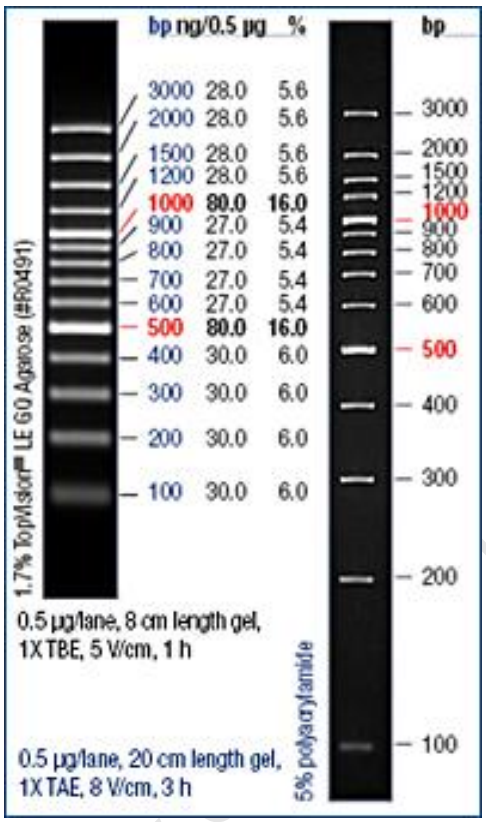

14.5. Cycle sequencing reaction mixture

Reagent	Final concentration	Volume
Template DNA	100 µg/ µl	2 µl
Forward or reverse primer	3.2 pmol/µl	4 µl
Dilution Buffer (Applied Biosystems)	5 X	4 µl
5 x Terminator mix (Applied Biosystems)	-	2 µl
Sterile distilled water	-	8 µl
Total		20 µl

14.6. Protocol for ethanol precipitation of DNA

1. Add 2 µl sodium acetate (1.5M NaAcetate, pH >8, 250 mM EDTA) to DNA
2. Add absolute ethanols at a volume of 2.5 x that of DNA solution
3. Mix and leave to stand for 1 hr (-80°C) or O/N (-20°C)
4. Centrifuge at 10 000 rpm for 10 min

5. Discard supernatant

6. Add 50 µl of 70% ethanol

7. Centrifuge at 10 000 rpm for 10 min

8. Discard supernatant

9. Air dry pellet for at least one hour

10. Resuspend pellet in 10 µl HiDi formamide (Applied Biosystems, USA)

11. Run sample on sequencer

14.7. Annotated region of the CFTR gene to be amplified

```
   1  AATTGGAAGCAAATGACATCACAGCAGGTCAGAGAAAAAGGGTTGAGCGGCAGGCACCCA
  61  GAGTAGTAGGTCTTTGGCATTAGGAGCTTGAGCCCAGACGGCCCTAGCAGGGACCCCAGC
 121  GCCCGAGAGACCATGCAGAGGTCGCCTCTGGAAAAGGCCAGCGTTGTCTCCAAACTTTTT
 181  TTCAGCTGGACCAGACCAATTTTGAGGAAAGGATACAGACAGCGCCTGGAATTGTCAGAC
 241  ATATACCAAATCCCTTCTGTTGATTCTGCTGACAATCTATCTGAAAAATTGGAAAGAGAA
 301  TGGGATAGAGAGCTGGCTTCAAAGAAAAATCCTAAACTCATTAATGCCCTTCGGCGATGT
 361  TTTTTCTGGAGATTTATGTTCTATGGAATCTTTTTATATTTAGGGGAAGTCACCAAAGCA
 421  GTACAGCCTCTCTTACTGGGAAGAATCATAGCTTCCTATGACCCGGATAACAAGGAGGAA
 481  CGCTCTATCGCGATTTATCTAGGCATAGGCTTATGCCTTCTCTTTATTGTGAGGACACTG
 541  CTCCTACACCCAGCCATTTTTGGCCTTCATCACATTGGAATGCAGATGAGAATAGCTATG
 601  TTTAGTTTGATTTATAAGAAGACTTTAAAGCTGTCAAGCCGTGTTCTAGATAAAATAAGT
 661  ATTGGACAACTTGTTAGTCTCCTTTCCAACAACCTGAACAAATTTGATGAAGGACTTGCA
 721  TTGGCACATTTCGTGTGGATCGCTCCTTTGCAAGTGGCACTCCTCATGGGGCTAATCTGG
 781  GAGTTGTTACAGGCGTCTGCCTTCTGTGGACTTGGTTTCCTGATAGTCCTTGCCCTTTTT
 841  CAGGCTGGGCTAGGGAGAATGATGATGAAGTACAGAGATCAGAGAGCTGGGAAGATCAGT
 901  GAAAGACTTGTGATTACCTCAGAAATGATTGAAAATATCCAATCTGTTAAGGCATACTGC
 961  TGGGAAGAAGCAATGGAAAAAATGATTGAAAACTTAAGACAAACAGAACTGAAACTGACT
1021  CGGAAGGCAGCCTATGTGAGATACTTCAATAGCTCAGCCTTCTTCTTCTCAGGGTTCTTT
1081  GTGGTGTTTTTATCTGTGCTTCCCTATGCACTAATCAAAGGAATCATCCTCCGGAAAATA
1141  TTCACCACCATCTCATTCTGCATTGTTCTGCGCATGGCGGTCACTCGGCAATTTCCCTGG
1201  GCTGTACAAACATGGTATGACTCTCTTGGAGCAATAAACAAAATACAGGATTTCTTACAA
1261  AAGCAAGAATATAAGACATTGGAATATAACTTAACGACTACAGAAGTAGTGATGGAGAAT
1321  GTAACAGCCTTCTGGGAGGAGGGATTTGGGGAATTATTTGAGAAAGCAAAACAAAACAAT
1381  AACAATAGAAAAACTTCTAATGGTGATGACAGCCTCTTCTTCAGTAATTTCTCACTTCTT
1441  GGTACTCCTGTCCTGAAAGATATTAATTTCAAGATAGAAAGAGGACAGTTGTTGGCGGTT
1501  GCTGGATCCACTGGAGCAGGCAAGACTTCACTTCTAATGGTGATTATGGGAGAACTGGAG
1561  CCTTCAGAGGGTAAAATTAAGCACAGTGGAAGAATTTCATTCTGTTCTCAGTTTTCCTGG
1621  ATTATGCCTGGCACCATTAAAGAAAATATCATCTTTGGTGTTTCCTATGATGAATATAGA
1681  TACAGAAGCGTCATCAAAGCATGCCAACTAGAAGAGGACATCTCCAAGTTTGCAGAGAAA
1741  GACAATATAGTTCTTGGAGAAGGTGGAATCACACTGAGTGGAGGTCAACGAGCAAGAATT
1801  TCTTTAGCAAGAGCAGTATACAAAGATGCTGATTTGTATTTATTAGACTCTCCTTTTGGA
1861  TACCTAGATGTTTTAACAGAAAAAGAAATATTTGAAAGCTGTGTCTGTAAACTGATGGCT
1921  AACAAAACTAGGATTTTGGTCACTTCTAAAATGGAACATTTAAAGAAAGCTGACAAAATA
1981  TTAATTTTGCATGAAGGTAGCAGCTATTTTTATGGGACATTTTCAGAACTCCAAAATCTA
2041  CAGCCAGACTTTAGCTCAAAACTCATGGGATGTGATTCTTTCGACCAATTTAGTGCAGAA
2101  AGAAGAAATTCAATCCTAACTGAGACCTTACACCGTTTCTCATTAGAAGGAGATGCTCCT
2161  GTCTCCTGGACAGAAACAAAAAAACAATCTTTTAAACAGACTGGAGAGTTTGGGGAAAAA
2221  AGGAAGAATTCTATTCTCAATCCAATCAACTCTATACGAAAATTTTCCATTGTGCAAAAG
2281  ACTCCCTTACAAATGAATGGCATCGAAGAGGATTCTGATGAGCCTTTAGAGAGAAGGCTG
2341  TCCTTAGTACCAGATTCTGAGCAGGGAGAGGCGATACTGCCTCGCATCAGCGTGATCAGC
2401  ACTGGCCCCACGCTTCAGGCACGAAGGAGGCAGTCTGTCCTGAACCTGATGACACACTCA
2461  GTTAACCAAGGTCAGAACATTCACCGAAAGACAACAGCATCCACACGAAAAGTGTCACTG
2521  GCCCCTCAGGCAAACTTGACTGAACTGGATATATATTCAAGAAGGTTATCTCAAGAAACT
```

```
2581 GGCTTGGAAATAAGTGAAGAAATTAACGAAGAAGACTTAAAGGAGTGCTTTTTTGATGAT
2641 ATGGAGAGCATACCAGCAGTGACTACATGGAACACATACCTTCGATATATTACTGTCCAC
2701 AAGAGCTTAATTTTTGTGCTAATTTGGTGCTTAGTAATTTTTCTGGCAGAGGTGGCTGCT
2761 TCTTTGGTTGTGCTGTGGCTCCTTGGAAACACTCCTCTTCAAGACAAAGGGAATAGTACT
2821 CATAGTAGAAATAACAGCTATGCAGTGATTATCACCAGCACCAGTTCGTATTATGTGTTT
2881 TACATTTACGTGGGAGTAGCCGACACTTTGCTTGCTATGGGATTCTTCAGAGGTCTACCA
2941 CTGGTGCATACTCTAATCACAGTGTCGAAAATTTTACACCACAAAATGTTACATTCTGTT
3001 CTTCAAGCACCTATGTCAACCCTCAACACGTTGAAAGCAGGTGGGATTCTTAATAGATTC
3061 TCCAAAGATATAGCAATTTTGGATGACCTTCTGCCTCTTACCATATTTGACTTCATCCAG
3121 TTGTTATTAATTGTGATTGGAGCTATAGCAGTTGTCGCAGTTTTACAACCCTACATCTTT
3181 GTTGCAACAGTGCCAGTGATAGTGGCTTTTATTATGTTGAGAGCATATTTCCTCCAAACC
3241 TCACAGCAACTCAAACAACTGGAATCTGAAGGCAGGAGTCCAATTTTCACTCATCTTGTT
3301 ACAAGCTTAAAAGGACTATGGACACTTCGTGCCTTCGGACGGCAGCCTTACTTTGAAACT
3361 CTGTTCCACAAAGCTCTGAATTTACATACTGCCAACTGGTTCTTGTACCTGTCAACACTG
3421 CGCTGGTTCCAAATGAGAATAGAAATGATTTTTGTCATCTTCTTCATTGCTGTTACCTTC
3481 ATTTCCATTTTAACAACAGGAGAAGGAGAAGGAAGAGTTGGTATTATCCTGACTTTAGCC
3541 ATGAATATCATGAGTACATTGCAGTGGGCTGTAAACTCCAGCATAGATGTGGATAGCTTG
3601 ATGCGATCTGTGAGCCGAGTCTTTAAGTTCATTGACATGCCAACAGAAGGTAAACCTACC
3661 AAGTCAACCAAACCATACAAGAATGGCCAACTCTCGAAAGTTATGATTATTGAGAATTCA
3721 CACGTGAAGAAAGATGACATCTGGCCCTCAGGGGGCCAAATGACTGTCAAAGATCTCACA
3781 GCAAAATACACAGAAGGTGGAAATGCCATATTAGAGAACATTTCCTTCTCAATAAGTCCT
3841 GGCCAGAGGGTGGGCCTCTTGGGAAGAACTGGATCAGGGAAGAGTACTTTGTTATCAGCT
3901 TTTTTGAGACTACTGAACACTGAAGGAGAAATCCAGATCGATGGTGTGTCTTGGGATTCA
3961 ATAACTTTGCAACAGTGGAGGAAAGCCTTTGGAGTGATACCACAGAAAGTATTTATTTTT
4021 TCTGGAACATTTAGAAAAAACTTGGATCCCTATGAACAGTGGAGTGATCAAGAAATATGG
4081 AAAGTTGCAGATGAGGTTGGGCTCAGATCTGTGATAGAACAGTTTCCTGGGAAGCTTGAC
4141 TTTGTCCTTGTGGATGGGGGCTGTGTCCTAAGCCATGGCCACAAGCAGTTGATGTGCTTG
4201 GCTAGATCTGTTCTCAGTAAGGCGAAGATCTTGCTGCTTGATGAACCCAGTGCTCATTTG
4261 GATCCAGTAACATACCAAATAATTAGAAGAACTCTAAAACAAGCATTTGCTGATTGCACA
4321 GTAATTCTCTGTGAACACAGGATAGAAGCAATGCTGGAATGCCAACAATTTTTGGTCATA
4381 GAAGAGAACAAAGTGCGGCAGTACGATTCCATCCAGAAACTGCTGAACGAGAGGAGCCTC
4441 TTCCGGCAAGCCATCAGCCCCTCCGACAGGGTGAAGCTCTTTCCCCACCGGAACTCAAGC
4501 AAGTGCAAGTCTAAGCCCCAGATTGCTGCTCTGAAAGAGGAGACAGAAGAAGAGGTGCAA
4561 GATACAAGGCTTTAGAGAGCAGCATAAATGTTGACATGGGACATTTGCTCATGGAATTGG
4621 AGCTCGTGGGACAGTCACCTCATGGAATTGGAGCTCGTGGAACAGTTACCTCTGCCTCAG
4681 AAAACAAGGATGAATTAAGTTTTTTTTTAAAAAAGAAACATTTGGTAAGGGGAATTGAGG
4741 ACACTGATATGGGTCTTGATAAATGGCTTCCTGGCAATAGTCAAATTGTGTGAAAGGTAC
4801 TTCAAATCCTTGAAGATTTACCACTTGTGTTTTGCAAGCCAGATTTTCCTGAAAACCCTT
4861 GCCATGTGCTAGTAATTGGAAAGGCAGCTCTAAATGTCAATCAGCCTAGTTGATCAGCTT
4921 ATTGTCTAGTGAAACTCGTTAATTTGTAGTGTTGGAGAAGAACTGAAATCATACTTCTTA
4981 GGGTTATGATTAAGTAATGATAACTGGAAACTTCAGCGGTTTATATAAGCTTGTATTCCT
5041 TTTTCTCTCCTCTCCCCATGATGTTTAGAAACACAACTATATTGTTTGCTAAGCATTCCA
5101 ACTATCTCATTTCCAAGCAAGTATTAGAATACCACAGGAACCACAAGACTGCACATCAAA
5161 ATATGCCCCATTCAACATCTAGTGAGCAGTCAGGAAAGAGAACTTCCAGATCCTGGAAAT
5221 CAGGGTTAGTATTGTCCAGGTCTACCAAAAATCTCAATATTTCAGATAATCACAATACAT
5281 CCCTTACCTGGGAAAGGGCTGTTATAATCTTTCACAGGGGACAGGATGGTTCCCTTGATG
5341 AAGAAGTTGATATGCCTTTTCCCAACTCCAGAAAGTGACAAGCTCACAGACCTTTGAACT
5401 AGAGTTTAGCTGGAAAAGTATGTTAGTGCAAATTGTCACAGGACAGCCCTTCTTTCCACA
5461 GAAGCTCCAGGTAGAGGGTGTGTAAGTAGATAGGCCATGGGCACTGTGGGTAGACACACA
5521 TGAAGTCCAAGCATTTAGATGTATAGGTTGATGGTGGTATGTTTTCAGGCTAGATGTATG
5581 TACTTCATGCTGTCTACACTAAGAGAGAATGAGAGACACACTGAAGAAGCACCAATCATG
5641 AATTAGTTTTATATGCTTCTGTTTTATAATTTTGTGAAGCAAAATTTTTTCTCTAGGAAA
5701 TATTTATTTTAATAATGTTTCAAACATATATAACAATGCTGTATTTTAAAAGAATGATTA
5761 TGAATTACATTTGTATAAAATAATTTTTATATTTGAAATATTGACTTTTTATGGCACTAG
5821 TATTTCTATGAAATATTATGTTAAAACTGGGACAGGGGAGAACCTAGGGTGATATTAACC
5881 AGGGGCCATGAATCACCTTTTGGTCTGGAGGGAAGCCTTGGGGCTGATGCAGTTGTTGCC
5941 CACAGCTGTATGATTCCCAGCCAGCACAGCCTCTTAGATGCAGTTCTGAAGAAGATGGTA
6001 CCACCAGTCTGACTGTTTCCATCAAGGGTACACTGCCTTCTCAACTCCAAACTGACTCTT
6061 AAGAAGACTGCATTATATTTATTACTGTAAGAAAATATCACTTGTCAATAAAATCCATAC
6121 ATTTGT
```

```
Araujo – 5′ GTTTTCCTGGATTATGCCTGGCAC 3′ forward
Araujo – 5′ GTTGGCATGCTTTGATGACGCTTC 3′ reverse
```

Figure 14.1. Annotated CFTR sequence. CFTR sequence showing the position of primers. The forward primer is shown in orange, and the reverse in magenta. The deletion is highlighted in red. Amplification of the region results in a 95 bp sequence.

14.8. CFTR ΔF508 region primers

Name	Size	TM (°C)	Sequence
CFTR-F	95	58.6	gttttcctggattatgcctggcac
CFTR-R		59.4	gttggcatgctttgatgacgcttc

14.9. Construction of pCXN vector

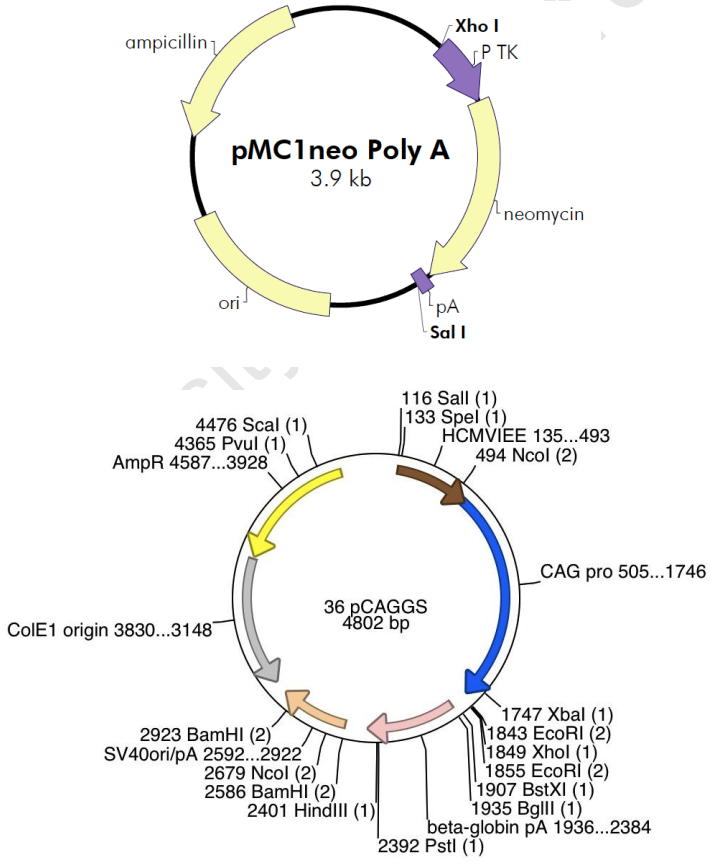

Figure 14.2. Vector maps of the pCAGGS and pMCneo Poly A vectors from which pCXN was constructed. The pCXN vector was constructed by cleavage of the pMCneo Poly A vector (top) at the *XhoI* and SalI sites, and ligation of the insert into pCAGGS at the *SalI* site. The CA4 cDNA sequence was cloned into the *EcoRI* site of pCXN.

14.10. pEGFP-N1 vector map showing multiple cloning site

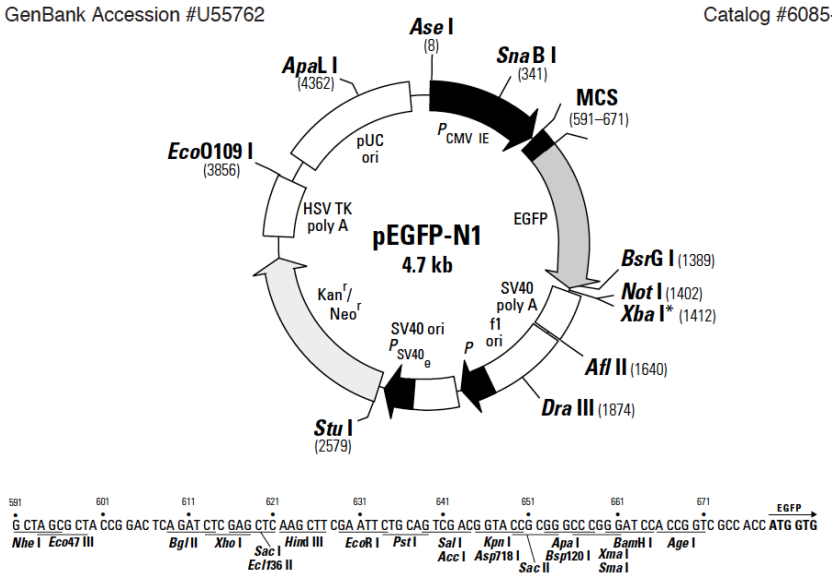

Figure 14.3. pEGFP-N1 vector map. A map showing the restriction and multiple cloning sites (MCS) of the pEGFP-N1 vector. The CA4 complete cDNA sequence was cloned into the vector using the *HindIII* and *SacI* restriction enzymes.

14.11. pGem-T Easy vector map

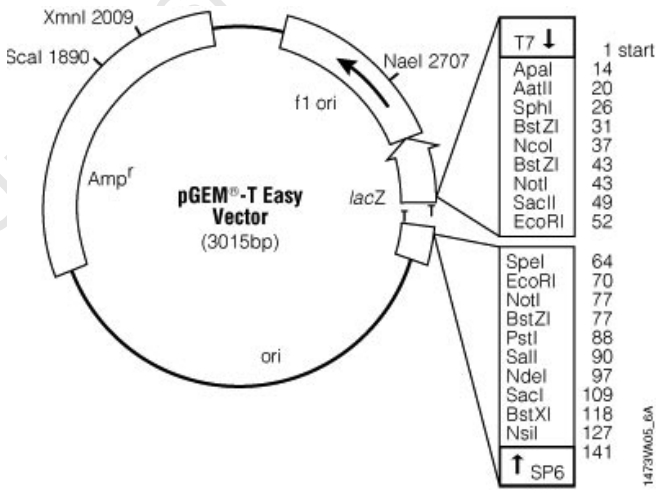

Figure 14.4. pGem-T Easy vector map. During the construction of CA4/pEGSH, a CA4 cDNA fragment generated by PCR was subcloned into the pGEM-T Easy vector via the T/A cloning site. The cDNA was then cloned into pEGSH via the *Kpn1* and *Xho1* restriction enzyme site

14.12. Mycoplasma test mounting fluid

20 mM Citric acid

55 mM $Na_2HPO_4.2H_2O$

50% Glycerol

pH to 5.5 and store at 4°C

14.13. Western blot analysis buffers

Resolving gel

12% Acryl-bisacryl-amide mix (30:08)

0.375 M Tris (pH 8.8)

0.1% SDS

0.1% TEMED

0.1% Ammonium persulphate

Stacking gel

5% Acryl-bisacryl-amide mix (30:08)

0.192 M Tris (pH6.8)

0.1% SDS

0.1% TEMED

0.1% Ammonium persulphate

Acryl-bisacryl-amide mix (30:08)

26 g acrylamide

1 g N,N'-methylenebisacrylamide

Make up to 100ml, heating at 37°C to dissolve chemicals. Store at 4°C and protect from light

Running buffer

1 g SDS

3.03 g Tris

14.41 g glycin

Make up to 1 litre

Transfer buffer

2.9 g glycine

5.8 g Tris

0.37 g SDS

200 ml isopropanol

Make up to 1 litre and store at store at 4°C

Phosphate buffered saline (PBS)/Tween

8 g NaCl

1.45 g $Na_2HPO_4.12H_2O$

0.2 g KCl

0.2 g KH_2PO_4

Make up to 1 litre, pH to 7.4

PBS/Tween

For membrane washes, add 0.1% Tween 1 x PBS

Stripping buffer

62.5 mM Tris-HCl (pH 6.7)

2% SDS

100 mM β-mercaptoethanol

14.14. Hank's Buffered Salt Solution

8 g NaCl

0.4 g KCl

60 mg KH_2PO_4

1 g Glucose

10 mg Phenol Red

48 mg Na_2HPO_4

98 mg $MgSO_4$

140 mg $CaCl_2$

350 mg $NaHCO_3$

14.15. shSCR (scrambled shRNA) Sequence

5'AAAAAGTGGGAAGGGCCCTGCAGGTGGGTCAGGCCCACAGGGCCCTTCCCACCGGTGTTTC GTCCTTTCCACAA 3'

The shSCR sequence (designed by Fiona Baine, Division of Human Genetics, University of Cape Town) is a non-specific shRNA that was used as a negative control for experiments in which expression of CAIV mRNA was silenced.

14.16. Proteins identified by mass spectrometry as being bound to CAIV

hek wt

13.1	cDNA FLJ43509 fis, clone PERIC2003699
15.2	Hemoglobin subunit alpha OS=Homo sapiens GN=HBA1 PE=1 SV=2 - [HBA_HUMAN]
16.0	Hemoglobin subunit beta OS=Homo sapiens GN=HBB PE=1 SV=2 - [HBB_HUMAN]
25.9	CLL-associated antigen KW-6 (Fragment)
38.8	Coiled-coil domain-containing protein 68
44.9	Isoform 2 of Arginine/serine-rich coiled-coil protein 2
47.3	Isoform 2 of Serum albumin
50.1	Similar to Elongation factor 1-alpha 1
51.5	Keratin, type I cytoskeletal 14 OS=Homo sapiens GN=KRT14 PE=1 SV=4 - [K1C14_HUMAN]
53.1	Type II hair keratin 1

54.6	55 kDa protein
56.6	Keratin, type II cuticular Hb2
58.8	Keratin, type I cytoskeletal 10 OS=Homo sapiens GN=KRT10 PE=1 SV=6 - [K1C10_HUMAN]
61.9	Keratin, type II cytoskeletal 1b
62.0	Keratin, type I cytoskeletal 9 OS=Homo sapiens GN=KRT9 PE=1 SV=3 - [K1C9_HUMAN]
65.2	Spermatogenesis-associated protein 16
65.8	Similar to Nestin
65.8	Keratin, type II cytoskeletal 2 epidermal
65.8	Keratin, type II cytoskeletal 2 oral
66.0	Keratin, type II cytoskeletal 1 OS=Homo sapiens GN=KRT1 PE=1 SV=6 - [K2C1_HUMAN]
67.6	Lamin-B2
69.7	Isoform 3 of Centrosomal protein kizuna
69.9	cDNA FLJ51903, highly similar to Stress-70 protein, mitochondrial
70.9	Isoform 1 of Coiled-coil domain-containing protein 67
75.6	cDNA FLJ43107 fis, clone CTONG2020108, highly similar to Protein CASP
78.1	cDNA FLJ51916, highly similar to Type II inositol-3,4-bisphosphate4-phosphatase
83.9	Isoform 1 of Olfactomedin-like protein 2B
85.2	Isoform 3 of Enhancer of polycomb homolog 1
86.0	Uncharacterized protein
89.6	Tumor necrosis factor alpha-induced protein 3
89.7	Isoform 1 of Progesterone-induced-blocking factor 1
91.4	Isoform 2 of Transmembrane protease serine 7
91.7	Chondroitin sulfate synthase 1
107.9	Zinc finger, NFX1-type containing 1
126.9	Uncharacterized protein
138.8	Isoform 2 of Protein diaphanous homolog 1
145.7	Splicing factor 3B subunit 1
145.8	Isoform 3 of B-cell CLL/lymphoma 9-like protein
156.9	cDNA FLJ45870 fis, clone OCBBF3005330, highly similar to FYVE finger-containing phosphoinositide kinase
157.4	Isoform 2 of Rap guanine nucleotide exchange factor 6
178.8	Protein tyrosine phosphatase, receptor type, F isoform 2 variant
180.0	Formin-2
206.7	Isoform 4 of Afadin
213.9	Voltage-gated L-type calcium channel alpha-1 subunit
223.4	myosin-11 isoform SM2A
223.5	Myosin-13
223.8	Myosin-3
227.8	228 kDa protein
241.5	Basic helix-loop-helix domain-containing protein KIAA2018
250.4	Isoform 3 of Pecanex-like protein 1

268.1	Isoform 5 of Centriolin
270.9	Isoform 2 of Dystrophin
271.5	Isoform 2 of Telomere-associated protein RIF1
301.6	Isoform 3 of Centromere-associated protein E
307.6	Uncharacterized protein
312.1	Matrix-remodeling-associated protein 5
331.6	Isoform DPI of Desmoplakin
335.7	Isoform 1 of Chromodomain-helicase-DNA-binding protein 7
350.7	Centrosome-associated protein 350
409.5	Isoform 1 of Abnormal spindle-like microcephaly-associated protein
477.3	478 kDa protein
516.0	stAR-related lipid transfer protein 9
632.4	Midasin
801.4	hypothetical protein LOC643677
986.0	nebulin isoform 1
1004.6	Isoform 4 of Nesprin-1

hek mut

9.0	9 kDa protein
15.2	Hemoglobin subunit alpha OS=Homo sapiens GN=HBA1 PE=1 SV=2 - [HBA_HUMAN]
16.0	Hemoglobin subunit beta OS=Homo sapiens GN=HBB PE=1 SV=2 - [HBB_HUMAN]
21.3	S-adenosylmethionine decarboxylase proenzyme isoform 2
25.8	Isoform 2 of Homer protein homolog 1
29.1	cDNA FLJ60029, highly similar to Keratin, type II cuticular Hb3
29.1	cDNA FLJ75207
31.6	Succinate dehydrogenase [ubiquinone] iron-sulfur subunit, mitochondrial
32.5	33 kDa protein
40.4	Uncharacterized protein
46.4	Uncharacterized protein
47.3	Isoform 2 of Serum albumin
50.1	Similar to Elongation factor 1-alpha 1
51.2	Keratin, type I cytoskeletal 16
51.5	Keratin, type I cytoskeletal 14 OS=Homo sapiens GN=KRT14 PE=1 SV=4 - [K1C14_HUMAN]
54.6	Ectonucleotide pyrophosphatase/phosphodiesterase family member 5
55.8	Isoform 2 of Uncharacterized aarF domain-containing protein kinase 4
58.8	Keratin, type I cytoskeletal 10 OS=Homo sapiens GN=KRT10 PE=1 SV=6 - [K1C10_HUMAN]
60.0	Keratin, type II cytoskeletal 6B OS=Homo sapiens GN=KRT6B PE=1 SV=5 - [K2C6B_HUMAN]

60.1	Isoform 6 of Shugoshin-like 1
62.0	Keratin, type I cytoskeletal 9 OS=Homo sapiens GN=KRT9 PE=1 SV=3 - [K1C9_HUMAN]
62.0	Isoform 9 of Collagen alpha-1(XIII) chain
62.3	Keratin, type II cytoskeletal 5 OS=Homo sapiens GN=KRT5 PE=1 SV=3 - [K2C5_HUMAN]
64.1	64 kDa protein
64.1	Keratinocyte proline-rich protein
65.8	Keratin, type II cytoskeletal 2 epidermal
65.9	Isoform 2 of DnaJ homolog subfamily C member 2
66.0	Keratin, type II cytoskeletal 1 OS=Homo sapiens GN=KRT1 PE=1 SV=6 - [K2C1_HUMAN]
67.0	cDNA FLJ53358, highly similar to Heterogeneous nuclear ribonucleoprotein R
76.0	Coiled-coil domain-containing protein 154
76.4	Isoform 3 of DNA polymerase kappa
87.5	Zinc finger protein 287
88.2	Ubiquitin carboxyl-terminal hydrolase 1
88.6	chromosome 19 open reading frame 29
98.5	Isoform 2 of WD repeat-containing protein 47
105.8	Isoform 2 of Mitotic checkpoint serine/threonine-protein kinase BUB1 beta
113.1	Isoform 1 of Solute carrier family 12 member 3
120.8	Uncharacterized protein
120.9	Isoform 2 of Electroneutral sodium bicarbonate exchanger 1
125.7	Isoform 1 of Protein phosphatase 1 regulatory subunit 3A
127.5	Uncharacterized protein
130.4	Uncharacterized protein
133.7	Insulin receptor substrate 4
139.9	Isoform 1 of EH domain-binding protein 1
142.7	Isoform 2 of S phase cyclin A-associated protein in the endoplasmic reticulum
144.2	Isoform 2 of Treacle protein
145.7	Isoform 1 of Misshapen-like kinase 1
150.6	Adenylate cyclase type 9
151.1	microtubule-associated tumor suppressor candidate 2 isoform a
151.1	Zinc finger protein 609
162.8	Isoform 4 of Membrane-associated guanylate kinase, WW and PDZ domain-containing protein 3
168.1	Isoform 1 of Pleckstrin homology domain-containing family H member 2
177.9	Dedicator of cytokinesis 8
193.4	Isoform 2 of Peripheral-type benzodiazepine receptor-associated protein 1
204.1	Uncharacterized protein
207.5	208 kDa protein
222.1	Isoform 2 of Dedicator of cytokinesis protein 4
223.4	myosin-11 isoform SM2A
225.4	Isoform 1 of Cytoskeleton-associated protein 5

227.8	228 kDa protein
228.9	Isoform 1 of Myosin-10
232.0	Isoform 1 of Fanconi anemia group M protein
237.0	Isoform 1 of 1-phosphatidylinositol-3-phosphate 5-kinase
265.2	CREB-binding protein
268.1	Isoform 5 of Centriolin
269.6	Isoform 2 of Transcriptional regulator ATRX
279.8	Isoform 2 of Collagen alpha-5(VI) chain
285.9	Leucine-rich repeat serine/threonine-protein kinase 2
299.4	Isoform 1 of Serine/arginine repetitive matrix protein 2
301.6	Isoform 3 of Centromere-associated protein E
337.6	DmX-like protein 1
337.6	Isoform 4 of Protein unc-80 homolog
358.0	Isoform 1 of Cadherin EGF LAG seven-pass G-type receptor 3
361.5	hypothetical protein LOC65250
367.5	Centromere protein F
409.5	Isoform 1 of Abnormal spindle-like microcephaly-associated protein
412.1	dystrophin Dp427l isoform
477.3	478 kDa protein
485.6	Isoform 2 of Dynein heavy chain 1, axonemal
492.3	Isoform 1 of Cytoplasmic dynein 2 heavy chain 1
528.7	Dynein heavy chain 5, axonemal
571.5	Isoform 3 of E3 ubiquitin-protein ligase UBR4
613.8	Isoform 1 of Microtubule-actin cross-linking factor 1, isoforms 1/2/3/5
669.7	Microtubule-actin cross-linking factor 1, isoform 4
801.4	hypothetical protein LOC643677
1010.4	Isoform 1 of Nesprin-1

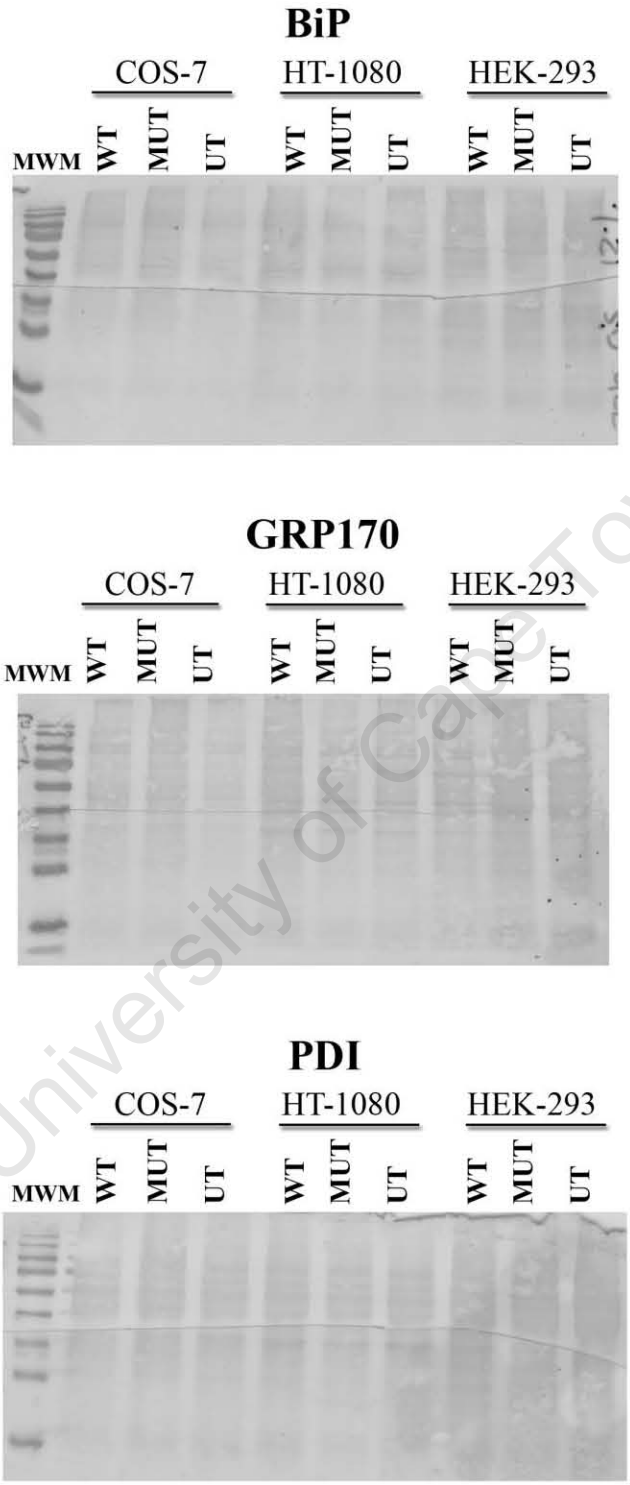

Figure 14.7. Chaperone western blots stained wirh Ponceau S to control for loading of protein from COS-7, HT-1080 and HEK-293 cells transfected with CAIV. MWM indicates the lane in which the molecular weight marker used to quantify size was run.